Modeling Investigation of Gas Hydrate Decomposition: Thermodynamic Approach and Molecular Dynamic Simulations

By

©Javad Kondori

A thesis submitted to the school of Graduate Studies in partial fulfilment of the requirements for the degree of

Doctor of Philosophy

Faculty of Engineering and Applied Science
Memorial University of Newfoundland

August 2019

St. John's, Newfoundland and Labrador
Canada

ABSTRACT

In the last few decades, there has been a great interest in the hydrate reservoirs for energy storage and source purposes. It has been proven that hydrates can contribute to ocean carbon cycling, global climate change, and coastal sediment stability. The permafrost and offshore environments contain enormous quantities of methane in the form of gas hydrates. In addition, the natural gas has been recently produced worldwide including in Alaska, Siberia, Japan, and North West Territories of Canada. However, the gas hydrates formation may lead to various forms of blockages in oil/gas production and transportation processes, resulting in high capital and operating costs.

Detailed experimental and modeling investigations of hydrate formation and decomposition can assist to better understand the mechanisms involved in gas production from hydrates. Thus, it is important to determine the equilibrium hydrate-forming conditions so that a systematic parametric sensitivity analysis is conducted to identify the vital process and thermodynamic parameters affecting this occurrence. This project focuses on the hydrate formation/dissociation conditions where equations of state and molecular dynamic (MD) simulations are used. Giving further information, this study provides a reliable model to determine the gas hydrate formation and decomposition conditions of pure, binary, and ternary systems of hydrate gases where the van der Waals Platteuw model is utilized by combining with extended UNIQUAC model and PC-SAFT equation of state. In addition, MD simulations are conducted to investigate the microscopic mechanisms/phenomena and intermolecular forces involved in gas (pure and mixture) hydrate decomposition, where the molecular interactions, structures, and behaviours of hydrate systems need to be appropriately explored. Through a systematic design of simulation runs, the impacts of temperature, pressure, cage occupancy, and inhibitors on the hydrate dissociation are studied. Furthermore, the diffusion coefficient, density, and heat capacity of gas hydrates with different structures and compositions of methane, carbon dioxide, propane, and isobutane

are determined through employing MD strategy. A very good agreement is noticed between the modeling results and the experimental data so that the value of AADT% for PC-SAFT equation of state is lower, compared to the previous EOS/thermodynamic models. The binary interaction parameters for different binary components are investigated by using experimental hydrate data, leading to better outcome compared with results obtained through fitting the VLE data. The trend of the heat capacity and density of methane hydrate obtained from the MD simulations shows a good match with the real data. The hydrate decomposition is not achieved at the equilibrium temperature at 100% cage occupancy; however, the decomposition of the methane hydrate lattice is observed when the cage occupancy reduces from 100% to 87.5% or 75% because of low stability and high diffusion coefficient of the methane molecules at low cage occupancies where the temperature and pressure are constant. The lattice parameter for the methane/water and methane/isobutane systems is calculated at a variety of pressures and temperatures. A good agreement between the experimental data and simulation results is noticed. The relative importance of inhibitors in terms of gas hydrate decomposition duration is assessed. Based on this criterion, the inhibitors are ordered as follows: methanol > ethanol >glycerol. The physical properties such as density and lattice parameter for different compositions of methane + carbon dioxide are obtained which are in agreement with those determined by experimental and theoretical techniques. According to the MD results, the structure with methane (25%) + carbon dioxide (75%) composition is almost stable under 300 K at 5 MPa; it means the best configuration to have a stable structure is when carbon dioxide and methane molecules are in large and small cavities, respectively. MD technique is used to investigate the bubble formation and evolution of carbon dioxide and methane after dissociation. Analysing the outcome of the present and previous works, the current study provides new reliable/useful information and data on the thermodynamic behaviours and molecular level of the hydrate dissociation process. It is expected that such a research investigation

offers effective tips/guidelines to deal with hydrate formation and dissociation in terms of utilization, prevention, and processing.

ACKNOWLEDGMENTS

I would like to acknowledge those special people without whom this dissertation would not been accomplished.

First and foremost, I express my sincere gratitude and thanks to my supervisor, Dr. Sohrab Zendehboudi. His spectacular insights and visions have always inspired me. I am greatly indebted to Dr. Sohrab Zendehboudi for his endless patient guidance throughout this research. He always supported me and guided me on exact paths to achieve my goal and complete my research tasks. I would like to thank my co supervisor Dr. Lesley James for her continued support and guidance towards my thesis completion. I would also like to express my sincere gratitude to my former supervisor, Dr. M. Enamul Hossain.

Most importantly, none of this would have been possible without the love and patience of my family. My beloved wife and my immediate family have been a constant source of love, concern, support, and strength all these years.

Last but not least, I would like to thank Memorial University (NL, Canada), Equinor (formerly Statoil) Canada, Innovate NL, and the Natural Sciences and Engineering Research Council of Canada (NSERC) for their financial support.

Table of Contents

LIST OF TABLES

LIST OF FIGURES

1. CHAPTER ONE

Introduction and Overview

Currently, gas hydrates have attracted increasing interests due to their high importance and wide applications in the future energy sources/storage [1], gas transportation [2], gas separation [3], and water treatment distillation [4]. Beside the considerable benefits of gas hydrates, they might create serious problems such as blockage and material/mechanical damage to equipment and pipeline systems in the oil and gas industries [5].

Gas hydrates, mainly methane hydrates, form valuable and huge gas resources in permafrost and deep ocean areas due to the fact at the standard condition, each cubic meter of natural gas hydrate contains about 160-180 cubic meters of natural gas [6]. Natural clathrate hydrates are crystalline ice-like compounds in which the guest molecules are trapped in the polyhedral cells created within the hydrogen-bonded water framework [6]. The clathrate hydrates can be formed at high pressures and low temperatures due to the van der Waals interactions between the guest gas molecules and water lattices, and the hydrogen bonds between water molecules [6]. Due to the size and characteristics of guest molecules in the cages, different hydrate structures namely; structure I, structure II, and structure H, can be created [6]. These three structures differ in the crystal structure in terms of the type and number of cages. The lattice parameter of cubic structure I is 12.05, which consists of two small (5^{12}) and six large ($5^{12}6^2$) cages. The small (pentagonal dodecahedral) and large cages (tetrakaidekahedral) are composed of 12 pentagonal water rings and 12 pentagonal plus two hexagonal faces, respectively.

The variations of temperature and pressure in process equipment especially in pipelines may lead to desirable conditions for formation of clathrate hydrates. Therefore, it is essential to propose effective, safe, and economical operating strategies in the oil and gas processes that may experience hydrate formation.

In the past decades, several researchers have studied natural gas production by methane hydrate dissociation through experimental (and pilot scale) and modelling/simulation investigations [8-16].

There are three major methods to produce natural gas (mainly methane) from gas hydrates; namely, depressurisation, thermal stimulation, and chemical injection [7]. In most recent studies, the depressurisation method has been recognised as the most promising approach for hydrate decomposition [8-11]. The hydrate formation or decomposition can be also affected by chemical or additive injection [18]. Thus, the role of additives in the dissociation acceleration and the formation inhibition needs to be studied comprehensively. A number of studies (in the open sources) investigate important prospects of additives in terms of improving storage capacity [19], dissociation [20], and formation rate [21] of gas hydrates.

The monitoring and controlling of hydrate formation and/or decomposition through experimental works at various process conditions are relatively difficult. In recent years, molecular dynamic (MD) simulations have been utilized as a reliable tool to study the structure [12], nucleation [13], growth [14], stability [15], and thermodynamic properties [16-18] of gas hydrates. In the MD simulations, the movement of each atom and/or molecule is determined by using the Newton's laws and the empirical potential functions are utilized to describe the interactions between all components in the simulation box. Recently, we prepared a comprehensive review on the theory and applications of MD simulations and different potential functions, which are used in the simulation of gas hydrates dissociation [19]. Wan et al. [20] employed MD simulations for methane gas hydrate dissociation in the systems that contained alcohol as an additive. In addition, Zhang and Pan [14] obtained the dynamic and structural properties of the methane hydrates, for example, mean square displacement, potential energy, density profile, and radial distribution function (RDF). Zhang et al. [21] conducted MD simulations to demonstrate the water- methane structure in the gas hydrate clathrate and to calculate the diffusion coefficient of water molecules by using mean square displacement (MSD). Also, Sakamaki et al. [22] studied the thermodynamic and mechanical characteristics of methane hydrate structure; the MD technique was employed in their research study to calculate the interfacial tension within a wide range

of pressure. Thus, it seems necessary to investigate the influence of different additives on methane hydrate clathrate decomposition. Although the structural and dynamic properties of clathrate hydrates have been investigated by a number of researchers in the past years, the MD simulations have not been used to calculate the thermophysical or physical properties such as density, thermal conductivity, heat capacity, and viscosity. The measurements of these parameters in gas hydrate systems at high- pressure and low-temperature conditions are difficult and expensive. Hence, the MD simulations and thermodynamic models appear to be suitable ways for determination of the characteristics of different hydrate systems. The density of hydrate was measured in some experimental studies [23, 24]. The MD tools can be used as an appropriate approach to calculate and monitor the density of gas hydrate over various stages such as formation, nucleation, and decomposition of clathrate hydrates. In addition, the heat capacity of methane hydrate at different temperatures and pressures is a vital property for heat loss calculations, which is studied in this research work.

As the first phase in this research work, the hydrate phase equilibrium conditions in different systems are obtained by employing the van der Waals and Platteuw model coupled with the perturbed-chain statistical associating fluid theory (PC-SAFT) equation of state and universal quasi chemical (UNIQUAC) model. The equilibrium hydrate-forming conditions are determined for several pure and mixtures of gas systems in the presence and/or absence of inhibitors under different thermodynamic and process conditions. The inhibitors studied in this research project include KCl, $CaCl_2$, $MgCl_2$, NaCl, glycerol, ethanol, and methanol. The UNIQUAC model is used to calculate the water activity in the aqueous phase of alcohols and salts. Also, the optimal interaction parameters for the components in the aqueous phase are determined to be used in the UNIQUAC model.

In this project, we also perform a series of molecular dynamic (MD) simulations for gas hydrate decomposition at different temperatures, pressures, and cage occupancies. Furthermore, different inhibitors such as methanol and glycerol are selected as a regular additive in this research work as they

are common inhibitors in the oil and gas transportation and the gas hydrate exploration. Thus, the structural and dynamic properties of gas hydrates with inhibitors are also analysed at different thermodynamic conditions. The mean square displacement, diffusion coefficient, radial distribution function, as well as the thermodynamic properties of gas hydrates in mixture of carbon dioxide, methane, propane, and isobutane for structure I and II at various temperatures and pressures, in the presence and absence of inhibitors (methanol, ethanol, and glycerol), are investigated.

The main contributions/phases of this research project are given below:

- The PC-SAFT equation of state is used to calculate the gas hydrate formation temperatures.
- The UNIQUAC model and association contribution are combined for different gaseous systems in the presence of different alcohols (ethanol, methanol, and glycerol) and salts (KCl, NaCl, $CaCl_2$, and $MgCl_2$).
- The binary interactions parameter of two-component cases in the UNIQUAC model (u_{ij}) is determined.
- The structural and thermodynamic properties (MSD, RDF, diffusion coefficient, and lattice parameter) of methane gas hydrate in structure I and II are studied to investigate the stability and decomposition process of hyrates.
- The density and heat capacity of methane hydrates at different conditions are calculated using MD simulations.
- The effects of inhibitors on stability and decomposition phenomenon of hydrates are investigated by comparing the results of cases with and without inhibitors.
- The ranking of various inhibitors (in terms of time and temperature of gas hydrate decomposition) for mixtures of methane, propane, and isobutane gas hydrate structure II is determined.

- Different compositions of methane and carbon dioxide are tested to find the most stable case(s) at different temperatures. According to the MD results, the structure with methane (25%) + carbon dioxide (75%) composition is almost stable under 300 K at 5 MPa; it means the best configuration to have a stable structure is when carbon dioxide and methane molecules are in large and small cavities, respectively.
- The physical properties such as density and lattice parameter for different compositions of methane + carbon dioxide are obtained. The comparison is made between the modeling results of this work and the outcomes of the studies available in the literature.
- MD technique is also employed to investigate the bubble formation and evolution of carbon dioxide and methane bubbles after dissociation.

This thesis consists of a series of manuscripts either published or under review for publication, as listed below:

Chapter Two has been published in the Journal of Petroleum Science and Engineering. The manuscript provides a systematic literature review on the hydrate dissociation where various processes such as depressurization, thermal stimulation, inhibitor injection, and gas swapping are discussed. In addition, the review work investigates key features of molecular dynamics simulations including main governing equations, assumptions, and potential functions concerning the decomposition of methane hydrate. Chapter Three has been published in the industrial & Engineering Chemistry Research Journal, ACS Publications. The PC-SAFT equation of state is employed to model the hydrate phase in different systems. The gas hydrate formation conditions are determined for pure gases, sour gases, and different mixtures of gases in the uninhibited and inhibited systems. Chapter Four has been published in the Fuel Journal. A series of molecular dynamic simulations for methane hydrate decomposition at different temperatures, pressures, and cage occupancies are performed. Furthermore, methanol is used as an appropriate additive in this research work as it is a common inhibitor in oil and gas transportation and

gas hydrate exploration. Chapter Five has been published in the Journal of Chemical Engineering Research and Design. The dynamic and structural properties of mixtures including methane, propane, and isobutane that appear in structure II of gas hydrates are studied. The impact of three inhibitors including methanol, ethanol, and glycerol on the decomposition phenomenon is demonstrated through employing MD simulations. Chapter Six includes a technical manuscript, which is published in Journal of Molecular Liquid. In this phase of study, we plan to investigate the stability and dissociation of CH_4 and CO_2 hydrates at different compositions and temperatures. In addition, the physical and dynamic characteristics of the system are calculated. The dynamic behaviors of CH_4 and CO_2 bubbles after hydrate decomposition are discussed. Chapter Seven contains a summary, conclusions, and recommendations for future work.

References

[1] Englezos, P. and J.D. Lee, *Gas hydrates: A cleaner source of energy and opportunity for innovative technologies.* Korean Journal of Chemical Engineering, 2005. **22**(5): p. 671-681.

[2] Fitzgerald, A. and M. Taylor. *Offshore gas-to-solids technology*. in *Offshore Europe*. 2001. Society of Petroleum Engineers.

[3] Kang, S.-P. and H. Lee, *Recovery of CO2 from flue gas using gas hydrate: thermodynamic verification through phase equilibrium measurements.* Environmental science & technology, 2000. **34**(20): p. 4397-4400.

[4] Javanmardi, J. and M. Moshfeghian, *Energy consumption and economic evaluation of water desalination by hydrate phenomenon.* QNRS Repository, 2011. **2011**(1): p. 622.

[5] Carroll, J.J., *Natural Gas Hydrates: A Guide for Engineers*. 2009.

[6] Sloan Jr, E.D. and C. Koh, *Clathrate hydrates of natural gases*. 2007: CRC press.

[7] Burshears, M., T. O'brien, and R. Malone. *A multi-phase, multi-dimensional, variable composition simulation of gas production from a conventional gas reservoir in contact with hydrates*. in *SPE Unconventional Gas Technology Symposium*. 1986. Society of Petroleum Engineers.

[8] Demirbas, A., *Methane hydrates as potential energy resource: Part 2–Methane production processes from gas hydrates.* Energy Conversion and Management, 2010. **51**(7): p. 1562-1571.

[9] Kurihara, M., A. Sato, H. Ouchi, H. Narita, Y. Masuda, T. Saeki, and T. Fujii. *Prediction of gas productivity from eastern Nankai Trough methane hydrate reservoirs*. in *Offshore Technology Conference*. 2008. Offshore Technology Conference.

[10] Moridis, G. *Numerical studies of gas production from methane hydrates*. in *SPE Gas Technology Symposium*. 2002. Society of Petroleum Engineers.

[11] Liu, Y., M. Strumendo, and H. Arastoopour, *Simulation of methane production from hydrates by depressurization and thermal stimulation.* Industrial & Engineering Chemistry Research, 2008. **48**(5): p. 2451-2464.
[12] English, N.J. and J.M.D. MacElroy, *Theoretical studies of the kinetics of methane hydrate crystallization in external electromagnetic fields.* Journal of Chemical Physics, 2004. **120**(21): p. 10247-10256.
[13] Sarupria, S. and P.G. Debenedetti, *Homogeneous nucleation of methane hydrate in microsecond molecular dynamics simulations.* Journal of Physical Chemistry Letters, 2012. **3**(20): p. 2942-2947.
[14] Zhang, J. and Z. Pan, *Effect of potential energy on the formation of methane hydrate.* Journal of Petroleum Science and Engineering, 2011. **76**(3): p. 148-154.
[15] Okano, Y. and K. Yasuoka, *Free-energy calculation of structure-H hydrates.* The Journal of chemical physics, 2006. **124**(2): p. 024510.
[16] Wei, C. and Z. Hong-Yu, *Molecular dynamics simulation of the structure I empty gas hydrate.* Chinese physics letters, 2002. **19**(5): p. 609.
[17] Mirzaeifard, S., P. Servio, and A.D. Rey, *Molecular Dynamics Characterization of Temperature and Pressure Effects on the Water-Methane Interface.* Colloid and Interface Science Communications, 2018. **24**: p. 75-81.
[18] Mirzaeifard, S., P. Servio, and A.D. Rey, *Molecular dynamics characterization of the water-methane, ethane, and propane gas mixture interfaces.* Chemical Engineering Science, 2019.
[19] Kondori, J., S. Zendehboudi, and M.E. Hossain, *A review on simulation of methane production from gas hydrate reservoirs: Molecular dynamics prospective.* Journal of Petroleum Science and Engineering, 2017. **159**: p. 754-772.
[20] Wan, L.H., K.F. Yan, X.S. Li, and S.S. Fan, *Molecular dynamics simulation of methane hydrate dissociation process in the presence of thermodynamic inhibitor.* Wuli Huaxue Xuebao/ Acta Physico - Chimica Sinica, 2009. **25**(3): p. 486-494.
[21] Zhang, J., S. Piana, R. Freij-Ayoub, M. Rivero, and S.K. Choi, *Molecular dynamics study of methane in water: diffusion and structure.* Molecular Simulation, 2006. **32**(15): p. 1279-1286.
[22] Sakemoto, R., H. Sakamoto, K. Shiraiwa, R. Ohmura, and T. Uchida, *Clathrate Hydrate Crystal Growth at the Seawater/Hydrophobic−Guest−Liquid Interface.* Crystal Growth & Design, 2010. **10**(3): p. 1296-1300.
[23] Waite, W.F., J.C. Santamarina, D.D. Cortes, B. Dugan, D. Espinoza, J. Germaine, J. Jang, J. Jung, T.J. Kneafsey, and H. Shin, *Physical properties of hydrate-bearing sediments.* Reviews of geophysics, 2009. **47**(4).
[24] Kiefte, H., M. Clouter, and R. Gagnon, *Determination of acoustic velocities of clathrate hydrates by Brillouin spectroscopy.* The Journal of Physical Chemistry, 1985. **89**(14): p. 3103-3108.

2. CHAPTER TWO

Literature Review (A Review on Simulation of Methane Production from Gas Hydrate Reservoirs: Molecular Dynamics Prospective, Published)

Preface

A version of this manuscript has been published in the Journal of Petroleum Science and Engineering 159 (2017): 754-772. I am the primary author of this paper. Along with the co-authors, Sohrab Zendehboudi, M Enamul Hossain. I carried out most of the literature review, data collection and the comparison of different methods for methane production from hydrates. I prepared the first draft of the manuscript and subsequently revised the manuscript based on the co-authors' feedback as well as the comments received from the peer review process. The co-author, M Enamul Hossain, helped in reviewing and revising the manuscript. The co-author, Sohrab Zendehboudi, contributed through providing the manuscript's outlines, comments on various parts of the manuscript, and technical points/critiques on previous works in the related field. Sohrab Zendehboudi also assisted in reviewing and revising the manuscript.

Abstract

Hydrate reservoirs have steadily emerged as an important contributor in energy storage. To better understand the role of hydrates in gas production, it is vital to know the challenges related to the hydrate dissociation. To highlight the main technical challenges, further research and engineering investigations are needed for interactions between the molecules, phase behaviours, and detailed mechanisms of hydrate formation and dissociation. This review paper describes the gas hydrate reservoirs, hydrate dissociation, and previous research works related to gas engineering. This study briefly presents the key theoretical concepts and drawbacks of different techniques/kinetics of decomposition; consisting of depressurising, thermal stimulation, chemical injection, and gas swapping. This will be followed by the theory on the molecular dynamics simulation and its application in various decomposition methods. Owing to the limitations of existing experimental and theoretical approaches, development of more accurate theoretical models and equations of state (EOSs) is inevitable. The molecular dynamics simulation strategy has been used as a strong research tool with adequately small scales in both space and time. The practical implication of molecular dynamics (MD) simulation in hydrate dissociation methods is illustrated at the end of this study for further clarification. The complex nature of hydrates clearly implies that new potential functions for current MD tools are required to satisfactorily comprehend the hydrate molecular structure and mechanisms of hydrate decomposition.

Keywords: Methane Hydrate Reservoir, Hydrate Dissociation, Kinetics of Decomposition, Molecular Dynamics Simulation, Potential Function.

2.1. Introduction

Sir Humphry Davy discovered the hydrate in 1810. He observed that a crystalline solid was created by an aqueous solution of chlorine when it was cooled. Then, in early 1820, John Faraday conducted some experiments that confirmed the Davy's results. However, it remained a matter of "academic" enthusiasm, until Hammerschmit [1] claimed in 1934 that hydrates (as the main reason) are responsible

for obstruction of gas and oil transportation in pipeline systems. Since then, the hydrate inhibition methods have been persistently tested through various research activities by scientists across the world [2-8]. In this field of research, apart from the gas hydrate formation conditions, the impacts of inhibitors on the equilibrium conditions have been widely studied. The soaring cost of hydrate inhibition has been one of the important concerns in the gas and oil energy sectors since 1970.

Gas hydrates are solid ice-like substances formed from water when the natural gas (e.g., mainly methane) combines with water under high-pressure and low-temperature conditions. As the gas hydrates contain a vast quantity of methane gas and globally occur in profound water and permafrost areas, they can provide a viable (and additional) energy resource [9]. Natural gas hydrates (NGHs) are non-stoichiometric compounds which are made of water molecules at particular thermodynamic conditions, depending on the temperature, pressure, and composition. Each standard cubic meter of NGH can result in approximately 160–180 cubic meters of natural gas under normal conditions [10].

The best conditions required for gas hydrate formation are usually low temperatures (<300 K) and high pressures (>0.6 MPa) [11, 12]. Hydrate structures are classified into three categories, depending on the size of guest molecules, and type and number of cavities that cause water molecules to change their arrangements. These three common structures are called structure (type) I [13], structure (type) II [14], and structure (type) H[15]. The most significant structural differences between various classes of hydrates are summarized in Table 2-1. The unit cell of structure I hydrates includes two types of cavities; namely, two small pentagonal cavities known as dodecahedrons (5^{12}), and six larger cavities which are named tetrakaidecahedron ($5^{12}6^2$) [16].

Table 2-1: Parameters of three popular hydrate structures (modified after reference [11]).

Hydrate crystal structure	**I**		**II**		**H**		
Crystal type	Cubic		Cubic		Hexagonal		
Space group	Pm3n (no. 223)		Fd3m (no. 227)		P6/mmm (no. 191)		
Lattice parameter	α=12 Å α=β=γ=90˚		α=17.3 Å α= β=γ=90˚		α=12.2 Å, c=10.1 Å α= β=90 ˚, γ=120 ˚		
Number of waters per unit cell	46		136		34		
Cavity	Small	Large	Small	Large	Small	Medium	Large
Number of cavities per unit cell	2	6	16	8	3	2	1
Average cavity radius (Å)	3.95	4.33	3.91	4.73	3.91	4.06	5.71
Coordination number	20	24	20	28	20	36	

Table 2-1 demonstrates that the small cavity is approximately spherical, due to a low amount of change in the radius of 3.95 and 3.91 Å in types I and II of hydrates, respectively [11]. The structure I of hydrates is usually created by one guest molecule such as carbon dioxide, ethane, and methane. A unit cell of structure II comprises 136 water molecules which include 16 small cavities (5^{12}) and 8 large cavities ($5^{12}6^2$) [17] . Structure H contains small, large, and $4^3 5^6 6^3$ cages. The formation of structure H hydrates requires two molecules; including, a large organic guest molecule (such as neohexane), and a help gas (such as methane) [18]. Figure 2-1 displays the detailed information on the hydrate crystal cell structures. In all types of hydrates, maximum one guest molecule generally can be resided in each cage. Even for severe cases (e.g., extremely high pressures), there is a possibility of having multiple-cage occupancies, with uncommon small guests like hydrogen or/and xenon [11].

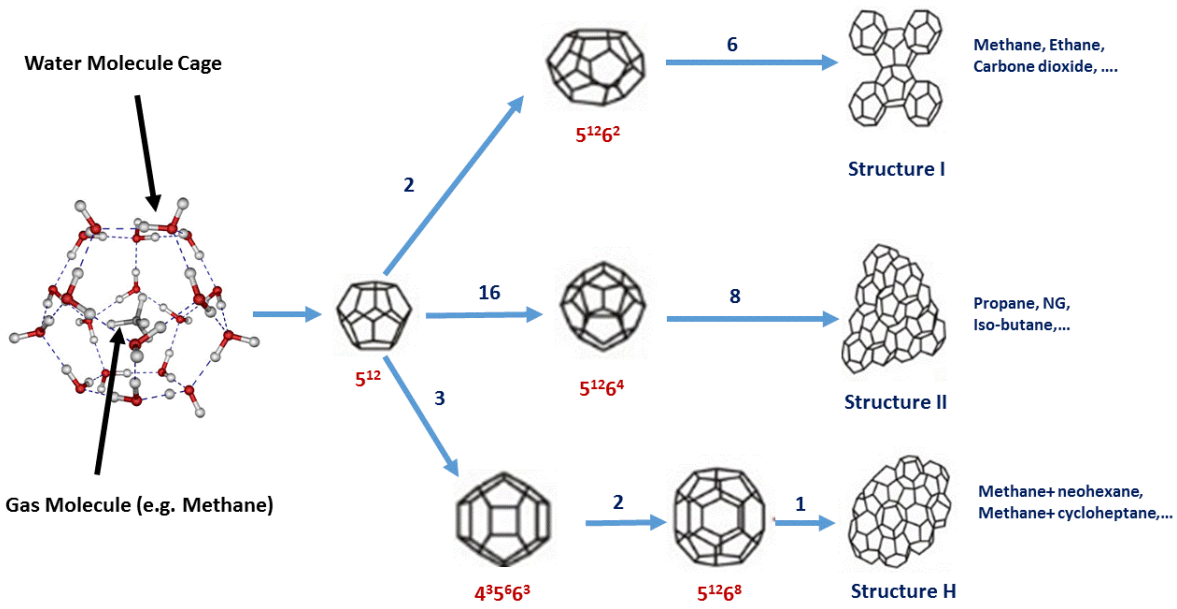

Figure 2-1: Simple schematic of three common unit crystal structures of the gas hydrates (modified after reference [11]).

More than 27 percent of the land (e.g., mainly freezing rocks) and 90 percent of the sea have the potential to contain gas hydrate reserves [19]. Moreover, the changes of pressure and temperature in longer distance especially in pipeline systems are more favorable conditions for hydrate formation. Therefore, it is vital to offer an economical, effective, and safe operation in the gas and oil production sites. Generally, the phase equilibrium of a gas hydrate is investigated through various operational strategies such as depressurising and thermal stimulation. According to this approach, the exploitation procedures of a gas hydrate can be arranged as depressurisation, thermal stimulation, chemical injection, and gas swapping [20]. Recent studies illustrate that the depressurisation method (when the pressure of the deposit is decreased to a value lower than the dissociation pressure at the dominant temperature) is the most promising technique for hydrate dissociation [21-24]. Although the hydrate formation and decomposition conditions have been investigated by some researchers at various conditions, further experimental and theoretical studies on the hydrate kinetics and gas hydrate decomposition should be carried out to understand the phenomenon mechanisms. For instance, the hydrate formation and decomposition have been studied by researchers to investigate a variety of key aspects such as formation

and decomposition kinetics of hydrates in different solutions (e.g., ionic and non-ionic liquids), decomposition enthalpies, formation conditions for the refrigerants in aqueous solutions, gas consumption in formations, and induction time in the bentonite clay suspension systems [25-31].

Molecular dynamics (MD) is an interesting and efficient computer simulation method. A deep understanding of microscopic mechanisms can be achieved through MD simulations. MD simulation technique has been proven as a powerful research tool to analyse the behaviour of complex systems so that it gives information on structural and dynamical properties at the molecular level. It involves solving the classical equations of motion in the system. MD simulation studies of NGH have evolved during the past years [32-35].

The present work focuses on important aspects (e.g., hydrate dissociation, and methane production) of gas hydrate reservoirs which have been highlighted in the literature over recent years. In fact, it provides a brief review of hydrate dissociation under depressurisation, thermal stimulation, inhibitor injection, and gas swapping. In addition, the article investigates the various features of molecular dynamics simulations including main governing equations, assumptions, and potential functions concerning the decomposition of methane hydrate.

2.2. Gas Hydrate Reservoirs

Global energy demand is continuing to rise. There has been an increased interest in hydrates as an energy source, because gas hydrates are more available than other resources in the world and many governments/countries can benefit from them. In addition, the production cost for hydrate reservoirs is only 10–20% more than the cost for the standard (conventional) natural gas production technologies [36]. Knowing the fact that in the late 21st century there will be a sharply decline in hydrocarbon resources because of the human population growth, hydrate reservoirs seem to be a promising energy resource in the near future. Hydrates can be considered as a huge source of natural gas, because one cubic foot of solid gas hydrates contains an amount of gas which is 150 to 170 times higher, compared

to one cubic foot of the corresponding natural gas at the standard conditions [37]. Hence, by altering gas to the hydrate, a massive volume of gas can be stored under special temperature and pressure conditions[38].

The volume of gas hydrates and types, elastic, and petrophysical properties of the sediments/rocks appear to be vital to describe gas hydrate reservoirs [39]. Holbrook et al. [39] showed that the lower limit of gas hydrate stability (e.g., bottom-simulating reflector, BSR) is found in about 450 meter below the seafloor (mbsf). There are diagenetic carbonates as nodules and lamina in upper and lower limits of the BSR without the mineralogical or sedimentological interruption. The mineralogy and composition of these diagenetic carbonates in equilibrium state should be used to determine the formation conditions of gas hydrates [40]. In the Blake Ridge, the thickness of diagenetic carbonate sediments (nodules or/and laminae) has been reported to be within the range of 1-10 millimetres [41]. In addition, there are some small cubic crystals of sulfide components such as pyrite. Pierre et al. utilized scanning electron microscopy (SEM) and transmission electron microscopy (TEM) tests to characterize the crystals of smear slides [40]. Based on the tests results, they observed that the hexagonal structures in the forms of single, twinned, and aggregated crystals are smaller than 1 micrometer [40]. Kvenvolden et al. [42] conducted a research work on the oxygen isotopic compositions of the diagenetic carbonates. They demonstrated that the gas hydrates formation occurs in the BSR upper limit of all sedimentary sections. According to the geophysical methods, it has been proved that methane hydrates are available throughout the world's oceans, primarily on the continental shelves (Figure 2-2) [43]. Figure 2-2 demonstrates that the minimum amount of gas hydrate sources (10 kg/m2) is normally found in the extended border zones. The estimation of global hydrate resources has been published by many scientists [44-48].

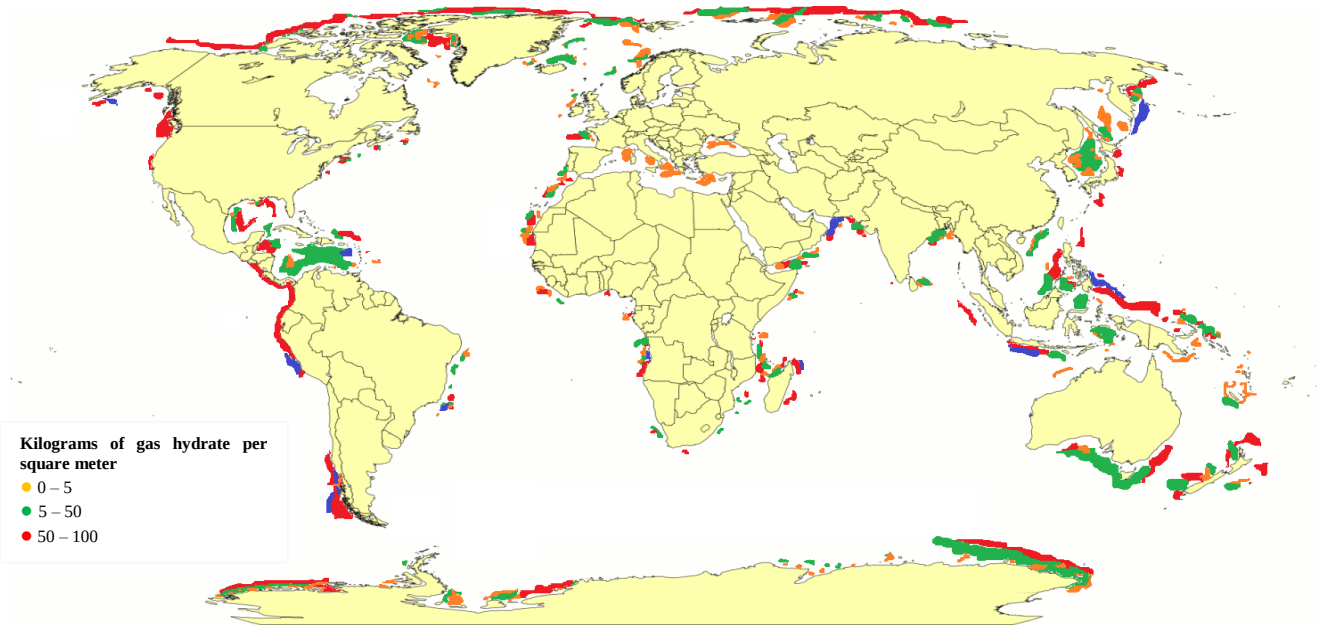

Figure 2-2: Global methane hydrate distribution in the ocean, primarily on the continental shelves (modified after reference [43]).

According to the literature, the deposits of hydrates in both shale and sand formations have an economic potential. Although there is a high likelihood of hydrates in the porous systems with high porosity and permeability, hydrate production in marine and arctic sediments have always attracted attention of industrial and academic sectors in terms of technical, economic, and environmental prospects [48]. For example, Makogon [49] introduced a methodology to calculate the amount of subsurface gas hydrates. In another work, Kvenvolden [50] discussed about all estimations of gas hydrate resources. This research study predicted 21×10^{15} m^3 methane in the hydrate sources [50- 52]. The maximum amount of gas hydrates (above 100 kg/m^2) is also located in the continental margins of Alaska, Peru, Japan, Chile, Argentina, Indonesia, Taiwan, and Gulf of Oman (up to 157 kg/m^2 stored gas hydrate) [43]. The gas hydrate reservoirs are considered as a huge energy source, compared to other hydrocarbon reserves (Figure 2-3) [43]. The gas hydrate inventory varies considerably according to various reports in the literature; nonetheless, the amount is still very large. [53].

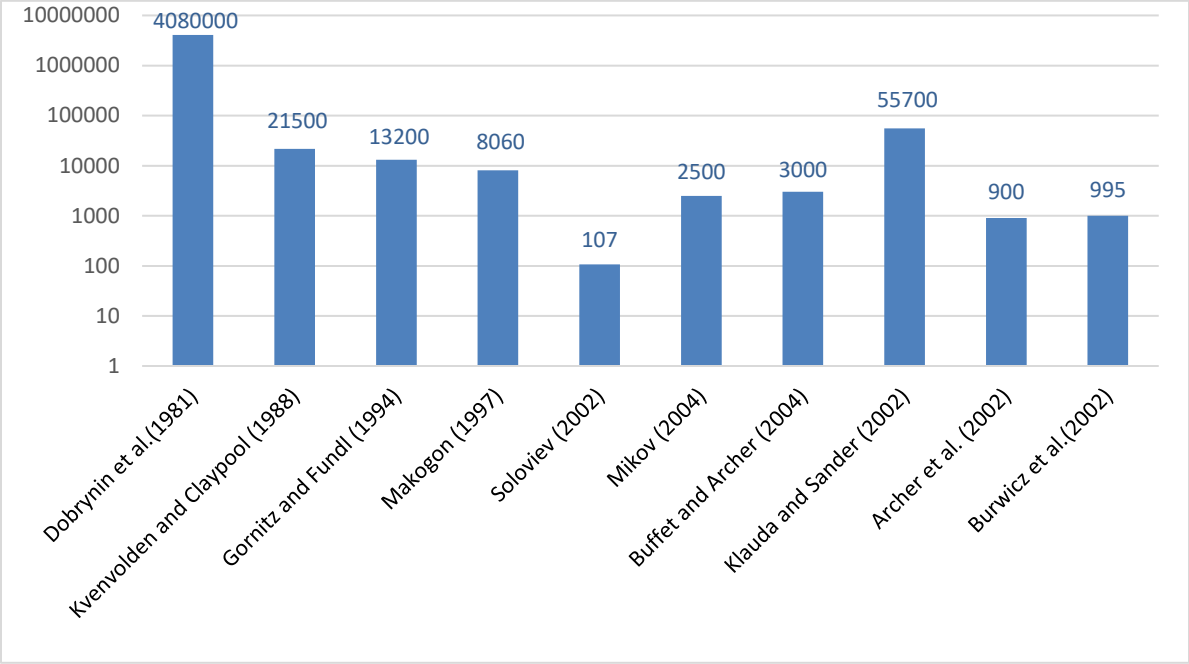

Figure 2-3: Approximate global gas hydrate index in the marine zones. The relative approximation ranges are tagged in Giga tones Carbon (GtC) (modified after reference [43]).

2.2.1. Classification of Methane Hydrate Reservoirs

There are three main classes of gas hydrate reservoirs in terms of geological characteristics, thermodynamic behaviors, and production strategies (Figure 4) [54, 55]. Class 1 reservoirs are made of a hydrate-bearing layer and an underlying two-phase zone which contains liquid water and gas. Class 1 (Figure 2-4a) reservoirs are also called hydrate-capped gas reservoirs [56]. The hydrate, liquid, and gas are in equilibrium.

Figure 2-4: Classification of gas hydrate reservoirs [55].

This class of reservoirs can be divided into two categories based on the presence of components in the hydrate zone: hydrate and gas (Category 1G) and hydrate and water (Category 1W) [57]. Class 2 reservoirs are composed of a hydrate-bearing interval with an underlying water-zone where the free gas is absent (Figure 2-4b). As all components in hydrate layer have the same temperature and pressure (i.e., thermodynamic equilibrium conditions) and there is no free gas in the multi-component system, the amount of produced gas and production rate are very low in this kind of gas hydrate reservoirs [57]. Class 3 includes a single hydrate-bearing zone. This type of gas hydrate reservoirs (e.g., Class 2) experiences the slow production rates during the decomposition process as the temperature and pressure conditions fall in the stability region (Figure 2-4c) [58].

Among three different decomposition methods, the depressurization is appropriate for all classes of the hydrate reservoirs as this technique is simple, cheap, and fast. The fast alteration of pressure and temperature might lead to the secondary hydrate formation in gas reservoirs [58-60]. Hence, the warm water injection (e.g., thermal stimulation method) near the well can be efficient to destroy the new hydrates (and ice) and lower the possibility of well chocking.

2.2.2. Hydrate Decomposition Kinetics

The production of hydrate methane means decomposing methane hydrate in the reservoirs and collecting the resultant methane gas in wells and downstream facilities. The kinetics of hydrate decomposition has been investigated for a few systems. Yin *et al*. [61] discussed about 14 different kinetic models of hydrate dissociation. The most important models since 1980s are presented in Table 2-2. The models are divided into three different types based on the solution method; namely, analytical, numerical, and empirical methodologies [61].

Table 2-2: Summary of gas hydrate dissociation kinetic models.

Researcher	Heat Transfer	Mass Transfer	System	Intrinsic Kinetics	Porous Media	Solution Method
Ullerich *et al*.[62]	√	√	Hydrate+ Water+ Methane Gas	–	–	Numerical
Kim-Bishnoi [63]	–	√	Hydrate+ Water+ Methane Gas	√	–	Analytical
Holder *et al*. [92]	√	√	Hydrate+ Water+ Methane Gas	–	–	Numerical
Burshears at al. [20]	√	√	Hydrate+ Water+ Mixture of Methane, Ethane and Propane)	√	–	Numerical
Selim-Sloan [64]	√	√	Hydrate+ Water+ Methane Gas	–	√	Analytical
Jamaluddin *et al*. [65]	√	√	Hydrate+ Water+ Methane Gas	√	–	Numerical
Yousif *et al*. [93]	√	√	Hydrate+ Salted Water+ Methane Gas	√	√	Numerical
Tsypkin [66]	√	√	Hydrate+ Water+ Ice+ Methane Gas	–	√	Analytical
Makogon *et al*. [79]	√	√	Hydrate+ Water+ Methane Gas	–	√	Analytical
Khairkhah *et al*. [67]	√	√	Hydrate+ Water+ Methane Gas	√	√	Numerical
Masuda *et al*. [68]	√	√	Hydrate+ Water+ Methane Gas	√	√	Numerical

Clarke *et al*. [69]	√	√	Hydrate+ Water+ Mixture of Methane and Ethane)	√	–	Numerical
Moridis [70]	√	√	Hydrate+ Water+ Methane Gas	√	√	Numerical
Hong *et al*. [60]	√	√	Hydrate+ Water+ Methane Gas	√	√	Analytical
Komai *et al*. [71]	√	√	Hydrate+ Water+ Methane Gas	√	–	Numerical
Ahmadi *et al*. [72]	√	√	Hydrate+ Water+ Natural Gas	√	√	Numerical
Sean *et al*. [73]	√	√	Hydrate+ Water+ Methane Gas	√	–	Numerical
Nazridoust *et al*. [74]	√	√	Hydrate+ Water+ Methane Gas	√	√	Numerical
Oyama *et al*. [102]	√	√	Hydrate+ Water+ Methane Gas	√	√	Theoretical
Gamwo *et al*. [75]	√	√	Hydrate+ Water+ Methane Gas	√	√	Numerical
Windmeier *et al*. [76]	√	√	Hydrate+ Water+ Methane Gas	√	–	Empirical

Ullerich *et al*. [62] described a numerical model without employing adjustable parameters to forecast decomposition of hydrates. This model exhibits an acceptable agreement with the experimental data. They also found that the thermal conduction poorly contributes to hydrate decomposition in the absence of sediments; however, the thermal conduction is more important in the in-situ cases of hydrate decomposition in sediments [62]. Kim *et al*. [63] suggested a method for the rate of natural gas hydrate decomposition and obtained the rate constant using the empirical data/findings for methane. Their experiments included measurement of the amount of collected methane within hydrate decomposition in a semi-batch stirred-tank reactor over an isothermal process. To calculate the intrinsic rate, the initial particle size was supposed to be constant, considering the Stokes law and settling time. In addition, it was assumed that all components have the same size before dissociation [63]. Selim *et al*. [64] introduced a mathematical model for the hydrate decomposition under thermal stimulation in porous media where heat flux and physical properties were constant. The model was based on one- dimensional semi- infinitive region, $0 < x < \infty$. They assumed that the hydrate fills the entire pore volume and has an initial uniform temperature, T_i. At time $t = 0$, the temperature at $x = 0$ was increased by a constant heat flux q_s and the temperature of the boundary was altered from T_i to T_o. It was also

observed that the hydrate decomposition starts and the boundary surface moves to a positive x-direction($x = X(t)$, which separates the undecomposed hydrate region from the water/gas system. At $t > 0$, the decomposed hydrate region occupies the zone, $0 < x < X(t)$, while the undecomposed hydrate occupies the region, $0 < X(t) < x < \infty$. They believed that the producing water from decomposition remains immobile and occupies the pores of the decomposed zone, and the thermophysical properties are constant. Internal effects, viscous dissipation, and possibility of external or mutual energy were ignored in their study. Having these assumptions, the differential form of the momentum balance equation is given below:

$$\varphi \frac{\partial \rho_g}{\partial t} + \frac{\partial (\rho_g v_x)}{\partial x} = 0 \qquad 0 < x < X(t), \qquad t > 0 \qquad (2\text{-}1)$$

where

$$v_x = \frac{\kappa}{\mu} \frac{\partial P}{\partial x} \qquad 0 < x < X(t), \qquad t > 0 \qquad (2\text{-}2)$$

In the above equations, φ stands for the porosity and ρ_g and v_x refer to the superficial gas velocity and gas density, respectively. κ, μ, and P represent the permeability, gas viscosity, and gas pressure, respectively. The differential forms of the mass and energy balance equations are listed below:

$$\rho_I C_{p_1} \frac{\partial T_I}{\partial t} + \frac{\partial}{\partial x}\left(\rho_g C_{p_g} v_x T_I\right) = k_I \frac{\partial^2 T_I}{\partial x^2} + T\beta \frac{DP}{Dt} \qquad 0 < x < X(t), t > 0 \qquad (2\text{-}3)$$

$$\frac{\partial T_{II}}{\partial t} = \alpha_{II} \frac{\partial^2 T_{II}}{\partial x^2} \qquad X(t) < x, t > 0 \qquad (2\text{-}4)$$

$$\rho_g = \frac{MwP}{RT_I} \qquad 0 < x < X(t), t > 0 \qquad (2\text{-}5)$$

where $T(x,t)$ is the temperature, C_P represents the heat capacity at a constant pressure, k stands for the effective thermal conductivity, β represents the coefficient of thermal expansion of gas, Mw and R are the gas molecular weight and universal gas constant, respectively. In the above equations, subscripts I and II refer to the dissociated zone and hydrate zone, respectively. The subscript g is also

for the gas phase. The initial and boundary conditions describing the decomposition process for the above equations are as follows:

$$\begin{cases} T_I = T_{II} & x = 0, \quad t > 0 \\ P_I = P_{II} & x = 0, \quad t > 0 \\ T_I = T_I = T_D & x = X(t), \quad t > 0 \end{cases} \tag{2-6}$$

$$\omega\varphi\rho_H \frac{dX}{dt} + \rho_g v_x = 0 \qquad x = X(t), \quad t > 0 \tag{2-7}$$

$$k_{II} \frac{\partial T_{II}}{\partial x} - k_I \frac{\partial T_I}{\partial x} = \varphi\rho_H \Delta H_D \frac{dX}{dt} \qquad x = X(t), \quad t > 0 \tag{2-8}$$

$$P_D = exp\left(A - \frac{B}{T_D}\right) \qquad x = X(t), \quad t > 0 \tag{2-9}$$

$$T_{II} = T_i \qquad x = \infty, \quad t > 0 \tag{2-10}$$

$$T_{II} = T_i \qquad 0 < x < \infty, \quad t > 0 \tag{2-11}$$

$$X(t) = 0 \qquad t = 0 \tag{2-12}$$

where ω and ΔH_D represent the mass of gas produced per unit mass of hydrate and heat of dissociation, respectively. Subscripts (*D*) and (*i*) refer to the dissociation and initial conditions, respectively. Equations (2-7) and (2-8) are the mass and energy balance equations at the front of the dissociation region, respectively. Thermodynamic equilibrium relationship (e.g., Antoine equation) between the gas pressure and the hydrate dissociation temperature at the dissociation interface is described by Equation (2-9). In Equation (2-9), A and B denote the component-specific constants in the Antoine equation. Selim *et al*. [64] applied a fourth degree polynomial to approximate the exact solution in their study. The expressions for $\rho_g(X,T), v_x(x,t)$, $P(x,t), T_I(x,t), T_{II}(x,t), X(t)$, and η are given below:

$$\frac{T_I - T_0}{T_D - T_0} = \frac{erf(a\eta + b) - erf(b)}{erf(a\xi + b) - erf(b)} \tag{2-13}$$

$$\frac{T_I - T_i}{T_D - T_i} = \frac{erf(\eta)}{erf(\xi)} \tag{2-14}$$

$$P^2 = P_0^2 + 4\frac{\omega\varphi(\rho_H)(\alpha_{II})\mu R}{\kappa\ Mw}\ \xi\int_0^{\eta} T_I(\eta)d\eta \quad (2\text{-}15)$$

$$X(t) = \xi\sqrt{4\alpha_{II}t} \quad (2\text{-}16)$$

$$\eta = \frac{x}{\sqrt{(4\alpha_{II}t)}} \quad (2\text{-}17)$$

in which, ξ is a number which depends on only physical parameters of initial and boundary conditions. Table 2-3 includes the magnitude of thermal, geological, and physical parameters used in Selim *et al*. study [64]. They showed that the decomposition rate decreases with increasing porosity of the hydrate phase. Decomposition rate is independent of the gas viscosity and porous system permeability. It was also found that lower thermal conductivity in the hydrate region and higher thermal diffusivity in the dissociation region lead to higher decomposition rates.

Table 2-3: Parameters used in dislocated model [61, 64].

Porosity, ϕ	0.3
Permeability, κ	1.38×10^{-13} m^2
Thermal Diffusion of Dissociation Zone, α_I	2.89×10^{-6} m^2/s
Thermal Diffusion of Hydrate Zone, α_{II}	6.97×10^{-7} m2/s
Thermal Conductivity of Dissociation Zone, k_I	5.57 W/m.K
Thermal Conductivity of Hydrate Zone, k_{II}	2.73 W/m.K
Hydrate Density, ρ_H	913 kg/m^3
Hydrate Heat of Dissociation,	$\Delta H_D = 215.59\times10^3 - 394.945T$ (J/kg)
	$\Delta H_D = 446.12\times10^3 - 132.638T$ (J/kg)
Antonine Equation	$P_D = \exp(49.3185 - 9459/T_{\backslash D}$ (Pa)
Gas Heat Capacity (J/kg.K)	$C_P = 1.23879\times10^3 + 3.1303T + 7.905\times10^{-4}T - 6.858\times10^{-7}T^3$
Gas Viscosity (Pa.s)	$\mu = [2.4504\times10^{-3} + 2.8764\times10^{-5}T + 3.279\times10^{-9}T^2 - 3.7838\times10^{-12}T^3] + [2.0891\times10^{-5}\rho_g + 2.5127\times10^{-7}\rho_g^2 - 5.822\times10^{-10}\rho_g^3 + 1.8387\times10^{-13}\rho_g^4]$

Through an extensive investigation, Jamaluddin *et al*. [65] used two mechanistic methods (intrinsic kinetics and heat transfer) to analyze the methane hydrate dissociation. Their results showed that the rate of dissociation depends on the activation energy. It was also found that both kinetic and intrinsic rates control the dissociation rate where the system pressure and surface roughness factor change [65]. Tsypkin [66] considered two moving phase transition boundaries to construct a new decomposition model for the gas hydrate. Gas hydrate decomposed in one boundary and ice melted on the other. A high-permeable system was utilized where the dissociation in the front moved faster than the ice melting. Dissociation region was divided into three zones which were separated by two boundaries. The researcher developed a proper equation for the mass and heat transfer during the hydrate decomposition, showing the corresponding zone between the dissociation and ice melting. Khairkhah *et al*. [67] concluded that an accurate estimation of gas production from hydrate reservoirs through modeling/simulation methodologies should incorporate two-phase fluid flow, kinetic rate, heat transfer, and dissociation model. Masuda *et al*. [68] provided a numerical model for predicting the flow behaviour of water and gas with hydrate decomposition in a porous medium. Their results were verified with the data obtained from the methane gas hydrate decomposition in Berea sandstone cores. In addition, Clarke *et al*.[69] offered a new mathematical model to calculate the intrinsic rate of gas hydrate dissociation where the gas mixtures contain methane and ethane. They performed experiments to investigate the kinetics of gas hydrate dissociation. Moridis [70] suggested EOSHYDR2 module for calculation of gas hydrate decomposition under equilibrium for both marine and permafrost reservoirs. They used EOSHYDR2 to model gas hydrate decomposition, non-isothermal hydrate formation, transport phenomena, and phase behavior for various hydrate cases. Moridis [60, 70] simulated gas hydrate decomposition of simple methane and mixture of methane and alkanes hydrates by employing exact thermochemical parameters. Hong *et al*. (60) simulated gas generation from a hydrate reservoir in a porous medium by using a simple analytical model. They studied the influences of different

parameters such as operating conditions, kinetic rate, and formation properties on the gas production. In addition, different equilibrium models were examined in their work. Komai *et al*. [71] conducted an experimental investigation for methane hydrate decomposition below the melting point using the Raman spectroscopy. They presented a kinetic model to explain the decomposition of methane hydrate by applying non- steady state approximation diffusion-controlled regime. The governing equation used in their work was the Fick's law as expressed below[71]:

$$\eta \frac{\partial C}{\partial t} = D \frac{1}{r^2} \frac{\partial}{\partial r} \left(r^2 \frac{\partial C}{\partial r} \right) \tag{2-18}$$

where *D*, *C*, and *r* refer to the diffusion coefficient of methane in the ice layer, concentration of methane in the hydrate, and radius of the hydrate particle, respectively. It should be noted that the mass transfer of methane occurs through the spherical wall of the ice layer. Thus, the initial and boundary conditions are as follows:

$$\begin{cases} C = C_B & t = 0 \\ C = C_B & r = r_0, t > 0 \\ C = C_H & r = X(t), t > 0 \end{cases} \tag{2-19}$$

In the above boundary conditions, $X(t)$ and r_0 refer to the radius of the hydrate particle (depending on the time) and the initial hydrate radius, respectively. C_B and C_H denote the concentration of methane in the bulk gas phase and the hydrate phase, respectively. Employing the initial and boundary conditions, the solution of the diffusion equation can be achieved in terms of the elapsed time and hydrate radius as follows:

$$\frac{C - C_B}{C_H - C_B} = \frac{x(r_0 - x)}{r(r_0 - x)} - \frac{2x}{\pi r} \sum_{n=1}^{\infty} \frac{1}{n} \sin \frac{n\pi(r - x)}{r_0 - x} \exp\left(-\frac{n^2 \pi^2 D t}{(r_0 - x)^2}\right) \tag{2-20}$$

They noted that the fugacity/fugacity coefficient can be calculated using a suitable thermodynamic correlation or equation of state (EOS) at different pressures. At the initial period of hydrate decomposition, it can be written $\mathrm{x} \cong r_0$ and $\mathrm{t} \cong 0$. For the small interval, they assumed that the

expression $\xi = \frac{(r_0 - x)}{\sqrt{Dt}}$ remains almost constant. According to this assumption, the following solution is attained:

$$\frac{1}{2}\xi = \varphi\left[\frac{r_0}{x} + 2\sum_{n=1}^{\infty}\exp(-\frac{n^2\pi^2}{\xi^2})\right] \cong \varphi\left[1 + 2\sum_{n=1}^{\infty}\exp(-\frac{n^2\pi^2}{\xi^2})\right] \quad (2\text{-}21)$$

where

$$\xi = \frac{(r_0 - x)}{\sqrt{Dt}} \quad (2\text{-}22)$$

Using the expression ξ and the relationship $\mathrm{I(t)} \cong [\frac{\mathrm{x(t)}}{r_0}]^3$, they calculated $I(\mathrm{t})$ through the following equation:

$$\frac{(1 - I(t)^{\frac{1}{3}})^2}{\xi^2} = \frac{Dt}{r_0^2} \quad (2\text{-}23)$$

There is a linear relationship between $\frac{(1 - I(t)^{\frac{1}{3}})^2}{\xi^2}$ and (t) based on their experiments. Their study showed that the results of diffusion-controlled dissociation regime and non-steady state approximation are in a very good agreement with the real data. It was also found that the decomposition rate of methane hydrate increases with increasing the temperature, while this rate declines as the pressure goes up. Ahmadi *et al*. [72] solved the governing equation by using the finite-difference numerical technique to analyse natural gas generation from hydrate reservoirs. They forecasted the generation rate, and temperature and pressure profiles for various reservoir temperatures and well pressures. For instance, a correlation which is valid for 1-D systems was suggested for the natural gas production in gas hydrate reservoirs. Their results showed that a small alteration in temperature cannot be effective in natural gas production[72]. Sean *et al*. [73] combined the numerical simulation outputs obtained from computational fluid dynamic (CFD) and experimental results to develop a method for determination of

the intrinsic rate of gas hydrate decomposition. They showed that the boundary temperature of the methane hydrate is equal to the temperature of the ambient water. Thus, they claimed that the gas hydrate decomposition at the surface can take place at constant temperature conditions [73]. Nazridoust *et al*. [74] carried out a study concerning the hydrate decomposition in a porous medium by employing a computer simulation method. They used FLUENT code to simulate hydrate module for gas hydrate dissociation. Based on their research investigation, it was concluded that the FLUENT code has no capability to simulate the hydrate formation/dissociation. It was also found that the natural gas generation is a function of pressure, core permeability, and temperature. They also noticed that the temperature in the decomposition front declines due to the hydrate decomposition and after that rises because of the heat transfer. Through increasing the system temperature, the gas and water generation rates are increased. Gamwo *et al*. [75] utilized the HydrateResSim package which is a heat-flow, multi-component, and multi-flow simulation program. The model includes the equilibrium and kinetic frameworks to characterize methane generated from the gas hydrate decomposition. The simulation program can be used for four-phase flow and three-component systems to describe the methane production, as well. In addition, Windmeier *et al*. [76] conducted a theoretical study (consecutive desorption, CDM) about gas hydrate dissociation to comprehend the mechanisms of dissociation kinetics and intrinsic gas hydrate dissolution.

2.2.3. Gas Hydrate Reservoirs Production Methods

The production method that includes temperature rising is called “thermal stimulation” and the technique that entails the pressure reduction is called “depressurisation method”, and combination of change in temperature and pressure refers to "chemical injection". Therefore, the operation of the “rising temperature” or “declining pressure” of layers bearing methane hydrate is the practical way of the methane hydrate production. Due to the dependency of hydrate stability on the temperature and pressure in the reservoirs, production methods are strongly affected by the P-T diagram of the reservoirs. Several

conventional methods have been suggested for generation of natural gas from the hydrate reservoirs, including thermal stimulation, depressurisation, gas swapping, or/and a combination of these techniques [10, 77-80]. The alteration of temperature and pressure for three methods is shown in Figure 2-5.

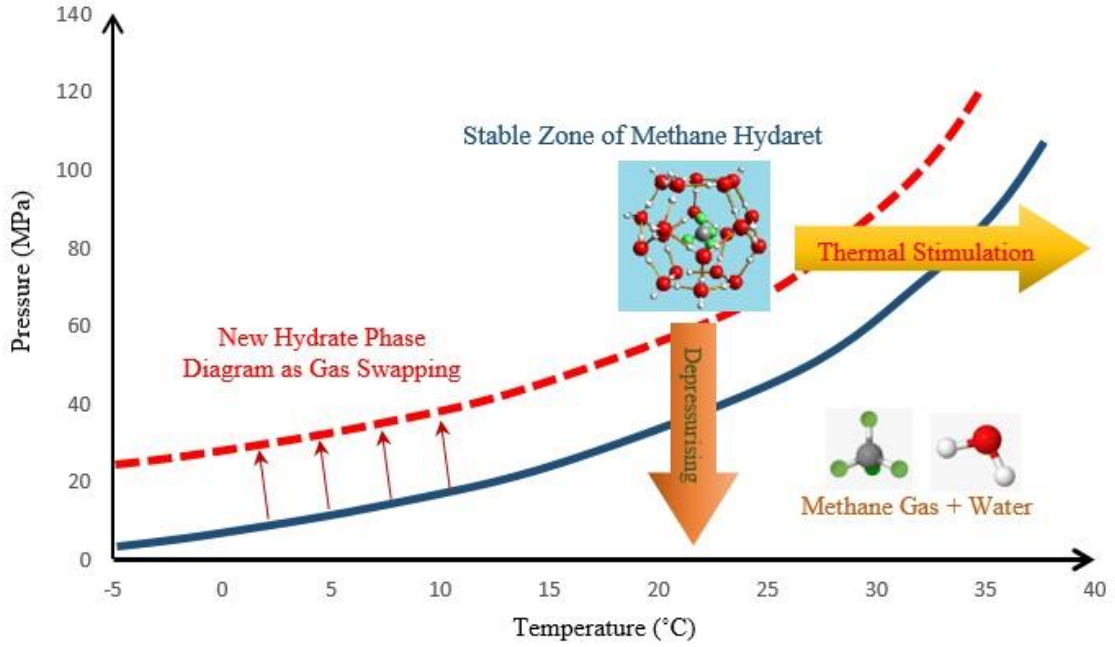

Figure 2-5: Methane hydrate phase diagram.

Commercial gas generation from methane hydrate reservoirs has not been commenced yet; however, a few prosperous flow tests have been conducted in oceanic and arctic environments. The only gas generation test in an oceanic environment is the eastern Nankai Trough case on March 12–18, 2013, as a part of the research in Japan [81]. The most important arctic hydrate generation test was performed at the Mallik site in the Mackenzie Delta, Northwest Territories, Canada, 2002 [82]. Throughout a week, both thermal stimulation and depressurisation methods were employed to produce gas from the hydrates. The most common method of hydrate dissociation is depressurisation. This method first involves lowering the pressure at the prevailing temperature inside the reservoir and facilitating the methane hydrate to be decomposed. In the thermal stimulation approaches, hot water, injected steam or/and a heated liquid (indirectly via sonic or/and electric tools) are used as a source. The other method

is the chemical injection such that the chemicals are utilized to change the natural gas hydrate equilibrium conditions outside the thermodynamic states of hydrate stability zone. There are two different types of inhibitors: thermodynamic and kinetic inhibitors [10]. Thermodynamic inhibitors with strong hydrogen bonding (like ethylene glycol and methanol) shift the equilibrium hydrate stability curve. In addition, the kinetic inhibition is able to alter the hydrate equilibrium within the hydrate stability zone, and small crystals delay the nucleation as well as the growth of gas hydrate [12, 83-85]. There are also newly developed methods such as CO_2 gas exchange through sequestration of CO_2 into NGH-filled sediments [86], use of fluorine gas, and microwave technology [87]. Figure 2-6 depicts three different methods for methane hydrate decomposition [88]. In the first process (a), the pressure is changed by installing a pump. Due to the pressure drop, the hydrate dissociates slowly and the methane is produced. In the second method (b), methane is released from the hydrates when they are induced with a gas. Carbon dioxide displaces the methane in the clathrate cages. The last method (c) is the thermal stimulation which includes injecting hot water into the well, resulting in the methane hydrate production. In the following sections, four hydrate decomposition techniques for natural gas generation are briefly reviewed.

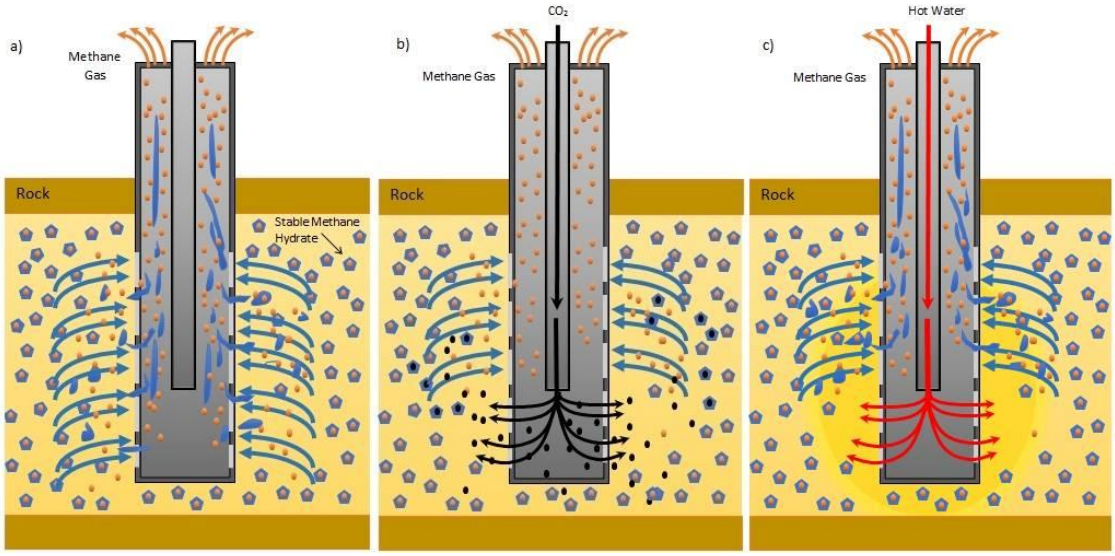

Figure 2-6: Methods of production of hydrate methane. (a): Depressurising, (b): Chemical injection, (c): Thermal stimulation (modified after reference [88]).

Depressurizing: Different mechanisms have been established to provide commercial gas generation from the gas hydrate reservoirs. The only technique that has been successfully used to economically produce gas from the gas hydrates is the depressurisation method. Depressurisation is a gas generation method that decomposes methane hydrate by declining pressure in the wellbore drilled through hydrate-bearing sediments. Past studies indicated that the depressurisation method (where the pressure of the system is decreased below the decomposition pressure at the prevailing temperature) is one of the most promising techniques for hydrate dissociation. Through reducing pressure, methane hydrate becomes thermodynamically unstable and decomposes due to the geothermal heat flow and sensible heat of the sediments. Therefore, depressurisation is likely the first-generation method performed outside the laboratory. The best operating conditions for this method are high temperature, high permeability, and high geothermal heat flux [89, 90]. Verigin *et al*. [91] offered an isothermal depressurisation model for a one-dimensional linear system of gas hydrates in a semi-infinite stratum, where the heat was considered to flow immediately from the environment to the hydrate bulk. Holder *et al*. [92] developed a methane hydrate general depressurisation model in which the heat of decomposition is achieved from the sensible heat of the reservoir itself. They showed that the hydrate gas can be produced around 20 to 30% of the total gas production. Burshears *et al*. [20] modified the previous model [92] to be used for other kinds of gas hydrates. Yousif *et al*. [93, 94] studied a 1-D numerical model to mathematically analyze the decomposition in a sandstone system using the depressurisation method by applying the mass and momentum balance conservation laws for each phase. The numerical and experimental results revealed that the methane gas is produced along with an appreciable amount of water in the hydrate decomposition process within the porous model. Sun *et al*. [95] used an experimental methodology to investigate the impacts of gas composition, porous medium, and additive to obtain adequate knowledge/ understanding of the depressurising dissociation operation. Goel *et al*. [96] modified a model to estimate the efficiency of the hydrate decomposition in a porous medium by using radial diffusivity equation

where the gas mass balance in a gas hydrate well was analytically solved. Based on the depressurisation method, Sung *et al*. [97] utilized a numerical mathematical technique to obtain a 3-D multiphase (e.g., water, gas, and hydrate) system where an implicit pressure- explicit saturation technique was employed. Results of their study demonstrated the effects of the momentum and mass transfer mechanism while increasing permeability. Ji *et al*.[98] presented a parametric sensitivity analysis about the methane production by decreasing well's pressure in the reservoir. The results illustrated that the gas generation rate is dependent on the temperature and pressure of the reservoir, and zone permeability [98]. The depressurising method was also studied by Kono *et al*. [99] to examine the decomposition rate of CH_4 hydrate which was adjusted by controlling the porous sediment parameters. Sun *et al*.[100] also investigated the gas generation from sediments including methane hydrate by depressurisation. They noticed that the laboratory-scale tests were often decomposition controlled, but the field-scale processes were mainly affected by the flow rate and flow regime. They also showed that the rate of gas generation is more susceptible to the surrounding heat transfer coefficient than the longitudinal conduction coefficient. Ruan *et al.* [101] provided a numerical simulation for gas generation in gas hydrate reservoirs by depressurization in the longitudinal and radial directions, they concluded that the gas generation in the longitudinal direction is slower than that in the radial direction. Also, they investigated the effects of permeability, initial hydrate saturation, intrinsic porosity on the gas generation. Oyama *et al*. [102] carried out an experimental and theoretical study and defined a decomposition model as a function of mass transfer and heat transfer rate over the gas generation process. The results showed that the rates of gas generation and decomposition are affected by the production pressure. It was also concluded that one of the most significant factors affecting the dissociation is the heat transfer from the surrounding [102]. In addition, an economical sensitivity study and a simplified analytical method on modelling of gas generation from hydrate by depressurisation have been implemented by Khataniar *et al*. [103]. Increasing the recovery factor is an important goal that needs to be clarified through systematic

experimental and theoretical investigations [104]. Konno *et al*. showed in their latest work that the cyclic depressurisation is a stable heat source methodology driven by the geothermal heat flow. The technique is economically and environmentally sound [104]. A part of related research studies on the depressurisation operation are summarized in Table 2-4 for further information.

Table 2-4: Summary of experimental studies on gas hydrate dissociation by depressurizing.

Researchers	System	Purpose	Pressure (atm)	Temperature (K)
Verigin *et al*. [91]	Natural Gas Hydrate	Introduced an isothermal depressurisation model in a semi-infinite stratum.	Less than 100	263
Holder *et al*. [92]	Methane Hydrate	Presented a methane-hydrate global depressurisation model.	More than 30	295
Burshears *et al*. [20]	Ar, N_2, CO_2 and H_2S Hydrates	Developed Holder model to some another kind of gas hydrates.	40-200	283
Yousif *et al*. [93]	Methane Hydrate	Modified a 1D numerical model to simulate mathematically model in porous media sandstone.	20-35	274
Sung *et al*. [97]	Methane Hydrate	Developed a numerical, 3D and multiphase model by using an implicit pressure explicit saturation technique.	40	280.15
Ji *et al*. [98]	Methane Hydrate	Conducted a parametric study of methane production by depressurizing.	20-160	282
Kono *et al*. [99]	Methane Hydrate	Investigated the rate of CH4 hydrate dissociation by the control of porous sediments properties.	67-135	273.5
Oyama *et al*. [102]	Methane Hydrate	Developed a decomposition model through an experimental study on gas production to elucidate the dissociation characteristics.	103	285.45

Thermal Stimulation: Thermal stimulation is accomplished by increasing temperature above the hydration temperature at an equilibrium condition. In thermal stimulation, the energy usage in the decomposition and generation should not be greater than the energy that can be recovered from the produced gases to meet the economic criteria. Some experimental works on the decomposition behaviour of hydrates by thermal stimulation have been performed [105]. For example, Kawamura *et al*.[106] provided the hydrate decomposition kinetics by dissociating pellet-shaped samples, that mimic naturally happening hydrates in ocean sediments, with a viscous fluid or/and pure water at different temperatures. A high number of thermal stimulation experiments have been employed by adding heated fluids or steam and thus must make up for the intrinsic losses associated with moving heated fluids

through the downhole and overburden to the hydrate residues [107]. Kamata *et al*. [108] studied a dissociation test of methane hydrate sediment by the thermal recovery technology. They showed that pressure and temperature in the sample fluctuate between the stability of methane hydrate and decomposition when the water is at a high temperature [108]. Thermal stimulation is used as the supplementary means for decomposing hydrate by depressurisation because of the limitation of thermal conduction in the porous media [109, 110]. Su *et al*. [110] concluded that the heat may be taken back by the liquids flowing in the well before it reaches the hydrate decomposition front, and then the heat impact is significantly decreased and most heat lost. Hence, the producing plan and synchronic heating are impossible for generating gas from the hydrate residues. Heat is operated along the r-axis direction from the heated well but fluids (e.g., gas and water) flow oppositely when a thermal stimulation is applied for generating gas, synchronously. Liang *et al*. [111] claimed that the gas generation rate boosts up with time until it gains a maximum amount, and afterwards it starts to decline. However, the water generation rate remains approximately constant during the generation process. The hydrate content of the sediment, flow rate, and water injection temperature affect the energy ratio of thermal stimulation generation. Jang and Santamarina [112] have offered a new simulation method for both depressurisation and thermal stimulation production processes in which the volume expansion is incorporated. Considering the gas diffusion and fluid expansion in a pore network modeling method, they showed that the initial hydrate saturation, sediment pore size distribution, and gas expansion factor can play an important role in gas recovery efficiency. It was also found that the gas expansion is a significant factor affecting the in-situ pore pressure. They showed that the simulated gas recovery efficiency is lower for systems with less gas expansion factors, i.e., systems with higher initial pore pressure. Their work showed that the high-volume expansion and thus high recovery efficiency are found in shallow reservoirs with low initial pressures.

Chemical Injection: Depressurization is the most common gas hydrate production method as it appears to be economical. Unlike the inhibitor injection or thermal stimulation, it does not need supplementary costs. Since it takes more time compared to inhibitor injection and thermal stimulation in decomposition, it has a low generation rate, and, therefore a low productivity. It also has been shown that the dissociation is endothermic in this technique. Therefore, there is a chance of gas hydrate reformation while the dissociation reaction occurs [98, 113]. Thermal excitation is more energy efficient than other three methods because the gas hydrates are more sensitive to heat and respond most readily to heat sources. Furthermore, the injected energy can distribute not only across the gas hydrate layer in reservoir but also it can be spread out in the surrounding zones that may not contain gas hydrates [114]. This high amount of energy loss is remarked to be the main weakness of the thermal stimulation technology. The chemical injection method includes injecting inhibitors into the gas hydrates to dissociate hydrates in the reservoir. In general, the common inhibitors are methanol and brine. However, the economic and environmental prospects are their drawbacks to be widely utilized in the real cases [115, 116]. A few reports have been produced about the methane hydrate decomposition in porous media where various chemicals are added. Ngema *et al.* [117] provided a series of hydrate decomposition data for refrigerants and different concentrations of $CaCl_2$, also they offered correlations for gas hydrate decomposition data for mentioned systems. Kamath *et al*. [118] conducted a number of tests examining depressurisation and injection of hot brine solution. Li *et al*. [119] experimentally studied the methane generation treatment from the gas hydrate in a porous system by injecting hot brine with various temperatures and concentrations. They concluded that the generation yield is changed by both concentration and brine temperature. However, the effect of the concentration of the injected brine solution on production efficiently in the porous rocks with different porosities and permeabilities has not been studied yet.

Gas Swapping: The gas swapping method involves injecting another guest molecule into a gas hydrate reservoir for hydrates formation. In the gas replacement, new guest gas molecules take the place of methane molecules in gas hydrates and then release methane as a fluid. CO_2 is often used, but sometimes combination of CO_2 and other compounds are used to encourage the guest gas molecule replacement. The swapping efficiency can become above 60% in the bulk hydrate where the hydrate is surrounded by the gas phase [120]. However, the efficiency desires to decline because of the multi-phase condition and lower permeability in sediments. The CO_2 injection lowers the fugacity of CH_4 in the gas side, which is the consequence of the CH_4 hydrate decomposition. This method combines the benefits of the natural gas hydrate production and the CO_2 sequestration operations. However, the CO_2 hydrate formation is responsible to lower the permeability of the natural gas hydrate sediments. Subsequently, the production rate in this method is very slow [121]. The ConocoPhillips, in a joint program with the U.S. Department of Energy, and the Japan Oil, Gas, and Metals National Corporation performed the first field program designed to study the potential of CO_2−CH_4 displacement in methane hydrate reservoirs in the Prudhoe Bay Unit in the Alaska North Slope on May 5, 2012 [122]. The low permeability of hydrate region could be considered as a principal problem in the chemical injection method, which prevents the diffusion of injected fluids. In addition, retardation of injected chemicals by fluid mixing obstructs the spread of injected chemicals. CO_2 swapping alters the molecular frame. It exchanges the methane molecules with the CO_2 molecules [123]. This is desirable not only because of the potential method to generate gas from the methane hydrates but also as a method that may lead to CO_2 capturing. However, further comprehensive research is needed to confirm that the method is technically and commercially feasible [124].

Table 2-5: Advantages and disadvantages of four types of gas hydrate decompositions.

Method	Advantages	Disadvantages
Depressurizing	No need to input excess energy, Having potential to use in gas hydrate reservoirs with low hydrate saturation, high porosity, and low free gas	Resulting in ground subsidence and submarine landslides, hydrate reformation may occur due to endothermic depressurization, production of water
Thermal Stimulation	Production rate can be controlled by changing the rate of injected heat	Slow production rate, inefficient (high heat losses), Costly
Chemical Injection	Production rate can be improved in a short time period	Not feasible to use in gas hydrate reservoirs with low permeability, environmental issues, costly, thermal adjustment
Gas Swapping	Good strategy for CO_2 capture and sequestration	Not feasible to use in gas hydrate reservoirs with low permeability, environmental issues, costly, slow production rate

Table 2-5 provides the main advantages and disadvantages of all types of gas hydrate production methods. The thermal stimulation integrated with depressurisation appears to be the most viable technique for the marine natural gas hydrate production. To increase the energy efficiency, a number of new methods including chemical oxygen-iodine laser technology [125], down-hole combustion [126], microwave [127], geothermal energy technology [128], and electromagnetic technology [129] have been proposed for the natural gas generation. In summary, each dissociation method has particular merits and drawbacks. Despite being a simple method and offering persistent heat transfer, the heat loss by the thermal stimulation is in the range of 10% to 75% of the injected total energy [64, 111, 114] The main drawback of the thermal stimulation is the heat losses mainly in the permafrost zones. The microwave heating technique, despite its simple running and high heating rate, uses a high extent of electrical power during wave transfer and disregards a high-power magnetron. Although, the depressurization methodology is cheap and does not need a steady dissociation, it is slow in methane production and has a low efficiency. The electromagnetic supply method has high heat efficiency, but

operation of the apparatus in this method is intricate, and a considerable amount of power is required. Despite the small primary energy level, and practical implication, the chemical injection method is costly. It does not have a high production rate, and the equipment corrosion might be experienced in this method. Thus, this approach is not practical for hydrate dissociation in the submarine zones. In summary, none of these methods for natural gas hydrate dissociation are yet commercial in terms of application. Hydrate can be effectively generated if these various techniques are integrated. The combination of the heating and depressurization leads to a better performance. In other words, the methane hydrate is decomposed by the thermal stimulation and free gas is exploited by the depressurization method. Based on the literature review, the combination of three main decomposition methods may be crucial for the long-term gas exploitation, as pure inhibitor methods and/or thermal dissociation methods have relatively limited effectiveness, while they need high costs.

2.3. Molecular Dynamics Simulation

Molecular dynamics (MD) is a computer simulation method which is employed in various engineering and science disciplines to calculate motion and equilibrium of each individual atom or molecule. MD simulations emerged as a powerful and popular gadget to show molecular scale conception of microscopic mechanisms. It helps to attain the knowledge concerning the structural and dynamical properties at the molecular level for a high number of systems, from gas mixtures and simple liquids [130-132] to complex materials such as polymers [133-136], and nanoparticles [137, 138]. The key steps of the complete molecular dynamic are reported in Figure 2-7 [139]. The first step involves computing all atoms coordinates (x). The second step shows the principal calculation loop of a molecular dynamics simulation to determine the force on each atom, which is obtained from the sum of all potentials.

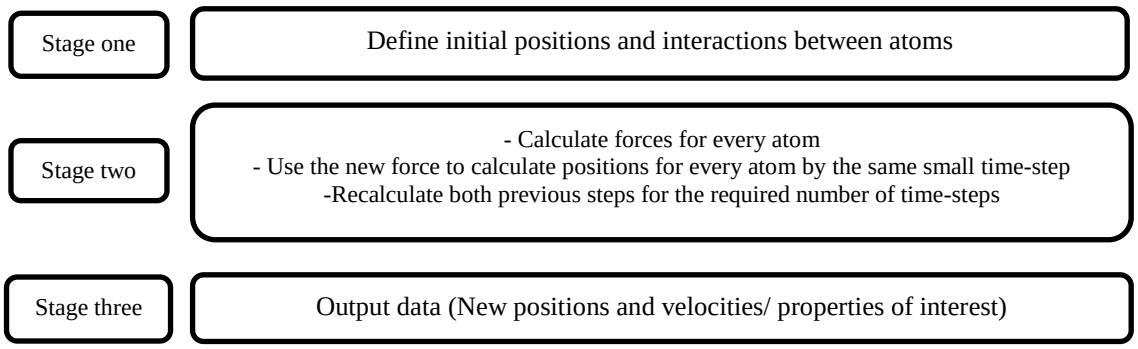

Figure 2-7: Schematic stages of a typical MD simulation (modified after reference [139]).

After that, the forces are used to move each atom forward on time. The forces can be calculated by solving a set of classical equations of motion for all particles in all molecules. In the classical mechanics, the force is defined as follows:

$$F_i = m_i \frac{d^2 r_i}{dt^2} = m_i \frac{dV_i}{dt} = m_i \, a_i \qquad (2\text{-}24)$$

where r_i and F_i stand for the atom position and force acting, respectively. In Equation (2-24), the universal force field includes the intermolecular interactions and interactions between the atoms bonded to each other. Non-bonded interaction contains the van der Waals energy and electrostatic effects. Intermolecular interactions consist of improper dihedral, angle bending, bond stretching, and torsional rotation. Each of them has a functional form as presented below:

$$E = \left(E_W + E_\theta + E_R + E_\phi\right)_{Bonded} + \left(E_{VDW} + E_{el}\right)_{Non-bonded} \qquad (2\text{-}25)$$

There are many algorithms for solving the equation of motion [140-143]. The Verl*et al*gorithm [141] computes the new positions at $t + \Delta t$, using the atom acceleration at time (t) and the position from the prior step, $x(t - \Delta t)$, as written below:

$$x(t + \Delta t) = 2x(t) - x(t - \Delta t) + \frac{d^2 x(t)}{dt^2} \Delta t^2 \qquad (2\text{-}26)$$

Using velocity and position at time zero, we can compute positions and velocities at all other times. In the leapfrog algorithm [144], positions at time (t) and velocities at time $t - (\frac{\Delta t}{2})$ calculate forces, new positions, and velocities through the following relationships:

$$x(t + \Delta t) = x(t) + \frac{dx(t)}{dt}(t + \frac{\Delta t}{2})\Delta t \quad (2\text{-}27)$$

where,

$$\frac{dx(t)}{dt}\left(t + \frac{\Delta t}{2}\right) = \frac{dx(t)}{dt}\left(t - \frac{\Delta t}{2}\right) + \frac{d^2x(t)}{dt^2}\Delta t \quad (2\text{-}28)$$

In the second stage, each iteration is obtained by a classical small time-step($\Delta t = 10^{-15}s$).

The last stage in the algorithm (Figure 2-7) is to generate the outputs. In the output path, the statistical mechanics can be used to calculate different thermodynamical and dynamical properties such as density, viscosity coefficient, mechanical parameters, electrical potentials, and terms of energy [139]. There are various molecular dynamic computer programs which include TINKER [145], NAMD [146], DL_POLY [147], CHARM [148], GROMACS [149], and LAMMPS [150].

There have been some efforts to use molecular dynamics in hydrate dissociation. The next sections discuss the application of the molecular dynamics simulation in hydrate dissociation research area. As there are many constituents in the molecular systems, it is difficult to determine the characteristics of such complex systems mathematically. The molecular dynamic simulations overcome this problem by using certain numerical techniques. However, long MD simulations lead to a difficult problem from a mathematical point of view. For instance, cumulative errors can be generated during the numerical integration. This issue can be addressed by general-purpose minimization algorithms.

2.3.1. Molecular Dynamics Simulation of Hydrate Dissociation

Depressurising and Thermal Stimulation: Dissociation process of gas hydrate with molecular dynamics simulation especially with depressurising and thermal stimulation is briefly described in this section. There are a few reports on the decomposition mechanisms using MD simulation, because it is difficult to perform the dissociation process by decreasing the pressure of hydrate systems. For instance, Báez *et al.* [151] accomplished molecular dynamic simulations of dissolution of hydrate clusters including liquid phases and water molecules composed of pure water and melted hydrate. They prepared a system for 160 picoseconds at 40 bars and 270 K. It was found that the crystal hydrate dissolution is slower than the atomic systems. In the dissociation step, gas molecules move through the liquid to create a gas- rich region. In addition, it was concluded from their study that the cavities are located at the interface release part of their cages in dodecahedral and tetrakaidecahedral. English *et al.* also studied the CO_2 hydrate, and obtained the results similar to the Báez's findings [151]. A detailed fluctuation–dissipation analysis via Onsager's hypothesis for methane hydrate [153], and CO_2 hydrate dissociation [152] was conducted by them, as well. In the case of CO_2 hydrate dissociation, they combined the non-equilibrium molecular dynamics dissociation and non-equilibrium mass-transfer models [152]. Ding *et al.* [154] simulated the decomposition process of structure I methane hydrates at a constant pressure and temperature. They also used SPC and OPLS for water and methane potentials so that the hydrate microstructure was determined by site-by-site radial distribution function (RDF) for oxygen and carbon atoms. NPT MD simulations were performed by the DL- POLY MD software package where temperatures T= 315, 320 and 325 K and pressure P = 30 bar, total simulation time = 500 picoseconds, and time-step = 1 femtosecond. They concluded that the decomposition for guest molecules happens when the diffusion coefficient for water is higher than that for guest molecules in a stable condition of hydrate. They divided hydrate dissociation into two stages so that firstly, the cell size is increased by the diffusion of host molecules and the lattice framework ultimately breaks. In the second step, the

methane molecules exit from the disintegrated hydrate cages [154]. Myshakin *et al.* [155] introduced a thermally induced dissociation technique for the methane hydrate. Undesired effects of super-heating or super-cooling were ignored in their work upon the attendance of a liquid phase at the interface. In the MD simulation runs conducted by the GROMACS package, the methane hydrate-water and hexagonal ice-water models with the COS/G2 force field were used for water. For methane, the five-site nonpolarizable model with partial charges on carbon and hydrogen atoms was used. The NVT model was utilized for simulation of hexagonal ice-water. At the beginning, open cages at the interfaces experienced the decomposition. They reported that molecular dynamic simulations of the dissociation are completed by 85%, 95%, and 100% of primary capacity of the methane cages. The results showed that there is a relationship between the occupancy and hydrate dissociation rate on the cage [156]. Iwai *et al.* [157] studied the decomposition processes of carbon dioxide and methane hydrates. They used the software WinMASPHYCPro2.2 produced by Fujitsu with the following assumptions: alternative boundary condition, controlling temperature by Nose procedure [158], controlling pressure by Parrinello- Rahman procedure [159], 1 fs for each time-step, and half of the primary cell length is equal to the potential cut. Other input data/ conditions were as follows: unit cell consists of 8 guest molecules and 46 water molecules, the pressure is 5.0 MPa, and the equilibrium calculations are obtained at T=270 K and 370 K. They reported that the 5-site (TIP5P) and TraPPE [160] models are accepted by the methane molecules and the carbon dioxide hydrate is less stable than the methane hydrate under the similar conditions. Smirnov *et al.* [161] examined melting of methane hydrate for pressures up to 5000 bar for various water models. The kinetic stability boundary for analogous nucleation is identified by them. They also indicated that the methane hydrate decomposes at low temperatures by lowering the occupancy of cages [161].

Gas Swapping: Widespread attention in recent years has focused on the important prospects of CO_2 storage in clathrate hydrates so that displacing methane by CO_2 in methane hydrate sediments in the permafrost or ocean depths has been suggested by several researchers. However, still there are various technical and operational challenges with the process. For instance, releasing a significant amount of methane into the atmosphere is considered as a serious health and environmental threat. Chatti *et al.* [162] and Komatsu *et al*. [163] offered interesting insights (applying decomposition process in cool storage, refrigeration, transportation, and separation processes) into the CO_2 sequestration in clathrates. Geng *et al.* [164] have performed the molecular dynamics simulation to evaluate the potential of methane reformation while there is a methane replacement in hydrate by carbon dioxide molecules. MD simulations of methane, CO_2 and methane/CO_2 hydrates at 260, 270 and 280 K under 5 MPa were carried out by them. Yan *et al*. [165] also measured the active parameters of CO_2, H_2, and CO_2/H_2 hydrate by MD. Their effort led to defining the most thermodynamically-favoured hydrate that may make CO_2/H_2 syngas in an integrated gasification combined cycle to separate CO_2 from the syngas. They concluded that the formation of the mixed hydrate is thermodynamically conceivable. In another research work, Tung *et al*. [166] explained the process of CH_4 replacement by CO_2 in methane hydrates through employing MD. They used TIP4P-Ew [167] for water, EPM2 [168] for CO_2, and OPLS-AA [169] for methane, as the force field models to determine the interactions in the molecular model. An angular order parameter (AOP) of a water molecule was utilized to identify the hydrate phase molecules, and also to examine the difference between the angles expected in a tetrahedral hydrogen-bonding cages. They showed that the water rigidity increases as AOP lowers. It was also concluded that in regions near the interface, the CO_2 components can be replaced with the methane molecules in about 20 ns. The results indicated that there is not a liquid layer of CO_2 at the interface [166]. Qi *et al*. [170] developed an interfacial molecular dynamic simulation similar to Tung *et al*. [166]. They showed that in CH_4 hydrates, the region adjacent to the interface between the gas phase and hydrate is the most

probable place to replace CO_2 with CH_4. Bai *et al*. [171] worked on microsecond molecular dynamics simulation to figure out the replacement mechanisms of CH_4 by CO_2 in the methane hydrates. The impacts of memory effect, mass transfer limitations, and chemical potentials of guest molecules on this replacement were studied in their work. They concluded that the amorphous layer makes a considerable obstacle to mass transfer of guest molecules in the replacement process. It was also demonstrated that the replacement rate between CO_2 and CH_4 and prevention from further CH_4 decomposition can be decreased due to formation of the amorphous layers.

Chemical Injection: In this section, the previous studies accomplished via molecular dynamics simulations regarding gas hydrate dissociation by thermodynamic inhibitors like inorganic salts are briefly described. For example, Yagasaki *et. al* [172] provided a molecular dynamic simulation of the methane hydrate decomposition by NaCl, the effect of NaCl concentration and temperature in kinetics of hydrate decomposition were studied. Qi *et al*. [173] conducted a MD simulation study for desalination of the electrolyte solutions by hydrate. The simulations results showed that at the pressure greater than that of pure water, one can have a couple of Na^+-Cl^- ions in one cell hydrate. Qi *et al* used TIP4P-4 [167], OPLS [169], and Born-Mayer-Huggins [174] potential models to quantitatively determine water-water, methane-methane, and Na^+-Cl^- interactions, respectively. Tung *et al*. [175] also investigated the hydrate crystal growth in the brine solution of NaCl. Xu *et al*. [176] scrutinized the methane hydrate decomposition process in the brine solution of $CaCl_2$, NaCl, and KCl using molecular dynamics simulation in the Material Studio environment. They considered a two-phase model for the inorganic solution and hydrate system. The lower phase contains of a $\boldsymbol{2 \times 2 \times 3}$-unit cell of methane hydrates including 96 methane molecules and 552 water molecules. Above this phase, there is a brine solution of the inorganic salts (including $\boldsymbol{Na^+}$and $\boldsymbol{Cl^-}$ atoms) with the network size of 2.406 nm × 2.406 nm × 3.609 nm, as demonstrated in Figure 2-8.

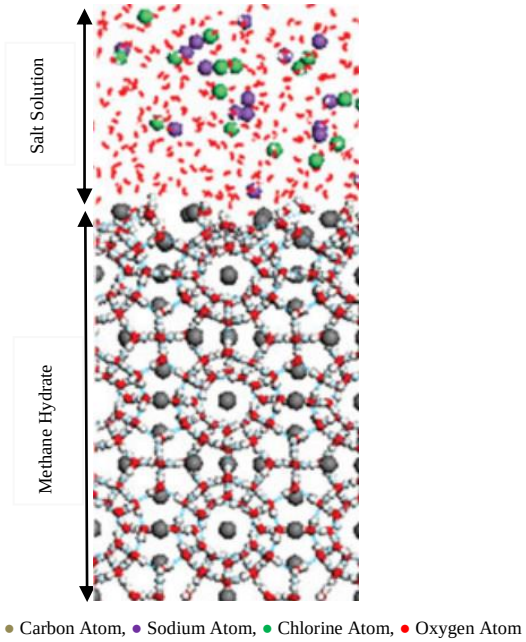

Figure 2-8: Crystal structures of methane hydrate and salt solution [176].

Molecular dynamic simulation was carried out with the NVT group (i.e., numbers of components (N), temperature (T), and volume (V) of the system remain constant) at 273 K and various boundary conditions where the time step was set to be 0.5 fs. They performed simulation runs in two steps. At the first step, the body of hydrate structure was disabled to assoil the excess interfacial tension between the salt solution and hydrate. In the next step, the hydrate structure missed the discriminant layer, and the decomposition simulation was run for 600 ps [176]. Figure 2-9 demonstrates the hydrate dissociation in various salt solutions at 600 ps. The decomposition rate is obtained from the simulation process. The decomposition rate also rises when the amount of salt increases [176]. The hydrogen bonds of water components are the major forces to reinstate the crystalline shape of hydrate [153].

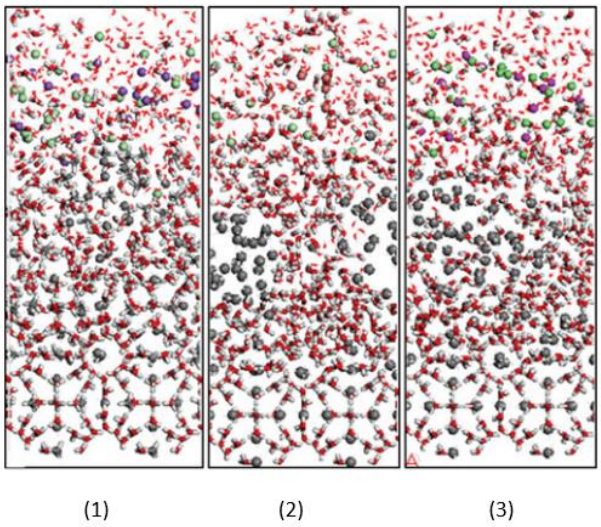

Figure 2-9: Verification of methane hydrate dissociation in various salt solutions [176].

(1- 20% NaCl, 2- 20% KCl 3- 20% $CaCl_2$)

They concluded that the structure of water molecules changes in the presence of inorganic salts so that it helps the hydrate decomposition. Furthermore, the inorganic salt diffusion coefficient decreases by increasing the salt concentration [176].

2.3.2. Potential Functions

To capture the molecular forces and the interaction of water and aqueous solutions, it is vital to conduct fundamental research studies using the molecular dynamics and statistical mechanics simulations. The selection of the water model has an effect on the observed parameters, even when only bulk behaviour is investigated in the absence of interfaces. A crucial decision for computing the potential parameters is to select the values that fit them. The number of the parameters required for this modeling strategy should be low so that the fitting is simplified as much as possible. It should be also large enough to present the resulting potential predictive tools for the other properties. In the case of water, a series of potentials including two positive charges on the hydrogens and a LJ interaction site on the oxygen have been primarily offered. These models involve an alteration in the site of the negative charge, when the

charge is placed on the oxygen for the elongated simple point charge (defined as a SPC potential), as expressed below[177]:

$$u(r_{ij}) = \frac{q_i q_j}{4\pi\varepsilon_0 r_{ij}} + 4\varepsilon\left[\left(\frac{\sigma}{r_{ij}}\right)^{12} + \left(\frac{\sigma}{r_{ij}}\right)^{6}\right] \quad (2\text{-}29)$$

where r_{ij} is the distance between two molecules, q refers to the charge on molecules, ε and σ stand for the Lenard-jones parameters, and ε_0 is the permittivity of free space. When the alter is located on bisector of the H-O-H, the TIP4P model is specified [167] and the electron is "lone pairs" in the TIP5P model [178]. Furthermore, the LJ potential describes the interactions between the water and methane molecules. It is then significant to choose the accurate potential models to compute the potential parameters of water [179]. This is mainly applicable in the case of the most common models, namely TIP4P and SPC. For the methane hydrate, it can be questionable that mostly TIP4P water model along with an ab initio-fitted five-site methane model [180] can be the best for parameters including the melting point and density. The first direct calculation to achieve ice-water interfacial parameters was performed using an improved version of the cleaving methods for the TIP4P model [181, 182]. Davidchack *et al*. [183] conducted calculations which were improved by including the full electrostatic interactions. The values for the TIP4P and TIP5P-E models were also reported at equilibrium (along with argon hydrate) conditions. A comparison between models used in the studies for water, TIP3P, TIP4P, and TIP5P, was made by Vega *et al*. [184], in which TIP5P and TIP4P water were judged to be of a similar quality. TIP3P water performs poorer, but it has the advantage of simplicity and allows thus for larger simulations. Additionally, the TIP3P model is a part of the CHARMM package and is often utilized in simulations of biological systems. Another evaluation of TIP4P, TIP5P, SPC, and SPCE water has led to the conclusion that TIP4P water and SPC water are the best for reproducing experimental values [185]. Chialvo *et al*. [160] used SPC, SPCE, and TIP5P models for water. As a result, all these models led to a similar outcome. Paschek [186] investigated the results of different cases

while employing the TIP4P, TIP5P, and SPC/E models of water. The main conclusion of this project is that the models are not able to calculate the excess chemical potential of methane in water when the temperature is in the range of 270-370 K. Recently, two models have accurately described the density of pure water at this temperature interval. They are the TIP4P/Ew provided by Horn *et al*. [187] and the TIP4P/2005 proposed by Abascal *et al*. [188]. Docherty *et al*. [189] introduced a model which is able to calculate the excess chemical potential of methane in water over a broad range of temperatures. The monomer geometries and parameters for the five potential functions (SPC, TIP3P, BF, TIPS2, and TIP4P) are summarized in Table 2-6.

Table 2-6: Monomer geometry and parameters for potential functions (liquid water at 25˚C and 1 atm)[167].

	SPC	**TIP3P**	**BF**	**TIPS2**	**TIP4P**
r(OH)	1.0	0.975	0.96	0.957	0.957
r(OO)	2.75	2.74	2.72	2.79	2.75
<HOH, deg	109.47	104.52	105.7	104.52	104.52
q(O)	-0.82	-0.834	0	0	0
q(H)	0.41	0.417	0.49	0.535	0.52
$-E_i$ (Kcal/mol)	10.18	9.86	10.49	9.88	10.07

The chemical potential of methane molecule can be achieved by considering all of the hydrogens, as methane is typically the main component of these hydrates.

Beside the LJ potential function, other popular models are the TraPPE (transferable potentials for phase equilibria) [190], OPLS-AA (Optimal Parameterization for the Liquid State) [191], and a united-atom model (UA) [192] as potential functions to calculate the potential parameters for methane. The parameters for both potential functions are tabulated in Table 2-7.

Table 2-7: Parameters for potential functions (methane gas, R = 8.31451 J gmol^{-1} K^{-1}) [195].

Model	**σ/Å**	**(ε/R)/K**	**q/e**	**r_{CH}/ Å**
OPLS-AA C	3..50	33.21	-0.240	1.0947
OPLS-AA H	2.50	15.09	0.060	
UA CH_4	3.73	147.5	0.000	
TraPPE	3.73	148.0	0.000	

The CO_2 hydrates study performed by Radhakrishnan *et al*. [193] focused on free-energy hypersurface as a function of various order parameters of Landau–Ginzburg approach free-energy hyper surface. In this context, the molecular dynamic simulations carried out by Storr *et al*. [35] led to promising new chances for free-energy methods. Also, Qi *et al*. [170] have used OPLS-AA model [191] to determine the inter-molecular interactions between the guest-guest molecules. The interaction between guest monomers is defined by Equation (30) [170]:

$$u_{mn} = \sum_m \sum_n \left(\frac{1}{4\pi\varepsilon_0}\frac{q_i q_j}{r_{ij}} + \frac{\acute{A}_{ij}}{r_{ij}^{12}} - \frac{\acute{B}_{ij}}{r_{ij}^{6}}\right) \quad (2\text{-}30)$$

where $\acute{A}_{ij}$ and $\acute{B}_{ij}$ were the pair-parameters between the host and guest components which are calculated by Equation (31) and Equation (32):

$$\acute{A}_{ij} = \sqrt{\acute{A}_{ii} \times \acute{A}_{jj}} \quad (2\text{-}31)$$

$$\acute{B}_{ij} = \sqrt{\acute{B}_{ii} \times \acute{B}_{jj}} \quad (2\text{-}32)$$

Table 2-8 displays the charge of atoms (q) for carbon dioxide and methane. Comparing Equation (30) and Equation (31), it can be concluded that the site-parameters $\acute{A}_{ij}$ and $\acute{B}_{ij}$ can be determined in terms of the Lennard–Jones parameters ε and σ for each site, $\acute{A}_{ii} = 4\varepsilon_i\sigma_i^{12}$, $\acute{B}_{ii} = 4\varepsilon_i\sigma_i^{6}$, $\acute{A}_{jj} = 4\varepsilon_j\sigma_j^{12}$, and $\acute{B}_{jj} = 4\varepsilon_j\sigma_j^{6}$.

Table 2-8: Atomic charges for OPLS-AA model [170].

Molecule	Atom	q/e
CO_2	C	+0.4578
	O	-0.2289
CH_4	C	-0.3744
	H	+0.0936

The pair-parameters of atoms in the guest molecules are listed in Table 2-9 [170]. The decomposition rate of methane from gas hydrate is dependent on the cage occupancy [194].

It was shown that if the occupancy of hydrate decreases at a constant temperature, the dissociation rate of hydrates will increase over long term methane release.

Table 2-9: Pair-parameters in OPLS-AA model [170].

Atom pair	A (kcal Å^6/mol)	B (kcal Å^6/mol)
C−C	3.248063E+6	1.167984E+3
O−O	3.799967E+5	5.649754E+2
C−O	1.11097E+6	8.123314E+2
C−H	1.967738E+5	2.388105E+2
H−H	1.192093E+4	4.882812E+1
O−H	6.730463E+4	1.660924E+2
C−O(H_2O)	1.083413E+6	7.609159E+2
C−H(H_2O)	1.967738E+5	2.388105E+2
O−H(H_2O)	6.730463E+4	1.660924E+2
O−O(H_2O)	3.705714E+5	5.292160E+2
H−O(H_2O)	6.563523E+4	1.555798E+2
H−H(H_2O)	1.192093E+4	4.882812E+1

It implies that the hydrates networks with full occupancy of the cages (100%) have greater stability compared to the empty cages which are resistant against the dissociation. English [153] also concluded that the rate of hydrate decomposition is not a function of cage occupancy.

2.4. Technical Challenges

Research on new methods and techniques related to hydrate formation, inhibition, and decomposition has been considered in terms of theoretical studies and practical production operations since 1990s. For example, extensive research works have been carried out with focus on different aspects of gas hydrate simulation (e.g., nucleation, growth, formation, and decomposition) through using molecular dynamics simulation to calculate the important parameters attributed to the hydrate geology and hydrate geochemistry.

The previous studies clearly convey the message that a comprehensive study through employing strong modeling tools such as molecular dynamics simulation strategy is required to capture the important aspects of hydrates such as disassociation mechanisms, thermodynamic behaviours, and hydrate kinetics to remove the inherent limitations of previous models.

To the best of our knowledge, there are no systematic research works in the open sources that deal with molecular dynamic simulations to forecast the behavior of water/gas/hydrate systems over hydrate formation and dissociation phenomena at various thermodynamic and process conditions. In addition, MD simulations of three methods addressed in this manuscript for gas production have not been conducted at the same operational conditions, implying an appropriate comparison between the simulation methods is not possible. The above shortcomings increase motivations of our research team to focus on this topic where development and utilization of new and powerful tools/models such as EOSs, transport phenomena models, optimization strategies, and molecular dynamics simulations are targeted. The current challenges are clearly highlighted in various sections of this study.

2.5. Future Research Guidelines and Conclusions

A large amount of methane is stored in gas hydrate reserves around the world, nearly 10^{17} cubic meters. Due to this potential energy source and the massive extent of gas hydrates, the hydrates have attracted a great attention from governments and scientists. This study provides an overview of the research works conducted on the decomposition of methane hydrate gas reservoirs. Although, a considerable progress has been made in this area, the dissociation mechanisms of gas hydrates have not been adequately understood yet. For instance, the relationship between the crystal type and decomposition behaviours of clathrate hydrates is still indistinct. The main conclusions of this review manuscript are as follows:

1. There are a few studies about the hydrate formation and decomposition of methane hydrate at the microscopic level. Considering various uses for gas hydrates, further experimental and theoretical investigations should be conducted in this field so that more accurate and cost-effective techniques are developed.
2. An appropriate gas reservoir simulation should be able to identify the key characteristics of gas reservoirs, to predict the future of reservoir production, and to develop effective hydrocarbon withdrawal plans. Therefore, a systematic/comprehensive simulation and modeling strategy for investigation of gas hydrate production mechanisms seems inevitable.
3. One of the main challenges in the area of gas hydrates is how to accurately model the behaviours of brine/gas/hydrates where the permeability, porosity, and temperature of underground formations hold high values. In addition, the free gas layer and intermediate zones in gas hydrate reserves require further experimental and theoretical studies at micro to macro scales. Despite of various engineering and research works on the gas hydrate formation and dissociation reported in the literature, comprehensive and precise models (e.g., for prediction of thermo-

physical properties, reaction kinetics, and production rate) for natural gas hydrate reservoir cases should be developed through using real data and theoretical information.

4. With the aid of MD simulation, it is feasible to determine the geometric parameters of gas hydrate molecules, to explore the interfacial phenomena of various water/gas/hydrate/porous medium systems, and to obtain electromagnetic fields for the hydrate cages and potential functions for methane, water, and carbon dioxide over the hydrate formation and gas production processes in gas hydrate reservoirs. In addition, it is important to explore new features of hydrate cages and their impact on decomposition rate, and combination of two or three practical methods for hydrate decomposition using MD in order to choose an effective production approach.
5. The interface between the liquid water and methane hydrate during methane hydrate decomposition can be systematically explored by a new powerful approach, called molecular dynamics simulations. New potential functions are substantial to investigate the detailed molecular nature and to figure out the mechanisms of hydrate decomposition.

Acknowledgements

The authors would like to thank the Natural Sciences and Engineering Research Council of Canada (NSERC); Research & Development Corporation of Newfoundland and Labrador (RDC), funding no. 210992; and Statoil Canada Ltd., funding no. 211162 for providing financial support to accomplish this research under Statoil Chair in Reservoir Engineering at the Memorial University of Newfoundland, St. John's, NL, Canada.

Nomenclatures

A Component-specific constants in the Antonine equation

B Component-specific constants in the Antonine equation

$\acute{A}$ Pair-parameters between host and guest components

$\acute{B}$	Pair-parameters between host and guest components	
C	Concentration of methane	$\mathrm{mol/m^3}$
C_B	Concentration of methane in bulk gas phase	$\mathrm{mol/m^3}$
C_H	Concentration of methane in hydrate	$\mathrm{mol/m^3}$
C_p	Effective heat capacity	$\mathrm{J/kg.\,K}$
C_{p_g}	Gas heat capacity	$\mathrm{J/kg.\,K}$
D	Diffusion coefficient	$\mathrm{m^2/s}$
E	Potential function	J/mol
E_W	Improper dihedrals potential	J/mol
E_θ	Angle bending potential	J/mol
E_R	Bonding stretching potential	J/mol
E_ϕ	Torsional rotation potential	J/mol
E_{VDV}	van der Waals potential	J/mol
E_{el}	Electrostatic potential	J/mol
F_i	Force action	N
$G(t)$	Cumulative gas produced	$\mathrm{m^3}$
k	Effective thermal conductivity	$\mathrm{J/s.\,m.\,K}$
Mw	Gas molecular mass	kg/kgmol
P	Gas pressure	Pa
P_0	Pressure at $x = 0$	Pa
P_D	Dissociation pressure	Pa
$q(x,t)$	Heat flux	$\mathrm{J/s.\,m^2}$
q	Electrostatic charge of atoms	e
$T(x,t)$	Temperature	K
T_0	Temperature at $x = 0$	K
T_D	Dissociation temperature	K
T_I	Initial temperature	K

t	Time	s
v_x	Superficial gas velocity	m/s
x	Axial position	m

Greek letters

α	Effective thermal diffusivity	m^2/s
β	Coefficient of thermal expansion of gas	K^{-1}
ΔH_D	Hydrate heat of dissociation	J/kg
ϕ	Porosity	
η	Similarity variable	
κ	Permeability	m^2
σ	Lennard–Jones parameters	m
ε	Lennard–Jones parameters	J/mol
ε_0	Permittivity	F/m
μ	Gas viscosity	$Pa.s$
ξ	Constant in diffusion calculation	
ζ	Constant in diffusion calculation	
ρ	Effective density	kg/m^3
ρ_g	Gas density	kg/m^3
ρ_H	Hydrate density	kg/m^3
ω	Mass of gas produced per unit mass of hydrate	

Subscripts

I	Dissociated zone
II	Hydrate zone
D	Dissociation
g	Gas
H	Hydrate

i	Initial condition
0	Boundary condition at $x = 0$

Abbreviations

AOP	Angular Order Parameter
BF	Bernal-Fowler Potential Function
BSR	Bottom-Simulating Reflector
CDM	Consecutive Desorption Method
CFD	Computational Fluid Dynamic
EOS	Equation of State
GtC	Giga Tones Carbon
MD	Molecular Dynamic
NGH	Natural Gas Hydrate
$OPLS - AA$	Optimal Parameterization for the Liquid State
SEM	Scanning Electron Microscopy
TEM	Transmission Electron Microscopy
$TRAPPE$	Transferable Potentials for Phase Equilibria
$TIP3P$	Transferable Intermolecular Potential with 3 Points
$TIP4P$	Transferable Intermolecular Potential with 4 Points
UA	United- Atom Model

References

[1] E. Hammerschmidt, Formation of gas hydrates in natural gas transmission lines, Industrial & Engineering Chemistry, 26 (1934) 851-855.

[2] M. Wu, S. Wang, H. Liu, A study on inhibitors for the prevention of hydrate formation in gas transmission pipeline, Journal of Natural Gas Chemistry, 16 (2007) 81-85.

[3] Z. Huo, E. Freer, M. Lamar, B. Sannigrahi, D. Knauss, E. Sloan, Hydrate plug prevention by anti-agglomeration, Chemical Engineering Science, 56 (2001) 4979-4991.

[4] Y. Seo, S.-P. Kang, Inhibition of methane hydrate re-formation in offshore pipelines with a kinetic hydrate inhibitor, Journal of Petroleum Science and Engineering, 88 (2012) 61-66.

[5] J.D. Lee, P. Englezos, Unusual kinetic inhibitor effects on gas hydrate formation, Chemical engineering science, 61 (2006) 1368-1376.

[6] R.A. Fair, Hydrate prevention in-gas production, in: Google Patents, 1967.

[7] O. Urdahl, K. Kinnari, R. Holme, Operational experience by apply-ing direct electrical heating for hydrate prevention, in: Offshore TechnologyConference, 2003.

[8] C. Gengliang, Formation and prevention of hydrate during process of gas exploitation and transmission, Natural Gas Industry, 24 (2004) 89-91.

[9] T.S. Collett, A.H. Johnson, C.C. Knapp, R. Boswell, Natural gas hydrates: a review, (2009).

[10] E.D. Sloan Jr, C. Koh, Clathrate hydrates of natural gases, CRC press, 2007.

[11] E.D. Sloan, Fundamental principles and applications of natural gas hydrates, Nature, 426 (2003) 353-363.

[12] E.D. Sloan, Gas hydrates: review of physical/chemical properties, Energy & Fuels, 12 (1998) 191-196.

[13] L. Pauling, R.E. Marsh, The structure of chlorine hydrate, Proceedings of the National Academy of Sciences, 38 (1952) 112-118.

[14] W. Claussen, A second water structure for inert gas hydrates, The Journal of Chemical Physics, 19 (1951) 1425-1426.

[15] J.A. Ripmeester, J.S. Tse, C.I. Ratcliffe, B.M. Powell, A new clathrate hydrate structure, Nature, 325 (1987) 135-136.

[16] A. Khan, Stabilization of hydrate structure H by N2 and CH4 molecules in 435663 and 512 cavities, and fused structure formation with 51268 cage: a theoretical study, The Journal of Physical Chemistry A, 105 (2001) 7429-7434.

[17] B.H. Wu, Measurement and prediction of gas hydrate equilibrium conditionin the presence of inhibitors, in: Chemical and Biological Engineering, TheUniversity of British Columbia, 1994.

[18] W. Shin, S. Park, H. Ro, D.-Y. Koh, J. Seol, H. Lee, Phase equilibrium measurements and the tuning behavior of new sII clathrate hydrates, The Journal of Chemical Thermodynamics, 44 (2012) 20-25.

[19] K. Kvenvolden, A primer on the geological occurrence of gas hydrate, Geological Society, London, Special Publications, 137 (1998) 9-30.

[20] M. Burshears, T. O'brien, R. Malone, A multi-phase, multi-dimensional, variable composition simulation of gas production from a conventional gas reservoir in contact with hydrates, in: SPE Unconventional Gas Technology Symposium, Society of Petroleum Engineers, 1986.

[21] A. Demirbas, Methane hydrates as potential energy resource: Part 2–Methane production processes from gas hydrates, Energy Conversion and Management, 51 (2010) 1562-1571.

[22] M. Kurihara, A. Sato, H. Ouchi, H. Narita, Y. Masuda, T. Saeki, T. Fujii, Prediction of gas productivity from eastern Nankai Trough methane hydrate reservoirs, in: Offshore Technology Conference, Offshore Technology Conference, 2008.

[23] G. Moridis, Numerical studies of gas production from methane hydrates, in: SPE Gas Technology Symposium, Society of Petroleum Engineers, 2002.

[24] Y. Liu, M. Strumendo, H. Arastoopour, Simulation of methane production from hydrates by depressurization and thermal stimulation, Industrial & Engineering Chemistry Research, 48 (2008) 2451-2464.

[25] H. Kakati, A. Mandal, S. Laik, Phase Stability and Kinetics of CH4 + CO2 + N2 Hydrates in Synthetic Seawater and Aqueous Electrolyte Solutions of NaCl and CaCl2, Journal of Chemical & Engineering Data, 60 (2015) 1835-1843.

[26] J. Kondori, J. Javanmardi, A. Eslamimanesh, A.H. Mohammadi, Thermodynamic consistency test for isobaric experimental data of water content of methane, Fluid Phase Equilibria, 347 (2013) 54-61.

[27] V.K. Saw, I. Ahmad, A. Mandal, G. Udayabhanu, S. Laik, Methane hydrate formation and dissociation in synthetic seawater, Journal of Natural Gas Chemistry, 21 (2012) 625-632.

[28] K. Nazari, M.R. Moradi, A.N. Ahmadi, Kinetic Modeling of Methane Hydrate Formation in the Presence of Low-Dosage Water-Soluble Ionic Liquids, Chemical Engineering & Technology, 36 (2013) 1915-1923.

[29] V.K. Saw, M. Gudala, G. Udayabhanu, A. Mandal, S. Laik, Kinetics of methane hydrate formation and its dissociation in presence of non-ionic surfactant Tergitol, Journal of Unconventional Oil and Gas Resources, 6 (2014) 54-59.

[30] P.T. Ngema, P. Naidoo, A.H. Mohammadi, D. Richon, D. Ramjugernath, Thermodynamic stability conditions of clathrate hydrates for refrigerant (R134a or R410a or R507) with MgCl2 aqueous solution, Fluid Phase Equilibria, 413 (2016) 92-98.

[31] V.K. Saw, G.N. Udayabhanu, A. Mandal, S. Laik, Methane Hydrate Formation and Dissociation in the presence of Bentonite Clay Suspension, Chemical Engineering & Technology, 36 (2013) 810-818.

[32] C. Moon, P.C. Taylor, P.M. Rodger, Molecular dynamics study of gas hydrate formation, Journal of the American Chemical Society, 125 (2003) 4706-4707.

[33] J. Zhang, R. Hawtin, Y. Yang, E. Nakagava, M. Rivero, S. Choi, P.M. Rodger, Molecular dynamics study of methane hydrate formation at a water/methane interface, The Journal of Physical Chemistry B, 112 (2008) 10608-10618.

[34] E. Freer, E. Sloan, An engineering approach to kinetic inhibitor design using molecular dynamics simulations, Annals of the New York Academy of Sciences, 912 (2000) 651-657.

[35] M.T. Storr, P.C. Taylor, J.-P. Monfort, P.M. Rodger, Kinetic inhibitor of hydrate crystallization, Journal of the American Chemical Society, 126 (2004) 1569-1576.

[36] Y.F. Makogon, S.A. Holditch, T.Y. Makogon, Natural gas-hydrates — A potential energy source for the 21st Century, Journal of Petroleum Science and Engineering, 56 (2007) 14-31.

[37] J.S. Gudmundsson, M. Parlaktuna, A.A. Khokhar, Storage of Natural Gas as Frozen Hydrate.

[38] R. Masoudi, B. Tohidi, Gas hydrate production technology for natural gas storage and transportation and CO2 sequestration, in: SPE Middle East Oil and Gas Show and Conference, Society of Petroleum Engineers, 2005.

[39] W.S. Holbrook, H. Hoskins, W.T. Wood, R.A. Stephen, D. Lizarralde, Methane Hydrate and Free Gas on the Blake Ridge from Vertical Seismic Profiling, Science, 273 (1996) 1840-1843.

[40] C. Pierre, J.M. Rouchy, A. Gaudichet, Diagenesis in the gas hydrate sediments of the Blake Ridge: mineralogy and stable isotope compositions of the carbonate and sulfide minerals, in: Proc Ocean Drilling Program Sci Results, 2000, pp. 139-146.

[41] C.K. Paull, R. Matsumoto, P.J. Wallace, N.R. Black, W.S. Borowski, T.S. Collett, J.E. Damuth, G.R. Dickens, P.K. Egeberg, K. Goodman, R.F. Hesse, Y. Hiroki, S.W. Holbrook, H. Hoskins, J. Ladd, E. Lodolo, T.D. Loreson, R.J. Musgrave, T. Nahr, H. Okada, C. Pierre, C. Ruppel, M. Satoh, R. Thiery, Y. Watanabe, H. Wehner, W.J. Winters, W.T. Wood, Proc. Ocean Drill. Program: Initial Rep., 164 (1996) 99.

[42] P.G. Brewer, F.M. Orr Jr, G. Friederich, K.A. Kvenvolden, D.L. Orange, Gas hydrate formation in the deep sea: In situ experiments with controlled release of methane, natural gas, and carbon dioxide, Energy and Fuels, 12 (1998) 183-188.

[43] E. Pinero, M. Marquardt, C. Hensen, M. Haeckel, K. Wallmann, Estimation of the global inventory of methane hydrates in marine sediments using transfer functions, Biogeosciences, 10 (2013) 959-975.

[44] V.M. Dobrynin, Y.P. Korotajev, D.V. Plyuschev, Gas hydrates-one of the possible energy sources, in: Long-Term Energy Resources, edited by: Meyer, R. G. and Olson, Pitman, Boston, MA, (1981) 727–729.

[45] Y. Makogon, Perspectives of development of gas hydrate accumulations, Gasovaya Promyshlennost, 3 (1981) 16-18.

[46] L. Harvey, Z. Huang, Evaluation of the potential impact of methane clathrate destabilization on future global warming, Journal of Geophysical Research: Atmospheres, 100 (1995) 2905-2926.

[47] W. Holbrook, H. Hoskins, W. Wood, Methane hydrate and free gas on the Blake Ridge from vertical seismic profiling, Oceanographic Literature Review, 4 (1997) 337-338.

[48] A.H. Johnson, GLOBAL RESOURCE POTENTIAL OF GAS HYDRATE–ANew CALCULATION, Natural Gas & Oil, 304 (2011) 285-4541.

[49] Y. Makogon, Special characteristics of the natural gas hydrate fields exploration in the zone of hydrate formation, TsNTI MINGASPROMa, Moscow, 17 (1966).

[50] K.A. Kvenvolden, Potential effects of gas hydrate on human welfare, Proceedings of the National Academy of Sciences, 96 (1999) 3420-3426.

[51] W.T. Wood, J.F. Gettrust, N.R. Chapman, G.D. Spence, R.D. Hyndman, Decreased stability of methane hydrates in marine sediments owing to phase-boundary roughness, Nature, 420 (2002) 656-660.

[52] R. Hesse, Pore water anomalies of submarine gas-hydrate zones as tool to assess hydrate abundance and distribution in the subsurface: What have we learned in the past decade?, Earth-Science Reviews, 61 (2003) 149-179.

[53] K.C. Hester, P.G. Brewer, Clathrate hydrates in nature, Annual review of marine science, 1 (2009) 303-327.

[54] G. Moridis, T. Collett, Strategies for gas production from hydrate accumulations under various geologic conditions, Lawrence Berkeley National Laboratory, (2003).

[55] M. Kurihara, H. Ouchi, H. Narita, Y. Masuda, Gas production from methane hydrate reservoirs, in: Proceedings of the 7th International Conference on Gas Hydrates (ICGH), Edinburgh, UK, 2011.

[56] S. Gerami, M. Pooladi-Darvish, Material balance and boundary-dominated flow models for hydrate-capped gas reservoirs, in: SPE Annual Technical Conference and Exhibition, Society of Petroleum Engineers, 2006.

[57] G.J. Moridis, Toward production from gas hydrates: current status, assessment of resources, and simulation-based evaluation of technology and potential, Lawrence Berkeley National Laboratory, (2008).

[58] G.J. Moridis, M.T. Reagan, Gas production from class 2 hydrate accumulations in the permafrost, in: SPE Annual Technical Conference and Exhibition, Society of Petroleum Engineers, 2007.

[59] M. Kurihara, H. Ouchi, T. Inoue, T. Yonezawa, Y. Masuda, S. Dallimore, T. Collett, Analysis of the JAPEX/JNOC/GSC et al. Mallik 5L-38 gas hydrate thermal-production test through numerical simulation, BULLETIN-GEOLOGICAL SURVEY OF CANADA, 585 (2005) 139.

[60] H. Hong, M. Pooladi-Darvish, P.R. Bishnoi, Analytical Modelling of Gas Production From Hydrates in Porous Media, (2003).

[61] Z. Yin, Z.R. Chong, H.K. Tan, P. Linga, Review of gas hydrate dissociation kinetic models for energy recovery, Journal of Natural Gas Science and Engineering, (2016).

[62] J.W. Ullerich, M.S. Selim, E.D. Sloan, THEORY AND MEASUREMENT OF HYDRATE DISSOCIATION, AIChE Journal, 33 (1987) 747-752.

[63] H.C. Kim, P.R. Bishnoi, R.A. Heidemann, S.S.H. Rizvi, Kinetics of methane hydrate decomposition, Chemical Engineering Science, 42 (1987) 1645-1653.

[64] M.S. Selim, E.D. Sloan, Heat and mass transfer during the dissociation of hydrates in porous media, AIChE Journal, 35 (1989) 1049-1052.

[65] A.K.M. Jamaluddin, N. Kalogerakis, P.R. Bishnoi, Modelling of decomposition of a synthetic core of methane gas hydrate by coupling intrinsic kinetics with heat transfer rates, Canadian Journal of Chemical Engineering, 67 (1989) 948-954.

[66] G.G. Tsypkin, A mathematical model of dissociation for gas hydrates coexisting with ice in natural strata, Izvestiya Akademii Nauk. Mekhanika Zhidkosti I Gaza, (1993) 84-92.

[67] D. Khairkhah, M. Pooladi-Darvish, P. Bishnoi, T. Collett, S. Dallimore, Production potential of the Mallik field reservoir, BULLETIN-GEOLOGICAL SURVEY OF CANADA, (1999) 377-390.

[68] Y. Masuda, Y. Fujinaga, S. Naganawa, K. Fujita, K. Sato, Y. Hayashi, Modelling and experimental studies on dissociation of methane gas hydrates in Berea sandstone cores; presented at 3rd International Conference on Gas Hydrates, July 18-22, Salt Lake City, Utah, (1999).

[69] M.A. Clarke, P.R. Bishnoi, Measuring and modelling the rate of decomposition of gas hydrates formed from mixtures of methane and ethane, Chemical Engineering Science, 56 (2001) 4715-4724.

[70] G.J. Moridis, Numerical Studies of Gas Production from Methane Hydrates, SPE J., 8 (2003) 359.

[71] T. Komai, S.P. Kang, J.H. Yoon, Y. Yamamoto, T. Kawamura, M. Ohtake, In situ Raman spectroscopy investigation of the dissociation of methane hydrate at temperatures just below the ice point, J. Phys. Chem. B, 108 (2004) 8062.

[72] G. Ahmadi, C. Ji, D.H. Smith, Numerical solution for natural gas production from methane hydrate dissociation, Journal of Petroleum Science and Engineering, 41 (2004) 269-285.

[73] W.-Y. Sean, T. Sato, A. Yamasaki, F. Kiyono, CFD and experimental study on methane hydrate dissociation Part I. Dissociation under water flow, AIChE Journal, 53 (2007) 262-274.

[74] K. Nazridoust, G. Ahmadi, Computational modeling of methane hydrate dissociation in a sandstone core, Chemical Engineering Science, 62 (2007) 6155-6177.

[75] I.K. Gamwo, Y. Liu, Mathematical Modeling and Numerical Simulation of Methane Production in a Hydrate Reservoir, Industrial & Engineering Chemistry Research, 49 (2010) 5231-5245.

[76] C. Windmeier, L.R. Oellrich, Theoretical study of gas hydrate decomposition kinetics - Model development, Journal of Physical Chemistry A, 117 (2013) 10151-10161.

[77] T. Collett, J.-J. Bahk, R. Baker, R. Boswell, D. Divins, M. Frye, D. Goldberg, J. Husebø, C. Koh, M. Malone, M. Morell, G. Myers, C. Shipp, M. Torres, Methane Hydrates in Nature—Current Knowledge and Challenges, Journal of Chemical & Engineering Data, 60 (2015) 319-329.

[78] P. Englezos, Clathrate hydrates, Ind. Eng. Chem. Res., 32 (1993) 1251-1274.

[79] Y.F. Makogon, Hydrates of Natural Gas, Pennwell Books, 1981.

[80] A.K. Sum, C.A. Koh, E.D. Sloan, Clathrate Hydrates: From Laboratory Science to Engineering Practice, Industrial & Engineering Chemistry Research, 48 (2009) 7457-7465.

[81] OGMEC. News Releases 2012, March 19., in, <https://www.jogmec.go.jp/english/news/release /news_01_000006. html>.

[82] S.R. Dallimore, T.S. Collett, T. Uchida, Summary of Mallik 21[ndash]38 Well, GSC Bull., 544 (1999) 1-10.

[83] C.A. Koh, R.E. Westacott, W. Zhang, K. Hirachand, J.L. Creek, A.K. Soper, Mechanisms of gas hydrate formation and inhibition, Fluid Phase Equilibria, 194–197 (2002) 143-151.

[84] J.P. Lederhos, J.P. Long, A. Sum, R.L. Christiansen, E.D. Sloan, Effective kinetic inhibitors for natural gas hydrates, Chemical Engineering Science, 51 (1996) 1221-1229.

[85] P.K. Notz, S.B. Bumgardner, B.D. Schaneman, J.L. Todd, Application of Kinetic Inhibitors to Gas Hydrate Problems, (1996).

[86] A. Graue, B. Kvamme, B. Baldwin, J. Stevens, J.J. Howard, E. Aspenes, G. Ersland, J. Husebo, D. Zornes, MRI visualization of spontaneous methane production from hydrates in sandstone core plugs when exposed to CO2, SPE Journal, 13 (2008) 146-152.

[87] A. Arora, S.S. Cameotra, C. Balomajumder, Techniques for Exploitation of Gas Hydrate (Clathrates) an Untapped Resource of Methane Gas, Journal of Microbial & Biochemical Technology, 2015 (2015).

[88] Marine Resources – Opportunities and Risks, in, 2014.

[89] Y. Konno, Y. Masuda, Y. Hariguchi, M. Kurihara, H. Ouchi, Key Factors for Depressurization-Induced Gas Production from Oceanic Methane Hydrates, Energy & Fuels, 24 (2010) 1736-1744.

[90] Y. Konno, Y. Jin, K. Shinjou, J. Nagao, Experimental evaluation of the gas recovery factor of methane hydrate in sandy sediment, RSC Advances, 4 (2014) 51666-51675.

[91] N. Verigin, I. Khabibullin, G. Khalikov, Linear problem of the dissociation of the hydrates of a gas in a porous medium, Fluid Dynamics, 15 (1980) 144-147.

[92] G.D. Holder, P.F. Angert, Simulation of gas production from a reservoir containing both gas hydrates and free natural gas, in: SPE annual technical conference and exhibition, Society of Petroleum Engineers, 1982.

[93] M.H. Yousif, H.H. Abass, M.S. Selim, E.D. Sloan, Experimental and theoretical investigation of methane-gas-hydrate dissociation in porous media, SPE Reserv. Eng., (1991) 69-76.

[94] M.H. Yousif, B.P. Research, E.D. Sloan, Experimental Investigation of Hydrate Formation and Dissociation in Consolidated Porous Media, SPE Reserv. Eng., 6 (1991) 452.

[95] C.Y. Sun, G.J. Chen, Methane hydrate dissociation above 0 °c and below 0°C, Fluid Phase Equilibria, 242 (2006) 123-128.

[96] N. Goel, M. Wiggins, S. Shah, Analytical modeling of gas recovery from in situ hydrates dissociation, Journal of Petroleum Science and Engineering, 29 (2001) 115-127.

[97] W.-M. Sung, D.-G. Huh, B.-J. Ryu, H.-S. Lee, Development and application of gas hydrate reservoir simulator based on depressurizing mechanism, Korean Journal of Chemical Engineering, 17 (2000) 344-350.

[98] C. Ji, G. Ahmadi, D.H. Smith, Natural gas production from hydrate decomposition by depressurization, Chemical Engineering Science, 56 (2001) 5801-5814.

[99] H.O. Kono, S. Narasimhan, F. Song, D.H. Smith, Synthesis of methane gas hydrate in porous sediments and its dissociation by depressurizing, Powder Technology, 122 (2002) 239-246.

[100] X. Sun, N. Nanchary, K. Mohanty, 1-D modeling of hydrate depressurization in porous media, Transport in Porous Media, 58 (2005) 315-338.

[101] X. Ruan, Y. Song, H. Liang, M. Yang, B. Dou, Numerical Simulation of the Gas Production Behavior of Hydrate Dissociation by Depressurization in Hydrate-Bearing Porous Medium, Energy & Fuels, 26 (2012) 1681-1694.

[102] H. Oyama, Y. Konno, Y. Masuda, H. Narita, Dependence of depressurization-induced dissociation of methane hydrate bearing laboratory cores on heat transfer, Energy & Fuels, 23 (2009) 4995-5002.

[103] S. Khataniar, V.A. Kamath, S.D. Omenihu, S.L. Patil, A.Y. Dandekar, Modelling and economic analysis of gas production from hydrates by depressurization method, The Canadian Journal of Chemical Engineering, 80 (2002) 135-143.

[104] Y. Konno, Y. Masuda, K. Akamine, M. Naiki, J. Nagao, Sustainable gas production from methane hydrate reservoirs by the cyclic depressurization method, Energy Conversion and Management, 108 (2016) 439-445.

[105] J.Y. Lee, B.J. Ryu, T.S. Yun, J. Lee, G.-C. Cho, Review on the gas hydrate development and production as a new energy resource, KSCE Journal of Civil Engineering, 15 (2011) 689-696.

[106] T. Kawamura, K. Ohga, K. Higuchi, J. Yoon, Y. Yamamoto, T. Komai, H. Haneda, Dissociation behavior of pellet-shaped methane-ethane mixed gas hydrate samples, Energy & fuels, 17 (2003) 614-618.

[107] W. Pang, W. Xu, C. Sun, C. Zhang, G. Chen, Methane hydrate dissociation experiment in a middle-sized quiescent reactor using thermal method, Fuel, 88 (2009) 497.

[108] Y. Kamata, T. Ebinuma, R. Omura, H. Minagawa, H. Narita, Y. Masuda, Y. Konno, Decomposition experiment of methane hydrate sediment by thermal recovery method, in: Proceedings of the 5th International Conference on Gas Hydrates, 2005, pp. 81-85.

[109] G.J. Moridis, M.T. Reagan, S.J. Kim, Y. Seol, K. Zhang, Evaluation of the gas production potential of marine hydrate deposits in the Ulleung basin of the Korean East Sea, SPE Journal, 14 (2009) 759-781.

[110] Z. Su, Y. Cao, N. Wu, Y. He, Numerical analysis on gas production efficiency from hydrate deposits by thermal stimulation: Application to the Shenhu Area, south China sea, Energies, 4 (2011) 294-313.

[111] L.G. Tang, R. Xiao, C. Huang, Z.P. Feng, S.S. Fan, Experimental Investigation of Production Behavior of Gas Hydrate under Thermal Stimulation in Unconsolidated Sediment, Energy & Fuels, 19 (2005) 2402-2407.

[112] J. Jang, J.C. Santamarina, Recoverable gas from hydrate-bearing sediments: Pore network model simulation and macroscale analyses, J. Geophys. Res., 116 (2011) 1.

[113] M.H. Yousif, P.M. Li, M.S. Selim, E.D. Sloan, Depressurization of natural gas hydrates in berea sandstone cores, Journal of Inclusion Phenomena and Molecular Recognition in Chemistry, 8 (1990) 71-88.

[114] V. Kamath, S.P. Godbole, EVALUATION OF HOT-BRINE STIMULATION TECHNIQUE FOR GAS PRODUCTION FROM NATURAL GAS HYDRATES, JPT, Journal of Petroleum Technology, 39 (1987) 1379-1388.

[115] F.E. Anderson, J.M. Prausnitz, Inhibition of gas hydrate by methanol, AIChE J., 32 (1986) 1321.

[116] J. Sira, S. Patil, V. Kamath, Study of hydrate dissociation by methanol and glycol injection, in: SPE Annual technical conference and exhibition, Society of Petroleum Engineers, 1990.

[117] P.T. Ngema, P. Naidoo, A.H. Mohammadi, D. Richon, D. Ramjugernath, Experimental Clathrate Hydrate Dissociation Data for Systems Comprising Refrigerant + CaCl2 Aqueous Solutions, Journal of Chemical & Engineering Data, 61 (2016) 827-836.

[118] V.A. Kamath, P.N. Mutalik, J.H. Sira, S.L. Patil, Experimental study of brine injection and depressurization methods for dissociation of gas hydrates, SPE Form. Eval., (1991) 477.

[119] X. Li, L. Wan, G. Li, Q. Li, Z. Chen, K. Yan, Experimental investigation into production behavior of methane hydrate in porous sedment with hot brine stimulation, Ind. Eng. Chem. Res., 47 (2008) 9696.

[120] Y. Park, M. Cha, J.-H. Cha, K. Shin, H. Lee, K.-P. Park, D.-G. Huh, H.-Y. Lee, S.-J. Kim, J. Lee, Swapping carbon dioxide for complex gas hydrate structures, in: ICGH 6th International Conference on Gas Hydrates, Citeseer, 2008.

[121] N. Goel, In situ methane hydrate dissociation with carbon dioxide sequestration: Current knowledge and issues, Journal of petroleum science and engineering, 51 (2006) 169-184.

[122] The Igńik Sikumi Gas Hydrate Exchange, Trial Project Team, Ignik Sikumi gas hydrate˙ field trial completed. Fire in the Ice; US, Department of Energy, Office of Fossil Energy, National Energy, Technology Laboratory, Pittsburg, PA, 12 (2012) 1-3.

[123] A. Graue, B. Kvamme, B.A. Baldwin, J. Stevens, J.J. Howard, G. Ersland, J. Husebo, D.R. Zornes, Magnetic resonance imaging of methane-carbon dioxide hydrate reactions in sandstone pores, in: SPE Annual Technical Conference and Exhibition, Society of Petroleum Engineers, 2006.

[124] Y. Park, D.-Y. Kim, J.-W. Lee, D.-G. Huh, K.-P. Park, J. Lee, H. Lee, Sequestering carbon dioxide into complex structures of naturally occurring gas hydrates, Proceedings of the National Academy of Sciences, 103 (2006) 12690-12694.

[125] K. Josui, N. Miyakawa, K. Tei, D. Sugimoto, T. Fujioka, Excavation of methane hydrate using COIL, Proc. SPIE, 6101 (2006) 610127.

[126] M.J. Castaldi, Y. Zhou, T.M. Yegulalp, Down-hole combustion method for gas production from methane hydrates, Journal of petroleum Science and Engineering, 56 (2007) 176-185.

[127] D.-L. Li, D.-Q. Liang, S.-S. Fan, X.-S. Li, L.-G. Tang, N.-S. Huang, In situ hydrate dissociation using microwave heating: Preliminary study, Energy Conversion and Management, 49 (2008) 2207-2213.

[128] N. Fulong, J. Guosheng, T. Fenglin, Utilizing geothermal energy to exploit marine gas hydrate, NATURAL GAS INDUSTRY, 26 (2006) 136.

[129] M.R. Islam, A new recovery technique for gas production from Alaskan gas hydrate, J. Pet. Sci. Eng., 11 (1994) 267.

[130] S.D. Stoddard, J. Ford, Numerical experiments on stochastic behavior of a Lennard-Jones gas system, Phys Rev A, 8 (1973).

[131] D.J. Adams, E.M. Adams, G.J. Hills, The computer simulation of polar liquids, Mol Phys, 38 (1979).

[132] V.P. Sokhan, D.J. Tildesley, The free surface of water: molecular orientation, surface potential and nonlinear susceptibility, Mol Phys, 92 (1997).

[133] K. Kremer, G.S. Grest, Dynamics of entangled linear polymer melts: a molecular-dynamics simulation, J Chem Phys, 92 (1990).

[134] F. Varnik, J. Baschnagel, K. Binder, Molecular dynamics results on the pressure tensor of polymer films, J Chem Phys, 113 (2000).

[135] D.C. Rapaport, The art of molecular dynamics simulation, Cambridge University Press, Cambridge, 2004.

[136] J.-L. Barrat, J. Baschnagel, A. Lyulin, Molecular dynamics simulations of glassy polymers, Soft Matter, 6 (2010).

[137] T. Belytschko, S. Xiao, G. Schatz, R. Ruoff, Atomistic simulations of nanotube fracture. Phys Rev B 65(23): 235430, in, 2002.

[138] V. Coluci, N. Pugno, S. Dantas, D. Galvao, A. Jorio, Atomistic simulations of the mechanical properties of 'super' carbon nanotubes. Nanotechnology 18(33): 335702, in, 2007.

[139] M. Orsi, Molecular dynamics simulation of humic substances, Chemical and Biological Technologies in Agriculture, 1 (2014) 1-14.

[140] D. Beeman, Some multistep methods for use in molecular dynamics calculations, Journal of Computational Physics, 20 (1976) 130-139.

[141] L. Verlet, Computer" experiments" on classical fluids. I. Thermodynamical properties of Lennard-Jones molecules, Physical review, 159 (1967) 98.

[142] W.C. Swope, H.C. Andersen, P.H. Berens, K.R. Wilson, A computer simulation method for the calculation of equilibrium constants for the formation of physical clusters of molecules: application to small water clusters, J Chem Phys, 76 (1982).

[143] C.W. Gear, Numerical initial value problems in ordinary differential equations, Prentice Hall PTR, 1971.

[144] R.W. Hockney, POTENTIAL CALCULATION AND SOME APPLICATIONS, in, Langley Research Center, Hampton, Va., 1970.

[145] The site of TINKER software, in.

[146] The site of NAMD software, in.

[147] I.T. Todorov, W. Smith, K. Trachenko, M.T. Dove, Journal of Materials Chemistry, 16 (2006).

[148] B.R. Brooks, R.E. Bruccoleri, B.D. Olafson, D.J. States, S. Swaminathan, M. Karplus, CHARMM: a program for macromolecular energy, minimization, and dynamics calculations, J Comput Chem, 4 (1983).

[149] B. Hess, C. Kutzner, E. Lindahl, Gromacs 4, algorithms for highly efficient, load-balanced, and scalable molecular simulation, J Chem Theory Comput, 4 (2008).

[150] S. Plimpton, Fast parallel algorithms for short-range molecular dynamics, J Comput Phys, 117 (1995).

[151] L.A. Baez, P. Clancy, Computer simulation of the crystal growth and dissolution of natural gas hydrates, Annals of the New York Academy of Sciences, 715 (1994) 177-186.

[152] N.J. English, E.T. Clarke, Molecular dynamics study of CO2 hydrate dissociation: Fluctuation-dissipation and non-equilibrium analysis, Journal of Chemical Physics, 139 (2013).

[153] N.J. English, J.K. Johnson, C.E. Taylor, Molecular-dynamics simulations of methane hydrate dissociation, Journal of Chemical Physics, 123 (2005).

[154] L. Ding, C. Geng, Y. Zhao, H. Wen, Molecular dynamics simulation on the dissociation process of methane hydrates, Molecular Simulation, 33 (2007) 1005-1016.

[155] H. Yu, W.F. van Gunsteren, Charge-on-spring polarizable water models revisited: from water clusters to liquid water to ice, The Journal of chemical physics, 121 (2004) 9549-9564.

[156] E.M. Myshakin, H. Jiang, R.P. Warzinski, K.D. Jordan, Molecular dynamics simulations of methane hydrate decomposition, Journal of Physical Chemistry A, 113 (2009) 1913-1921.

[157] Y. Iwai, H. Nakamura, Y. Arai, Y. Shimoyama, Analysis of dissociation process for gas hydrates by molecular dynamics simulation, Molecular Simulation, 36 (2010) 246-253.

[158] S. Nosé, A unified formulation of the constant temperature molecular dynamics methods, The Journal of Chemical Physics, 81 (1984) 511-519.

[159] M. Parrinello, A. Rahman, Polymorphic transitions in single crystals: A new molecular dynamics method, Journal of Applied Physics, 52 (1981) 7182-7190.

[160] A. Chialvo, M. Houssa, P. Cummings, Molecular dynamics study of the structure and thermophysical properties of model sI clathrate hydrates, The Journal of Physical Chemistry B, 106 (2002) 442-451.

[161] G.S. Smirnov, V.V. Stegailov, Melting and superheating of sI methane hydrate: Molecular dynamics study, Journal of Chemical Physics, 136 (2012).

[162] I. Chatti, A. Delahaye, L. Fournaison, J.P. Petitet, Benefits and drawbacks of clathrate hydrates: A review of their areas of interest, Energy Conversion and Management, 46 (2005) 1333-1343.

[163] H. Komatsu, M. Ota, R.L. Smith, H. Inomata, Review of CO 2–CH 4 clathrate hydrate replacement reaction laboratory studies–properties and kinetics, Journal of the Taiwan Institute of Chemical Engineers, 44 (2013) 517-537.

[164] C.-Y. Geng, H. Wen, H. Zhou, Molecular Simulation of the Potential of Methane Reoccupation during the Replacement of Methane Hydrate by CO2, The Journal of Physical Chemistry A, 113 (2009) 5463-5469.

[165] Y. Ke-Feng, L. Xiao-Sen, S. Li-Hua, C. Zhao-Yang, X. Zhi-Ming, Molecular dynamics simulation of promotion mechanism of store hydrogen of clathrate hydrate, (2011).

[166] Y.-T. Tung, L.-J. Chen, Y.-P. Chen, S.-T. Lin, In Situ Methane Recovery and Carbon Dioxide Sequestration in Methane Hydrates: A Molecular Dynamics Simulation Study, The Journal of Physical Chemistry B, 115 (2011) 15295-15302.

[167] W.L. Jorgensen, J. Chandrasekhar, J.D. Madura, R.W. Impey, M.L. Klein, Comparison of simple potential functions for simulating liquid water, The Journal of Chemical Physics, 79 (1983) 926-935.

[168] J.G. Harris, K.H. Yung, Carbon dioxide's liquid-vapor coexistence curve and critical properties as predicted by a simple molecular model, The Journal of Physical Chemistry, 99 (1995) 12021-12024.

[169] W.L. Jorgensen, D.S. Maxwell, J. Tirado-Rives, Development and testing of the OPLS all-atom force field on conformational energetics and properties of organic liquids, Journal of the American Chemical Society, 118 (1996) 11225-11236.

[170] Y. Qi, M. Ota, H. Zhang, Molecular dynamics simulation of replacement of CH4 in hydrate with CO2, Energy Conversion and Management, 52 (2011) 2682-2687.

[171] D. Bai, X. Zhang, G. Chen, W. Wang, Replacement mechanism of methane hydrate with carbon dioxide from microsecond molecular dynamics simulations, Energy & Environmental Science, 5 (2012) 7033-7041.

[172] T. Yagasaki, M. Matsumoto, Y. Andoh, S. Okazaki, H. Tanaka, Dissociation of Methane Hydrate in Aqueous NaCl Solutions, The Journal of Physical Chemistry B, 118 (2014) 11797-11804.

[173] Y. Qi, W. Wu, Y. Liu, Y. Xie, X. Chen, The influence of NaCl ions on hydrate structure and thermodynamic equilibrium conditions of gas hydrates, Fluid Phase Equilibria, 325 (2012) 6-10.

[174] A.M. Stoneham, R. Taylor, Handbook of interatomic potentials, in, UKAEA Atomic Energy Research Establishment, 1981.

[175] Y.-T. Tung, L.-J. Chen, Y.-P. Chen, S.-T. Lin, Molecular dynamics study on the growth of structure I methane hydrate in aqueous solution of sodium chloride, The Journal of Physical Chemistry B, 116 (2012) 14115-14125.

[176] J. Xu, T. Gu, Z. Sun, X. Li, X. Wang, Molecular dynamics study on the dissociation of methane hydrate via inorganic salts, Molecular Physics, 114 (2016) 34-43.

[177] H. Berendsen, J. Grigera, T. Straatsma, The missing term in effective pair potentials, Journal of Physical Chemistry, 91 (1987) 6269-6271.

[178] M.W. Mahoney, W.L. Jorgensen, A five-site model for liquid water and the reproduction of the density anomaly by rigid, nonpolarizable potential functions, The Journal of Chemical Physics, 112 (2000) 8910-8922.

[179] J. Abascal, E. Sanz, R.G. Fernández, C. Vega, A potential model for the study of ices and amorphous water: TIP4P/Ice, The Journal of chemical physics, 122 (2005) 234511.

[180] E.A. Mastny, C.A. Miller, J.J. de Pablo, The effect of the water/methane interface on methane hydrate cages: the potential of mean force and cage lifetimes, The Journal of chemical physics, 129 (2008) 034701.

[181] J.Q. Broughton, G.H. Gilmer, Molecular dynamics investigation of the crystal–fluid interface. VI. Excess surface free energies of crystal–liquid systems, The Journal of chemical physics, 84 (1986) 5759-5768.

[182] R.L. Davidchack, B.B. Laird, Direct calculation of the crystal–melt interfacial free energies for continuous potentials: Application to the Lennard-Jones system, The Journal of chemical physics, 118 (2003) 7651-7657.

[183] R.L. Davidchack, R. Handel, J. Anwar, A.V. Brukhno, Ice Ih–Water Interfacial Free Energy of Simple Water Models with Full Electrostatic Interactions, Journal of chemical theory and computation, 8 (2012) 2383-2390.

[184] C. Vega, J.L. Abascal, M. Conde, J. Aragones, What ice can teach us about water interactions: a critical comparison of the performance of different water models, Faraday discussions, 141 (2009) 251-276.

[185] J. Zielkiewicz, Structural properties of water: Comparison of the SPC, SPCE, TIP4P, and TIP5P models of water, The Journal of chemical physics, 123 (2005) 104501.

[186] D. Paschek, Temperature dependence of the hydrophobic hydration and interaction of simple solutes: An examination of five popular water models, The Journal of chemical physics, 120 (2004) 6674-6690.

[187] H.W. Horn, W.C. Swope, J.W. Pitera, J.D. Madura, T.J. Dick, G.L. Hura, T. Head-Gordon, Development of an improved four-site water model for biomolecular simulations: TIP4P-Ew, The Journal of chemical physics, 120 (2004) 9665-9678.

[188] J.L.F. Abascal, C. Vega, A general purpose model for the condensed phases of water: TIP4P/2005, The Journal of Chemical Physics, 123 (2005) 234505.

[189] H. Docherty, A. Galindo, C. Vega, E. Sanz, A potential model for methane in water describing correctly the solubility of the gas and the properties of the methane hydrate, Journal of Chemical Physics, 125 (2006).

[190] M.G. Martin, J.I. Siepmann, Transferable potentials for phase equilibria. 1. United-atom description of n-alkanes, The Journal of Physical Chemistry B, 102 (1998) 2569-2577.

[191] A.D. MacKerell Jr, D. Bashford, M. Bellott, R.L. Dunbrack Jr, J.D. Evanseck, M.J. Field, S. Fischer, J. Gao, H. Guo, S. Ha, D. Joseph-McCarthy, L. Kuchnir, K. Kuczera, F.T.K. Lau, C. Mattos, S. Michnick, T. Ngo, D.T. Nguyen, B. Prodhom, W.E. Reiher Iii, B. Roux, M. Schlenkrich, J.C. Smith, R. Stote, J. Straub, M. Watanabe, J. Wiórkiewicz-Kuczera, D. Yin, M. Karplus, All-atom empirical potential for molecular modeling and dynamics studies of proteins, Journal of Physical Chemistry B, 102 (1998) 3586-3616.

[192] B. Guillot, Y. Guissani, S. Bratos, A computer-simulation study of hydrophobic hydration of rare gases and of methane. I. Thermodynamic and structural properties, The Journal of chemical physics, 95 (1991) 3643-3648.

[193] R. Radhakrishnan, B.L. Trout, A new approach for studying nucleation phenomena using molecular simulations: Application to CO2 hydrate clathrates, The Journal of chemical physics, 117 (2002) 1786-1796.

[194] E.M. Myshakin, H. Jiang, R.P. Warzinski, K.D. Jordan, Molecular dynamics simulations of methane hydrate decomposition, The Journal of Physical Chemistry A, 113 (2009) 1913-1921.

[195] D.P. Luis, A. García-González, H. Saint-Martin, A Theoretical Study of the Hydration of Methane, from the Aqueous Solution to the sI Hydrate-Liquid Water-Gas Coexistence, International journal of molecular sciences, 17 (2016) 378.

3. CHAPTER THREE

Evaluation of Gas Hydrate Formation Temperature for Gas/Water/Salt/Alcohol Systems: Utilization of Extended UNIQUAC Model and PC-SAFT Equation of State (published)

Preface

A version of this manuscript has been published in the Industrial & Engineering Chemistry Research 57 (41) (2018): 13833-13855. I am the primary author of this paper. With the help and advice of the co-authors, Sohrab Zendehboudi and Lesley James, I developed the conceptual thermodynamic model and designed the manuscript's structure. Most of the literature review, data collection, and the performance comparison of different methods and previous experimental works were done by me as the first author. I prepared the first draft of the manuscript and subsequently revised the manuscript based on the co-authors' feedback and comments received from journal reviewers. The co-author, Sohrab Zendehboudi, helped in developing the method, results interpretation, and statistical analysis. The co-author, Sohrab Zendehboudi, also considerably contributed to entirely correcting the text in terms of technical and editorial aspects. Lesley James thoroughly reviewed and revised the manuscript.

Abstract

Naturally occurring gas hydrates are of great importance in terms of strategic energy source. Hydrates affect coastal sediment stability, global climate change, and ocean carbon cycling. It is vital to understand the thermodynamic conditions of gas hydrates to control/manage and inhibit hydrate formation. A variety of equations of state (EOSs) have been utilized to model the thermodynamic behavior of gas hydrates. In this study, the PC-SAFT equation of state combined with van der Waals Platteuw model is employed to determine the clathrate hydrate formation temperature of pure gases (e.g., methane, ethane, propane, isobutane, carbon dioxide, and hydrogen sulfide) and binary and ternary systems of hydrate gases. In addition, the gas hydrate formation conditions are investigated where methanol, ethanol, glycerol, NaCl, KCl, $CaCl_2$, and $MgCl_2$ as inhibitors are present. The UNIQUAC model is utilized in this work to obtain the hydrate formation conditions in systems with inhibitors. The interaction parameters between water, alcohols, salts, and gasses are considered in the thermodynamic modeling. The long-range interaction contribution term is also incorporated in the model to determine the hydrate formation temperature in the presence of salts and alcohols. To achieve more accurate results, the association contribution is taken into account to calculate the residual Helmholtz energy. It is found that the PC-SAFT equation of state is able to predict the hydrate formation conditions with high precision. The comparison between the calculated and experimental data reveals that the average absolute error in this study is lower than that in the earlier works. The modeling strategy employed in this research study can be applicable to forecast the thermodynamic behaviors of natural or synthetic gas hydrates within a broad range of process conditions.

Keywords: PC-SAFT Equation of State, Gas Hydrate, Association Contribution, Phase Equilibria, Inhibitor

3.1. Introduction

Natural gas and light oils are considered as the world's primary sources of energy. Over production, transportation, and downstream operations, they generally experience a major problem, which is the formation of gas hydrate, leading to equipment blockage or/and shutdown. Thus, the inhibition of gas hydrate formation in various petroleum operations seem necessary. To attain this goal, thermodynamic and process research studies to forecast the hydrate phase equilibria in the presence of water, salts, and alcohols in upstream or/and downstream processes are inevitable.

Clathrate hydrates are the crystalline and ice-like compounds that are found at high-pressure and low-temperature conditions such that gas or volatile liquid molecules appropriate for hydrate formation are trapped within rigid cages of water molecules.

There are three hydrate structures, depending on the size of the gas molecule and type and number of cavities. The most common gas hydrate structures are namely; structure (type) I [1], structure (type) II [2], and structure (type) H [3]. Small molecules such as methane and ethane normally create structure I, while the larger molecules are observed in structure II and structure H. For instance, propane and isobutene form structure II and combinations of methane gas and cycloheptene form structure H.

In the last few decades, a considerable number of studies have been conducted to investigate a variety of applications of gas hydrates in the world; including water desalination/treatment technology[4], purification of gas mixtures [5], refrigeration and air conditioning systems in the form of hydrate slurry [6], gas transportation [7], gas storage, and carbon capture and sequestration [8]. Englezos [9] published a systematic literature review on the technological developments, environmental and energy concepts, and fundamental aspects of natural gas hydrates. Chatti et al. [2] also performed a literature review on different prospects of gas hydrates such as utilization, benefits and drawbacks, and characterization. The utilization and formation occurrence of clathrate hydrates in various industries mainly separation processes are presented in a review paper prepared by Eslamimanesh et al.[3]. In addition, Kondori et

al. [10] conducted a comprehensive review study on different kinds of gas hydrate reservoirs. They showed the limitations of existing experimental and theoretical approaches and offered an appropriate procedure on the development of more accurate theoretical models.

The prohibition ways/strategies for hydrate formation and prediction of hydrate formation conditions are the most important aspects in gas hydrate studies. There are several research works in the open sources to develop models for simulation/modeling of the clathrate hydrate formation. The majority of the modeling strategies have employed a statistical mechanistic model, which was primarily developed by van der Waals and Platteeuw [11], to describe the hydrate phase. To determine the thermodynamic equilibrium conditions, the equations of state (EOSs) and activity coefficient models are generally utilized. A number of researchers including Parrish and Prausnitz [12], Ng and Robinson [13], and Holder et al. [14] modified the van der Waals model [11] to design various chemical engineering processes while dealing with multiple phases. Anderson et al. [15] proposed a model based on the equality of fugacities to determine the hydrate equilibrium conditions by using a modified Redlich Kwong (RK) equation of state for the vapor phase and a modified UNIQUAC model for the liquid phase where various gaseous mixtures and methanol (as an inhibitor) were examined. To investigate the impact of methanol on the gas hydrate formation, Englezos et al. [16] used the Trebble–Bishnoi [17] equation of state. Tavasoli et al. [18] also estimated the hydrate formation conditions in both uninhibited and inhibited systems through using the Elliot, Suresh, and Donohue (ESD) equation of state. In another study, Karamoddin et al. [19] compared the results obtained from three different EOSs (e.g., Soave-Redlich-Kwong (SRK), Valdarama-Patel-Teja (VPT), and cubic-plus-association (CPA)) for determination of the hydrate formation conditions of refrigerants. Chapoy et al. [20] used the CPA equation of state to obtain the gas hydrate formation conditions of pure gases. Eslamimanesh et al. [21] developed a model to determine the hydrate formation conditions of hydrogen sulfide and carbon dioxide where the modified conventional Clapyron equation was used. Li et al. [22] conducted a

thermodynamic study on prediction of hydrate formation in sour natural gas systems containing H_2S and CO_2. They utilized CPA equation of state in their research investigation. Recently, Kwaterski et al. [23] introduced an approach to study the influences of dissolved salts such as NaCl, KCl, and $CaCl_2$ on the thermodynamic conditions of the gas phase in the hydrate systems. They applied the E-NRTL activity coefficient model for hydrate formation systems of carbon dioxide + methane + electrolyte + water.

The ongoing development of onshore and offshore petroleum fields increases the risks of operating difficulties resulted from the formation of gas hydrates. Various strategies are currently being used for lowering the hydrate problems in hydrocarbon production, pipeline, and process facilities. To decide on an effective inhibition method, we need to accurately estimate hydrate formation conditions. The hydrate formation temperature and pressure of various pure gases; namely, methane, ethane, propane, hydrogen sulfide, nitrogen, *i*-butane, ammonia, and carbon dioxide are investigated in this study. Hydrate structures are divided into two categories, depending on the size of the guest molecules listed above. The structure I is considered for all the above gases except for systems which include propane and *i*-butane.

In addition, Li [24] developed a thermodynamic model based on the statistical associating fluid theory (SAFT) to investigate gas hydrate formation condition in the absence and in the presence of inhibitors. Using the SAFT equation of state, the Helmholtz free energy of each component is calculated by summing up of the dispersion interaction, hard sphere extraction, and association terms. The SAFT equation of state has been successfully used for the phase equilibria of numerous complex components; for example, electrolyte solutions [25], ionic liquids [26], aromatics [27], polymers [28], and alcohols [29]. The association interaction between the molecules can be captured by the SAFT equation of state. After introducing the SAFT equation of state, many researchers proposed the new versions of the SAFT such as S-SAFT, soft-SAFT, MS-SADT, and PC-SAFT to improve the performance/accuracy of the

SAFT equation of state in thermodynamic equilibrium calculations [30-32]. Firstly, the perturbed chain SAFT (PC-SAFT) equation of state was used by Gross et al. [33]. In the PC-SAFT equation of state, the dispersion energy is calculated, considering both hard chains and hard spheres. In the context of gas hydrate, Li [34] studied hydrate formation of methane, ethane, and propane by using the first version of SAFT. Liang et al. [35] and Leekumjorn et al. [36] illustrated new methods to calculate the PC-SAFT parameters for different systems.

To the best of our knowledge, there is no gas hydrate modeling study for gas mixtures using the PC-SAFT equation of state and UNIQUAC model. The integration/combination of PC-SAFT EOS and UNIQUAC model has never been used to forecast the hydrate formation conditions in the presence of inhibitors, electrolytes, and ionic liquids.

In the present work, the PC-SAFT equation of state is employed to model the hydrate phase in different systems. The PC-SAFT equation of state is coupled with the van der Waals and Platteuw model. The gas hydrate formation conditions are investigated for pure gas, sour gas, and different mixtures of gases in the uninhibited and inhibited systems. Under various thermodynamic conditions, the three-phase equilibria calculations are studied for various systems (pure and mixture) of the gas, liquid, hydrates, and inhibitors such as methanol, ethanol, glycerol, NaCl, KCl, $CaCl_2$, and $MgCl_2$. The optimal values of all the possible UNIQUAC interaction parameters between the components in the aqueous phase are considered. The activity of water in the aqueous mixtures of alcohols and salts is also determined by using UNIQUAC.

3.2. Modeling Approach

Under phase equilibrium condition, the equality of temperature, pressure, and chemical potentials (fugacity) of a component in all involved phases is the basis of calculations related to the gas hydrate formation conditions. For three phase vapor-liquid-hydrate equilibria, the fundamental equation for the equilibrium condition in the gas hydrates is given below:

$$\mu_w^H = \mu_w^\alpha \tag{3-1}$$

where μ_w^H and μ_w^α stand for the chemical potential of water in the hydrate phase and other coexisting phases, respectively. In this study, the equilibrium conditions between water, hydrate, and vapor phases are investigated. van der Waals and Platteuw [11] introduced a model to determine the chemical potential of the component in the hydrate phase with the following assumptions; i) There is no more than one gas molecule in each cavity, ii) The interaction between encaged molecules is neglected, and iii) The guest molecules follow the ideal gas behavior. The water chemical potential function in the hydrate network (van der Waals and Platteuw [11]) is calculated by Equation (2-1) as follows:

$$\mu_w^H = \mu_w^\beta + RT\sum_i^N \upsilon_i \ln\left(1 - \frac{C_{mi} f_i}{1 + \sum_{mi} C_{mi} f_i}\right) \tag{3-2}$$

where μ_w^β represents the chemical potential of water in an empty cage of hydrate network, f_i stands for the fugacity of the gaseous compounds which are achieved using the PC-SAFT equation of state (further details are found in the next sections), υ_i refers to the number of cavities of type *m* per water molecule in the lattice, and R and T denote the universal gas constant and temperature, respectively. C_{mi} in Equation (3-2) is the Langmuir constant, which is described by the following expression [12] :

$$C_{mi} = \frac{4\pi}{kT}\int_0^\infty \exp\left[\frac{-\omega(r)}{kT}\right] r^2 dr \tag{3-3}$$

in which, $\omega(r)$ symbolizes the spherically symmetric cell potential and k signifies the Boltzmann's constant, which is calculated by summation over all gas-water interactions in the cavity. The Kihara potential function is applied to calculate $\omega(r)$, as shown below:

$$\omega(r) = 2z\varepsilon\left[\frac{\sigma^{12}}{R^{11} r}(\delta^{10} + \frac{a}{R}\delta^{11}) - \frac{\sigma^6}{R^5 r}(\delta^4 + \frac{a}{R}\delta^5)\right] \tag{3-4}$$

and

$$\delta^N = \left[\frac{1-(r/R)-(a/R)-\left[1-(r/R)-(a/R)\right]^{-N}}{N} \right] \tag{3-5}$$

where r and R represent the distance of the guest molecule from the cavity center (radius of the cavity) and cell radius, respectively; z refers to the coordination number; $\sigma + 2a$ is the collision diameter; a stands for the core radius; and ε is the symbol for the energy parameter in the Kihara potential function. Parrish and Prausnitz [12] proposed the following correlation to calculate the Langmuir constant:

$$C_{mi} = \frac{A_{mi}}{T} \exp\left(\frac{B_{mi}}{T}\right) \tag{3-6}$$

In Equation (3-6), A_{mi} and B_{mi} introduce two constants which can be obtained, when the theoretical value of C_{mi} is determined by using Equation (3-3).

The water chemical potential in the liquid or ice phase, μ_w^{α}, (the right side of Equation (3-1)) is achieved as follows:

$$\mu_w^{\alpha} = \mu_w^{\circ} + RT \ln a_w \tag{3-7}$$

in which, μ_w° and a_w denote the chemical potential and activity of pure water in the ice or liquid phase, respectively. The chemical potential difference of water in the pure liquid (or ice phase) and in the unoccupied hydrate lattice ($\Delta\mu_w^{\alpha}$) is given below:

$$\Delta\mu_w^{\alpha} = \mu_w^{\alpha} - \mu_w^{\beta} \tag{3-8}$$

The chemical potential difference of water in the hydrate phase and the unoccupied hydrate lattice ($\Delta\mu_w^{H}$) can be also defined as follows:

$$\Delta\mu_w^H = \mu_w^H - \mu_w^\beta \tag{3-9}$$

Consequently, the equilibrium quality of chemical potential (see Equation (3-1)) turns to the following expression:

$$\Delta\mu_w^H = \Delta\mu_w^\alpha \tag{3-10}$$

The left side of Equation (8) is commonly expressed as follows [14]:

$$\Delta\mu_w^\alpha = RT\left[\frac{\Delta\mu_w^\circ}{RT_0} - \int_{T_0}^{T}\frac{\Delta H_w^\alpha}{RT^2}dT + \int_{P_0}^{P}\frac{\Delta v_w^\alpha}{RT}dP - \ln a_w\right] \tag{3-11}$$

Where $\Delta\mu_w^\circ$ represents the difference in the chemical potential of pure water in the unoccupied lattice and liquid water at a temperature equal to 273.15 K. ΔH_w^α and Δv_w^α signify the difference in the molar enthalpy and the difference in the molar volume between the occupied network of hydrate and liquid water, respectively. T_0 and P_0 introduce the reference temperature (e.g., 273.15 K) and reference pressure (e.g., 1 atm), respectively. The magnitude of ΔH_w^α can be determined by using Equation (3-12), as shown below:

$$\Delta H_w^\alpha = \Delta H_w^0 + \int_{T_0}^{T}\Delta C_{p_w}dT \tag{3-12}$$

where ΔC_{p_w} is the water heat capacity, which is obtained by the following correlation:

$$\Delta C_{p_w} = \Delta C_{p_w}^0 + b\left(T - 273.15\right) \tag{3-13}$$

Based on Equations (3-8) to (3-13), all constants required for the phase equilibria calculations are listed in Table 3-1 [37]. The water activity is calculated by the UNIQUAC model [38], which is described in the Supporting Information .

Table 3-1: Thermodynamic parameters of unoccupied hydrate lattice at 273 K and 1 atm [39].

Properties	Structure I	Structure II
$\Delta\mu_w^{\alpha}\,(J/mol)$	1264	883
$\Delta H_w^0\,(J/mol)$	-4858	-5201
$\Delta v_w^{\alpha}(cm^3/mol)$	4.6	5.0
$\Delta C_{p_w}^0\,(J/mol.K)$	38.120	
$b(J/mol)$	0.141	

3.2.1. PC-SAFT EOS

In the context of phase equilibria, two classical thermodynamic methods are usually employed; namely, the cubic equations of state and liquid activity coefficient models [40]. In addition to the conventional tools/ models, the association models have been used over the last decades, which can show and explain the effect of hydrogen bonding in targeted systems including both polar and non-polar components.

The statistical association fluid theory (SAFT) is one of the most reliable and accurate models in the perturbation theory [41]. In the SAFT equation of state, all molecules are considered as spherical segments with equal size, which are characterized by five pure-component parameters; including, number of segments (m), diameter of segment (σ), energy of segment (ε), volume of association ($\kappa_{A_iB_i}$), and energy of association ($\varepsilon_{A_iB_i}$). It should be mentioned that the last two terms are utilized only if the molecule is self-associating. Gross and Sadowski [33] introduced the PC-SAFT equation of state (EOS). The PC-SAFT EOS has two main differences with the SAFT equation of state [27] so that the dipole-dipole interaction term is added to the PC-SAFT EOS and the Lenard-Jones equation is used for the segment contribution. In the PC-SAFT equation of state, the dispersion interactions are considered between the connected segments instead of disconnected segments. The interaction term can be

employed with a good reliability for the chain molecules such as solutions containing hydrocarbons or/and polymers. PC-SAFT equation of state exhibits a high accuracy to predict the vapor-liquid and liquid-liquid equilibrium conditions of small and large molecules over a wide range of pressure, temperature, and composition for systems of associating, non-associating, polar and non-polar components, and polymers [42]. Due to its great precision in forecasting the thermophysical properties of various mixtures, particularly polymeric systems, nowadays PC-SAFT EOS experiences more applications in modeling (and simulation) of polymerization systems and predicting of thermodynamic or/and thermophysical properties. Utilization of PC-SAFT EOS model for mixtures requires the accurate estimation of pure component parameters such as segment number, diameter, and energy.

The PC-SAFT is presented in terms of reduced Helmholtz free energy to describe the thermodynamic properties of a system. The residual Helmholtz free energy of a system ($\bar{a}^{res}$) is the sum of three terms, which show the contributions of various interaction forces between the molecules. In the PC-SAFT EOS, the residual Helmholtz free energy is expressed as follows:

$$\bar{a}^{res} = \bar{a}^{hard-chain} + \bar{a}^{dispersion} + \bar{a}^{association} \tag{3-14}$$

where the residual Helmholtz free energy, $\bar{a}^{res}$, is calculated by the following equation:

$$\bar{a}^{res} = \frac{A}{N \kappa T} \tag{3-15}$$

In Equation (3-15), the parameter κ represents the Boltzmann constant, *N* shows the total number of molecules, and *T* refers to the absolute temperature. In Equation (3-14), the hard-chain contribution ($\bar{a}^{hard-chain}$) includes the hard chain formation and the sphere contribution. Dispersion forces ($\bar{a}^{dispersion}$) denote the attractions between non-polar and weakly-polar molecules. The association contribution ($\bar{a}^{association}$) consists of any specific interactions such as electron donor-acceptor interactions and

hydrogen. The corresponding equations for determination of important thermodynamic parameters (e.g., gas compressibility factor and fugacity coefficient) by using PC-SAFT are given in the Supporting Information.

3.2.2. Input Parameters and Data

In this study, 7 pure components are used in 16 various systems within broad ranges of pressure, temperature, and composition. For simple non-association systems, we need to have three main parameters such as the segment number (m), diameter of segment (σ), and potential well depth energy (ε / k)[33,43]. To include any associating component, the association energy for sites A and B (κ^{AB}), effective association volume (ε^{AB} / k), and the above three parameters are required [43]. Table 3-2 provides the pure-component parameters for all components in this study. The binary interaction parameters (k_{ij}) [44] and cross- association interactions (ν_{ij} and λ_{ij}) [33] are listed in Table 3-2.

Table 3-2: Pure-component parameters of the PC-SAFT equation of state.

Component	m	σ (Å)	ε / k (K)	κ^{AB}	ε^{AB} / k (K)	Reference
Water	2.6166	2.0689	132.44	0.293973	1767.1	[43]
Methanol	1.779	3.088	194.18	0.0488	2668.7	[43]
Ethanol	2.8243	2.9659	191.25	0.0545	2321.8	[43]
Glycerol	1.5728	4.190	554.73	0.0007	4364.57	[45]
Methane	1.000	3.7039	150.03	-	-	[33]
Ethane	1.6069	3.5206	191.42	-	-	[33]
Propane	2.0020	3.6184	208.11	-	-	[33]
iButane	2.6166	3.7574	216.53	-	-	[33]
CO_2	2.0729	2.7852	169.21	-	-	[33]
N_2	1.2053	3.3130	90.96	-	-	[33]
H_2S	1.6941	3.0214	226.79	-	-	[43]

Na^+	1	2.4566	2044.09	0.001	2630	[46]
K^+	1	3.26	1350.31	0.001	1400	[46]
Mg^{2+}	1	2.4803	3360.36	0.001	3490	[46]
Ca^{2+}	1	3.321	2205.76	0.001	2218	[46]
Cl^-	1	3.28	2260.41	0.001	2120	[46]

Table 3-3: Binary interaction parameters and binary association parameters.

Binary system	k_{ij}	v_{ij}	λ_{ij}	Ref.	**Binary system**	k_{ij}	v_{ij}	λ_{ij}	Ref.
Methane/CO_2	0.0919	-	-	[47]	Methanol/Ethane	0.110	-	-	[48]
Methane/ N_2	0.0311	-	-	[47]	Methanol/CO_2	-0.087	-	-	[48]
Methane/ H_2S	0.885	-	-	[47]	Ethanol/CO_2	0.076	-	-	[48]
Methane/iButane	0.0256	-	-	[47]	Propane/iButane	-0.0078	-	-	[48]
Methane/ Propane	0.014	-	-	[47]	CO_2/ H_2S	0.0974	-	-	[49]
Methane/Ethanol	0.0911	-	-	[50]	CO_2/Ethane	0.014	-	-	[48]
Water/Ethanol	0.0569	0.2817	-0.0802	[43]	Water/Methanol	0.435	0.30614	0.09324	[43]
Water/NaCl	0.3213	-	-	[51]	Ethanol/Methanol	-0.0009	-	-	[43]
Methane/ NaCl	0.8738	-	-	[51]	Water/Glycerol	-0.280	0.0293	0.0213	[45]
CO_2/ NaCl	0.2659	-	-	[51]	Water/KCl	-0.2836	-	-	[51]
Propane/NaCl	0.72	-	-	[51, 52]	Methane/KCl	1.482	-	-	[51]
iButane/NaCl	0.7	-	-	[51, 52]	Propane/KCl	1.36	-	-	[51, 52]
N_2/NaCl	0.007	-	-	[51, 52]	iButane/KCl	1.35	-	-	[51, 52]

3.2.3. Modeling Algorithm

Figure 3-1 shows the computational procedure to determine the thermodynamic conditions of the hydrate formation temperature. The procedure is as follows:

- The input parameters are the pressure and initial composition in the gas phase (water free),

- Assume the water activity $(a_w)=1$ for the aqueous phase,

- Guess a temperature for the hydrate formation,

- Obtain the fugacity for all gaseous components using the PC-SAFT equation of state,

- Calculate $\Delta\mu_w^{\alpha}$ and $\Delta\boldsymbol{\mu}_w^{H}$ through employing Equations (3-7) - (3-13),

- If the magnitudes of $\Delta\mu_w^{\alpha}$ and $\Delta\boldsymbol{\mu}_w^{H}$ are equal, the guessed temperature in the third step is correct; otherwise, the temperature needs to be updated and the program returns to the third step,

- Having a new temperature and equality of fugacity, the solubility of gases in the aqueous phase can be achieved using Equation (S-5),

- Calculate a new activity for water in the aqueous phase using the UNIQUAC model (see the Supporting Information) and repeat all the above steps from the second step by considering a new a_w and recalculate a new temperature,

- If the magnitudes of the new and old temperatures are equal, the new temperature is correct and it is considered as the temperature of the hydrate formation; otherwise, the temperature needs to be updated and the program returns to the second step where the new a_w and the last updated temperature are used. To provide further details, the algorithm required to conduct phase equilibrium calculations is provided in the Supporting Information. The MALAB© software is used for programming in this research work.

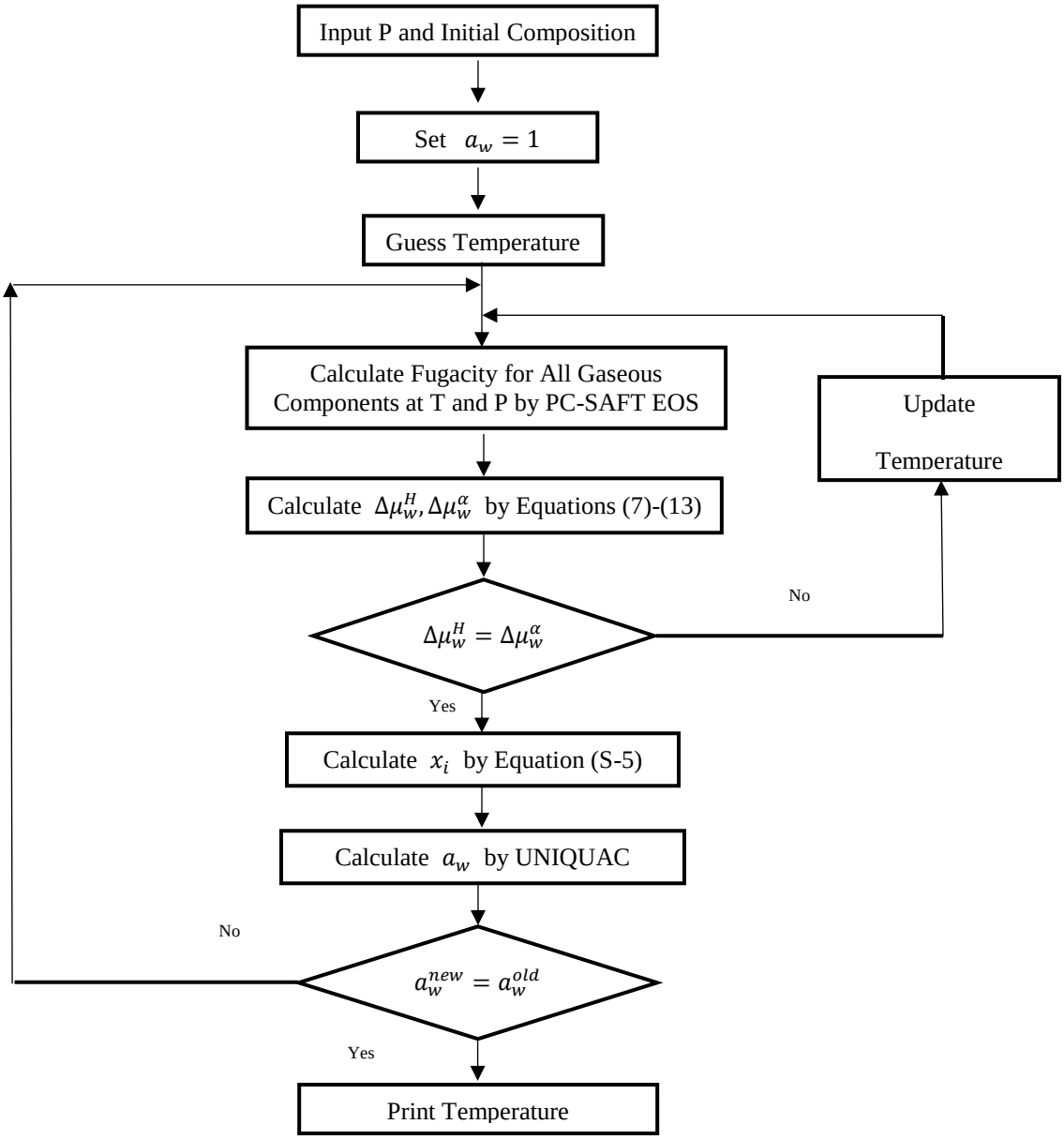

Figure 3-1: Flow diagram for calculation of hydrate formation temperature.

3.3. Results and Discussion

We use UNIQUAC model to obtain the water activity and PC-SAFT EOS is also employed to determine the fugacity of gas components. The effect of electrolyte and ions is considered while obtaining the parameters of PC-SAFT EOS and UNIQUAC model.

Table 3-4 shows the hydrate formation conditions for hydrates with pure gases. As can be seen in Table 4, a very good match is noticed between the experimental data and calculated values based on the minimum error percentage, maximum error percentage, and average absolute error percentage where the PC-SAFT equation of state is employed. The mean error percentage or average absolute percent deviation in temperature (AADT%) and pressure (AADP%) are calculated by the following equations:

$$AADT\% = 100 \times \sum_{i=1}^{N_p} \frac{1}{N_p} \frac{\left| T^{\exp} - T^{cal} \right|}{T^{\exp}} \tag{3-16}$$

$$AADP\% = 100 \times \sum_{i=1}^{N_p} \frac{1}{N_p} \frac{\left| P^{\exp} - P^{cal} \right|}{P^{\exp}} \tag{3-17}$$

where N_p stands for the number of data points in each dataset, and superscripts *exp* and *cal* are attributed to the experimental data and the calculated value of hydrate temperature (or/and pressure). The UNIQUAC interaction parameters of water, salts or/and alcohols systems are obtained where the overall AADT% for all systems containing inhibitors is minimized through using the pattern search technique in the MATLAB software. It should be mentioned that the hydrate formation data of pure gasses in the presence of inhibitors are used to obtain the parameters (listed in Table S2 of the Supporting Information) through regression technique.

Table 3-4: Values of the minimum error and maximum error percentages, AADT%, and AADP% while predicting hydrate formation conditions for pure gases.

Guest	Range of P (MPa)	Range of T (K)	N_P	Min. Error	Max. Error	AADT%	AADP%	Ref.	Guest	Range of P (MPa)	Range of T (K)	N_P	Min. Error	Max Error	AADT%	AADP%	Ref.
Methane	1.79-9.78	262.4-285.9	18	0.0038	0.6441	0.1033	1.0890	[53]		0.368-0.547	276.7-278.5	9	0.0019	0.0396	0.0160	1.0254	[54]
	33.99-77.5	295.7-302	4	0.0892	0.3264	0.1640	5.4582	[55]	ibutane	0.109-0.167	273.2275.1	10	0.1704	0.0549	0.0216	1.3746	[56]
	9.62-68.09	285.7-301.6	9	0.0117	0.0807	0.0407	1.4221	[57]		0.115-0.169	273.2-275	20	0.0027	0.0805	0.0395	2.2306	[58]
	15.9-237.5	290.2-315.1	14	0	0.0002	0.0001	0.0001	[59]	CO_2	1.324-4.323	273.7-282.9	17	0.0015	0.0607	0.0244	0.9693	[60]
	2.65-28.57	273.2-294.3	8	0.0066	0.1137	0.0655	2.1493	[61]		1.048-4.502	271.8-283.2	35	0.0002	0.1012	0.0425	1.5921	[62]

	7.1-13.11	283.2-288.7	3	0.057	0.0779	0.0671	2.1602	[63]		1.338-4.085	273.3-281.1	76	0.0038	0.283	0.1269	4.8312	[64]
	3.02-18.55	275.2-291.2	7	0.0022	0.2136	0.0563	1.6698	[65]	N_2	24.93-328.8	277.6-305.5	14	0.0200	0.2318	0.0706	2.0194	[59]
Ethane	0.294-0.441	260.9-287	13	0.0038	0.7414	0.1214	2.4108	[66]		14.48-95.8	272--291	37	0.0016	0.1028	0.0330	0.9229	[67]
	0.51-2.73	273.7-286.5	18	0.017	0.0765	0.0395	1.4863	[53]		55-439	285.6-309.4	29	0.0061	0.2216	0.088	2.268	[68]
	0.78-2.62	277.5-286.5	7	0.0526	0.1080	0.0872	3.4174	[69]		16.27-35.16	273.2-281.1	8	0.0017	0.2305	0.0645	1.9589	[61]
	5.0-20.34	288-290.6	6	0.0011	0.0267	0.0107	2.005	[70]		19.09-45.35	274.5-283.0	3	0.0066	0.0862	0.0359	1.0171	[71]
	0.848-3.082	277.8-287.2	10	0.007	0.0841	0.0395	1.6736	[72]	H_2S	0.31-2.241	283.2-302.7	4	0.0039	0.1879	0.1086	3.31	[73]
	19.48-83.75	290.4-298.3	26	0.0022	0.055	0.0218	1.192	[74]		0.093-2.239	272.8-302.7	13	0.0050	0.8508	0.1148	2.0506	[75]
Propane	0.165-0.472	273.228	10	0.0093	0.061	0.0324	1.8104	[76]		1.61-2.07	298.6-300.8	12	0.0057	0.247	0.0572	1.497	[77]
	0.183-0.27	273.7-275.4	3	0.0049	0.0251	0.0118	0.7507	[60]									

Figure 3-2 shows the methane hydrate formation conditions in the presence of pure water where the experimental data collected from the literature are used for the comparison and validation purposes. In general, AADT% for pure methane hydrate formation condition is about 0.0635%, implying reliability and high capability of PC-SAFT in predicting hydrate behaviors.

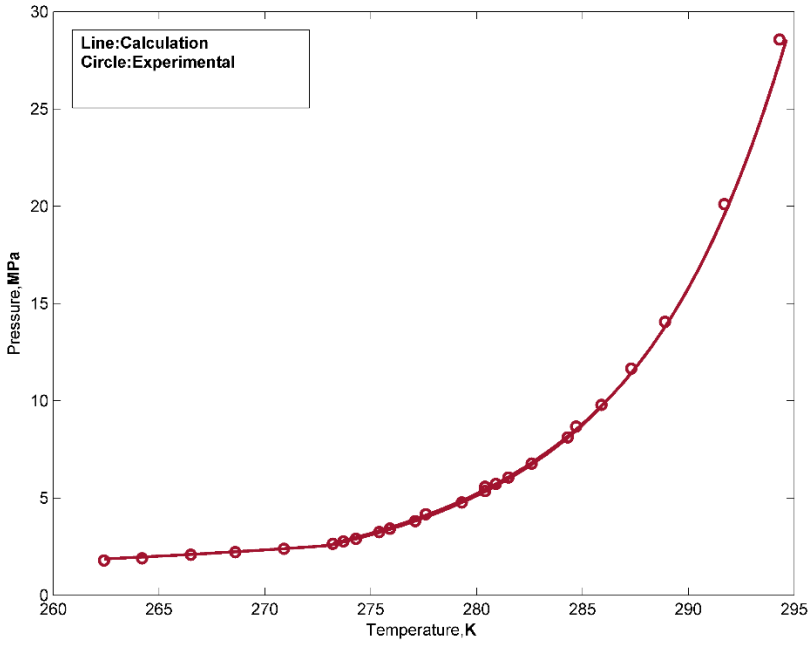

Figure 3- 2: Hydrate formation conditions of methane [53, 61].

Figures 3-2 and 3-4 depict the hydrate formation conditions for ethane, propane, isobutane, carbon dioxide, nitrogen, and hydrogen sulfide. The magnitudes of AADT% for ethane, propane, isobutane, carbon dioxide, nitrogen, and hydrogen sulfide are 0.0491%, 0.0228%, 0.0335%, 0.0902%, 0.0591%, and 0.0901%, respectively. The results attained in this study reveal that there is an acceptable agreement between the modeling results and real data while dealing with pure gases. The mean value of AADP% for all pure gases in this study is 2.1748% (for 443 points), while the magnitudes of AADP% for other studies are reported to be 1.521% with SRK EOS/UNIQUAC [78], 4.33% with cubic plus-association (CPA)EOS [79] , 5.65% with the fugacity-based model [80], 2.88% with the modified version of the Peng–Robinson equation of state (PRSV1 EOS) [81], and 2.66% with PRSV2 equation of state [82] to estimate the equilibrium pressure. Providing more detailed calculations/information on Table 3-4 and Figures 3-2 to 3-4, the Supporting Information includes a high number of calculated and

experimental hydrate temperature and pressure for pure gases, as listed in Table S4 and Table S5.

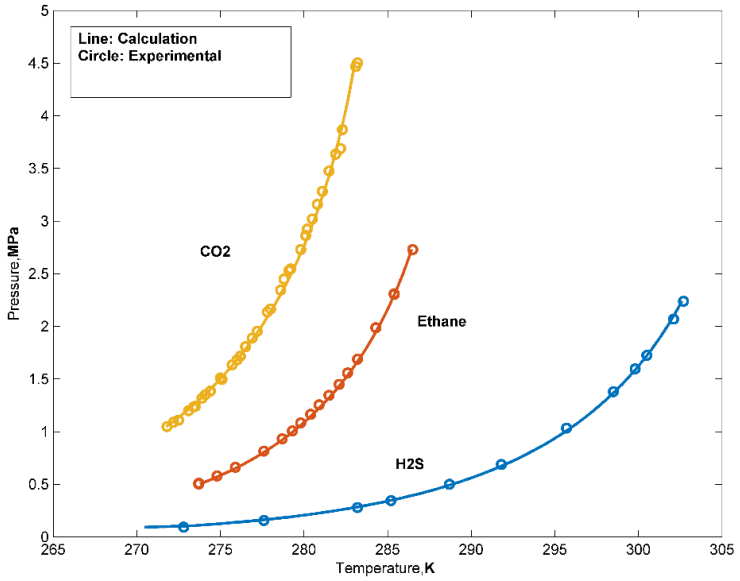

Figure 3-3: Hydrate formation conditions of ethane[53], carbon dioxide[62], and hydrogen sulfide [75].

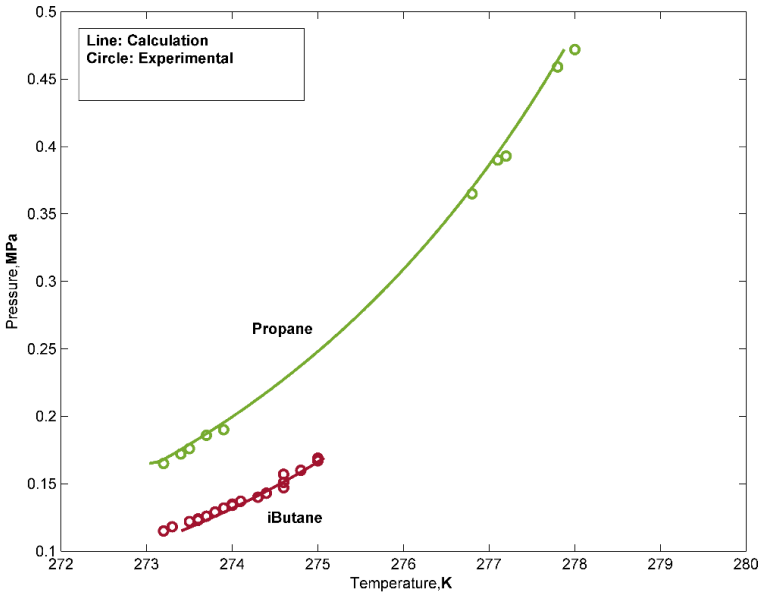

Figure 3-4: Hydrate formation conditions of propane [76] and ibutane [58].

Table 3-5 lists the equilibrium conditions for the hydrate formation temperature of gas mixtures of methane + ethane, methane + propane, methane + isobutane, methane + nitrogen, methane + carbon dioxide, methane + hydrogen sulfide, ethane + propane, ethane + carbon dioxide, and propane + isobutane. It is worth noting that the methane and ethane hydrates alter from Structure I to Structure II when the mole percentage of methane in the mixture is between 72.2 mole% and 75.0 mole%. Thus, it can be concluded that Structure II hydrate can form from a mixture with a methane concentration (mole%) greater than 75%. Based on this criterion/rule, the equilibrium conditions are determined for Structure II when the mole fraction of methane is above 0.75 [83].

Table 3-5: Minimum error and maximum error percentages and AADT% while estimating hydrate formation temperature for gas mixture systems.

Gas 1	Gas 2	Range of P (MPa)	Range of T (K)	N_P	Min. Error	Max. Error	AADT %	Ref	Gas 1	Gas 2	Range of P (MPa)	Range of T (K)	N_P	Min. Error	Max Error	AADT%	Ref.
CH_4	98.4% C_2H_6	1.81-3.08	283.9-287.8	4	0.0908	0.222	0.155	[69]		76.25% C_3H_8	0.263-0.83	274.7-280.1	6	0.111	0.265	0.178	[65]
	95.3% C_2H_6	0.99-2.99	279.4-287.6	6	0.081	1.015	0.326	[69]		62.9% C_3H_8	0.27-0.945	274.5-428 .3	6	0.136	0.261	0.202	[65]
	82.3% C_2H_6	1.42-3.0	281.6-287.0	5	0.028	0.121	0.076	[69]		(100-0)% C_3H_8	0.78-3.37	275.15	17	0	0.206	0.044	[88]
	43.6% C_2H_6	1.289-2.434	277.6-283.2	3	0.010	0.059	0.032	[53]		(100-0)% C_3H_8	0.509-4.495	278.15	14	0.014	0.308	0.11	[88]
	9.6% C_2H_6	1.524-3.965	274.8-283.2	4	0.603	1.342	0.844	[53]	CH_4	1.4% iC_4H_{10}	6.79-62.23	288.6-302.1	7	0.237	1.0354	0.669	[57]
	5% C_2H_6	1.841-4.771	274.8-283.2	4	0.575	1.368	0.844	[53]		4.6% iC_4H_{10}	6.72-3.33	294.3-305.44	13	0.085	0.376	0.226	[57]
	2.9% C_2H_6	2.158-4.034	274.8-280.4	3	0.461	0.758	0.59	[53]		(36-99) iC_4H_{10}	0.505-10.07	274.8-2990.9	47	0.017	1.06	0.345	[89]
	2.2% C_2H_6	2.365-6.088	274.8-283.2	5	0.183	0.493	0.304	[53]		(0-100) iC_4H_{10}	0.128-3.09	274.35	21	0.043	0.856	0.205	[88]
	1.2% C_2H_6	2.2806-5.08	274.8-280.4	3	0.007	0.644	0.228	[53]		(0-100) iC_4H_{10}	0.78-3.37	274.83-275.1	17	0	0.094	0.044	[88]
	19.1% C_2H_6	7-68.57	288.8-304.1	8	0.013	0.202	0.164	[57]	CH_4	(10-85) $\%CO_2$	1.45-10.95	273.7-287.4	42	0.014	0.574	0.175	[85]
	5.4% C_2H_6	6.39-68.43	284.9-303	8	0.121	0.316	0.190	[57]		(0-100) $\%CO_2$	3.04-5.46	280.3	30	0.006	0.236	0.0849	[90]
CH_4	72.8 % N_2	7.9-28.49	273.2-288.0	8	0.011	0.633	0.434	[61]		96.54% CO_2	1.1- 4.8	273.5-282.3	9	0.053	0.352	0.332	[91]
	76.0 % N_2	8.62-35.96	273.2-289.1	7	0.592	0.061	0.341	[61]		(0-100) $\%CO_2$	2.0-5.0	277.2-283.56	40	0.032	1.44	0.306	[92]
	89.2 % N_2	12.55-28.79	273.2-283.2	6	0	0.662	0.121	[61]		(0-100) $\%CO_2$	0.774-2.527	271.2-278.05	12	0.161	0.847	0.48	[93]
	(0-100)% N_2	2.64-32.42	273.2-279.8	25	0.035	0.880	0.423	[61]	C_2H_6	(14.3-72) $\%C_3H_8$	0.5-2.02	273.1-283.3	60	0.004	1.22	0.397	[86]

	10.74 % N_2	2.99-10.1	273.2-285.3	8	0.051	0.111	0.071	[84]		(12.7-89.2) %CO_2	3.9-35.96	273.2-295.2	44	0.001	1.12	0.306	[61]
	12.7 % N_2	7.4-31.31	282.8-295.2	10	0.045	0.274	0.148	[61]		(0-100) %CO_2	2.64-32.42	273.2-279.8	25	0.001	0.881	0.42	[61]
	26.9 % N_2	3.9-24.33	273.2-294.4	6	0.593	1.12	0.411	[61]	**C_3H_8**	(0-100) %ibutane	0.101-0.171	272.1.272.2	13	0.049	0.413	0.33	[94]
CH_4	63.8%C_3H_8	0.272-0.687	274.8-280.4	3	0.008	0.140	0.076	[53]		(20.6-88.8) %ibutane	0.213-0.49	275.25-277.5	6	0.233	0.446	0.36	[95]
	28.8% C_3H_8	0.365-1.151	274.8-283.2	4	0.001	0.096	0.062	[53]	**CH_4+CO_2 + H_2S**								
	11.7% C_3H_8	0.552-1.558	274.8-283.2	4	0.003	0.053	0.038	[53]		87.6+7.40+4.95	1.045-8.22	274.2-290.2	9	0.088	0.897	0.348	[87]
	4.8% C_3H_8	0.814-2.227	274.8-283.2	4	0.010	0.124	0.049	[53]		82.4+10.7+6.78	1.11-8.024	276.2-291.2	12	0.101	0.380	0.251	[96]
	2.6% C_3H_8	1.151-3.013	274.8-283.2	4	0.088	0.153	0.133	[53]		82.91+7.1+9.93	1.192-7.91	278.2-293.2	9	0.038	0.466	0.282	[96]
	1.0% C_3H_8	1.627-4.358	274.8-283.1	5	0.021	0.079	0.056	[53]		77.7+7.3+14.98	0.646-7.91	277.2-295.7	9	0.034	0.752	0.252	[96]
	5.5% C_3H_8	7.41-62.23	293.1-304.9	6	0.044	1.07	0.785	[57]		75.4+6.81+17.7	0.95-8.68	282.2-297.2	11	0.087	0.718	0.290	[96]
	3.5% C_3H_8	6.93-68.98	290.5-304.4	9	0	1.64	0.951	[57]		66.38+7+26.62	0.582-8.08	281.2-299.7	9	0.065	0.878	0.383	[96]

The minimum error percentage, maximum error percentage, and AADT% are also provided in Table 3-5. Figures 3-5 to 3-7 illustrate a comparison between the experimental and calculated hydrate formation temperature for some binary systems. According to Table 3-5 and Figures 3-5 through 3-7, PC-SAFT is able to offer accurate hydrate formation data for the binary gas systems so that the extent of AADT% for 591 data points in 9 different systems utilized in this study is 0.302%. Furthermore, the maximum and minimum values of AADT% in all gas mixture are 1.64% and 0%, respectively. It can be concluded that the PC-SAFT equation of state is a proper EOS to obtain thermodynamic information/ conditions of hydrate for both pure gases and gaseous mixtures.

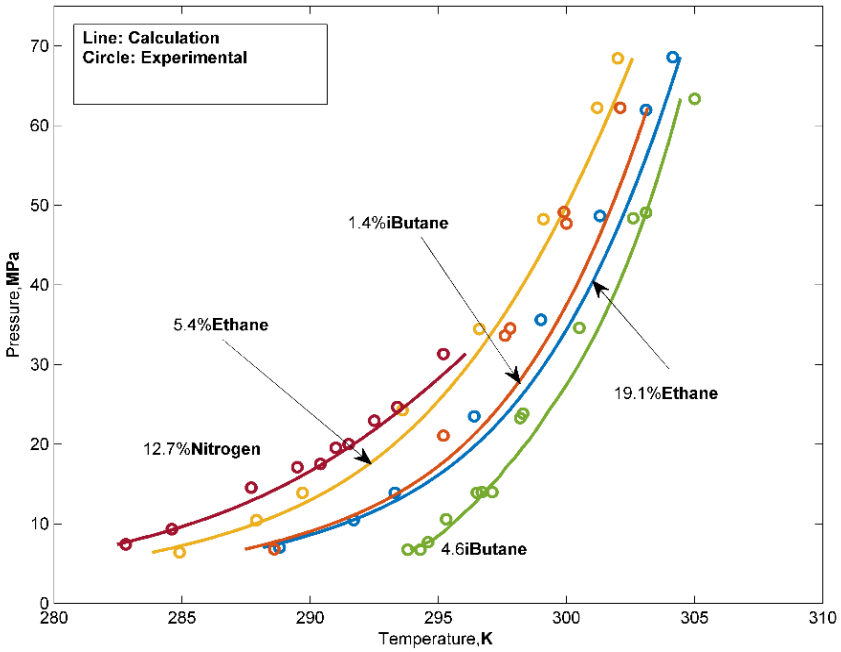

Figure 3-5: Experimental and calculated hydrate formation temperatures of CH_4 with C_2H_6[57], iC_4H_{10}[57], and N2 [84] for different weight fractions.

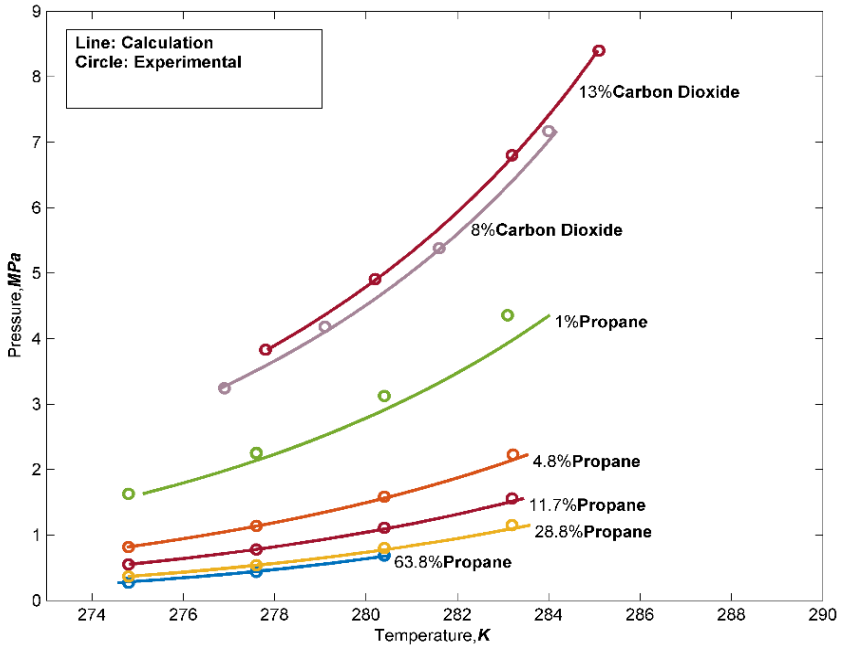

Figure 3-6: Experimental and calculated hydrate formation temperatures of CH_4 with CO_2 [85] and C_3H_8 [53] for various concentrations.

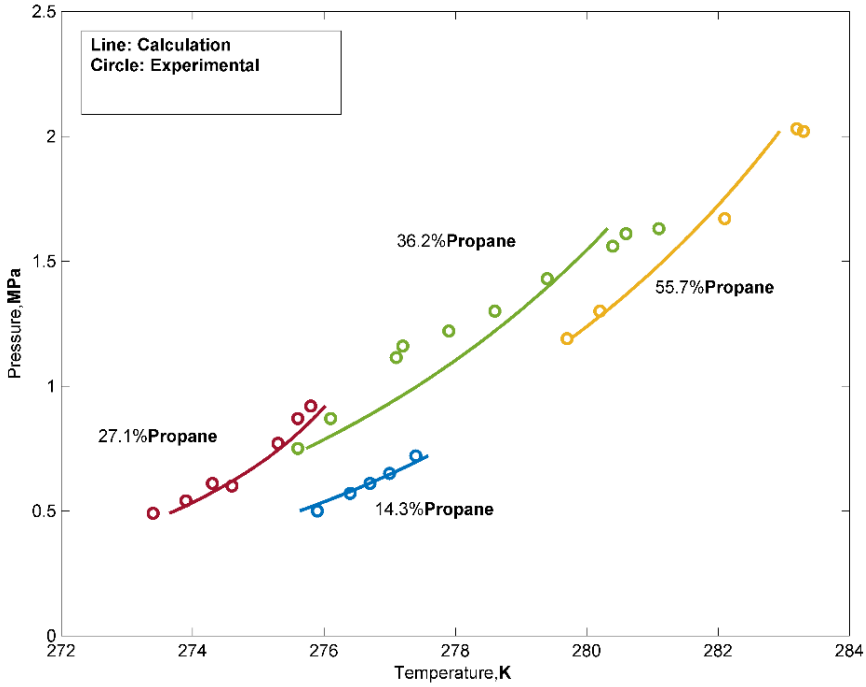

Figure 3-7: Experimental and calculated hydrate formation temperatures of C_2H_6 with C_3H_8 for different weight fractions of C_3H_8 [86].

There is one important point about Figure 3-5 that needs to be discussed here. Indeed, there are small and large cages in structure II of hydrates. It is clear that at high concentration/mole fraction of *i*-butane in the methane/*i*-butane mixtures, there are adequate number of *i*-butane molecules with a bigger size (compared to the methane molecules) that occupy large cages so that methane molecules are placed only in small cages. However, this molecule placement pattern does not occur when the mole fraction of *i*-butane in the mixture is small (e.g., 1.4%). Thus, the large cages of structure II are occupied by both CH_4 and *i*-C_4H_{10} for the cases with a small concentration of *i*-butane. On the other hand, the *i*-butane parameters were only used in our calculations to determine the difference in chemical potentials between ice and the empty hydrate lattices for the large cages ($\Delta\mu_w^\circ$) due to the assumption made in this study and lack of adequate information, which causes an error. Hence, a higher error in the prediction of hydrate

temperature is noticed for the mixture with a low concentration of *i*-butane, compared to the case having a greater mole fraction for *i*-butane.

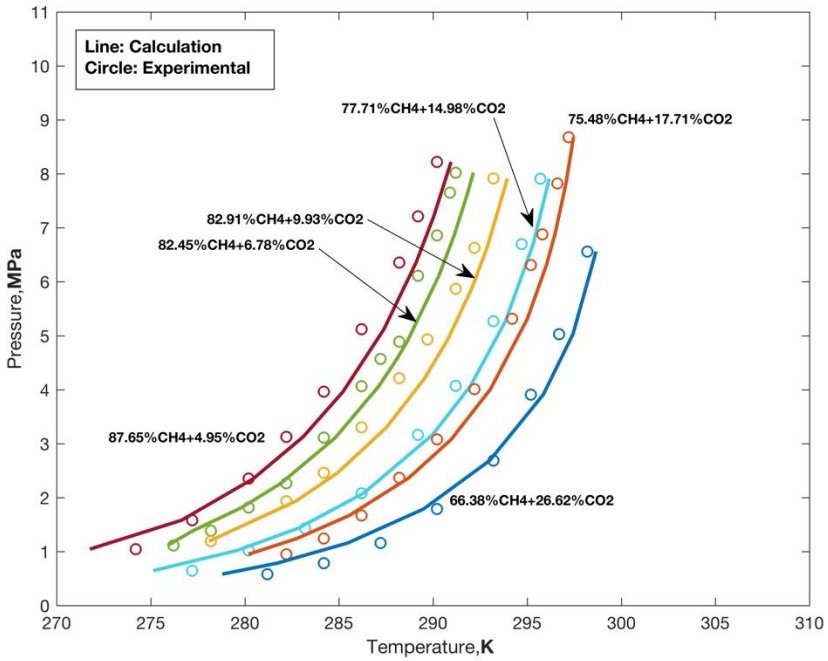

Figure 3-8: Experimental and calculated hydrate formation temperature of CH_4+CO_2 + H_2S for various concentrations of H_2S [87].

Figure 3-8 demonstrates the calculated and experimental hydrate formation conditions for one ternary system (methane + carbon dioxide + hydrogen sulfide) which can be a representative of a natural gas mixture or a sour gas stream. The selected data and binary interaction coefficients are given in Tables 3-2 and 3-3. The results imply that the overall AADT% for the ternary gas systems in this study is 0.295 % for 59 points in six different concentrations (see Table 3-5). It should be noted that the experimental error and possible errors in the extent of interaction forces can be the main factors for the observed deviation.

Table 3-6: Minimum and maximum error percentages and AADT% while estimating hydrate formation temperature in the presence of alcohols for pure gas systems.

Gas Phase	Liquid Phase	Range of P (MPa)	Range of T (K)	N_P	Min. Error	Max. Error	AADT %	Ref	Gas Phase	Liquid Phase	Range of P (MPa)	Range of T (K)	N_P	Min. Error	Max Error	AADT%	Ref.
CH_4	10%Methanol	4.378-19.30	274.2-287.0	5	0.023	0.213	0.145	[101]	C_3H_8	5% Methanol	0.234-0.468	272.1-274.8	5	0.022	0.179	0.098	[70]
	20%Methanol	3.516 -19.65	266.3-281.7	4	0.011	0.540	0.247	[101]		10.4%Methanol	0.185-0.434	268.3-271.8	6	0.14	0.251	0.207	[70]
	30%Methanol	3.985-18.70	261.1-274.7	4	0.226	0.426	0.279	[101]		10%Methanol	0.232-0.441	269.7-272.5	3	0.014	0.045	0.026	[102]
	40%Methanol	2.654-33.81	249.4-271.1	4	0.244	0.601	0.355	[101]		20%Methanol	0.112-0.37	260.3-265.3	3	0.083	0.234	0.172	[102]
	50%Methanol	6.819-21.07	251.4-259.7	4	0.514	1.342	0.635	[101]		30%Methanol	0.135-0.264	252.9-255.8	3	0.169	0.203	0.189	[102]
	60%Methanol	4.716-33.99	239.4-255.1	4	0.521	1.284	0.740	[101]		40%Methanol	0.121-0.175	242.5-244.3	3	0.287	0.460	0.369	[102]
	6% Methanol	3.48-5.94	273.9-279.5	5	0.003	0.016	0.014	[103]		5% Methanol	0.206-0.492	272.4-276.3	14	0.017	0.058	0.039	[104]
	10%Methanol	1.97-6.54	265.4-278.1	8	0.061	0.493	0.229	[103]		10%Methanol	0.209-0.463	269.3-272.8	13	0	0.030	0.012	[104]
	20%Methanol	3.06-6.88	265.4-273.3	5	0.123	0.742	0.498	[103]	C_3H_8	5% Ethanol	0.202-0.489	272.4-276.3	13	0	0.015	0.010	[104]
	10%Methanol	2.14-18.82	266.2-286.4	6	0.005	0.302	0.179	[70]		10% Ethanol	0.213-0.469	270.9-274.29	11	0.002	0.052	0.015	[104]
	20%Methanol	2.83-18.75	263.2-280.2	6	0.021	0.385	0.149	[70]		15% Ethanol	0.209-0.44	268.5-271.8	9	0.018	0.042	0.024	[104]
	4.2%Methanol	2.76-10.79	272-285.1	11	0.0866	0.374	0.237	[105]	C_3H_8	10% Glycerol	0.206-0.491	272.3-276.1	13	0.002	0.030	0.015	[104]
	10%Methanol	2.62-9.78	268.2-281.5	5	0.054	0.101	0.080	[105]		20% Glycerol	0.19-0.449	269.5-273.3	12	0.211	0.248	0.230	[104]
	20%Methanol	2.95-10.11	264.5-276.6	5	0.026	0.144	0.079	[105]	CO_2	10%Methanol	1.012-2.56	266.7-274.7	4	0.191	0.475	0.308	[106]
	35%Methanol	2.88-9.87	254.5-266.0	4	0.054	0.148	0.120	[105]		20%Methanol	0.9-3.16	260.3-270.7	4	0192	0.582	0.375	[106]
	50%Methanol	3.26-10.11	245.2-255.1	4	0.200	0.469	0.325	[105]		30%Methanol	0.893-3.82	253.8-265.5	4	0.266	0.558	0.415	[106]
CH_4	5% Ethanol	3.45-6.2	273.9-280.1	4	0.010	0.057	0.039	[107]		40%Methanol	1.385-2.913	250.2-256	4	0.399	0.521	0.473	[106]
	10% Ethanol	2.98-7.4	271.1-280.2	4	0.004	0.135	0.056	[107]		10%Methanol	1.35-3.72	269.3-277.3	7	0.003	0.198	0.116	[108]
CH_4	10 % Glycerol	2.72-14.8	272.2-288.5	7	0.067	0.166	0.120	[102]		20%Methanol	1.67-3.1	265.6-270.4	4	0.006	0.212	0.094	[108]
	40 % Glycerol	3.29-13.33	266.1-279	7	0.044	0163	0.084	[102]	CO_2	10%Ethanol	1.75 -3.42	273-278.2	6	0.007	0.178	0.089	[108]
	25% Glycerol	4.39-20.53	273.8-288.2	4	0.021	0.860	0.333	[109]		20% Ethanol	1.55-3.45	273-278.2	5	0.042	0.223	0.105	[108]
	50% Glycerol	4.53-20.53	264.2-276.2	4	0.379	1.025	0.650	[109]	CO_2	10% Glycerol	1.25-3.39	271.5-279.7	6	0.024	0.426	0.205	[70]
C_2H_6	10%Methanol	0.417-2.91	268.1-282.0	4	0	0.077	0.019	[110]		40% Glycerol	1.42-3.3	264.7-272.4	4	0.251	0.395	0.307	[70]
	20%Methanol	0.55-2.65	263.3-275.5	4	0	0.084	0.065	[110]		10% Glycerol	1.391-3.345	272.2-280.2	6	0.010	0.351	0.171	[111]
	20%Methanol	0.552-0.904	264.3-269.4	4	0.087	0.133	0.131	[112]		20% Glycerol	1.502-3.556	270.4-277.1	8	0.219	0.607	0.327	[111]
	30%Methanol	0.667-1.463	260.9-267.0	4	0.005	0.132	0.052	[112]		30% Glycerol	2.03 -2.981	270.1-273.2	5	0.026	0.144	0.075	[111]
C_2H_6	5% Ethanol	0.59-1.34	273.6-280.0	4	0.008	0.171	0.038	[107]	H_2S	5% Methanol	0.1-0.9	271.1-291.7	7	0.014	0.551	0.170	[113]

	10% Ethanol	0.81-2.23	274.4-282.0	4	0.033	0.091	0.049	[107]	15%Methanol	0.18-1.5	269.4-291.5	8	0.077	0.689	0.344	[113]
C_2H_6	10% Glycerol	1.151-3.013	274.8-283.2	4	0.088	0.153	0.133	[102]	5% Ethanol	0.13-0.81	273.4-291	6	0.003	1.003	0.460	[113]
	40% Glycerol	1.627-4.358	274.8-283.1	5	0.021	0.079	0.056	[102]	10% Ethanol	0.13-0.81	272.6-289	6	0.015	0.689	0.278	[113]

Table 3-6 provides the hydrate formation conditions of different pure gas systems in the presence of methanol, ethanol, and glycerol as inhibitors. As one can see, the results of this study exhibit a good agreement with the available literature data. The overall absolute deviation in temperature for systems including pure gases and alcohols is 0.183% based on 376 data points, while the magnitudes of overall error percentage are 0.478 and 0.865 for the research works conducted by Javanmardi et al. [97] and Zuo et al. [98], respectively. Figures 3-9 to 3-11 provide the experimental and predicted hydrate formation temperature for the single gas hydrate systems where methanol, ethanol, and glycerol are present.

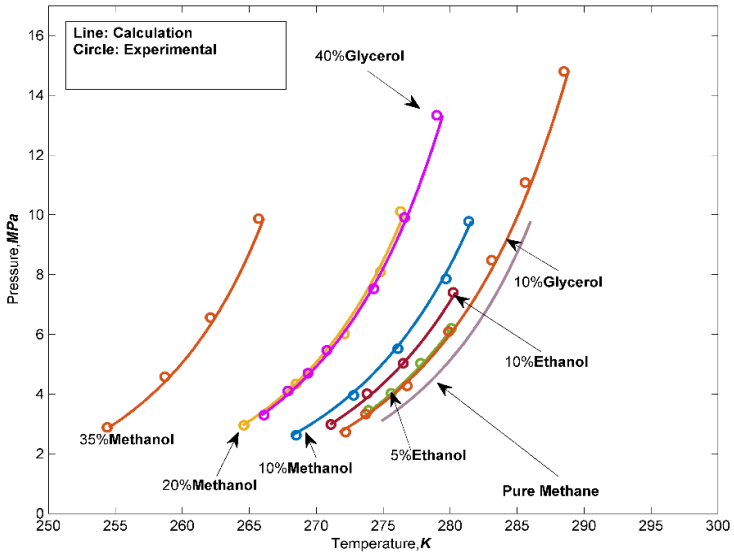

Figure 3-9: Experimental and calculated hydrate formation temperature of the CH_4+alcohols with different compositions [112].

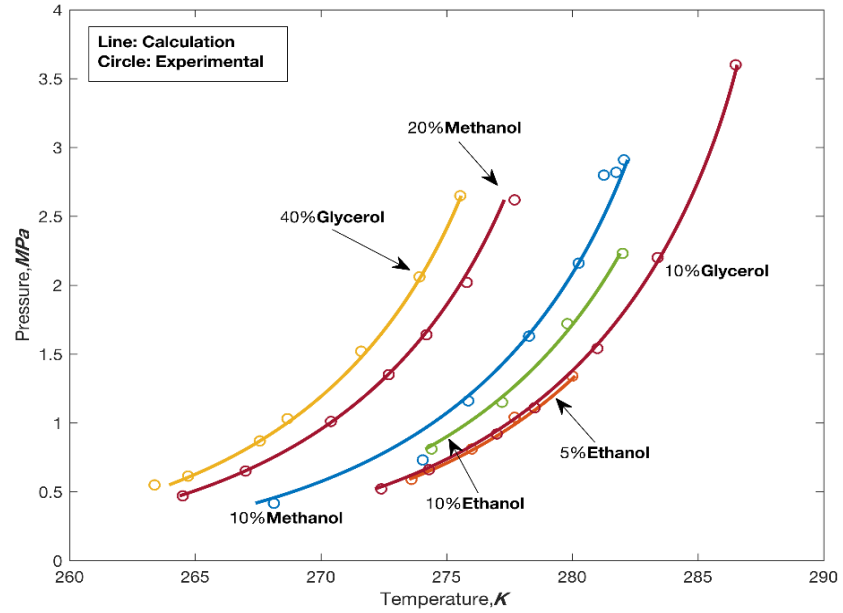

Figure 3-10: Experimental and calculated hydrate formation temperature of C_2H_6 + alcohols systems with different compositions [102, 110].

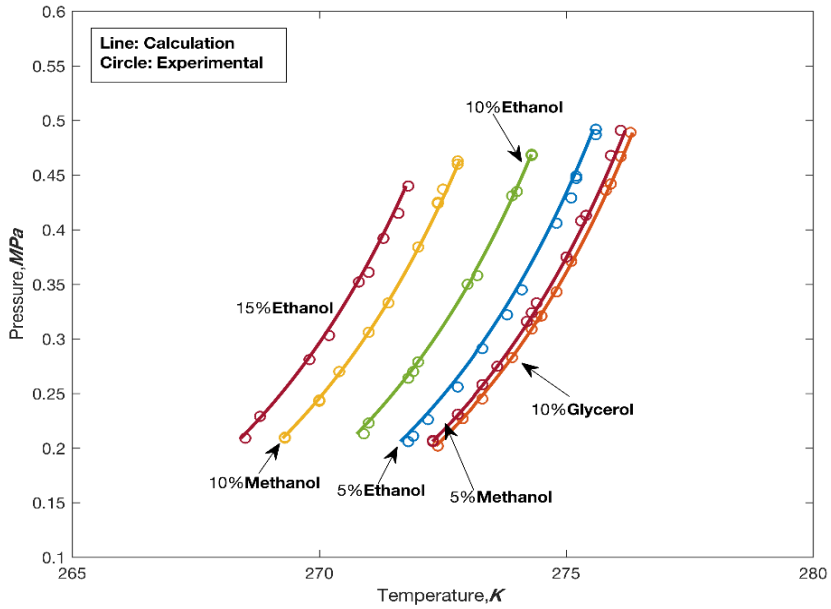

Figure 3-11: Experimental and predicted hydrate formation temperature of C_3H_8 + alcohols with various concentrations [104].

As depicted in Figures 3-9 to 3-11, the estimated hydrate conditions are very close to the experimental data at various compositions. It is important to note that the model calculations at some high pressures or/and high concentrations of alcohols show higher deviations which can be related to unsaturation occurrence of data, errors of experimental apparatus, and uncertainties of interaction parameters. The outcomes attained from the proposed model for single electrolyte solutions and pure gas hydrate systems are tabulated in Table 3-7. The overall AADT% for single electrolyte solutions is 0.1% using 93 different systems, exhibiting a much better accuracy compared to previous works [99,100]. A very good agreement between the experimental data and estimated values confirms this claim.

Table 3-7: The magnitudes of the minimum error and maximum error percentages and AADT% while estimating hydrate formation temperature in the presence of salts for pure gas systems.

Gas Phase	Liquid Phase	Range of P (MPa)	Range of T (K)	N_P	Min. Error	Max. Error	AADT%	Ref	Gas Phase	Liquid Phase	Range of P (MPa)	Range of T (K)	N_P	Min. Error	Max Error	AADT%	Ref
CH_4	3.936% NaCl	2.69-7.55	268.3-278.0	6	0.010	0.066	0.041	[114]		10.5 % $MgCl_2$	1.4-2.29	276.3-280.51	5	0.059	0.325	0.167	[115]
	7.785% NaCl	2.94-11.0	261.85-272.8	7	0.007	0.336	0.233	[114]	C_3H_8	5% NaCl	0.2-0.4	271.5-275.1	4	0.002	0.09	0.066	[116]
	5.976% NaCl	2.39-8.5	263.35-268.6	5	0.041	0.205	0.117	[114]		3.1% NaCl	0.221-0.414	273.1-275.95	5	0.008	0.026	0.013	[117]
	8.909% NaCl	4.78-9.55	263.25-269.2	5	0.079	0.205	0.174	[114]		10% NaCl	0.241-0.531	270.05-272.8	5	0.022	0.228	0.103	[117]
	3% NaCl	2.754-4.30	272.69-277.2	6	0.006	0.0148	0.011	[118]		15% NaCl	0.221-0.455	266.15-268.6	5	0.026	0.135	0.123	[117]
	15% NaCl	3.93-26.5	269.4-285.05	3	0.007	0.055	0.0382	[118]		20% NaCl	0.2-0.331	266.15-268.6	4	0.002	0.099	0.0432	[117]
	20% NaCl	5.02-15.38	268.55-277.2	3	0.039	0.291	0.138	[118]		3% NaCl	0.22-0.506	273-276.6	7	0.039	0.081	0.064	[119]
	3.986% NaCl	4.5-7.57	272.7-277.7	3	0.049	0.094	0.074	[120]		5% NaCl	0.194-0.51	271.3-275.6	8	0.020	0.121	0.081	[119]
	5.978% NaCl	4.23-8.57	269.2-275.1	3	0.128	0.441	0.243	[120]		10% NaCl	0.19-0.442	268.9-272.1	6	0.005	0.126	0.081	[119]
	2.001% NaCl	6.6-67.81	280.6-299.06	11	0.081	0.218	0.147	[121]	C_3H_8	5% KCl	0.18-0.46	272-276.2	4	0.024	0.044	0.050	[116]
	3.611% NaCl	7.51-71.56	279.1-296.03	11	0.038	0.385	0.228	[121]		10% KCl	0.228-0.42	271.05-273.4	5	0.096	0.223	0.170	[117]
	5.994% NaCl	7.92-70.56	274.4-291	10	0.015	0.289	0.136	[121]		15% KCl	0.22-0.393	269.05-271.2	5	0.057	0.211	0.221	[117]
	8.014% NaCl	7.85-71.3	270.6-285.76	10	0.012	0.299	0.142	[121]		20% KCl	0.228-0.33	266.45-267.5	5	0.089	0.339	0.149	[117]
	5% NaCl	3.58-9.6	274.2-283.6	5	0.029	0.162	0.068	[122]		5.02% KCl	0.166-0.40	271.6-275.14	3	0.21	0.254	0.245	[123]
CH_4	15% KCl	6.24-17.28	276.45-284.9	3	0.016	0.064	0.039	[124]		10.03% KCl	0.166-0.43	269.44-273.7	3	0.112	0.189	0.146	[123]
	5% KCl	2.71-8.96	271.6-283.2	6	0.043	0.136	0.084	[116]	C_3H_8	5% $CaCl_2$	0.18-0.46	271.8-276.2	4	0.0083	0.104	0.043	[116]
	10% KCl	2.78-8.82	270.1-281.5	7	0.048	0.227	0.150	[116]		7.5% $CaCl_2$	0.234-0.42	271.55-274.1	5	0.009	0.442	0.0282	[117]

CH_4	10 % $MgCl_2$	4.32-24.78	274.28-287.3	4	0.151	0.274	0.229	[124]
	1 % $MgCl_2$	5.83-22.65	280.89-292.3	5	0.005	0.050	0.028	[125]
	5 % $MgCl_2$	3.46-21.52	273.9-290.07	6	0.008	0.427	0.0204	[125]
	10 % $MgCl_2$	6.24-19.42	276.3-285.7	5	0.197	0.234	0.216	[125]
	15 % $MgCl_2$	5.83-19.68	270.4-280.2	5	0.085	0.143	0.125	[125]
	3 % $MgCl_2$	2.91-11.84	272.85-280.2	6	0.015	0.114	0.079	[126]
	5 % $MgCl_2$	2.82-10.56	271.25-284.1	5	0.139	0.280	0.224	[126]
	10 % $MgCl_2$	3.76-12.95	272.35-282.6	7	0.073	0.367	0.277	[126]
	15 % $MgCl_2$	5.24-12.26	270.75-278.4	4	0.100	0.516	0.277	[126]
	5% $MgCl_2$	3.3-10.11	273.3-283.7	5	0.068	0.151	0.129	[129]
	10% $MgCl_2$	4.17-11.9	272.9-282	5	0.102	0.256	0.235	[129]
CH_4	0.84% $CaCl_2$	6.05-10.12	279.9-284.4	5	0.024	0.148	0.130	[120]
	1.7% $CaCl_2$	6.88-10.22	278.4-282.3	4	0.15	0.327	0.212	[120]
	2.68% $CaCl_2$	4.92-90.7	273.5-278.8	4	0	0.305	0.115	[120]
	4.62% $CaCl_2$	6.26-9.8	264.2-268.41	5	0.046	0.282	0.143	[120]
	5.32% $CaCl_2$	6.4-9.8	259.9-264	4	0.025	0.300	0.163	[120]
	5% $CaCl_2$	2.81-8.53	272-283	6	0.010	0.132	0.088	[116]
	15% $CaCl_2$	3.39-9.01	268-277.4	6	0.095	0.230	0.158	[116]
	17.5% $CaCl_2$	3.39-22.93	265.4-282.2	6	0.200	0.337	0.270	[125]
	10% $CaCl_2$	4.5-7.57	272.7-277.7	3	0.23	0.38	0.043	[120]
	20% $CaCl_2$	4.23-8.57	269.2-275.1	3	0.100	0.318	0.175	[120]
C_2H_6	10% NaCl	0.883-2.16	273.7-280.4	5	0.003	0.197	0.111	[128]
	15% NaCl	1.082-2.15	272.7-277.1	3	0.110	0.355	0.203	[128]
C_2H_6	5% KCl	0.47-1.85	271.4-282.3	6	0.023	0.340	0.184	[116]
	10% KCl	0.54-2.9	272.2-284.7	7	0.019	0.631	0.204	[116]
C_2H_6	5% $CaCl_2$	0.44-2.09	271.5-283.3	6	0.126	0.436	0.266	[116]
	15% $CaCl_2$	0.81-2.52	270-278.5	5	0.098	0.280	0.153	[116]
C_2H_6	5 % $MgCl_2$	1.12-2.47	280.0-286	5	0.090	0.119	0.197	[115]
	6.1% $MgCl_2$	1.17-2.37	279.45-285.5	5	0.004	0.213	0.084	[115]
	7.2% $MgCl_2$	1.38-2.55	279.8-285.08	5	0.019	0.275	0.178	[115]
	11.3% $CaCl_2$	0.248-0.37	269.65-271.3	4	0.174	0.251	0.227	[117]
	15.2% $CaCl_2$	0.234-0.35	266.3-267.95	5	0.007	0.014	0.0576	[117]
	5.02% $CaCl_2$	0.181-0.47	271.31-275.6	3	0.168	0.195	0.187	[117]
	10% $CaCl_2$	0.162-0.43	268.1-272.02	3	0.246	0.335	0.277	[123]
	15% $CaCl_2$	0.133-0.34	263.02-267.3	3	0.172	0.18	0.177	[123]
CO_2	5%NaCl	1.37-3.73	271.8-280.2	4	0.100	0.343	0.223	[116]
	10%NaCl	1.15-3.701	268.75-277.3	8	0.0022	0.647	0.299	[127]
	15.2%NaCl	1.39-3.142	267.45-275.4	5	0.158	0.461	0..338	[127]
	10%NaCl	2.15-3.227	273.2-276.1	4	0.005	0.224	0.109	[128]
	20%NaCl	1.51-3.116	263.2-268.8	4	0.003	0.156	0.078	[128]
	5%NaCl	1.30-3.004	271.18-277.9	4	0.156	0.502	0.278	[130]
	20.3%NaCl	0.606-2.63	263.29-266.8	3	0.315	0.639	0.523	[130]
	3%NaCl	1.060-2.63	263.29-266.8	4	0.315	0.639	0.523	[130]
	15%NaCl	1.212-3.23	265.3-273.01	4	0.062	0.241	0.161	[130]
CO_2	10%KCl	2.01-3.35	273.8-278	4	0.004	0.111	0.59	[116]
	10%KCl	1.937-3.61	273.5-278.4	4	0.011	0.24	0.165	[128]
	10%KCl	1.13-3.485	269.02-277.8	4	0.049	0.316	0.200	[130]
	15%KCl	1.606-2.63	263.29-266.8	3	0.091	0.232	0.176	[130]
	5%KCl	1.325-3.9	270.97-281.5	7	0.098	0.399	0.240	[130]
	3%KCl	1.325-3.83	272.6-281.09	6	0.015	0.395	0.171	[130]
CO_2	15% $CaCl_2$	2.1-3.6	270.2-274.7	4	0.003	0.034	0.019	[116]
	10%$CaCl_2$	0.94-3.65	267.4-278.05	7	0.032	0.65	0.241	[127]
	3%$CaCl_2$	1.82-3.702	275.52-280.8	4	0.006	0.326	0.149	[130]
H_2S	5%NaCl	0.15-1.91	273.7-297.4	7	0.02	0.700	0.211	[113]
	10%NaCl	0.18-1.8	274-295	7	0.031	0.334	0.146	[105]
H_2S	5%KCl	0.15-0.79	274.1-291.4	6	0.020	0.25	0.165	[105]
	10%KCl	0.15-0.82	273.29-290.2	6	0.008	0.18	0.07	[105]
H_2S	5%$CaCl_2$	0.11-0.95	272.2-293.2	7	0.014	0.312	0.122	[105]
	15%$CaCl_2$	0.22-1.98	273.1-293	7	0.132	0.378	0.247	[105]

Figures 3-12 and 3-13 illustrate the experimental and calculated hydrate formation temperature in the presences of a single salt for pure gas systems. It is found that the developed model is able to satisfactorily forecast the hydrate formation temperature at high concentrations of salts within a wide range of pressure and composition.

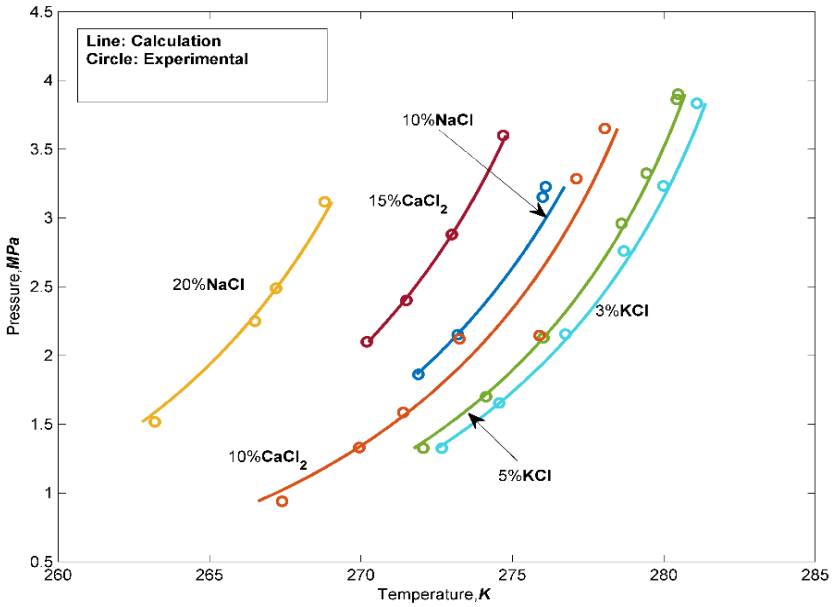

Figure 3-12: Experimental and calculated hydrate formation temperature of CO_2 + salts with different compositions [116, 127, 128, 131].

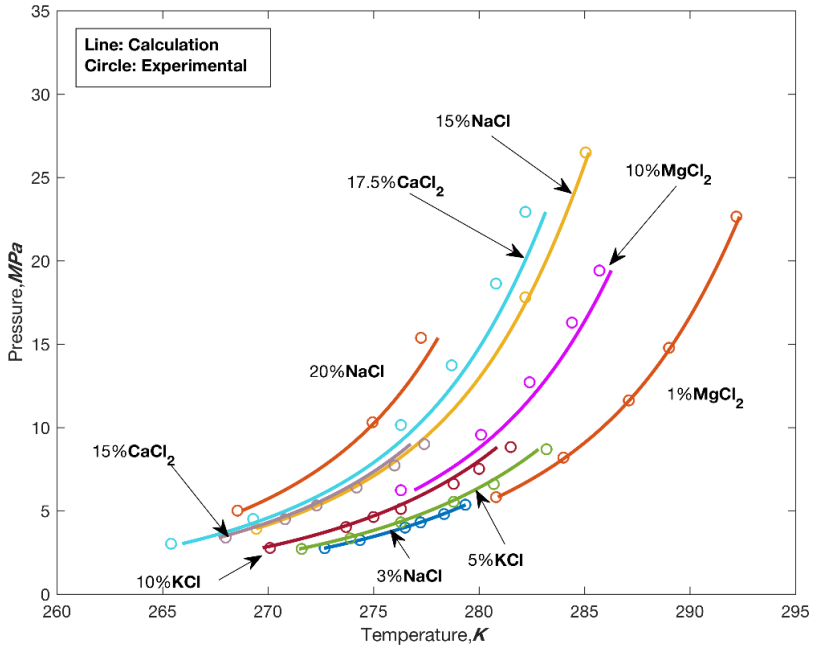

Figure 3-13: Experimental and calculated hydrate formation temperature of CH_4 + salts with various compositions [107, 118, 122, 125].

In addition, the average absolute percent deviation in hydrate temperature for mixture of salts, alcohols, and pure gas systems is determined as shown in Table 3-8 and Figure 3-14, based on the comparison of the calculated values and experimental data. There is a good match between the calculated values and real data, implying again higher reliability and accuracy of the model developed in this study, compared to the previous research studies [100, 132,133].

Table 3-8: Minimum error and maximum error percentages and AADT% while estimating hydrate formation temperature in the presence of salts and alcohols for pure gas systems.

Gas +Liquid Phase	Range of P (MPa)	Range of T (K)	N_p	Min. Error	Max. Error	AADT%	Ref	Gas+ Liquid Phase	Range of P (MPa)	Range of T (K)	N_p	Min. Error	Max Error	AADT%	Ref
CH_4+								CO_2+							
2%NaCl+10%Methanol	2.05-16.05	262.3-281.5	8	0.188	0.550	0.361	[139]	10%KCl+5%Methanol	0.91-2.9	265.33-274.71	8	0.008	0.633	0.351	[131]
2%NaCl+20%Methanol	2.05-14.05	258.4-274.9	6	0.057	0.711	0.572	[139]	15% $CaCl_2$+5%Methanol	1.328-2.809	265.23-274.19	6	0.387	0.695	0.494	[131]
2%NaCl+30%Methanol	4.05-16.05	258-268.5	7	0.036	0.418	0.230	[139]	10%NaCl+10%Methanol	1.184-2.872	264-270.83	7	0.044	0.25	0.167	[131]
2%NaCl+40%Methanol	4.05-16.05	249.9-261.2	7	0.223	0.418	0.314	[139]	10%KCl+10%Methanol	1.248-2.767	265.58-271.85	7	0.078	0.192	0.151	[131]
3%NaCl+30%Methanol	13.99-25.64	269.3-274.35	3	0.010	0.117	0.079	[140]	10% $CaCl_2$+10%Methanol	1.137-2.552	264.72-270.93	3	0.064	0.246	0.180	[131]

7%KCl+9%Methanol	7.446-28.88	275.95-286.35	3	0.008	0.845	0.434	[140]	5% $CaCl_2$+15%Methanol	1.243-2.73	264.76-270.83	3	0.087	0.309	0.167	[131]
10%$CaCl_2$+14%Methanol	11.85-26.07	274.05-280.35	3	0.038	0.355	0.150	[140]	5%NaCl+15%Methanol	1.16-2.809	264.72-274.19	3	0.0	0.838	0.348	[131]
8%NaCl+9%Methanol	7.826-26.33	273.85-283.45	3	0.037	0.355	0.244	[140]	5%NaCl+5%Methanol	1.48-3.038	270.63-276.85	3	0.082	0.226	0.144	[131]
10%NaCl+20%Methanol	5.11-10.97	253.9-260.1	5	0.236	0.540	0.424	[129]	**H_2S+**							
10%NaCl+15%Methanol	4.43-11.41	266.2-274.4	6	0.013	0.230	0.089	[129]	10%NaCl+10%Methanol	0.42-1.073	276.93-285.82	6	0.0342	0.448	0.245	[141]
5%NaCl+10%Methanol	4.88-8.73	272.1-277.5	4	0.294	0.438	0.348	[129]	15%NaCl+5%Methanol	0.441-0.95	278.4-284.92	4	0.104	0.282	0.173	[141]
CO_2+								5%NaCl+15%Methanol	0.41-0.95	278.99-285.62	3	0.005	0.149	0.1409	[141]
5%NaCl+10%Methanol	1.22-2.51	266.3-272.5	3	0.017	0.092	0.066	[106]	10%CaCl2+10%Methanol	0.412-0.879	278.99-285.62	3	0.024	0.182	0.118	[141]
15%NaCl+5%Methanol	1.271-2.707	263.39-269.2	3	0.0	0.246	0.129	[131]								

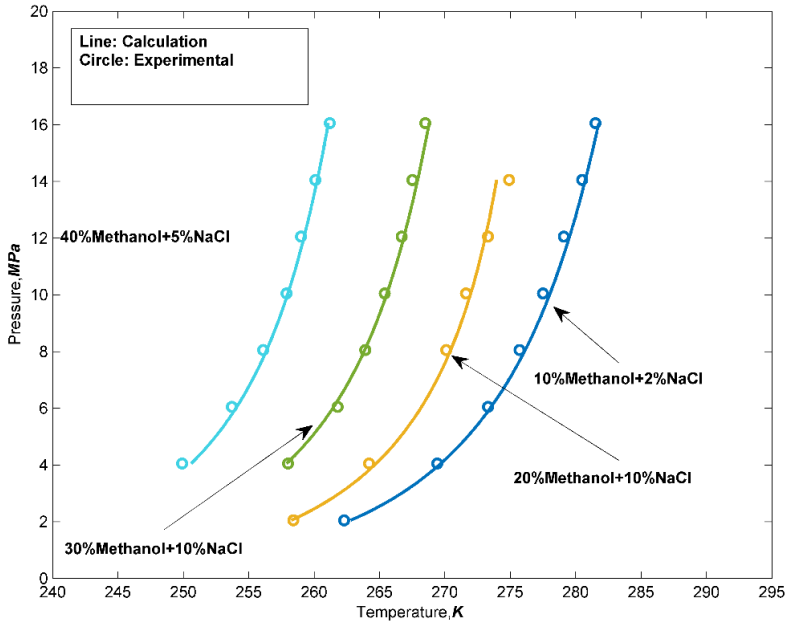

Figure 3- 14: Experimental and calculated hydrate formation temperature of CH_4 +mixture of methanol and salts with different concentrations [139].

At the end, this model is employed to determine the hydrate formation temperature for mixtures of natural gases in the presence of both salts and alcohols in the aqueous phase. Table 3-9 presents the modeling results of the hydrate formation condition for various gases (methane, ethane, propane, and carbon dioxide) where different concentrations of methanol and salts are examined.

Table 3-9: Minimum error and maximum error percentages and AADT% while estimating hydrate formation temperature in the presence of salts and alcohols for different gas mixtures.

Gas +Liquid Phase	Range of P (MPa)	Range of T (K)	N_p	Minimum Error	Maximum Error	AADT%	Ref.
80%CH_4+ 20%CO_2							
10%KCl+5%Methanol	2.172-9.705	267.58-280.42	3	0.004	0.04	0.101	[142]
10%$CaCl_2$+5%Methanol	266.51-280.35	2.211-10.348	3	0.020	0.24	0.017	[142]
15%NaCl+5%Methanol	2.151-9.371	262.37-274.85	3	0.025	0.064	0.043	[142]
5%NaCl+5%Methanol+ l5%KCl+5%$CaCl_2$	2.136-9.048	263.58-276.09	3	0.059	0.149	0.111	[142]
15%$CaCl_2$+5%Methanol	2.156-9.244	262.24-274.8	3	0.006	0.078	0.039	[142]
10%NaCl+10%Methanol	2.063-8.574	262.15-275.19	3	0.041	0.135	0.097	[142]
5%NaCl+5%Methanol	2.14-9.682	268.29-291.91	3	0.023	0.142	0.079	[142]
10%NaCl+10%Methanol	2.03-9.361	262.25-276.1	3	0.018	0.303	0.160	[142]
50%CH_4+ 50%CO_2							
5%NaCl+15%Methanol	2.564-6.888	266.08-274.12	3	0.009	0.15	0.078	[142]
10%NaCl+10%Methanol	2.153-6.785	264.46-274	3	0.028	0.142	0.086	[142]
78%CH_4+ 20%CO_2+ 2%Propane							
5%NaCl+5%Methanol	2.672-8.49	277.5-285.65	3	0.008	0.226	0.110	[143]
10%NaCl+10%Methanol	3.853-9.744	274.78-280.09	3	0.082	0.144	0.104	[143]
5%$CaCl_2$+5%Methanol	2.51-8.88	277.31-285.94	3	0.035	0.235	0.129	[143]
5%NaCl+5%KCL+ 10%Methanol	3.164-8.057	274.09-280.12	3	0.047	0.129	0.095	[143]

As it is clear, there is a very good agreement between the model estimations and real data. It is also concluded that the current model exhibits a better predictive performance in comparison with the models introduced in previous research investigations [97, 134]. Figure 3-15 illustrates the calculated results versus the experimental data for a part of the data points. It is expected that high solubility of hydrogen sulfide and carbon dioxide in the aqueous phase appreciably affects the water activity. Thus, the solubility is considered in the modeling strategy to improve the calculation accuracy while determining the water activity.

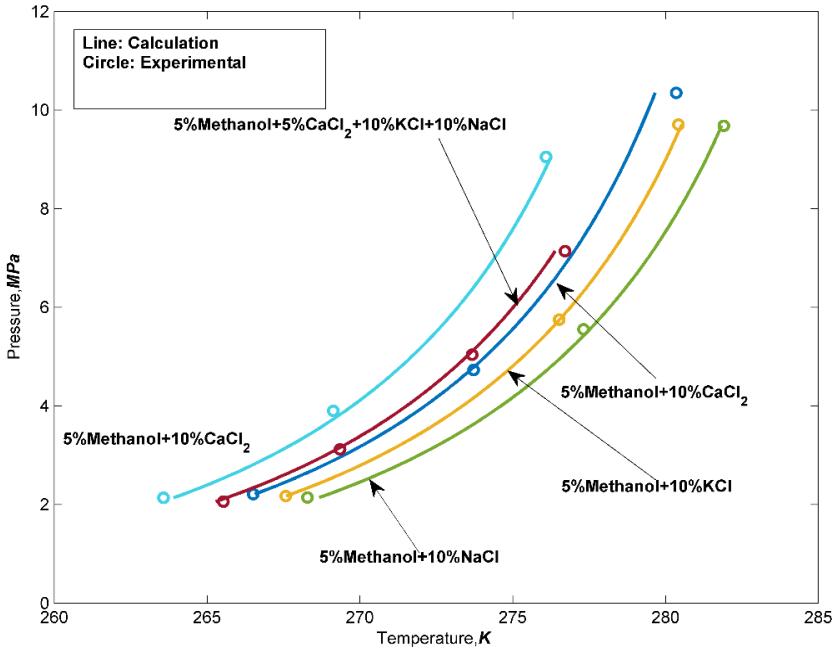

Figure 3-15: Experimental and calculated hydrate formation temperature of 80% CH_4 + 20% CO_2 + salts and alcohols with different concentrations [131].

In Figure 9, we also demonstrate the effect of inhibitors on methane hydrate condition where the hydrate formation condition of methane + pure water system is compared to that of the same gas system in the presence of the inhibitors. It implies that the hydrate formation condition moves to the left side of the P-T diagram to achieve a higher pressure/ lower temperature in comparison with the methane and pure water systems. Thus, the presence of inhibitors in the aqueous solution can change the hydrate formation condition. In other words, an increase in the inhibitor molality causes an increase in the equilibrium pressure at the same temperature. To provide more details and guidelines for researchers in this area, a series of experimental data and modeling results related to the water content or/and methane concentration extent (used for activity calculation) are listed in the Supporting Information (see Tables S-6 and S-7). A very good agreement is noticed between the modeling results and real

data for the methane solubility in the water phase, again confirming the reliability of the thermodynamic modeling approach in this research study.

In this work, the magnitude of association Z for the gas phase is very small due to the weak association effect in the gas phase. To prove this claim and attain more accurate results, the association term is considered in the modeling approach to calculate the compressibility factor and the association Helmholtz energy of the mixture. According to the results, this phenomenon shows minor impact on the gas compressibility factor. More information can be found in the Supporting Information, particularly Equation (S-27) and Equation (S-44). It is important to note that the association term is more important in the liquid phase (compared to the gas phase) where water and alcohols are present in the mixture.

To demonstrate the impact of the association terms, a comparison is made where the hydrate formation temperature is obtained for two different cases (Case 1 with association terms and Case 2 without association terms). The results presented to address this aspect are given in the Supporting Information. As seen in this document (Table S-8), Case 1 offers the predictions with a higher precision (or lower AADT%), compared to Case 2.

To further evaluate the extent of accuracy of the current study in comparison to other EOSs, the average absolute percent deviation in temperature (AADT%) of this thermodynamic work is compared to that of three previous studies including Du et al. [135], Khosravani et al. [82], and Delavar et al. [78] (see Table 3-10). Du et al. [135] utilized a modified version of Peng-Robinson (PR) EOS model based on Mollerup's random-nonrandom (RNR) theory to determine the vapor-liquid equilibria of strongly polar methanol-water-gas systems. In the another study, Khosravani et al. [82] employed the Stryjek and Vera modification of Peng–Robinson (PRSV2) equation of state and the linear function of binary interactions as a function

of temperature to describe the phase behavior of gas hydrates. In addition, Delavar et al. [78] calculated the phase equilibrium conditions of gas hydrates by using the GE-EOS and UNIQUAC activity coefficient models. As seen in Table 3-10, the phase equilibria model introduced in this study offers more accurate results in most cases so that there is a better match between the real data and predictions (e.g., lower AADT%), compared to the previous studies. The greater accuracy and reliability of the proposed modeling approach are mainly noticed at high concentrations of methanol.

Table 3-10: Comparison of the results of this study and previous hydrate models corresponding to the hydrate formation conditions for gas mixtures and alcohols/gas systems.

Gas	Inhibitor	P range (MPa)	Temp range (K)	Du et al. [135]	Khosravani et al.[82]	Delavar et al. [78]	Edgar et al.[136]	Li et al.[137]	Jiang et al.[138]	This work (AADP%)	This work (AADT%)	N_P*	Ref.
				(AADT%)			(AADP%)						
CH_4	10% Methanol	2.14–18.82	266–286.4	0.12	0.118	-	8.9	1.87	-	2.324	0.179	6	[70]
CH_4	20% Methanol	5.7–18.8	270–280	0.50	0.086	-	-	4.3	-	2.721	0.149	4	[70]
CH_4	4.2% Methanol	2.76–10.79	272.0–285.1	-	-	0.122	-	-	-	3.462	0.237	11	[105]
CH_4	10% Methanol	2.62-9.78	268.5-281.5	-	-	0.224	-	-	-	3.377	0.080	5	[105]
CH_4	20% Methanol	2.95-10.11	264.5-276.6	-	-	0.142	-		-	1.325	0.079	5	[105]
CH_4	25% Glycerol	4.39-20.53	273.8-286.2	-	-	-	-	0.36	-	4.02	0.333	4	[109]
CH_4	50% Glycerol	4.53-20.53	264.2-276.2	-	-	-	-	15.9	-	3.32	0.0935	4	[109]
C_3H_8	5% Methanol	0.23–0.46	272.1–274.8	0.42	0.142	-	9.4	9.4	-	2.761	0.098	8	[70]
C_3H_8	10.4%Methanol	0.185-0.46	268.3–271.8	0.56	0.051	-	12	-	-	3.413	0.207	6	[70]
C_2H_6	10% Methanol	0.417-2.91	268.1-282.0	-	0.064	0.128	6.8	-	-	2.791	0.019	4	[110]
C_2H_6	20% Methanol	0.55-2.65	263.5-274.1	-	0.072	0.087	24	-	-	3.621	0.065	4	[110]
H_2S	5% Methanol	0.1-0.9	271.1-291.7	-	-	0.178	-	-	-	4.281	0.17	7	[113]
H_2S	15% Methanol	0.18-1.5	269.4-291.5	-	-	0.448	-	-	-	1.892	0.344	8	[113]
CO_2	10% Glycerol	1.391-3.34	272.2-280.2	-	-	0.287	-	0.35	-	1.095	0.171	6	[111]
CO_2	20% Glycerol	1.502-3.55	270.4-277.1	-	-	-	-	2.32	-	2.645	0.327	8	[111]
CO_2	30% Glycerol	2.03 -2.98	270.1-273.2	-	-	-	-	2.74	-	2.874	0.075	5	[111]
CH_4	95.3% Ethane	0.99-2.99	279.4-287.6	-	-	-	-	-	4.02	3.7310	0.326	6	[69]
CH_4	82.3% Ethane	1.42-3.0	281.6-287.0	-	-	-	-	-	2.81	2.0337	0.076	5	[69]
CH_4	43.6% Ethane	1.289-2.434	277.6-283.2	-	-	-	-	-	4.65	1.0837	0.032	3	[53]
CH_4	19.1% Ethane	7-68.57	288.8-304.1	-	-	-	-	-	8.11	5.6887	0.164	8	[57]
CH_4	63.8% Propane	0.272-0.687	274.8-280.4	-	-	-	-	-	3.17	3.475	0.076	3	[53]
CH_4	28.8% Propane	0.365-1.151	274.8-283.2	-	-	-	-	-	0.91	0.8764	0.062	4	[53]
CH_4	4.8% Propane	0.814-2.227	274.8-283.2	-	-	-	-	-	0.30	1.051	0.049	4	[53]
CH_4	71.4% iButane	0.208-0.786	273.9.282.7	-	-	-	-	-	3.06	2.935	0.077	5	[89]
CH_4	84.8% iButane	0.304-2.03	274-288.9	-	-	-	-	-	5.99	3.032	0.078	4	[89]
CH_4	97.5% iButane	0.703-10.07	274.4-293.6	-	-	-	-	-	6.61	2.901	0.657	8	[89]

* Np refers to the number of points.

A comparison is also made between the modeling outputs of this study and other three research works; namely, Edgar et al. [136], Li et al. [137], and Jiang et al. [138] in terms of the average absolute percent deviation in pressure (AADP%). For instance, Edgar et al. [136] used the

cubic two-state (CTS) EOS to obtain the hydrate formation conditions of gas systems in the presence of methanol. Jiang et al.[138] and Li et al. [137] also investigated the gas hydrate formation conditions by employing the SAFT EOS for the systems containing pure gases and the gaseous mixtures in the presence of methanol. Comparing the magnitudes of AADP again confirms the effectiveness of PC-SAFT EOS coupled with an appropriate activity coefficient model such as UNIQUAC to forecast the hydrate formation pressure. According to Table 3-10, it can be concluded that the proposed thermodynamic model exhibits a better predictive performance than almost all other models so that more precise values for hydrate formation pressures of the pure single gas, gas mixtures, and gas systems in the presence of inhibitors such as NaCl and methanol are obtained while using the extended PC-SAFT/UNIQUAC model.

Gas hydrates generally lead to serious problems such as chock or blockage of gas flow within deep-water porous reservoirs, gas processing units, and gas transportation equipment that often cause significant operating concerns/problems and costs (both operational and capital expenses). Hence, it is vital to precisely forecast the hydrate formation conditions to find appropriate prevention/inhibition ways. To attain this crucial goal, development and utilization of reliable predictive tools considerably help researchers and engineers in gas industries to make logical decisions. With the aid of real data available in the literature, this study introduces a proper thermodynamic model with high accuracy that can be utilized in chemical and gas engineering software packages, which will be beneficial for implementation of engineering and research activities in the corresponding industrial and academic sectors.

3.4. Conclusions

Gas hydrates result in serious flow assurance problems in petroleum industry. A new thermodynamic model through using PC-SAFT equation of state for calculation of single and mixed clathrate hydrate formation conditions is developed in this study where the binary and ternary gas systems of methane, ethane, propane, isobutane, carbon dioxide, nitrogen, and hydrogen sulfide are considered. The association contribution and UNIQUAC model are incorporated in the modeling strategy. In this work, the association contributions between water, methanol, and ethanol are taken into account to obtain the thermodynamic conditions for the methane hydrate systems. A very good agreement is noticed between the modeling results and the experimental data so that the value of AADT% for PC-SAFT equation of state is lower, compared to the previous EOS/thermodynamic models. The binary interaction parameters for different binary components are investigated by using experimental hydrate data, leading to better outcome compared with results obtained through fitting the VLE data. Furthermore, the introduced thermodynamic approach is employed to determine the gas hydrate formation temperature in the presence of methanol, ethanol, glycerol, NaCl, KCl, $MgCl_2$, and $CaCl_2$. The results for the systems in the presence of inhibitors show a good match with the experimental hydrate formation data. Also, the AADT% values were less than other previous related works.

In addition to attaining a higher accuracy, the current study provides the best values for the physical parameters of PC-SAFT equation of state in gas hydrate systems.

Acknowledgements

The authors would like to acknowledge the financial support provided by the Memorial University (NL, Canada), the Natural Sciences and Engineering Research Council of Canada (NSERC), InnovateNL, and Equinor (formerly Statoil) Canada.

Supporting Information

The Supporting Information is available free of charge on the ACS Publications website. Further theory/information on UNIQUAC activity coefficient model and PC-SAFT EOS; an algorithm to calculate the value of fugacity; a brief procedure to obtain the aqueous composition; more experimental data and predictions for hydrate formation temperature and pressure of pure gases; comparison of the values of hydrate formation temperature for two different scenarios (with and without association energy terms).

Nomenclatures

Acronyms

$AADT$	Average absolute percent deviation in temperature
$AADP$	Average absolute percent deviation in pressure
CPA	Cubic-plus-association equation of state
CTS	Cubic two-state
ESD	Elliot, Suresh, and Donohue equation of state
EOS	Equation of state
SRK	Soave-Redlich-Kwong equation of state
RK	Redlich-Kwong equation of state
VLE	Vapor liquid equilibrium
VPT	Valdarama-Patel-Teja equation of state

Variables/Letters

A	Parameter in Kihara potential function
a	Core radius
$\bar{a}$	Helmholtz free energy
a_w	Activity of water
B	Parameter in Kihara potential function
C	Langmuir constant
C_p	Water heat capacity, $\mathrm{J/kg.K}$
d	Temperature-dependent segment diameter
f	Fugacity of gas component
g	Average radial distribution function
g_{ij}	Distribution function
H	Molar enthalpy
H_i	Henry's constant
k	Boltzmann's constant
k_{ij}	Binary interaction between two molecules
m	Segment number
N_p	Number of data points
P	Pressure, MPa
r	Radius of the cavity, m
R	Gas constant, $\mathrm{J/mol.K}$
R_i	Cell radius
T	Temperature, K
v	Molar volume, $\mathrm{mol/m^3}$
v_i^{∞}	Partial molar volume
x	Mole fraction

Z	Compressibility factor
z	Coordination number

Greek Letters

μ	Chemical potential
$\Delta^{A_iB_i}$	Association strength
ΔH_D	Hydrate dissociation heat, $\mathrm{J/kg}$
σ	Diameter of segment, m
ε	Energy parameter, J/mol
ε_{ij}	Association energy, J/mol
δ	Parameter in Kihara equation
ξ	Packing factor
κ_{ij}	Association volume
ϑ	Number of cavities
ϑ_{ij}	Binary association parameter in PC-SAFT
λ_{ij}	Binary association parameter in PC-SAFT
γ_i	Activity coefficient
θ_i	Local area fraction in the UNIQUAC model
Φ_i	Segment/volume fraction in the UNIQUAC model
ρ	Density, $\mathrm{kg/m^3}$
ω	Cell potential
ϕ	Fugacity of gas

Subscripts

pw	Pure water
i, j, k, x	Compound
w	Water

Superscripts

α	Other coexisting phases
β	Empty cage of hydrate case
$disp$	Dispersion
id	Ideal
hc	Hard-chain
hs	Hard sphere
N_P	Number of data
res	Residual
H	Hydrate
0	Pure water

References

[1] Englezos, P. and J.D. Lee, *Gas hydrates: A cleaner source of energy and opportunity for innovative technologies.* Korean Journal of Chemical Engineering, 2005. **22**(5): p. 671-681.

[2] Chatti, I., A. Delahaye, L. Fournaison, and J.P. Petitet, *Benefits and drawbacks of clathrate hydrates: A review of their areas of interest.* Energy Conversion and Management, 2005. **46**(9-10): p. 1333-1343.

[3] Eslamimanesh, A., A.H. Mohammadi, D. Richon, P. Naidoo, and D. Ramjugernath, *Application of gas hydrate formation in separation processes: A review of experimental studies.* The Journal of Chemical Thermodynamics, 2012. **46**: p. 62-71.

[4] Javanmardi, J. and M. Moshfeghian, *Energy consumption and economic evaluation of water desalination by hydrate phenomenon.* Applied thermal engineering, 2003. **23**(7): p. 845-857.

[5] Kang, S.-P. and H. Lee, *Recovery of CO2 from flue gas using gas hydrate: thermodynamic verification through phase equilibrium measurements.* Environmental science & technology, 2000. **34**(20): p. 4397-4400.

[6] Fournaison, L., A. Delahaye, I. Chatti, and J.-P. Petitet, *CO2 hydrates in refrigeration processes.* Industrial & engineering chemistry research, 2004. **43**(20): p. 6521-6526.

[7] Ogawa, T., T. Ito, K. Watanabe, K.i. Tahara, R. Hiraoka, J.i. Ochiai, R. Ohmura, and Y.H. Mori, *Development of a novel hydrate-based refrigeration system: A preliminary overview.* Applied Thermal Engineering, 2006. **26**(17-18): p. 2157-2167.

[8] Fitzgerald, A. and M. Taylor. *Offshore gas-to-solids technology*. in *Offshore Europe*. 2001. Society of Petroleum Engineers.

[9] Kerr, R.A., *Gas hydrate resource: smaller but sooner.* Science, 2004. **303**(5660): p. 946-947.
[10] Lee, H.J., J.D. Lee, P. Linga, P. Englezos, Y.S. Kim, M.S. Lee, and Y.D. Kim, *Gas hydrate formation process for pre-combustion capture of carbon dioxide.* Energy Fuels, 2009.
[11] Englezos, P., *Clathrate hydrates.* Industrial & engineering chemistry research, 1993. **32**(7): p. 1251-1274.
[12] Kondori, J., S. Zendehboudi, and M.E. Hossain, *A review on simulation of methane production from gas hydrate reservoirs: Molecular dynamics prospective.* Journal of Petroleum Science and Engineering, 2017. **159**: p. 754-772.
[13] Van der Waals, J.H., J.C. Platteeuw, and I. Priogine, *Advances in Chemical Physics, Vol. II*. 1959. 1.
[14] Parrish, W.R. and J.M. Prausnitz, *Dissociation pressures of gas hydrates formed by gas mixtures.* Industrial & Engineering Chemistry Process Design and Development, 1972. **11**(1): p. 26-35.
[15] Ng, H.-J. and D.B. Robinson, *The measurement and prediction of hydrate formation in liquid hydrocarbon-water systems.* Industrial & Engineering Chemistry Fundamentals, 1976. **15**(4): p. 293-298.
[16] Holder, G., G. Corbin, and K. Papadopoulos, *Thermodynamic and molecular properties of gas hydrates from mixtures containing methane, argon, and krypton.* Industrial & Engineering Chemistry Fundamentals, 1980. **19**(3): p. 282-286.
[17] Anderson, F. and J. Prausnitz, *Inhibition of gas hydrates by methanol.* AIChE journal, 1986. **32**(8): p. 1321-1333.
[18] Englezos, P., Z. Huang, and P. Bishnoi, *Prediction of natural gas hydrate formation conditions in the presence of methanol using the Trebble-Bishnoi equation of state.* Journal of Canadian Petroleum Technology, 1991. **30**(02).
[19] Trebble, M. and P. Bishnoi, *Development of a new four-parameter cubic equation of state.* Fluid phase equilibria, 1987. **35**(1-3): p. 1-18.
[20] Tavasoli, H., F. Feyzi, M.R. Dehghani, and F. Alavi, *Prediction of gas hydrate formation condition in the presence of thermodynamic inhibitors with the Elliott-Suresh-Donohue Equation of State.* Journal of Petroleum Science and Engineering, 2011. **77**(1): p. 93-103.
[21] Karamoddin, M. and F. Varaminian, *Experimental measurement of phase equilibrium for gas hydrates of refrigerants, and thermodynamic modeling by SRK, VPT and CPA EOSs.* The Journal of Chemical Thermodynamics, 2013. **65**(Supplement C): p. 213-219.
[22] Chapoy, A., H. Haghighi, R. Burgass, and B. Tohidi, *Gas hydrates in low water content gases: Experimental measurements and modelling using the CPA equation of state.* Fluid Phase Equilibria, 2010. **296**(1): p. 9-14.
[23] Eslamimanesh, A., A.H. Mohammadi, and D. Richon, *An improved Clapeyron model for predicting liquid water–hydrate–liquid hydrate former phase equilibria.* Chemical engineering science, 2011. **66**(8): p. 1759-1764.
[24] Li, L., L. Zhu, and J. Fan, *The application of CPA-vdWP to the phase equilibrium modeling of methane-rich sour natural gas hydrates.* Fluid Phase Equilibria, 2016. **409**(Supplement C): p. 291-300.

[25] Kwaterski, M. and J.-M. Herri, *Modelling of gas clathrate hydrate equilibria using the electrolyte non-random two-liquid (eNRTL) model.* Fluid Phase Equilibria, 2014. **371**: p. 22-40.
[26] !!! INVALID CITATION !!! 24.
[27] Ji, X. and H. Adidharma, *Thermodynamic modeling of CO 2 solubility in ionic liquid with heterosegmented statistical associating fluid theory.* Fluid Phase Equilibria, 2010. **293**(2): p. 141-150.
[28] Huang, S. and M. Radosz, *Equation of State for Small, Large, Polydisperse, and Associating Molecules.* Ind. Eng. Chem. Res., 1990. **29**: p. 2284.
[29] Huang, S. and M. Radosz, *Equation of State for Small, Large, Polydisperse, and Associating Molecules: Extension to Fluid Mixtures.* Ind. Eng. Chem. Res., 1991. **30**: p. 1994.
[30] Adidharma, H. and M. Radosz, *Prototype of an Engineering Equation of State for Heterosegmented Polymers.* Ind. Eng. Chem. Res., 1998. **37**: p. 4453.
[31] Adidharma, H. and M. Radosz, *Square-Well SAFT Equation of State for Homopolymeric and Heteropolymeric Fluids.* Fluid Phase Equilib., 1999. **158–160**: p. 165.
[32] Kinzl, M., G. Luft, H. Adidharma, and M. Radosz, *SAFT Modeling of Inert-Gas Effects on the Cloud-Point Pressures in Ethylene Copolymerization Systems: Poly(ethylene-co-vinyl acetate) + Vinyl Acetate + Ethylene and Poly(ethylene-co-hexene-1) + Hexene-1 + Ethylene with Carbon Dioxide, Nitrogen, or n-Butane.* Ind. Eng. Chem. Res., 2000. **39**: p. 541.
[33] Adidharma, H. and M. Radosz, *SAFT1 for Associating Fluids: Alkanols.* J. Phys. Chem. B, 2001. **105**: p. 9822.
[34] Fazlali, A., M. Nikookar, A. Agha-Aminiha, and A.H. Mohammadi, *Prediction of minimum miscibility pressure in oil reservoirs using a modified SAFT equation of state.* Fuel, 2013. **108**(Supplement C): p. 675-681.
[35] Fu, Y.-H. and S.I. Sandler, *A Simplified SAFT Equation of State for Associating Compounds and Mixtures.* Industrial & Engineering Chemistry Research, 1995. **34**(5): p. 1897-1909.
[36] Pàmies, J.C. and L.F. Vega, *Vapor−Liquid Equilibria and Critical Behavior of Heavy n-Alkanes Using Transferable Parameters from the Soft-SAFT Equation of State.* Industrial & Engineering Chemistry Research, 2001. **40**(11): p. 2532-2543.
[37] Gross, J. and G. Sadowski, *Perturbed-Chain SAFT: An Equation of State Based on a Perturbation Theory for Chain Molecules.* Ind. Eng. Chem. Res., 2001. **40**: p. 4.
[38] Li, X., H. Wu, P. Feng, L. Tang, and S. Fan, *Prediction of Equilibrium Hydrate Formation Conditions for Gas Mixtures Using the Statistical Associating Fluid Theory Equation of State.* Huaxue Xuebao, 2007. **65**: p. 59.
[39] Liang, X., W. Yan, K. Thomsen, and G.M. Kontogeorgis, *On petroleum fluid characterization with the PC-SAFT equation of state.* Fluid Phase Equilibria, 2014. **375**(Supplement C): p. 254-268.
[40] Leekumjorn, S. and K. Krejbjerg, *Phase behavior of reservoir fluids: Comparisons of PC-SAFT and cubic EOS simulations.* Fluid Phase Equilibria, 2013. **359**(Supplement C): p. 17-23.
[41] Munck, J., S. Skjold-Jørgensen, and P. Rasmussen, *Computations of the formation of gas hydrates.* Chemical Engineering Science, 1988. **43**(10): p. 2661-2672.

[42] Abrams, D.S. and J.M. Prausnitz, *Statistical thermodynamics of liquid mixtures: A new expression for the excess Gibbs energy of partly or completely miscible systems.* AIChE Journal, 1975. **21**(1): p. 116-128.
[43] Sloan, D.E. and C.A. Koh, *Clathrate Hydrates of Natural Gases*. 2008.
[44] Senol, I., *Perturbed-Chain Statistical Association Fluid Theory (PC-SAFT) Parameters for Propane, Ethylene, and Hydrogen under Supercritical Conditions.* disp, 2011. **2**: p. 1.
[45] Wertheim, M.S., *Fluids with highly directional attractive forces. IV. Equilibrium polymerization.* Journal of Statistical Physics, 1986. **42**(3): p. 477-492.
[46] Justo-Garcia, D.N., F. Garcia-Sanchez, N.L. Diaz-Ramirez, and A. Romero-Martinez, *Calculation of critical points for multicomponent mixtures containing hydrocarbon and nonhydrocarbon components with the PC-SAFT equation of state.* Fluid Phase Equilibria, 2008. **265**(1-2): p. 192-204.
[47] Mejbri, K., A. Taieb, and A. Bellagi, *Phase equilibria calculation of binary and ternary mixtures of associating fluids applying PC-SAFT equation of state.* The Journal of Supercritical Fluids, 2015. **104**: p. 132-144.
[48] Enick, R.M., G.P. Donahey, and M. Holsinger, *Modeling the High-Pressure Ammonia−Water System with WATAM and the Peng−Robinson Equation of State for Kalina Cycle Studies.* Industrial & Engineering Chemistry Research, 1998. **37**(5): p. 1644-1650.
[49] Meng, L., Y.-Y. Duan, and X.-D. Wang, *Binary interaction parameter k ij for calculating the second cross-virial coefficients of mixtures.* Fluid Phase Equilibria, 2007. **260**(2): p. 354-358.
[50] Fateen, S.-E.K., M.M. Khalil, and A.O. Elnabawy, *Semi-empirical correlation for binary interaction parameters of the Peng–Robinson equation of state with the van der Waals mixing rules for the prediction of high-pressure vapor–liquid equilibrium.* Journal of Advanced Research, 2013. **4**(2): p. 137-145.
[51] Stern, L.A., S. Circone, S.H. Kirby, and W.B. Durham, *Anomalous preservation of pure methane hydrate at 1 atm.* Journal of Physical Chemistry B, 2001. **105**(9): p. 1756-1762.
[52] Cai, J., J. Zhang, and W. Song, *Vapor–Liquid Equilibrium Measurements and Thermodynamic Modeling of the System (Methane+ Cyclohexane+ Ethanol).* Journal of Chemical & Engineering Data, 2015. **60**(4): p. 976-982.
[53] Soo, C.-B., *Experimental thermodynamic measurements of biofuel-related associating compounds and modeling using the PC-SAFT equation of state*. 2011, École Nationale Supérieure des Mines de Paris.
[54] Shadloo, A., M. Abolala, and K. Peyvandi, *Application of ion-based ePC-SAFT in prediction of density of aqueous electrolyte solutions.* Journal of Molecular Liquids, 2016. **221**: p. 904-913.
[55] Stradi, B.A., J.F. Brennecke, P. Kohn, and M.A. Stadtherr, *Reliable computation of mixture critical points.* AIChE Journal, 2001. **47**(1): p. 212-221.
[56] Masoudi, R., M. Arjmandi, and B. Tohidi, *Extension of Valderrama-Patel-Teja equation of state to modelling single and mixed electrolyte solutions.* Chemical Engineering Science, 2003. **58**(9): p. 1743-1749.
[57] Masoudi, R., B. Tohidi, A. Danesh, A.C. Todd, R. Anderson, R.W. Burgass, and J. Yang, *Measurement and prediction of gas hydrate and hydrated salt equilibria in*

aqueous ethylene glycol and electrolyte solutions. Chemical Engineering Science, 2005. **60**(15): p. 4213-4224.
[58] Deaton, W. and E. Frost Jr, *Gas hydrate composition and equilibrium data.* Oil Gas J, 1946. **45**: p. 170-178.
[59] Mooijer-van den Heuvel, M., C. Peters, and J. de Swaan Arons, *Gas hydrate phase equilibria for propane in the presence of additive components.* Fluid phase equilibria, 2002. **193**(1): p. 245-259.
[60] Kobayashi, R. and D.L. Katz, *Methane hydrate at high pressure.* J. Petrol Technol., 1949. **2579**: p. 66-70.
[61] Schneider, G. and J. Farrar, *US Dept. of Interior.* Res. Dev. Report, 1968(292): p. 37-49.
[62] McLeod, H.O. and J.M. Campbell, *Natural Gas Hydrates at Pressures to 10,000 lb./sq. in. abs.* J. Pet. Technol., 1961. **13**: p. 590.
[63] Rouher, O.S. and A.J. Barduhn, *Hydrates of iso-and normal butane and their mixtures.* Desalination, 1969. **6**(1): p. 57-73.
[64] Marshall, D.R., S. Saito, and R. Kobayashi, *Hydrates at high pressures: Part I. Methane-water, argon-water, and nitrogen-water systems.* AIChE Journal, 1964. **10**(2): p. 202-205.
[65] Deaton, W.M. and E.M. Frost, Jr., *Gas Hydrates and their Relation to the Operation of Natural Gas.* US Bur. Mines Monogr., 1946. **8**.
[66] Jhaveri, J. and D.B. Robinson, *Hydrates in the methane-nitrogen system.* The Canadian Journal of Chemical Engineering, 1965. **43**(2): p. 75-78.
[67] Larson, S.D., *Phase studies of the two component carbon dioxide-water system involving the carbon dioxide hydrate*. 1955, University of Illinois, Urbana.
[68] Galloway, T.J., W. Ruska, P.S. Chappelear, and R. Kobayashi, *Experimental measurement of hydrate numbers for methane and ethane and comparison with theoretical values.* Industrial & Engineering Chemistry Fundamentals, 1970. **9**(2): p. 237-243.
[69] Ohgaki, K., Y. Makihara, and K. Takano, *Formation of CO2 hydrate in pure and sea waters.* J. Chem. Eng. Jpn., 1993. **26**: p. 558.
[70] Verma, V.K., *Gas hydrates from liquid hydrocarbon-water systems*. 1974, University of Michigan.
[71] Roberts, O., E. Brownscombe, L. Howe, and H. Ramser, *Constitution diagrams and composition of methane and ethane hydrates.* Oil Gas J, 1940. **39**: p. 37-43.
[72] Van Cleeff, A. and G. Diepen, *Gas hydrates of nitrogen and oxygen.* Recueil des Travaux Chimiques des Pays-Bas, 1960. **79**(6): p. 582-586.
[73] Sugahara, K., Y. Tanaka, T. Sugahara, and K. Ohgaki, *Thermodynamic stability and structure of nitrogen hydrate crystal.* Journal of Supramolecular Chemistry, 2002. **2**(4): p. 365-368.
[74] Holder, G.D. and G.C. Grigoriou, *Hydrate Dissociation Pressures of (Methane + Ethane + Water). Existence of a Locus of Minimum Pressures.* J. Chem. Thermodynam., 1980. **12**: p. 1093.
[75] Ng, H.J. and D.B. Robinson, *Hydrate Formation in Systems Containing Methane, Ethane, Propane, Carbon Dioxide or Hydrogen Sulfide in the Presence of Methanol.* Fluid Phase Equilib., 1985. **21**: p. 145.

[76] Mohammadi, A.H., B. Tohidi, and R.W. Burgass, *Equilibrium data and thermodynamic modeling of nitrogen, oxygen, and air clathrate hydrates.* Journal of Chemical & Engineering Data, 2003. **48**(3): p. 612-616.
[77] Avlonitis, D., *Multiphase equilibria in oil-water hydrate forming systems.* Mémoire de, 1988.
[78] Bond, D.C. and N.B. Russell, *Effect of antifreeze agents on the formation of hydrogen sulphide hydrate.* Transactions of the AIME, 1949. **179**(01): p. 192-198.
[79] Nakano, S., K. Yamamoto, and K. Ohgaki, *Natural gas exploitation by carbon dioxide from gas hydrate fields—high-pressure phase equilibrium for an ethane hydrate system.* Proceedings of the Institution of Mechanical Engineers, Part A: Journal of Power and Energy, 1998. **212**(3): p. 159-163.
[80] Selleck, F., L. Carmichael, and B. Sage, *Phase behavior in the hydrogen sulfide-water system.* Industrial & Engineering Chemistry, 1952. **44**(9): p. 2219-2226.
[81] Miller, B. and E. Strong, *Hydrate storage of natural gas.* American Gas Association Monthly, 1946. **28**(2): p. 63-67.
[82] Carroll, J.J. and A.E. Mather, *Phase equilibrium in the system water-hydrogen sulphide: Hydrate-forming conditions.* The Canadian Journal of Chemical Engineering, 1991. **69**(5): p. 1206-1212.
[83] Delavar, H. and A. Haghtalab, *Prediction of hydrate formation conditions using GE-EOS and UNIQUAC models for pure and mixed-gas systems.* Fluid Phase Equilibria, 2014. **369**(Supplement C): p. 1-12.
[84] Martín, A. and C.J. Peters, *New Thermodynamic Model of Equilibrium States of Gas Hydrates Considering Lattice Distortion.* The Journal of Physical Chemistry C, 2009. **113**(1): p. 422-430.
[85] B. Klauda, J. and S. I. Sandler, *Phase behavior of clathrate hydrates: a model for single and multiple gas component hydrates.* Chemical Engineering Science, 2003. **58**(1): p. 27-41.
[86] Zhang, Y., P.G. Debenedetti, R.K. Prud'homme, and B.A. Pethica, *Accurate prediction of clathrate hydrate phase equilibria below 300 K from a simple model.* Journal of Petroleum Science and Engineering, 2006. **51**(1): p. 45-53.
[87] Khosravani, E., G. Moradi, and S. Sajjadifar, *Application of PRSV2 equation of state and explicit pressure dependence of the Langmuir adsorption constant to study phase behavior of gas hydrates in the presence and absence of methanol.* Fluid Phase Equilibria, 2012. **333**(Supplement C): p. 63-73.
[88] Maekawa, T., *Equilibrium conditions for gas hydrates of methane and ethane mixtures in pure water and sodium chloride solution.* Geochemical Journal, 2001. **35**(1): p. 59-66.
[89] Mei, D.-H., J. Liao, J.-T. Yang, and T.-M. Guo, *Experimental and modeling studies on the hydrate formation of a methane+ nitrogen gas mixture in the presence of aqueous electrolyte solutions.* Industrial & engineering chemistry research, 1996. **35**(11): p. 4342-4347.
[90] Unruh, C.H. and D.L. Katz, *Gas hydrates of carbon dioxide-methane mixtures.* Journal of Petroleum Technology, 1949. **1**(04): p. 83-86.
[91] Fan, S.-S. and T.-M. Guo, *Hydrate formation of CO2-rich binary and quaternary gas mixtures in aqueous sodium chloride solutions.* Journal of Chemical & Engineering Data, 1999. **44**(4): p. 829-832.

[92] Holder, G.D. and J.H. Hand, *Multiple-Phase Equilibriums in Hydrates from Methane, Ethane, Propane, and Water Mixtures.* AIChE J., 1982. **28**: p. 44.
[93] Sun, C.Y., G.J. Chen, W. Lin, and T.M. Guo, *Hydrate formation conditions of sour natural gases.* Journal of Chemical and Engineering Data, 2003. **48**(3): p. 600-602.
[94] Thakore, J.L. and G.D. Holder, *Solid vapor azeotropes in hydrate-forming systems.* Industrial & Engineering Chemistry Research, 1987. **26**(3): p. 462-469.
[95] Wu, B.J., D.B. Robinson, and H.J. Ng, *Three- and Four-Phase Hydrate Forming Conditions in Methane + Isobutane + Water.* J. Chem. Thermodynam., 1976. **8**: p. 461.
[96] Ohgaki, K., K. Takano, H. Sangawa, T. Matsubara, and S. Nakano, *Methane Exploitation by Carbon Dioxide from Gas Hydrates—Phase Equilibria for CO2-CH4 Mixed Hydrate System—.* Journal of chemical engineering of Japan, 1996. **29**(3): p. 478-483.
[97] Seo, Y.T. and L. Huen, *Multiple-Phase Hydrate Equilibria of the Ternary Carbon Dioxide, Methane, and Water Mixtures.* J. Phys. Chem. B, 2001. **105**: p. 10084.
[98] Hachikubo, A., A. Miyamoto, K. Hyakutake, K. Abe, and H. Shoji, *Phase equilibrium studies on gas hydrates formed from various guest molecules and powder ice*, in *Fourth International Conference on Gas Hydrates* 2002: Japan.
[99] Kamath, V.A., G.D. Holder, and P.F. Angert, *Three phase interfacial heat transfer during the dissociation of propane hydrates.* Chemical Engineering Science, 1984. **39**(10): p. 1435-1442.
[100] Paranjpe, S.G., S.L. Patil, V.A. Kamath, and S.P. Godbole, *Hydrate Equilibria for Binary and Ternary Mixtures of Methane, Propanes Isobutane, and n-Butane: Effect of Salinity* in *SPE Annual Conference 379, SPE 16871*. 1987, Dallas, TX.
[101] Wang, H., W. Sun, and C. Xia, *An easily recoverable and efficient catalyst for the heterogeneous cyclopropanation of olefins.* J. Mol. Catal., A: Chem., 2003. **206**: p. 199.
[102] Javanmardi, J., M. Moshfeghian, and R.N. Maddox, *An accurate model for prediction of gas hydrate formation conditions in mixtures of aqueous electrolyte solutions and alcohol.* The Canadian Journal of Chemical Engineering, 2001. **79**(3): p. 367-373.
[103] Zuo, Y., S. Gommesen, and T. Guo, *Equation of state based hydrate model for natural gas systems containing brine and polar inhibitor.* Chinese Journal of Chemical Engineering, 1996. **4**(3): p. 189-202.
[104] Hsieh, M.-K., Y.-T. Yeh, Y.-P. Chen, P.-C. Chen, S.-T. Lin, and L.-J. Chen, *Predictive method for the change in equilibrium conditions of gas hydrates with addition of inhibitors and electrolytes.* Industrial & Engineering Chemistry Research, 2012. **51**(5): p. 2456-2469.
[105] Chin, H.-Y., M.-K. Hsieh, Y.-P. Chen, P.-C. Chen, S.-T. Lin, and L.-J. Chen, *Prediction of phase equilibrium for gas hydrate in the presence of organic inhibitors and electrolytes by using an explicit pressure-dependent Langmuir adsorption constant in the van der Waals–Platteeuw model.* The Journal of Chemical Thermodynamics, 2013. **66**: p. 34-43.
[106] Haghighi, H., A. Chapoy, R. Burgess, S. Mazloum, and B. Tohidi, *Phase equilibria for petroleum reservoir fluids containing water and aqueous methanol solutions: Experimental measurements and modelling using the CPA equation of state.* Fluid Phase Equilibria, 2009. **278**(1-2): p. 109-116.
[107] Mohammadi, A.H., I. Kraouti, and D. Richon, *Experimental data and predictions of dissociation conditions for methane, ethane, propane, and carbon dioxide simple*

hydrates in the presence of glycerol aqueous solutions. Industrial & Engineering Chemistry Research, 2008. **47**(21): p. 8492-8495.
[108] Javanmardi, J., S. Babaee, A. Eslamimanesh, and A.H. Mohammadi, *Experimental measurements and predictions of gas hydrate dissociation conditions in the presence of methanol and ethane-1, 2-diol aqueous solutions.* Journal of Chemical & Engineering Data, 2012. **57**(5): p. 1474-1479.
[109] Maekawa, T., *Equilibrium conditions of propane hydrates in aqueous solutions of alcohols, glycols, and glycerol.* Journal of Chemical & Engineering Data, 2008. **53**(12): p. 2838-2843.
[110] Mohammadi, A.H. and D. Richon, *Phase equilibria of hydrogen sulphide clathrate hydrates in the presence of single or mixed salt aqueous solution.* The Journal of Chemical Thermodynamics, 2012. **53**: p. 82-85.
[111] Mohammadi, A.H. and D. Richon, *Phase equilibria of hydrogen sulfide and carbon dioxide simple hydrates in the presence of methanol,(methanol+ NaCl) and (ethylene glycol+ NaCl) aqueous solutions.* The Journal of Chemical Thermodynamics, 2012. **44**(1): p. 26-30.
[112] Mohammadi, A.H., W. Afzal, and D. Richon, *Experimental Data and Predictions of Dissociation Conditions for Ethane and Propane Simple Hydrates in the Presence of Distilled Water and Methane, Ethane, Propane, and Carbon Dioxide Simple Hydrates in the Presence of Ethanol Aqueous Solutions.* Journal of Chemical & Engineering Data, 2008. **53**(1): p. 73-76.
[113] Maekawa, T., *Equilibrium conditions for carbon dioxide hydrates in the presence of aqueous solutions of alcohols, glycols, and glycerol.* Journal of Chemical & Engineering Data, 2010. **55**(3): p. 1280-1284.
[114] Ng, H. and D.B. Robinson, in *First International Conference on Natural Gas Hydrates*, E.D. Sloan, J. Happel, and M.A. Hnatow, Editors. 1994: Annals of the New York Academy of Science. p. 450-462.
[115] Ng, H.-J. and D.B. Robinson, *Hydrate formation in systems containing methane, ethane, propane, carbon dioxide or hydrogen sulfide in the presence of methanol.* Fluid Phase Equilibria, 1985. **21**(1-2): p. 145-155.
[116] Breland, E. and P. Englezos, *Equilibrium Hydrate Formation Data for Carbon Dioxide in Aqueous Glycerol Solutions.* J. Chem. Eng. Data, 1996. **41**: p. 11.
[117] Mohammadi, A.H. and D. Richon, *Phase equilibria of methane hydrates in the presence of methanol and/or ethylene glycol aqueous solutions.* Industrial & Engineering Chemistry Research, 2009. **49**(2): p. 925-928.
[118] Mohammadi, A.H. and D. Richon, *Phase equilibria of hydrogen sulfide clathrate hydrates in the presence of methanol, ethanol, NaCl, KCl, or CaCl2 aqueous solutions.* Industrial & Engineering Chemistry Research, 2009. **48**(16): p. 7847-7851.
[119] De Roo, J., C. Peters, R. Lichtenthaler, and G. Diepen, *Occurrence of methane hydrate in saturated and unsaturated solutions of sodium chloride and water in dependence of temperature and pressure.* AIChE Journal, 1983. **29**(4): p. 651-657.
[120] Long, Z., J.-W. Du, D.-L. Li, and D.-Q. Liang, *Phase equilibria of ethane hydrate in MgCl2 aqueous solutions.* Journal of Chemical & Engineering Data, 2010. **55**(8): p. 2938-2941.
[121] Mohammadi, A.H., W. Afzal, and D. Richon, *Gas hydrates of methane, ethane, propane, and carbon dioxide in the presence of single NaCl, KCl, and CaCl2 aqueous*

solutions: Experimental measurements and predictions of dissociation conditions. The Journal of Chemical Thermodynamics, 2008. **40**(12): p. 1693-1697.

[122] Tohidi, B., R.W. Burgass, A. Danesh, and A.C. Todd, *Hydrate Inhibition Effect of Produced Water: Part 1—Ethane and Propane Simple Gas Hydrates*, in *Offshore Europe*. 1993, Society of Petroleum Engineers: Aberdeen, United Kingdom.

[123] Dholabhai, P., P. Englezos, N. Kalogerakis, and P. Bishnoi, *Equilibrium conditions for methane hydrate formation in aqueous mixed electrolyte solutions.* The Canadian journal of chemical engineering, 1991. **69**(3): p. 800-805.

[124] Maekawa, T., *Equilibrium Conditions of Clathrate Hydrates Formed from Propane and Aqueous Solutions of Propanone and Sodium Chloride.* Journal of Chemical & Engineering Data, 2010. **55**(9): p. 3645-3648.

[125] Kharrat, M. and D. Dalmazzone, *Experimental Determination of Stability Conditions of Methane Hydrate in Aqueous Calcium Chloride Solutions Using High Pressure Differential Scanning Calorimetry.* J. Chem. Thermodyn., 2003. **35**: p. 1498.

[126] Jager, M.D. and E.D. Sloan, *The effect of pressure on methane hydration in pure water and sodium chloride solutions.* Fluid Phase Equilibria, 2001. **185**(1-2): p. 89-99.

[127] Afzal, W., A.H. Mohammadi, and D. Richon, *Experimental Measurements and Predictions of Dissociation Conditions for Carbon Dioxide and Methane Hydrates in the Presence of Triethylene Glycol Aqueous Solutions.* J. Chem. Eng. Data, 2007. **52**: p. 2053.

[128] Bishnoi, P.R. and P.D. Dholabhai, *Experimental study on propane hydrate equilibrium conditions in aqueous electrolyte solutions.* Fluid Phase Equilibria, 1993. **83**: p. 455-462.

[129] Haghighi, H., A. Chapoy, and B. Tohidi, *Methane and Water Phase Equilibria in the Presence of Single and Mixed Electrolyte Solutions Using the Cubic-Plus-Association Equation of State.* Oil Gas Sci. Technol., 2009. **64**(2): p. 141.

[130] Atik, Z., C. Windmeier, and L.R. Oellrich, *Experimental gas hydrate dissociation pressures for pure methane in aqueous solutions of MgCl2 and CaCl2 and for a (methane+ ethane) gas mixture in an aqueous solution of (NaCl+ MgCl2).* Journal of Chemical & Engineering Data, 2006. **51**(5): p. 1862-1867.

[131] Kang, S.-P., M.-K. Chun, and H. Lee, *Phase equilibria of methane and carbon dioxide hydrates in the aqueous MgCl2 solutions.* Fluid phase equilibria, 1998. **147**(1-2): p. 229-238.

[132] Englezos, P. and S. Hall, *Phase equilibrium data on carbon dioxide hydrate in the presence of electrolytes, water soluble polymers and montmorillonite.* The Canadian Journal of Chemical Engineering, 1994. **72**(5): p. 887-893.

[133] Tohidi, B., A. Danesh, A. Todd, and R. Burgass, *Hydrate-free zone for synthetic and real reservoir fluids in the presence of saline water.* Chemical engineering science, 1997. **52**(19): p. 3257-3263.

[134] Mohammadi, A.H., I. Kraouti, and D. Richon, *Methane hydrate phase equilibrium in the presence of NaBr, KBr, CaBr2, K2CO3, and MgCl2 aqueous solutions: Experimental measurements and predictions of dissociation conditions.* The journal of chemical thermodynamics, 2009. **41**(6): p. 779-782.

[135] Dholabhai, P.D., N. Kalogerakis, and P.R. Bishnoi, *Equilibrium conditions for carbon dioxide hydrate formation in aqueous electrolyte solutions.* Journal of Chemical and Engineering Data, 1993. **38**(4): p. 650-654.

[136] Dholabhai, P.D., J.S. Parent, and P.R. Bishnoi, *Carbon dioxide hydrate equilibrium conditions in aqueous solutions containing electrolytes and methanol using a new apparatus.* Industrial & engineering chemistry research, 1996. **35**(3): p. 819-823.
[137] Masoudi, R., B. Tohidi, R. Anderson, R.W. Burgass, and J. Yang, *Experimental measurement and thermodynamic modelling of clathrate hydrate equilibria and salt solubility in aqueous ethylene glycol and electrolyte solutions.* Fluid Phase Equilibria, 2004. **219**(2): p. 157-163.
[138] Nasrifar, K., M. Moshfeghian, and R. Maddox, *Prediction of equilibrium conditions for gas hydrate formation in the mixtures of both electrolytes and alcohol.* Fluid phase equilibria, 1998. **146**(1-2): p. 1-13.
[139] Nasrifar, K. and M. Moshfeghian, *A model for prediction of gas hydrate formation conditions in aqueous solutions containing electrolytes and/or alcohol.* The Journal of Chemical Thermodynamics, 2001. **33**(9): p. 999-1014.
[140] Mohammadi, A.H. and B. Tohidi, *A Novel Predictive Technique for Estimating the Hydrate Inhibition Effects of Single and Mixed Thermodynamic Inhibitors.* The Canadian Journal of Chemical Engineering, 2005. **83**(6): p. 951-961.
[141] Du, Y. and T.-M. Guo, *Prediction of hydrate formation for systems containing methanol.* Chemical Engineering Science, 1990. **45**(4): p. 893-900.
[142] Galicia-Andrés, E. and M. Medeiros, *Hydrate Equilibrium Modelling with the Cubic two-state Equation of State.* Journal of the Mexican Chemical Society, 2016. **60**(4): p. 226-237.
[143] Li, X.-S., H.-J. Wu, Y.-G. Li, Z.-P. Feng, L.-G. Tang, and S.-S. Fan, *Hydrate dissociation conditions for gas mixtures containing carbon dioxide, hydrogen, hydrogen sulfide, nitrogen, and hydrocarbons using SAFT.* The Journal of Chemical Thermodynamics, 2007. **39**(3): p. 417-425.
[144] Jiang, H. and H. Adidharma, *Hydrate Equilibrium Modeling for Pure Alkanes and Mixtures of Alkanes Using Statistical Associating Fluid Theory.* Industrial & Engineering Chemistry Research, 2011. **50**(22): p. 12815-12823.
[145] Jager, M., C. Peters, and E. Sloan, *Experimental determination of methane hydrate stability in methanol and electrolyte solutions.* Fluid Phase Equilibria, 2002. **193**(1-2): p. 17-28.
[146] Najibi, H., A. Chapoy, H. Haghighi, and B. Tohidi, *Experimental determination and prediction of methane hydrate stability in alcohols and electrolyte solutions.* Fluid Phase Equilibria, 2009. **275**(2): p. 127-131.
[147] Mahadev, K.N. and P.R. Bishnoi, *Equilibrium conditions for the hydrogen sulfide hydrate formation in the presence of electrolytes and methanol.* The Canadian Journal of Chemical Engineering, 1999. **77**(4): p. 718-722.
[148] Dholabhai, P.D., J.S. Parent, and P.R. Bishnoi, *Equilibrium conditions for hydrate formation from binary mixtures of methane and carbon dioxide in the presence of electrolytes, methanol and ethylene glycol.* Fluid Phase Equilibria, 1997. **141**(1-2): p. 235-246.
[149] Dholabhai, P.D. and P.R. Bishnoi, *Hydrate equilibrium conditions in aqueous electrolyte solutions: mixtures of methane and carbon dioxide.* Journal of Chemical and Engineering Data, 1994. **39**(1): p. 191-194.

-

3.5.Supporting Information

This document provides more theoretical aspects of UNIQUAC activity coefficient model, further information on the theory and main equations involved in the PC-SAFT EOS model, an algorithm to determine the magnitude of fugacity, a brief procedure to calculate the aqueous composition, and a large number of real data and modeling results on the hydrate temperature and pressure for some pure gases. A comparison of the values of hydrate formation temperature for two different scenarios (with and without association energy terms) is also given in this Supporting Information.

S1. UNIQUAC Model

The UNIQUAC activity coefficient model is used to determine the water activity coefficient (γ) in aqueous phase, which is made of both residual and combinatorial terms (γ_i^{res} and γ_i^{com}), as follows:

$$\ln \gamma_i = \ln \gamma_i^{com} + \ln \gamma_i^{res} \tag{S-1}$$

$$\ln \gamma_i^{com} = \ln \frac{\Phi_i}{x_i} + \frac{z}{2} q_i \frac{\theta_i}{\Phi_i} + l_i + \frac{\Phi_i}{x_i} \sum x_i l_i \tag{S-2}$$

$$\ln \gamma_i^{res} = q_i \left[1 - \ln \left(\sum_j \theta_j \tau_{ji} \right) - \sum_j \frac{\theta_j \tau_{ij}}{\sum_k \theta_k \tau_{kj}} \right] \tag{S-3}$$

$$\theta_i = \frac{q_i x_i}{\sum_i q_i x_i}, \quad \Phi_i = \frac{r_i x_i}{\sum_i r_i x_i}, \quad l_i = (r_i - q_i)\frac{z}{2} - (r_i - 1) \tag{S-4}$$

in which γ_i, x_i, q_i, and r_i stand for the activity coefficient, mole fraction in the aqueous phase, structural surface, and volume parameters, respectively. The solubility of gases in the liquid

phase is determined based on the equality of the gas fugacity in the liquid and vapor phases and Henry's law [1]:

$$x_i = \frac{f_i^v}{H_i \exp(v_i^\infty ((P - P_i^{sat}) / RT))} \quad \text{(S-5)}$$

where v_i^∞ and H_i introduce the infinite partial molar volume and Henry's constant of component *i*, respectively. Both parameters v_i^∞ and H_i are a function of pressure and temperature. The values of the Henry's constant for the gas components are given by Mohebbi [2] and the values of infinite partial molar volume of the components are provided by Heidemann [3]. Thus, we are able to obtain the water mole fraction in the presence of inhibitors and salts where the solubility of gases in the aqueous phase is given.

The magnitudes of q_i and r_i for all components in the aqueous phase, which were taken from the literature, are listed in Table S1. The parameters Φ_i and θ_i represent the local area and segment (or volume) fraction of the component *i*, respectively. *z* is a constant, which is equal to 10. The binary interactions between two components (τ_{ij} or τ_{ij}) are achieved through using hydrate equilibrium data (e.g., curve-fitting procedure) as follows:

$$\tau_{ij} = \exp(\frac{u_{ij}}{T}) \quad \text{(S-6)}$$

The parameters of UNIQUAC model (u_{ij}) for all components (calculated in this work) are available in Table S2. It should be noted that the hydrate formation condition data for pure gases/ inhibitors are utilized to calculate the magnitudes of the parameters tabulated in Table S-2.

Table S1: *r* and *q* parameters used in the UNIQUAC model. [4]

	H_2O	NaCl	KCl	$CaCl_2$	$MgCl_2$	Methanol	Ethanol	Glycerol
r	0.92	6.246	6.477	11.032	11.977	1.431	2.5755	3.585
q	1.40	5.646	4.517	9.369	10.031	1.432	2.588	3.064

Table S2: The calculated u_{ij} for aqueous phase components in gas hydrate systems in the presence of inhibitors.

	H_2O	NaCl	KCl	$CaCl_2$	$MgCl_2$	Methanol	Ethanol	Glycerol
H_2O	0	2725.3	4656.68	-7680.4	3196.06	-8299.8	-12164	-3964.1
NaCl	-2973	0	-274.75	-9167.01	-	-12140	-	-
KCl	-3666.8	-247.7	0	-5946.1	-	10653	-	-
$CaCl_2$	-2105.9	10405	991.02	0	-	-11149	-	-
$MgCl_2$	-3518.1	9762	860.21	-	0	-	-	-
Methanol	-1436.9	3468.6	-495.5	6689.4	-	0	-	-
Ethanol	346.85	-	-	-	-	-	0	-
Glycerol	-1015.8	-	-	-	-	-	-	0

S2. PC-SAFT EOS

The PC-SAFT equation of state has three special parameters for non-associating fluids; including, the segment number (*m*), segment diameter (σ), and dispersion energy parameter (ε / k_b). The compressibility factor (*Z*) is given as summation of ideal (id), hard chain (hc), dispersion (disp) terms, and association (ass). Having this assumption, the compressibility factor is defined by the following equation:

$$Z = Z^{id} + Z^{hc} + Z^{disp} + Z^{ass} \tag{S-7}$$

where $Z = P\nu / RT$, $Z^{id} = 1$ (for ideal gases when pressure is very low). P is the pressure and ν stands for the molar volume. The magnitude of Z^{ass} is very small (close to zero) due to the weak association effect in the gas phase. Chapman et al. [5] introduced the following equation to calculate the homonuclear hard-sphere chain (Z^{hc}):

$$Z^{hc} = \overline{m} Z^{hs} - \sum_i x_i (m_i - 1) \dot{\rho} (g_{ii}^{hs})^{-1} \frac{\partial g_{ii}^{hs}}{\partial \dot{\rho}} \tag{S-8}$$

where

$$\overline{m} = \sum_i x_i m_i \tag{S-9}$$

in which, x_i and m_i denote the mole fraction and segment number of component i, respectively. $\dot{\rho}$ refers to the total number density of molecules. g_{ii}^{hs} represents the average radial distribution function of the hard sphere system, which is defined by the following equation [6]:

$$g_{ij}^{hs} = \frac{1}{1-\zeta_3} + \frac{d_i d_j}{d_i + d_j}\frac{3\zeta_2}{(1-\zeta_3)^2} + \left(\frac{d_i d_j}{d_i + d_j}\right)^2 \frac{2\zeta_2^2}{(1-\zeta_3)^3} \tag{S-10}$$

The derivative of g_{ii}^{hs} with respect to $\dot{\rho}$ is given below:

$$\dot{\rho}\frac{\partial g_{ii}^{hs}}{\partial \dot{\rho}} = \frac{\zeta_3}{(1-\zeta_3)^2} + \frac{d_i d_j}{d_i + d_j}\left(\frac{3\zeta_2}{(1-\zeta_3)^2} + \frac{6\zeta_2\zeta_3}{(1-\zeta_3)^3}\right) + \left(\frac{d_i d_j}{d_i + d_j}\right)^2\left(\frac{4\zeta_2^2}{(1-\zeta_3)^3} + \frac{6\zeta_2^2\zeta_3}{(1-\zeta_3)^4}\right) \tag{S-11}$$

The packing factor (ζ_n) is expressed by the following equation:

$$\zeta_n = \frac{\pi}{6}\dot{\rho}\sum_i x_i m_i d_i^n \qquad n \in \{0,1,2,3\} \tag{S-12}$$

The temperature-dependent segment diameter (d_i) can be calculated as follows:

$$d_i = \sigma_i\left[1 - 0.12\exp\left(-\frac{3\varepsilon_i}{kT}\right)\right] \tag{S-13}$$

in which, k denotes the Boltzmann constant. The total number density of molecules ($\dot{\rho}$) is determined as follows:

$$\dot{\rho} = \frac{6\zeta_3}{\pi \sum_i x_i m_i d_i^3} \tag{S-14}$$

The definition of the hard sphere contribution, Z^{hs}, in Equation (S-7) is given below:

$$Z^{hs} = \frac{\zeta_3}{1-\zeta_3} + \frac{3\zeta_1\zeta_3}{\zeta_0(1-\zeta_3)^2} + \frac{3\zeta_2^3 - 3\zeta_3\zeta_2^3}{\zeta_0(1-\zeta_3)^3} \tag{S-15}$$

The dispersion contribution of the compressibility factor (Z^{disp}) given in Equation (S-7) is computed by the following equation:

$$Z^{disp} = -2\pi\rho \frac{\partial(\zeta_3 I_1)}{\partial \zeta_3} \overline{m^2 \varepsilon \sigma^3} - \pi\rho\overline{m} \left(C_1 \frac{\partial(\zeta_3 I_2)}{\partial \zeta_3} + C_2 \zeta_3 I_2 \right) \overline{m^2 \varepsilon^2 \sigma^3} \tag{S-16}$$

The coefficients of Equation (S-16), $\overline{m^2 \varepsilon \sigma^3}$, and $\overline{m^2 \varepsilon^2 \sigma^3}$ are expressed as follows:

$$C_1 = \left(1 + \overline{m} \frac{8\zeta_3 - 2\zeta_3^2}{(1-\zeta_3)^4} + (1-\overline{m}) \frac{20\zeta_3 - 27\zeta_3^2 + 12\zeta_3^3 - 2\zeta_3^4}{\left((1-\zeta_3)(2-\zeta_3)\right)^2} \right)^{-1} \tag{S-17}$$

$$C_2 = -C_1^2 \left(\overline{m} \frac{-4\zeta_3^2 + 20\zeta_3 + 8}{(1-\zeta_3)^5} + (1-\overline{m}) \frac{2\zeta_3^3 + 12\zeta_3^2 - 48 + 40}{\left((1-\zeta_3)(2-\zeta_3)\right)^3} \right) \tag{S-18}$$

$$\overline{m^2 \varepsilon \sigma^3} = \sum_{i=1}^{N} \sum_{j=1}^{N} x_i x_j m_i m_j \left(\frac{\varepsilon_{ij}}{KT} \right) \sigma_{ij}^3 \tag{S-19}$$

$$\overline{m^2 \varepsilon^2 \sigma^3} = \sum_{i=1}^{N} \sum_{j=1}^{N} x_i x_j m_i m_j \left(\frac{\varepsilon_{ij}}{KT} \right)^2 \sigma_{ij}^3 \tag{S-20}$$

ε_{ij} , σ_{ij} , I_1 , and I_1 are also calculated by the following expressions:

$$\varepsilon_{ij} = \sqrt{\varepsilon_i \varepsilon_j}(1 - k_{ij}) \tag{S-21}$$

$$\sigma_{ij} = \frac{1}{2}(\sigma_i + \sigma_j) \tag{S-22}$$

$$I_1 = \sum_{i=0}^{6} a_i(\overline{m})\zeta_3^i \tag{S-23}$$

$$I_2 = \sum_{i=0}^{6} b_i(\overline{m})\zeta_3^i \tag{S-24}$$

In Equation (S-21), k_{ij} introduces the binary interaction between two molecules. $a_i(\overline{m})$ and $b_i(\overline{m})$ given in Equation (S-23) and Equation (S-24) are determined by the following relationships:

$$a_i(\overline{m}) = a_{0i} + \frac{\overline{m}-1}{\overline{m}} a_{1i} + \frac{\overline{m}-1}{\overline{m}} \frac{\overline{m}-2}{\overline{m}} a_{2i} \tag{S-25}$$

$$b_i(\overline{m}) = b_{0i} + \frac{\overline{m}-1}{\overline{m}} b_{1i} + \frac{\overline{m}-1}{\overline{m}} \frac{\overline{m}-2}{\overline{m}} b_{2i} \tag{S-26}$$

The universal model constants (e.g., a_{0i} and b_{0i}) in Equations (S-25) and (S-26) are tabulated in Table S3 [6].

Table S3: Universal model constants for Equations (S-25)and (S-26) [6].

i	a_{0i}	a_{1i}	a_{2i}	b_{0i}	b_{1i}	b_{2i}
0	0.9105631445	-0.3084016918	-0.0906148351	0.7240946941	-0.5755498075	0.0976883116
1	0.6361281449	0.1860531159	0.4527842806	2.2382791861	0.6995095521	-0.2557574982
2	2.6861347891	-2.5030047259	0.5962700728	-4.0025849485	3.8925673390	-9.1558561530
3	-26.547362491	21.419793629	-1.7241829131	-21.003576815	-17.215471648	20.642075974
4	97.759208784	-65.255885330	-4.1302112531	26.855641363	192.67226447	-38.804430052
5	-159.59154087	83.318680481	13.776631870	206.55133841	-161.82646165	93.626774077
6	91.297774084	-33.746922930	-8.6728470368	-355.60235612	-165.20769346	-29.666905585

The association contribution, Z^{ass}, in Equation (S-7) is given by the following relationship:

$$Z^{ass} = -\frac{1}{2}(1+\rho\frac{\partial \ln g}{\partial \rho})\sum_i x_i \sum_{A_i}(1-X^{A_i}) \tag{S-27}$$

The following equations are used to obtain the magnitudes of pressure (P) and fugacity coefficient (φ):

$$P = ZkT\dot{\rho}(10^{10}\frac{\dot{\mathrm{A}}}{m})^3 \tag{S-28}$$

$$\ln \varphi_k = \frac{\mu_k^{res}}{kT} - \ln Z \tag{S-29}$$

in which, φ_k and μ_k^{res} represent the fugacity coefficient and the residual chemical potential of *k*-component in the system, respectively. The chemical potential is determined by the following expression:

$$\frac{\mu_k^{res}(T,v)}{kT} = \bar{a}^{res} + (Z-1) + \left(\frac{\partial \bar{a}^{res}}{\partial x_i}\right)_{T,v,x_{i\neq k}} - \sum_{j=1}^{N}\left[x_j\left(\frac{\partial \bar{a}^{res}}{\partial x_j}\right)_{T,v,x_{j\neq k}}\right] \quad \text{(S-30)}$$

The residual Helmholtz free energy ($\bar{a}^{res}$) is obtained by Equation (14) in the main text of the manuscript. The hard-chain reference contribution ($\bar{a}^{hard-chain}$) is defined as follows:

$$\bar{a}^{hard-chain} = \bar{m}\bar{a}^{hs} - \sum_{i}^{N} x_i(m_i - 1)\ln g_{ii}^{hs}(\sigma_{ii}) \quad \text{(S-31)}$$

where

$$\bar{a}^{hs} = \frac{1}{\zeta_0}\left[\frac{3\zeta_1\zeta_2}{(1-\zeta_3)} + \frac{\zeta_2^3}{\zeta_3(1-\zeta_3)^2} + \left(\frac{\zeta_2^3}{\zeta_3^2} - \zeta_0\right)\ln(1-\zeta_3)\right] \quad \text{(S-32)}$$

Taking derivative of $\bar{a}^{hard-chain}$ with respect to the mole fraction of component k^{th} leads to the following equation:

$$\left(\frac{\partial \bar{a}^{hard-chain}}{\partial x_k}\right)_{T,\rho,x_{j\neq k}} = m_k \bar{a}^{hard-chain} + \bar{m}\left(\frac{\partial \bar{a}^{hs}}{\partial x_k}\right)_{T,\rho,x_{j\neq k}} - \sum_{i}^{N} x_i(m_i - 1)(g_{ii}^{hs})^{-1}\left(\frac{\partial g_{ii}^{hs}}{\partial x_k}\right)_{T,\rho,x_{j\neq k}} \quad \text{(S-33)}$$

Similarly,

$$\left(\frac{\partial g_{ii}^{hs}}{\partial x_k}\right)_{T,\rho,x_{j\neq k}} == \frac{\zeta_{3,xk}}{(1-\zeta_3)^2} + \frac{d_i d_j}{d_i + d_j}\left(\frac{3\zeta_{2,xk}}{(1-\zeta_3)^2} + \frac{6\zeta_2\zeta_{3,xk}}{(1-\zeta_3)^3}\right) + \left(\frac{d_i d_j}{d_i + d_j}\right)^2\left(\frac{4\zeta_2\zeta_{2,xk}}{(1-\zeta_3)^3} + \frac{6\zeta_2^2\zeta_{3\zeta_{2,xk}}}{(1-\zeta_3)^4}\right) \quad \text{(S-34)}$$

The dispersion reference contribution ($\bar{a}^{disp}$) is determined by the following expression:

$$\bar{a}^{disp} = -2\pi\rho I_1 \overline{m^2\varepsilon\sigma^3} - \pi\rho\bar{m}C_1 I_2 \overline{m^2\varepsilon^2\sigma^3} \tag{S-35}$$

Taking derivative of $\bar{a}^{disp}$ with respect to the mole fraction of component k^{th} results in:

$$\begin{aligned}\left(\frac{\partial \bar{a}^{disp}}{\partial x_k}\right)_{T,\rho,x_{j\neq k}} &= -2\pi\rho\left(I_{1,xk}\overline{m^2\varepsilon\sigma^3} + I_1\left(\overline{m^2\varepsilon\sigma^3}\right)_{xk}\right) - \\ &\pi\rho\left[\left(m_k C_1 I_2 + \bar{m}C_{1,xk}I_2 + \bar{m}C_1 I_{2,xk}\right)\overline{m^2\varepsilon^2\sigma^3} + \bar{m}C_1 I_2\left(\overline{m^2\varepsilon^2\sigma^3}\right)_{xk}\right]\end{aligned} \tag{S-36}$$

where

$$\left(\overline{m^2\varepsilon\sigma^3}\right)_{xk} = 2m_k\sum_j x_j m_j\left(\frac{\varepsilon_{kj}}{KT}\right)\sigma_{kj}^3 \tag{S-37}$$

$$\left(\overline{m^2\varepsilon^2\sigma^3}\right)_{xk} = 2m_k\sum_j x_j m_j\left(\frac{\varepsilon_{kj}}{KT}\right)^2\sigma_{kj}^3 \tag{S-38}$$

$$C_{1,xk} = C_2\zeta_{3,xk} - C_1^2\left\{m_k\frac{8\zeta_3 - 2\zeta_3^2}{(1-\zeta_3)^4} - m_k\frac{20\zeta_3 - 27\zeta_3^2 + 12\zeta_3^3 - 2\zeta_3^4}{\left((1-\zeta_3)(2-\zeta_3)\right)^4}\right\} \tag{S-39}$$

$$I_{1,xk} = \sum_{j=0}^{6}\left[a_j(\bar{m})\, j\zeta_{3,xk}\zeta_3^{j-1} + a_{j,xk}\zeta_3^j\right] \tag{S-40}$$

$$I_{2,xk} = \sum_{j=0}^{6}\left[b_j(\bar{m})\, j\zeta_{3,xk}\zeta_3^{j-1} + b_{j,xk}\zeta_3^j\right] \tag{S-41}$$

$$a_{j,xk} = \frac{m_k}{\bar{m}^2}a_{1j} + \frac{m_k}{\bar{m}^2}\left(3 - \frac{4}{\bar{m}}\right)a_{2i} \tag{S-42}$$

$$b_{j,xk} = \frac{m_k}{\bar{m}^2}b_{1j} + \frac{m_k}{\bar{m}^2}\left(3 - \frac{4}{\bar{m}}\right)b_{2i} \tag{S-43}$$

The last reference contribution in Equation (14) is the association reference contribution ($\bar{a}^{association}$). The association Helmholtz energy of a mixture ($\bar{a}^{association}$) is written as follows [7]:

$$\bar{a}^{associatin} = \sum_{i}^{N} x_i \left[\sum_{\mathrm{A}_i} (\ln X^{\mathrm{A},i} - \frac{X^{\mathrm{A},i}}{2}) + \frac{M_i}{2} \right] \tag{S-44}$$

in which, $X^{\mathrm{A},i}$ represents the mole fraction of molecules *i* which are not bonded at site A. This parameter is calculated by the following expression [7]:

$$X^{\mathrm{A}i} = \left(1 + N_{Av} \rho \sum_{j} \sum_{B_j} x_j X^{Bi} \Delta^{A_i B_j} \right)^{-1} \tag{S-45}$$

The first and second summations imply the summation over all sites on molecule *j* and summation over all components, respectively. $\Delta^{A_i B_j}$ is the association strength, which can be calculated by Equation (S-46) as given below:

$$\Delta^{A_i B_j} = \sigma_{ij}^3 g_{ij}^{hs} \kappa_{ij}^{\mathrm{AB}} \left(\exp\left(\frac{\varepsilon_{ij}^{\mathrm{AB}}}{k_b T} \right) - 1 \right) \tag{S-46}$$

in which, g_{ij} , κ_{ij} , and $\varepsilon_{ij}^{\mathrm{AB}} / k_b$ represent the radial distribution function, association volume function, and association energy, respectively. The association parameters indicating the interactions between two various molecules *i* and *j*, which are a function of pure association parameters, are determined by the following equations [7]:

$$\frac{\varepsilon_{ij}^{\mathrm{AB}}}{k_b} = (1 - \lambda_{ij}) \sqrt{\frac{\varepsilon_i^{\mathrm{AB}}}{k_b} \frac{\varepsilon_j^{\mathrm{AB}}}{k_b}} \tag{S-47}$$

$$\kappa_{ij}^{\mathrm{AB}} = (1 - \upsilon_{ij}) \sqrt{\kappa_i^{\mathrm{AB}} \kappa_j^{\mathrm{AB}}} \tag{S-48}$$

The λ_{ij} and υ_{ij} are two binary associating parameters that considerably increase the thermodynamic predictive potential of PC-SAFT for fluid mixtures especially around critical regions while dealing with phase equilibria [8].

S3. More Experimental Data and Predictions

In addition to Table 3-4, Table S4 and Table S5 present more real data and calculated values of hydrate temperature and pressure in this section for the following cases/sets:

- Range of P(33.99-77.5MPa) for methane; Ref. 48 (**Set 1**)
- Range of P(9.62-68.09MPa) for methane; Ref. 50(**Set 2**)
- Range of P(0.294-0.441MPa) for Ethane; Ref. 59 (**Set 3**)
- Range of P(0.78-2.62MPa) for Ethane; Ref. 62 (**Set 4**)
- Range of P(0.368-0.547MPa) for Propane; Ref. 47 (**Set 5**)
- Range of P(0.093-2.239MPa) for H_2S; Ref. 68 (**Set 6**)

Table S4: Experimental and predicted hydrate temperature for the experimental system pressure and the experimental and predicted hydrate pressure for the experimental system temperature.

Set 1				**Set 4**			
P (MPa)	**T (K)**	**Cal. T for exp.P**	**Cal. P for exp.T**	**P (MPa)**	**T (K)**	**Cal. T for exp.P**	**Cal. P for exp.T**
33.99	295.7	295.9638	32.8733	0.78	277.5	277.297745	0.799747
35.3	295.9	296.2636	33.7168	0.84	278.1	277.896050	0.86158
64.81	301	301.354	62.2775	1.04	279.9	279.59759	1.08080
77.5	302	302.9858	69.629	1.38	281.5	281.78238	1.32950
Set 2				1.66	283.3	283.15097	1.694545
9.62	285.7	285.7329	9.5846	2.1	284.5	284.79978	2.0093892
10.31	286.3	286.3487	10.253	2.62	286.5	286.218705	2.74688
10.1	286.1	286.16670	10.0243	**Set5**			
13.96	289	288.9391	14.062	0.368	276.7	277.297	0.3660
21.13	292.1	292.2566	20.710	0.377	277.0	277.896	0.3865

34.75	295.9	296.1386	33.717	0.405	277.2	279.597	0.4054
48.68	298.7	298.8773	47.6367	0.425	277.3	281.782	0.4187
62.4	300.9	301.01010	61.6576	0.433	277.4	283.150	0.4264
68.09	301.6	301.78869	66.6162	0.473	277.8	284.793	0.47118
Set 3				0.493	278.0	286.218	0.4868
9.62	285.7	285.732941	9.584681	0.51	278.2	277.297	0.5115
10.31	286.3	286.34873	10.25326	0.547	278.5	277.896	0.55323
10.1	286.1	286.166708	10.024328	**Set 6**			
13.96	289	288.9391	14.062996	0.093	272.8	270.478	0.1006
21.13	292.1	292.25664	20.71048	0.157	277.6	277.254	0.1625
34.75	295.9	296.138685	33.71701	0.28	283.2	283.06	0.2838
48.68	298.7	298.87734	47.656798	0.345	285.2	285.161	0.3463
62.4	300.9	301.010106	61.62561	0.499	288.7	288.855	0.4912
68.09	301.6	301.78869	66.676209	0.689	291.8	292.033	0.6728
				1.034	295.7	295.943	1.0075
				1.379	298.5	298.581	1.3664
				1.596	299.8	299.860	1.5848
				1.724	300.5	300.5150	1.7209
				2.068	302.1	301.992	2.0967
				2.239	302.7	302.602	2.2681

Table S5: The predicted hydrate pressure (in MPa) at various experimental temperatures per 0.1 K.

Set 1		**Set 2**		**Set 3**		**Set 4**		**Set 5**		**Set 6**	
T exp.	P cal.	T exp.	P cal.	T exp.	P cal.	T exp.	P cal.	T exp.	P cal.	T exp.	P cal.
295.7	32.8733	285.7	9.58429	260.9	0.31494	277.5	0.78602	276.77	0.36602	272.8	0.100698

295.8	33.2927	285.8	9.69198	261	0.31607	277.6	0.79598	276.87	0.37441	272.9	0.101604
295.9	33.7168	285.9	9.80114	261.1	0.31721	277.7	0.80608	276.97	0.38301	273	0.102542
296	34.1458	286	9.91177	261.2	0.31835	277.8	0.81633	277.07	0.39183	273.1	0.103509
296.1	34.5796	286.1	10.0239	261.3	0.3195	277.9	0.82671	277.17	0.40088	273.2	0.104504
296.2	35.01824	286.2	10.1376	261.4	0.320655	278	0.837246	277.27	0.410163	273.3	0.105524
296.3	35.46177	286.3	10.2528	261.5	0.321813	278.1	0.847927	277.37	0.419684	273.4	0.106568
296.4	35.9102	286.4	10.3697	261.6	0.322977	278.2	0.85876	277.47	0.429454	273.5	0.107634
296.5	36.36356	286.5	10.4881	261.7	0.324146	278.3	0.869747	277.57	0.43948	273.6	0.10872
296.6	36.82189	286.6	10.6082	261.8	0.325321	278.4	0.880891	277.67	0.44977	273.7	0.109824
296.7	37.2852	286.7	10.73	261.9	0.3265	278.5	0.892194	277.77	0.460334	273.8	0.110944
296.8	37.75351	286.8	10.8535	262	0.327685	278.6	0.90366	277.87	0.471181	273.9	0.112078
296.9	38.22687	286.9	10.9787	262.1	0.328876	278.7	0.915292	277.97	0.48232	274	0.113225
297	38.70528	287	11.1056	262.2	0.330072	278.8	0.927092	278.07	0.493761	274.1	0.114382
297.1	39.18878	287.1	11.2344	262.3	0.331273	278.9	0.939064	278.17	0.505516	274.2	0.115547
297.2	39.67738	287.2	11.3649	262.4	0.33248	279	0.95121	278.27	0.517594	274.3	0.116721
297.3	40.17113	287.3	11.4973	262.5	0.333692	279.1	0.963535	278.37	0.530008	274.4	0.117905
297.4	40.67003	287.4	11.6316	262.6	0.334909	279.2	0.97604	278.47	0.54277	274.5	0.119098
297.5	41.17412	287.5	11.7678	262.7	0.336132	279.3	0.988731			274.6	0.120301
297.6	41.68342	287.6	11.906	262.8	0.337361	279.4	1.00161			274.7	0.121515
297.7	42.19796	287.7	12.0461	262.9	0.338595	279.5	1.01468			274.8	0.122741
297.8	42.71775	287.8	12.1882	263	0.339835	279.6	1.027947			274.9	0.123979
297.9	43.24283	287.9	12.3323	263.1	0.341081	279.7	1.041412			275	0.12523
298	43.77322	288	12.4786	263.2	0.342332	279.8	1.055081			275.1	0.126493
298.1	44.30895	288.1	12.6269	263.3	0.343589	279.9	1.068957			275.2	0.12777
298.2	44.85003	288.2	12.7774	263.4	0.344851	280	1.083045			275.3	0.12906
298.3	45.3965	288.3	12.93	263.5	0.346119	280.1	1.097348			275.4	0.130363
298.4	45.94838	288.4	13.0849	263.6	0.347393	280.2	1.111871			275.5	0.131679
298.5	46.50569	288.5	13.242	263.7	0.348673	280.3	1.126619			275.6	0.133009
298.6	47.06846	288.6	13.4014	263.8	0.349959	280.4	1.141596			275.7	0.134352
298.7	47.63671	288.7	13.5631	263.9	0.35125	280.5	1.156807			275.8	0.135707
298.8	48.21047	288.8	13.7271	264	0.352547	280.6	1.172257			275.9	0.137076
298.9	48.78977	288.9	13.8935	264.1	0.35385	280.7	1.187951			276	0.138459

299	49.37462	289	14.0624	264.2	0.35516	280.8	1.203894	276.1	0.139854
299.1	49.96506	289.1	14.2337	264.3	0.356475	280.9	1.220092	276.2	0.141263
299.2	50.5611	289.2	14.4076	264.4	0.357796	281	1.23655	276.3	0.142686
299.3	51.16278	289.3	14.5839	264.5	0.359123	281.1	1.253274	276.4	0.144123
299.4	51.77011	289.4	14.7629	264.6	0.360456	281.2	1.27027	276.5	0.145575
299.5	52.38313	289.5	14.9444	264.7	0.361795	281.3	1.287544	276.6	0.14704
299.6	53.00186	289.6	15.1287	264.8	0.36314	281.4	1.305103	276.7	0.14852
299.7	53.62631	289.7	15.3156	264.9	0.364492	281.5	1.322952	276.8	0.150015
299.8	54.25653	289.8	15.5052	265	0.365849	281.6	1.341099	276.9	0.151524
299.9	54.89253	289.9	15.6976	265.1	0.367213	281.7	1.359552	277	0.153048
300	55.53434	290	15.8928	265.2	0.368583	281.8	1.378316	277.1	0.154588
300.1	56.18198	290.1	16.0909	265.3	0.369959	281.9	1.397401	277.2	0.156142
300.2	56.83548	290.2	16.2918	265.4	0.371342	282	1.416813	277.3	0.157712
300.3	57.49487	290.3	16.4957	265.5	0.37273	282.1	1.436561	277.4	0.159297
300.4	58.16017	290.4	16.7025	265.6	0.374125	282.2	1.456653	277.5	0.160898
300.5	58.8314	290.5	16.9124	265.7	0.375527	282.3	1.477098	277.6	0.162514
300.6	59.5086	290.6	17.1252	265.8	0.376935	282.4	1.497906	277.7	0.164147
300.7	60.19178	290.7	17.3412	265.9	0.378349	282.5	1.519085	277.8	0.165796
300.8	60.88097	290.8	17.5603	266	0.37977	282.6	1.540647	277.9	0.16746
300.9	61.57621	290.9	17.7825	266.1	0.381197	282.7	1.5626	278	0.169142
301	62.27751	291	18.008	266.2	0.382631	282.8	1.584957	278.1	0.170839
301.1	62.9849	291.1	18.2366	266.3	0.384071	282.9	1.607728	278.2	0.172554
301.2	63.6984	291.2	18.4686	266.4	0.385518	283	1.630924	278.3	0.174286
301.3	64.41806	291.3	18.7038	266.5	0.386972	283.1	1.654559	278.4	0.176034
301.4	65.14388	291.4	18.9424	266.6	0.388432	283.2	1.678646	278.5	0.1778
301.5	65.87589	291.5	19.1844	266.7	0.389899	283.3	1.703197	278.6	0.179583
301.6	66.61413	291.6	19.4298	266.8	0.391372	283.4	1.728227	278.7	0.181384
301.7	67.35862	291.7	19.6787	266.9	0.392853	283.5	1.753751	278.8	0.183203
301.8	68.10938	291.8	19.9311	267	0.39434	283.6	1.779784	278.9	0.185039
301.9	68.86644	291.9	20.187	267.1	0.395834	283.7	1.806343	279	0.186894
302	69.62984	292	20.4465	267.2	0.397335	283.8	1.833445	279.1	0.188767
		292.1	20.7097	267.3	0.398843	283.9	1.861109	279.2	0.190658

292.2	20.9764	267.4	0.400357	284	1.889353	279.3	0.192568
292.3	21.2469	267.5	0.401879	284.1	1.918199	279.4	0.194497
292.4	21.521	267.6	0.403407	284.2	1.947667	279.5	0.196445
292.5	21.799	267.7	0.404942	284.3	1.977781	279.6	0.198413
292.6	22.0807	267.8	0.406485	284.4	2.008565	279.7	0.200399
292.7	22.3662	267.9	0.408034	284.5	2.040045	279.8	0.202406
292.8	22.6556	268	0.40959	284.6	2.072248	279.9	0.204432
292.9	22.9489	268.1	0.411154	284.7	2.105204	280	0.206478
293	23.2461	268.2	0.412725	284.8	2.138945	280.1	0.208545
293.1	23.5473	268.3	0.414303	284.9	2.173505	280.2	0.210632
293.2	23.8525	268.4	0.415889	285	2.20892	280.3	0.212739
293.3	24.1617	268.5	0.417482	285.1	2.245229	280.4	0.214868
293.4	24.4749	268.6	0.419084	285.2	2.282475	280.5	0.217017
293.5	24.7923	268.7	0.420692	285.3	2.320704	280.6	0.219188
293.6	25.1138	268.8	0.422309	285.4	2.359966	280.7	0.221381
293.7	25.4394	268.9	0.423932	285.5	2.400317	280.8	0.223595
293.8	25.7692	269	0.425563	285.6	2.441816	280.9	0.225831
293.9	26.1033	269.1	0.427201	285.7	2.484529	281	0.228089
294	26.4416	269.2	0.428845	285.8	2.52853	281.1	0.230369
294.1	26.7841	269.3	0.430497	285.9	2.5739	281.2	0.232673
294.2	27.131	269.4	0.432154	286	2.620731	281.3	0.234999
294.3	27.4823	269.5	0.433818	286.1	2.669122	281.4	0.237348
294.4	27.8379	269.6	0.435489	286.2	2.719179	281.5	0.23972
294.5	28.1979	269.7	0.437168	286.3	2.771007	281.6	0.242116
294.6	28.5623	269.8	0.438855	286.4	2.824711	281.7	0.244536
294.7	28.9312	269.9	0.440551	286.5	2.880396	281.8	0.24698
294.8	29.3046	270	0.442258			281.9	0.249448
294.9	29.6825	270.1	0.443977			282	0.251941
295	30.0649	270.2	0.445708			282.1	0.254458
295.1	30.4519	270.3	0.447451			282.2	0.257001
295.2	30.8435	270.4	0.449207			282.3	0.259569
295.3	31.2398	270.5	0.450971			282.4	0.262163

295.4	31.6407	270.6	0.45274	282.5	0.264782
295.5	32.0463	270.7	0.454511	282.6	0.267427
295.6	32.4566	270.8	0.456281	282.7	0.270099
295.7	32.8733	270.9	0.45804	282.8	0.272798
295.8	33.2927	271	0.4598	282.9	0.275523
295.9	33.7168	271.1	0.46154	283	0.278276
296	34.1458	271.2	0.46328	283.1	0.281056
296.1	34.5796	271.3	0.46503	283.2	0.283864
296.2	35.01824	271.4	0.466805	283.3	0.2867
296.3	35.46177	271.5	0.468613	283.4	0.289565
296.4	35.9102	271.6	0.470471	283.5	0.292458
296.5	36.36356	271.7	0.472393	283.6	0.29538
296.6	36.82189	271.8	0.474393	283.7	0.298332
296.7	37.2852	271.9	0.47647	283.8	0.301313
296.8	37.75351	272	0.478582	283.9	0.304324
296.9	38.22687	272.1	0.480676	284	0.307365
297	38.70528	272.2	0.482697	284.1	0.310436
297.1	39.18878	272.3	0.484592	284.2	0.313539
297.2	39.67738	272.4	0.486308	284.3	0.316673
297.3	40.17113	272.5	0.487791	284.4	0.319838
297.4	40.67003	272.6	0.489009	284.5	0.323035
297.5	41.17412	272.7	0.490132	284.6	0.326265
297.6	41.68342	272.8	0.491451	284.7	0.329527
297.7	42.19796	272.9	0.493255	284.8	0.332821
297.8	42.71775	273	0.495834	284.9	0.33615
297.9	43.24283	273.1	0.49948	285	0.339511
298	43.77322	273.2	0.504467	285.1	0.342907
298.1	44.30895	273.3	0.510576	285.2	0.346337
298.2	44.85003	273.4	0.517034	285.3	0.349802
298.3	45.3965	273.5	0.523312	285.4	0.353302
298.4	45.94838	273.6	0.529541	285.5	0.356837
298.5	46.50569	273.7	0.535903	285.6	0.360408

298.6	47.06846	273.8	0.54239
298.7	47.63671	273.9	0.548948
298.8	48.21047	274	0.555573
298.9	48.78977	274.1	0.562282
299	49.37462	274.2	0.569079
299.1	49.96506	274.3	0.57596
299.2	50.5611	274.4	0.582927
299.3	51.16278	274.5	0.589981
299.4	51.77011	274.6	0.597124
299.5	52.38313	274.7	0.604357
299.6	53.00186	274.8	0.61168
299.7	53.62631	274.9	0.619096
299.8	54.25653	275	0.626605
299.9	54.89253	275.1	0.634209
300	55.53434	275.2	0.64191
300.1	56.18198	275.3	0.649708
300.2	56.83548	275.4	0.657604
300.3	57.49487	275.5	0.665601
300.4	58.16017	275.6	0.6737
300.5	58.8314	275.7	0.681902
300.6	59.5086	275.8	0.690209
300.7	60.19178	275.9	0.698622
300.8	60.88097	276	0.707142
300.9	61.57621	276.1	0.715772
301	62.27751	276.2	0.724513
301.1	62.9849	276.3	0.733366
301.2	63.6984	276.4	0.742333
301.3	64.41806	276.5	0.751416
301.4	65.14388	276.6	0.760617
301.5	65.87589	276.7	0.769937
301.6	66.61413	276.8	0.779377
		276.9	0.788941
		285.7	0.364015
		285.8	0.367659
		285.9	0.371341
		286	0.375059
		286.1	0.378815
		286.2	0.38261
		286.3	0.386443
		286.4	0.390316
		286.5	0.394228
		286.6	0.39818
		286.7	0.402172
		286.8	0.406206
		286.9	0.41028
		287	0.414397
		287.1	0.418556
		287.2	0.422757
		287.3	0.427002
		287.4	0.43129
		287.5	0.435623
		287.6	0.44
		287.7	0.444423
		287.8	0.448891
		287.9	0.453405
		288	0.457967
		288.1	0.462575
		288.2	0.467232
		288.3	0.471937
		288.4	0.47669
		288.5	0.481494
		288.6	0.486347
		288.7	0.491251
		288.8	0.496207

277	0.798629
277.1	0.808444
277.2	0.818387
277.3	0.828461
277.4	0.838667
277.5	0.849007
277.6	0.859484
277.7	0.8701
277.8	0.880856
277.9	0.891755
278	0.902799
278.1	0.913991
278.2	0.925332
278.3	0.936825
278.4	0.948473
278.5	0.960278
278.6	0.972243
278.7	0.98437
278.8	0.996661
278.9	1.00912
279	1.02175
279.1	1.034552
279.2	1.047531
279.3	1.060688
279.4	1.074027
279.5	1.087551
279.6	1.101264
279.7	1.115168
279.8	1.129266
279.9	1.143563
280	1.158061
280.1	1.172765

288.9	0.501214
289	0.506274
289.1	0.511387
289.2	0.516553
289.3	0.521774
289.4	0.52705
289.5	0.532382
289.6	0.53777
289.7	0.543214
289.8	0.548717
289.9	0.554278
290	0.559898
290.1	0.565578
290.2	0.571318
290.3	0.57712
290.4	0.582983
290.5	0.58891
290.6	0.5949
290.7	0.600954
290.8	0.607073
290.9	0.613258
291	0.61951
291.1	0.62583
291.2	0.632218
291.3	0.638675
291.4	0.645202
291.5	0.651801
291.6	0.658471
291.7	0.665214
291.8	0.672031
291.9	0.678923
292	0.685891

280.2	1.187677
280.3	1.202802
280.4	1.218143
280.5	1.233705
280.6	1.249491
280.7	1.265505
280.8	1.281752
280.9	1.298236
281	1.314962
281.1	1.331934
281.2	1.349157
281.3	1.366636
281.4	1.384375
281.5	1.402381
281.6	1.420658
281.7	1.439211
281.8	1.458047
281.9	1.477171
282	1.496588
282.1	1.516307
282.2	1.536331
282.3	1.556669
282.4	1.577327
282.5	1.598312
282.6	1.619631
282.7	1.641291
282.8	1.663301
282.9	1.685669
283	1.708402
283.1	1.731509
283.2	1.755
283.3	1.778883
292.1	0.692935
292.2	0.700057
292.3	0.707258
292.4	0.714538
292.5	0.721899
292.6	0.729342
292.7	0.736868
292.8	0.744478
292.9	0.752174
293	0.759955
293.1	0.767824
293.2	0.775782
293.3	0.78383
293.4	0.791969
293.5	0.8002
293.6	0.808525
293.7	0.816945
293.8	0.825461
293.9	0.834075
294	0.842788
294.1	0.851601
294.2	0.860516
294.3	0.869535
294.4	0.878658
294.5	0.887888
294.6	0.897226
294.7	0.906673
294.8	0.916231
294.9	0.925902
295	0.935687
295.1	0.945588
295.2	0.955607

283.4	1.803169
283.5	1.827867
283.6	1.852987
283.7	1.878541
283.8	1.90454
283.9	1.930995
284	1.95792
284.1	1.985326
284.2	2.013227
284.3	2.041638
284.4	2.070574
284.5	2.100049
284.6	2.13008
284.7	2.160684
284.8	2.19188
284.9	2.223686
285	2.256123
285.1	2.289211
285.2	2.322974
285.3	2.357436
285.4	2.392622
285.5	2.42856
285.6	2.465278
285.7	2.502809
285.8	2.541185
285.9	2.580444
286	2.620624
286.1	2.661768
286.2	2.703923
286.3	2.747139
286.4	2.791472
286.5	2.836985
295.3	0.965746
295.4	0.976007
295.5	0.98639
295.6	0.996899
295.7	1.007535
295.8	1.018301
295.9	1.029197
296	1.040227
296.1	1.051392
296.2	1.062695
296.3	1.074137
296.4	1.085722
296.5	1.097451
296.6	1.109326
296.7	1.121351
296.8	1.133528
296.9	1.145859
297	1.158347
297.1	1.170994
297.2	1.183803
297.3	1.196778
297.4	1.209921
297.5	1.223235
297.6	1.236722
297.7	1.250387
297.8	1.264233
297.9	1.278262
298	1.292478
298.1	1.306884
298.2	1.321485
298.3	1.336283
298.4	1.351283

286.6	2.883746
286.7	2.931831
286.8	2.981328
286.9	3.032336
287	3.084967

298.5	1.366488
298.6	1.381903
298.7	1.397531
298.8	1.413377
298.9	1.429446
299	1.44574
299.1	1.462266
299.2	1.479029
299.3	1.496032
299.4	1.513281
299.5	1.530782
299.6	1.548539
299.7	1.566559
299.8	1.584847
299.9	1.60341
300	1.622252
300.1	1.641382
300.2	1.660806
300.3	1.680529
300.4	1.700561
300.5	1.720908
300.6	1.741577
300.7	1.762578
300.8	1.783918
300.9	1.805605
301	1.82765
301.1	1.850061
301.2	1.872849
301.3	1.896023
301.4	1.919595
301.5	1.943575
301.6	1.967975

301.7	1.992808
301.8	2.018086
301.9	2.043823
302	2.070033
302.1	2.09673
302.2	2.123932
302.3	2.151653
302.4	2.179912
302.5	2.208726
302.6	2.238116
302.7	2.268101

S4. Fugacity Calculation

Figure S1 offers adequate details in the form of an algorithm to determine the magnitude of fugacity where PC-SAFT equation of state is employed. As it is clear from Figure S1, in addition to pressure, temperature, and mole fractions of the components, the PC-SAFT constants such as $m, \sigma, \varepsilon, \kappa, k_{ij}$, and ε^{AB} for all components via using Equations (S-9), (S-13), and (S-17) – (S-26) are required. The next step is to take a good initial estimate for the reduced density to calculate the compressibility factor and pressure. After that, we should find the magnitudes of important parameters including $d_i, g_{ii}^{hs}, C_1,$ and C_2 by Equations (S-9), (S-13), and (S-17) – (S-26). The compressibility factor can be then calculated through using Equation (S-7). Equation (S-28) will be utilized to obtain a new pressure. If the magnitudes of new and old pressures (P_{new} and P_{old}) are almost the same, the guessed reduced density is correct; otherwise, the above procedure is repeated to calculate the reduced density using the

new pressure. The next step is to calculate μ_k^{res} by Equations (S-17) and (S-30) to (S-48). The fugacity and fugacity coefficient are finally determined by Equation (S-29).

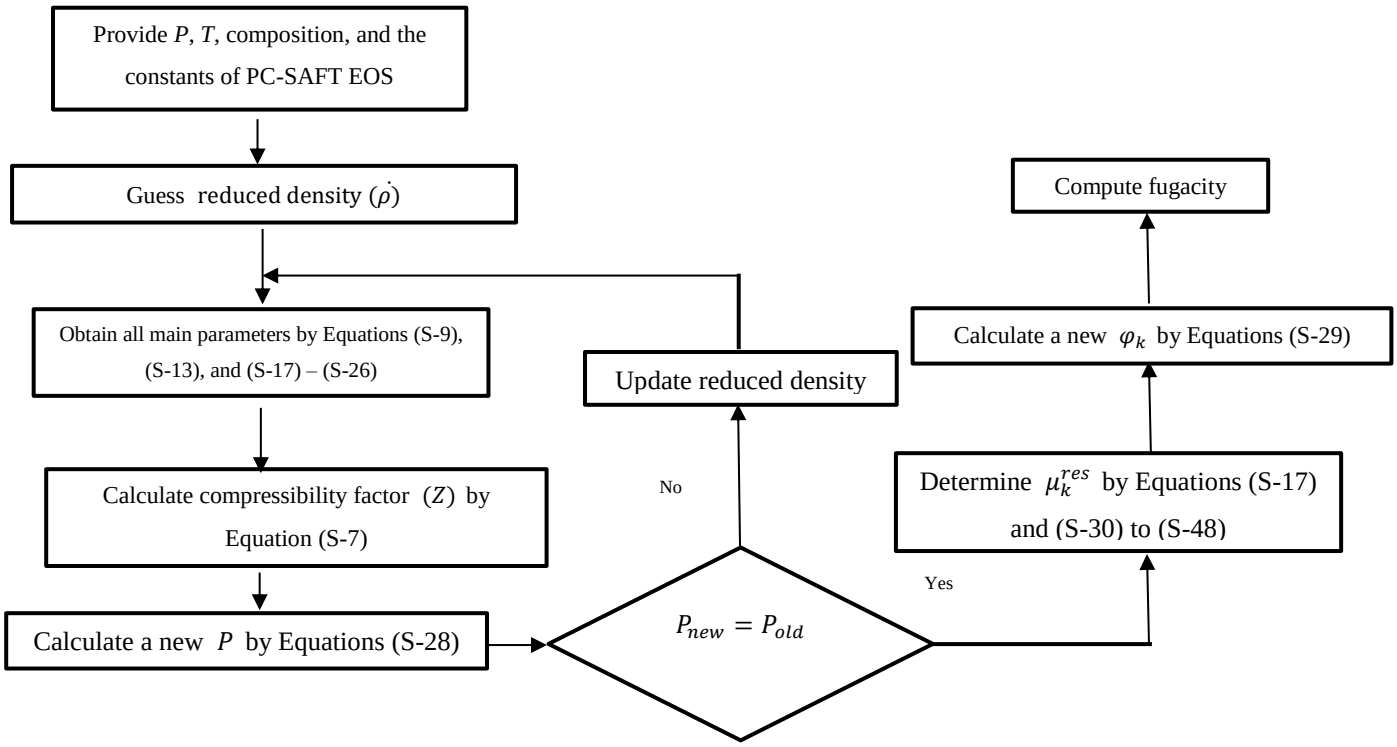

Figure S1: Flow diagram for calculation of fugacity for all gaseous components at various temperatures and pressures (T and P).

S5. Gas Solubility Calculation

In this section, a systematic procedure to calculate the solubility of gases in the aqueous phase is described. The solubility of the gasses in the aqueous phase is needed in the UNIQUAC model to determine the water activity. The equality of a component fugacity in both gas and liquid phases is the main criterion for thermodynamic equilibrium condition, as shown below:

$$f_i^v = f_i^l \qquad \text{(S-49)}$$

The fugacity of component *i* in the liquid phase is obtained by the following expression [9]:

$$f_i^l = H_i x_i exp(\frac{v_i^\infty (P - P_i^{sat})}{RT}) \quad \text{(S-50)}$$

where v_i^∞, x_i, P_i^{sat}, and H_i denote the infinite partial molar volume, mole fraction (in the liquid phase), vapor pressure, and Henry's constant of component *i*, respectively. Using Equation (S-49), one can rewrite Equation (S-50) as follows:

$$x_i = \frac{f_i^v}{H_i exp(\frac{v_i^\infty (P - P_i^{sat})}{RT})} \quad \text{(S-51)}$$

In this work, the Henry's constant (H_i) is a function of temperature as given by the following equation [10]:

$$H_i(Pa) = 1000 \times \exp(a + bT + \frac{c}{T} + dln(T)) \quad \text{(S-52)}$$

The infinite partial molar volume, which is dependent on the pressure and temperature, is expressed as follows [2]:

$$v_i^\infty (cm^3/mol) = (e + fT + gP) \quad \text{(S-53)}$$

All constants of Equations (S-52) and (S-53) are listed in Table S6 [2, 11].

Table S6: Constants used in Equations (S-52) and (S-53).

Gas	a	b	c	d	e	f	g
CH_4	147.788	-5768.3	-52.29	0.0186	100	-0.338	0.002457
C_2H_6	146.637	-5768.3	-51.85	0.01741	100	0.5201	0.01
C_3H_8	552.648	0.07845	-21334	-85.89	0	0.6189	0
i-C_4H_{10}	146.66	-5768.3	-52.42	0.02404	0	0	0
CO_2	21.621	-1499.8	-5.649	0.00020	32.8	0	0
H_2S	69.445	-3796.5	-21.625	-0.000015	34.9	0	0
N_2	78.852	-3745	-5.6494	0.00029	35.7	0	0

Table S7 presents a part of the typical results for the solubility of methane in water, where the methane hydrate system is studied. To calculate the gas solubility at each thermodynamic condition (e.g., temperature and pressure), the last value (updated) of gas fugacity, which is determined by employing an EOS through the procedure explained in Section S4, is used. Given the gas fugacity and model parameters provided in Table S6, the gas solubility can be computed through using Equations (S-51) - (S-53).

Table S7: Typical results for the methane solubility in water.

$T[K]$	*Pressure* $[MPa]$	$x_2^{exp} \times 10^4$	$x_2^{cal} \times 10^4$	***Absolute Error (%)***	φ_1^G	φ_2^G	***Reference***
298.15	2.351	4.97	5.23	5.23	0.787	0.961	[12]
	3.165	7.17	7.04	1.81	0.723	0.948	[12]
	4.544	10.00	9.54	4.60	0.623	0.927	[12]
	6.44	13.17	12.8	2.81	0.509	0.900	[12]
	8.894	16.78	15.97	4.83	0.389	0.868	[12]
	13.307	22.35	21.5	3.80	0.244	0.821	5
	17.202	25.85	24.7	4.45	0.168	0.789	5
	24.235	31.1	30.1	3.22	0.099	0.753	5

In Table S7, x_2^{exp} and x_2^{cal} stand for the experimental and calculated mole fraction of component 2 (methane) in the liquid phase, respectively.

As it is clear from the magnitudes of absolute error percentages in Table S7, there is a very agreement between the predictions and real data, again confirming the reliability of the thermodynamic modeling approach in this research study.

S6. Comparison between Results with and without Association Energy Terms

In this section, a series of results for gas hydrate formation temperature of CH_4/Methanol/Water systems are provided. There are two different cases discussed in this Supporting Information; the first scenario (Case 1) is to consider the association Helmholtz

energy ($\bar{a}^{association}$) of mixtures to calculate the residual Helmholtz free energy ($\bar{a}^{res}$) given by Equation (14) in the manuscript, where all three interaction parameters (k_{ij} , v_{ij} , and λ_{ij}) are used in the calculation/modeling procedure. The second case (Case 2) considers only binary interaction (k_{ij}) to obtain the temperature of hydrate formation in the presence of alcohols. Table S8 demonstrates a comparison between Case 1 and Case 2 in terms of AADT%. As it is clear from Table S8, the absolute error percentage is lower for Case 1 (the case with association terms), though Case 2 also offers acceptable accuracy while determining the temperature of hydrate formation. The impact of the association is low as a part of the water molecules are surrounded by the alcohol, in the presence of hydrate, leading to the weak association phenomenon.

Table S8: Effect of association energy terms on value of hydrate formation temperature.

Gas Phase	Liquid Phase	Pressure (MPa)	Experimental T (K)	Calculated T (K) [Case 1]	Calculated T (K) [Case 2]	AADT% [Case 1]	AADT% [Case 2]
CH_4	10% Methanol	2.62	268.5	268.23	269.06	0.10	0.21
		3.95	272.8	272.52	273.36	0.05	0.21
		5.52	276.1	275.95	276.79	0.09	0.25
		7.85	279.7	279.45	280.31	0.06	0.22
		9.78	281.4	281.57	282.44	0.01	0.37
	20% Methanol	2.95	264.6	264.58	265.69	0.01	0.41
		4.34	268.5	268.46	269.65	0.15	0.43
		6.01	272.1	271.7	272.91	0.11	0.30
		8.08	274.8	274.5	275.77	0.11	0.35
		10.11	276.3	276.6	277.88	0.10	0.57

References

[1] Abolala, M. and F. Varaminian, *Thermodynamic model for predicting equilibrium conditions of clathrate hydrates of noble gases+light hydrocarbons: Combination of Van der Waals–Platteeuw model and sPC-SAFT EoS.* The Journal of Chemical Thermodynamics, 2015. **81**: p. 89-94.

[2] Mohebbi, V., A. Naderifar, R. Behbahani, and M. Moshfeghian, *Determination of Henry's law constant of light hydrocarbon gases at low temperatures.* The Journal of Chemical Thermodynamics, 2012. **51**: p. 8-11.

[3] Heidemann, R.A. and J.M. Prausnitz, *Equilibrium data for wet-air oxidation. Water content and thermodynamic properties of saturated combustion gases.* Industrial & Engineering Chemistry Process Design and Development, 1977. **16**(3): p. 375-381.
[4] Delavar, H. and A. Haghtalab, *Thermodynamic modeling of gas hydrate formation conditions in the presence of organic inhibitors, salts and their mixtures using UNIQUAC model.* Fluid Phase Equilibria, 2015. **394**: p. 101-117.
[5] Chapman, W., K. Gubbins, G. Jackson, and M. Radosz, *New Reference Equation of State for Associating Liquids.* Ind. Eng. Chem. Res., 1990. **29**: p. 1709.
[6] Gross, J. and G. Sadowski, *Perturbed-Chain SAFT: An Equation of State Based on a Perturbation Theory for Chain Molecules.* Ind. Eng. Chem. Res., 2001. **40**: p. 4.
[7] Mejbri, K. and A. Bellagi, *Modelling of the thermodynamic properties of the water–ammonia mixture by three different approaches.* International Journal of Refrigeration, 2006. **29**(2): p. 211-218.
[8] Mejbri, K., A. Taieb, and A. Bellagi, *Phase equilibria calculation of binary and ternary mixtures of associating fluids applying PC-SAFT equation of state.* The Journal of Supercritical Fluids, 2015. **104**: p. 132-144.
[9] Prausnitz, J.M., R.N. Lichtenthaler, and E.G. de Azevedo, *Molecular Thermodynamics of Fluid-Phase Equilibria*. 1998: Pearson Education.
[10] Chapoy, A., A. Mohammadi, A. Valtz, C. Coquelet, and D. Richon, *Water and inhibitor distribution in gas production systems.* GPA Research Project, 2008. **987**.
[11] Akinfiev, N.N. and L.W. Diamond, *Thermodynamic description of aqueous nonelectrolytes at infinite dilution over a wide range of state parameters.* Geochimica et Cosmochimica Acta, 2003. **67**(4): p. 613-629.
[12] Aoyagi, K., K.Y. Song, and R. Kobayashi, *I. The water Content and Correlation of the Water Content of Methane in Equilibrium with Hydrate. II. The Water Content of a High Carbon Dioxide Simulated Prudhoe Bay Gas in Equilibrium with Hydrates*. 1980.

4. CHAPTER FOUR

New Insights into Methane Hydrate Dissociation: Utilization of Molecular Dynamics Strategy (Published)

Preface

A version of this manuscript has been published in the Fuel 249 (2019): 264-276. I am the primary author of this paper. Sohrab Zendehboudi and Lesley James provided me with valuable tips/guidelines to conduct the literature review, and the MD simulations. I prepared the first draft of the manuscript and then revised the manuscript based on the co-authors' feedback as well as the comments of the peer review process. The co-author Sohrab Zendehboudi also helped in model development, creating a proper manuscript structure, and revising all parts of the manuscript. The last co-author, Lesley James, provided comments on various section of the manuscript. She also edited the entire text.

Abstract

Hydrate reserves play a crucial role in energy storage and resources across the world. The gas hydrates formation may lead to various forms of blockages in oil/gas production and transportation processes, resulting in high capital and operating costs. Hence, it is important to determine the methane hydrate formation conditions and to find the vital process and thermodynamic parameters affecting this occurrence. In this study, molecular dynamic (MD) simulations are conducted to investigate the microscopic mechanisms/phenomena and intermolecular forces involved in methane hydrate decomposition, where molecular interactions, structures, and behaviours need to be appropriately determined/selected. Through a systematic parametric sensitivity analysis, the impacts of temperature, pressure, and cage occupancy on the hydrate dissociation are studied. Furthermore, the diffusion coefficient, density, and heat capacity of the methane hydrate are determined through employing MD strategy. The stability of water cages is also examined at various decomposition times, temperatures, and pressures. According to the radial distribution function and mean square displacement of oxygen-oxygen and carbon-carbon atoms, the stability of hydrate cages lowers with increasing temperature, while it increases with increasing the cage occupancy and pressure. Addition of inhibitors (e.g., methanol) to small cavities in the hydrate structure creates new hydrogen bonds between the water and inhibitor molecules in the cages, leading to acceleration of decomposition of hydrates. A good agreement is noticed between the outcomes of this research work and the results attained in experimental and theoretical studies available in the open sources. Analysing the outcome of the present and previous works, the current study provides new reliable/logical information on the molecular level of the hydrate dissociation process. It is expected that such a research investigation offers effective

tips/guidelines to deal with hydrate formation and dissociation in terms of utilization, prevention, and processing.

Keywords: Methane Hydrate; Dissociation; Molecular Dynamics; Cage Occupancy; Diffusion Coefficient

4.1. Introduction

Natural gas hydrates are crystalline ice-like compounds in which the guest molecules are trapped in the polyhedral cells created within the hydrogen-bonded water framework [1]. The gas hydrates can be formed at low temperatures and high pressures due to the van der Waals interactions between the guest gas molecules and water lattices, and the hydrogen bonds between water molecules [1]. Due to the size and properties of guest molecules in the cages, different hydrate structures namely, Structure I, Structure II, and Structure H can be created [1]. These three structures differ in the crystal structure in terms of the type and number of cages. The lattice parameter of cubic Structure I is 12.05, which consists of two small (5^{12}) and six large ($5^{12}6^2$) cages. The small (pentagonal dodecahedral) and large cages (tetrakaidekahedral) are composed of 12 pentagonal water rings and 12 pentagonal plus two hexagonal faces, respectively. Figure 4-1 demonstrates the lattice structure of the water molecules in Structure I gas hydrates for small and large cages.

Currently, gas hydrates have attracted increasing interests due to their wide applications in future energy sources/storage [2], gas transportation [3], gas separation [4], and water treatment distillation [5]. There are also research studies in the literature which discuss about problems (e.g., blockage) created by gas hydrates in equipment and pipeline systems in oil and gas industries [6].

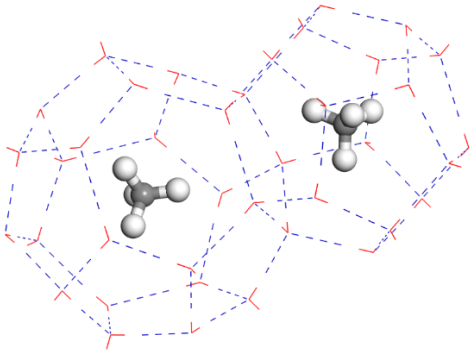

Figure 4-1: The lattice structure of small and large cages of water molecules in Structure I.

Gas hydrates, mainly methane hydrate, have provided valuable and huge gas resources in permafrost and profound areas due to the fact at the standard condition, each cubic meter of natural gas hydrate contains about 160-180 cubic meters of natural gas [1]. In the past decades, several researchers studied natural gas production by methane hydrate dissociation through experimental (and pilot scale) and modeling/simulation investigations [7-11]. There are three major methods to produce natural gas (mainly methane) from gas hydrates; namely, depressurisation, thermal stimulation, and chemical injection [12]. The hydrate formation or decomposition can be affected by chemical or additive injection [13]. Thus, the role of additives in the dissociation acceleration and the formation inhibition needs to be studied in detail. A number of studies are found in the literature to investigate important prospects of additives in terms of improving storage capacity [14], dissociation [15], and formation rate [16] of gas hydrates. The monitoring and controlling of hydrate formation and/or decomposition through experimental works at various process conditions is relatively difficult and inaccurate. In recent years, molecular dynamic (MD) simulations have been used as a reliable tool to study the structure [17], nucleation [18], growth [19], stability [20], and thermodynamic properties [21] of gas hydrates. In the MD simulations, the movement of each

atom and molecules is determined by using the Newton's laws and the empirical potential functions are utilized to describe the interactions between all components in the simulation box. In our most recent work, we prepared a comprehensive review on the applications of MD simulation and different potential functions, which are used in the simulation of gas hydrates dissociation [12]. Wan et al. [22] employed MD simulations for methane gas hydrate dissociation in the systems that contained alcohol as an additive. In addition, Zhang and Pan [19] obtained the dynamic and structural properties of the methane hydrates, for example, mean square

4.2. Simulation Information and Procedure

Several science and engineering disciplines need to compute the motion and equilibrium of atoms or molecules in each system by employing efficient computational strategies such as molecular dynamic (MD) simulations. The MD approach is a powerful tool to demonstrate the microscopic scale of various chemical and physical phenomena/systems. It provides better/detailed knowledge in molecular level regarding dynamic and structural characteristics of complex and/or simple chemical systems [27-29]. The primary stage of MD method is calculating all atoms coordinates and summation of all potential energies that provide the force on each atom. The force for molecules consists of the van der Waals, electrostatic, dihedral, angle bending, bond stretching, and torsional rotation [27-29]. In the classical mechanics, the Newton's law is utilized to obtain the position of each particle at a specific time by employing different algorithms to solve equation of motion [30-32]. In the last step of the simulation, the thermodynamic and dynamic properties are calculated by using the statistical mechanics.

. MD simulations are an effective strategy that allows for the analysis of systems at very low and high temperatures and pressure conditions. These thermodynamic conditions present

practical challenges when attempting to obtain experimental data, which highlights the advantages of using MD. At these thermodynamic conditions, we also need to calibrate or tune some parameters if an equation of state (EOS) is utilized. Another advantage of using MD simulations is that the tool needs only description of intermolecular and interatomic interactions as the inputs. In addition, the best way to analyze and find new features of the rare and expensive materials such as polymers or proteins is utilization of MD simulations under various process and thermodynamic conditions. Additionally, the special characters (e.g., forces and interactions) of molecules can be explored only with MD simulations. For instance, the diffusion and movement of small molecule of enzymes need the transient appearance of the protein's channel, which is feasible by using MD tools [33, 34]. The molecular dynamic simulations can be more useful to forecast and characterize the dynamic properties including mechanical and thermophysical characteristics in aerospace, electronics, and energy industries. However, the accuracy of MD simulations highly relies on the selection (or type) of potential functions. The regular size of the simulation cell size is in order of nm. Hence, the spatial correlation lengths and structure of any system should be less than the size of the simulation cell. Furthermore, MD simulations require to be ran using powerful computers with a high CPU so that the simulation runs might take fairly long time. Although the molecular dynamics simulation strategy has successfully simulated the complex systems, it has certain limitations in terms of the cell size and time of simulation runs.

In this research study, the molecular dynamic (MD) simulations are used to investigate the decomposition of methane hydrate, considering the effects of temperature, pressure and cage occupancy as well as the hydrate stability in the presence of methanol as an inhibitor. The MD simulations are performed by using the Forcite modules and consistent valence force field

(CVFF) of Materials Studio software [35]. The unit cell of hydrate Structure I is constructed by using oxygen atoms of water molecules positions, which are determined from x-ray diffraction [36]. A 3×3×3 supercell is built by replication of a unit cell to create a simulation box with 36.09×36.09×36.09 Å size and 1242 water molecules. The simulation box contains 54 small and 162 large cavities. Methane molecules are placed in all 162 of the large cages; the large cavities are filled with methane molecules for any cage occupancy. The methane molecules in small cavities are removed to simulate various cage occupancies so that they are replaced by the methanol molecules to investigate the inhibitor influence. Table 4-1 lists the required information of all different models, which are constructed.

Table 4-1: Summary of the concentration of guest molecules in initial simulation box.

Case	Occupancy (%)	Methane molecules		Methanol Molecules	
		Small cavity	Large cavity	Small cavity	Large cavity
1	100	54	162	0	0
2	87.5	27	162	0	0
3	75	0	162	0	0
4	100	52	162	2	0

The cage occupancy is calculated by the ratio of the number of methane molecules in the simulation box to 216, which indicate the maximum possible number of all methane molecules in the simulation box. For instance, in this study for 100% cage occupancy, the methane hydrate consists of 216 methane molecules (54 molecules in small cavities and 162 molecules in large cavities) and 1242 water molecules. In the case of 87.5% and 75% cage occupancy, the number of hydrates in the cavities is changed by 189 and 162, respectively. Two methanol molecules replace two methane molecules in small cavities to study the role of inhibitor in the

dissociation process. In this work, the decomposition process is evaluated for three different occupancies (100%, 87.5%, and 75%) without an inhibitor and in the presence of methanol molecules at three various temperatures (250, 260, and 270 K) at 50 MPa pressure. In addition, the impact of pressure is investigated for the methane hydrate case with 100% cage occupancy at temperature 280 K, where three different pressures (5, 10, and 50 MPa) are examined. Firstly, the energy minimization and geometry optimization for the initial simulation box are needed. To obtain the stable structure, both steepest descent and conjugate gradient methods of the Forcite module are employed [35]. In the steepest descent optimization method, a linear search is introduced on the basis of the direction of the energy downhill drop. In this strategy, the geometry minimization is first performed in the opposite direction at which the gradient holds the highest value at the initial point. The new line searches for a direction with the minimum energy by the orthogonal direction to the last gradient. This approach is repeated until the minimum energy is attained in all directions with an adequate tolerance. This methodology is usually used for structures, which are away from the equilibrium condition, to achieve a status with low energy. This technique is not generally efficient because the new directions must be perpendicular to the last direction. Hence, this method experiences considerable fluctuations to find a structure with the minimum energy and it will be very slow. Based on the above reason, the conjugate gradient method is used after minimizing the energy with the steepest descent [35]. In this method, the convergence speed is improved by using the information of the last direction for the next orthogonal direction search to avoid fluctuating around the minimum energy state. This strategy provides a proper set of conjugate directions, which move constantly toward the minimum energy. The space of energy is determined by the conjugate directions. It implies that the case with the minimum energy is found at the end of algorithm.

It can be concluded that it is a logical way to utilize the steepest descent method for the first optimization and then to implement the conjugate gradient methodology for reaching an accurate optimization. In this case, the chance of finding a structure with the minimum energy case is high at the end of geometry [35]. The constant volume and constant temperature (NVT) ensemble is performed for 20 ps to reach each targeted temperature. The constant pressure and constant temperature (NPT) ensemble MD simulations are carried out to demonstrate the decomposition process at all thermodynamic (T and P) conditions. The consistent valence forcefield (CVFF) is available in the Materials Studio package, which describes the parameters for water, hydrocarbons, amino acids, and many organic molecules [37]. It automatically uses the generic parameters when the explicit parameters are not found (e.g., automatic assignment of values for missing parameters). Liu et al. [38] employed the CVFF to calculate the intermolecular forces of all molecules in methane and carbon dioxide hydrate clathrate. In the CVFF, the water model for the potential function is the simple point charge (SPC). Utilization of SPC as a potential function for water molecules in the gas hydrate were recently studied by Burnham et al. [39] and Liu et al. [38]. According to their results, the one-site charges on oxygen and hydrogen in the water molecules are +0.41e and -0.82e, respectively. Also, the charges for the carbon and hydrogen for methane molecule in the CVFF feature of the Materials Studio are -0.4e and +0.1e, respectively. The energy expression for CVFF is given below [35, 40, 41]:

$$E = \sum_{b} D_b[1-e^{-\alpha(b-b_0)}] + \sum_{\theta} H_\theta \left(\theta-\theta_0\right)^2 + \sum_{\phi} H_\phi \left[1-S\cos(n\phi)\right] + \sum_{X} H_X X^2 +$$
$$\sum_{b}\sum_{b'} F_{bb'}(b-b_0)(b'-b_0') + \sum_{\theta}\sum_{\theta'} F_{\theta\theta'}(\theta-\theta_0)(\theta'-\theta_0') + + \sum_{b}\sum_{\theta} F_{b\theta}(b-b_0)(\theta-\theta_0) + \quad (4\text{-}1)$$
$$\sum_{\phi} F_{\phi\theta\theta'}\cos\phi(\theta-\theta_0)(\theta'-\theta_0') + \sum_{X} F_{XX'}XX' + + \sum \varepsilon\left[\left(\frac{r^*}{r}\right)^{12} - 2\left(\frac{r^*}{r}\right)^{6}\right] + \frac{q_i q_j}{\varepsilon r_{ij}}$$

where D, H, and F stand for the force constants; and b, θ, X and ϕ denote the bond length, bond angle, out-of-plane parameter, and dihedral angle, respectively. The zero condition represents the equilibrium value of that parameter. r_{ij} refers to the distance between particle *i* with charge q_i from particle *j* with charge q_j; ε introduces the well depth in van der Waals interaction term; and S and n are the sign convention and nonnegative integer coefficient parameters for the dihedral term, respectively.

In Equation (4-1), the first four terms represent the diagonal terms of valence of forcefield. The first term is the Morse potential, which is used for the bond-stretching term. The simple harmonic potential is added to this term. In most cases, the bond interactions are negligible, compared to the non-bond interactions. The second, third, and fourth terms are attributed to the energy deformation of bond angles, torsion angles, and out-of-plane interaction, respectively. The cross terms are represented by terms five to nine, which demonstrate the couplings through the internal coordinate deformation. For example, the coupling between the adjacent bonds stretching is shown by the fifth term. In addition, the dynamic properties of systems are calculated through using these terms. The last two terms in Equation (4-1) show the non-bonded interactions, where the tenth term represents the van der Waals interactions with the Lennard-Jones function and the eleventh term corresponds to the electrostatic interaction with the Coulomb function [35]. The CVFF force field is employed to explain the

molecular interactions in the methane hydrate clathrate. The van der Waals and long-range Coulomb interaction terms are computed by using the Ewald summation [35]. The temperature

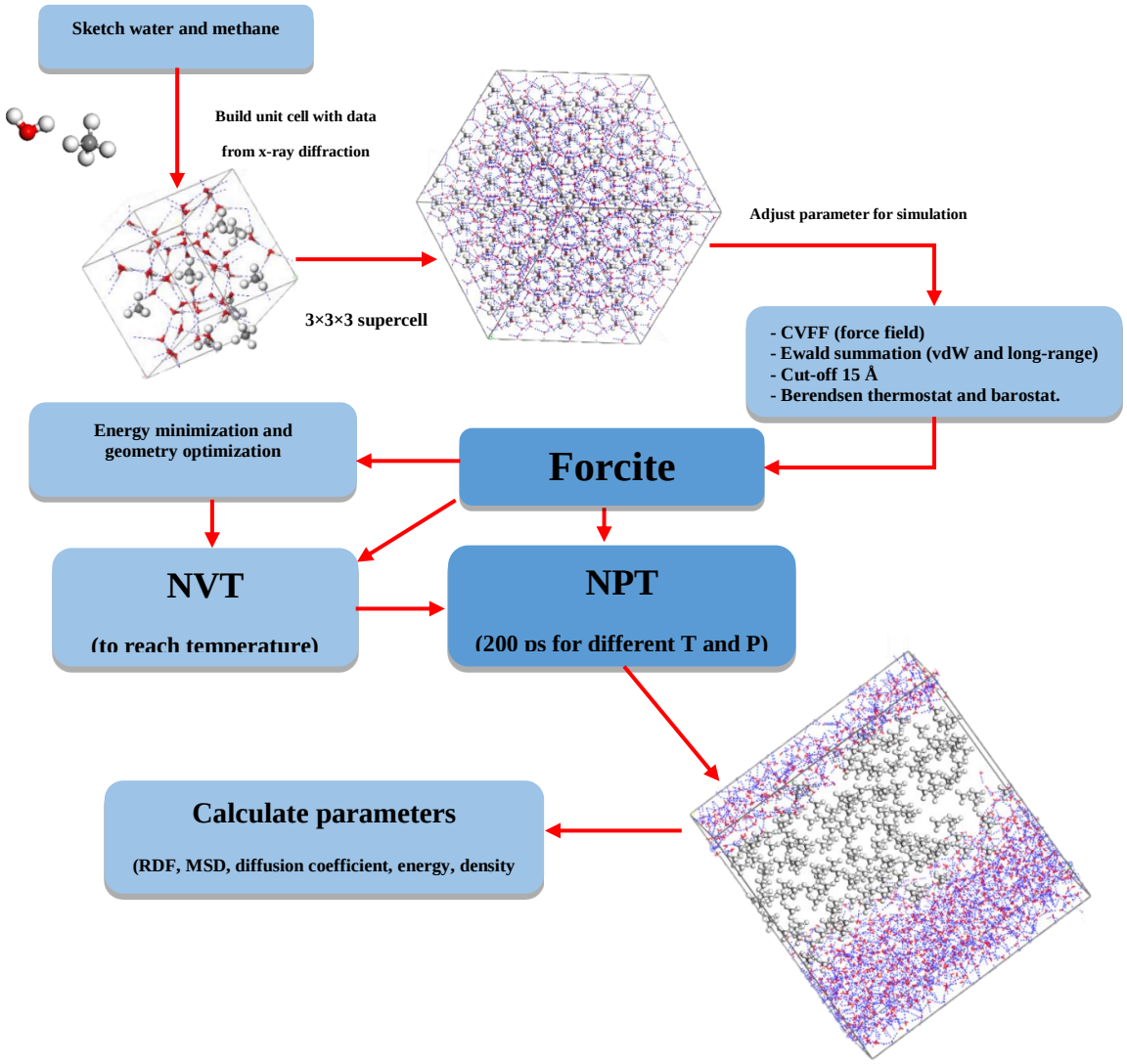

Figure 4-2: Main stages for MD simulation of methane hydrate decomposition.

and pressure of the objective system are adjusted by using the Berendsen thermostat and Berendsen barostat [42] with a decay constant of 0.2 ps and 0.1 ps, respectively. In addition, the van der Waals interactions in the simulation box are determined with a cut-off distance of 15.0 Å. Figure 4-2 demonstrates a simple schematic of the procedure for MD simulations of gas hydrate dissociation, where the Material Studio is employed.

4.3. Results and Discussion

Different cage occupancies, temperatures, and pressures and presence of additional molecules such as inhibitors (methanol) in methane hydrate dissociation are studied in this research work. The results achieved through using molecular dynamic simulations for the corresponding discussion are provided in this section. The structural and thermodynamic properties of clathrate hydrate are explored through discussing about the mean square displacement, radial distribution function, diffusion coefficient, potential energy, and structured snapshots.

4.3.1. Radial Distribution Function (RDF)

The microscopic and characteristic properties of methane hydrate structures are investigated to further explore the dissociation event of the hydrate clathrate. In this section, we analyse the radial distribution function (RDF) $g_{\alpha\beta}(r)$ at different temperatures, pressures, and cage occupancies. The occurrence probability to find the atom β in the distance of *r* from the atom α is RDF, $g_{\alpha\beta}(r)$, which is expressed below:

$$g_{\alpha\beta}(r) = \frac{V}{N_\alpha N_\beta}\left(\sum_{i=1}^{N_\alpha}\frac{n_i\beta(r)}{4\pi r^2\Delta r}\right) \tag{4-2}$$

In Equation (4-2), V denotes the volume of simulation box; N_α and N_β refer to the total number of α and β particles, respectively; and $n_i\beta(r)$ stands for the total number of β apart from atom α at the spherical distance of *r*. In this work, the g_{cc} (carbon-carbon) and g_{oo} (oxygen-oxygen) radial distribution functions are used to simulate the structure of water and methane in methane hydrate systems. The RDF is studied to assess the stability of methane

hydrate cages at different conditions in terms of temperature, cage occupancy, pressure, and absence or presence of methanol.

Temperature Impact. Figure 4-3 demonstrates the g_{oo} and g_{cc} at pressure 5 MPa and temperatures of 260, 270, and 280 K. The RDFs of oxygen-oxygen atoms in H_2O molecules are depicted in Panel (a) of Figure 4-3. The RDF is calculated from the NPT simulation for 100% cage occupancy of methane hydrate in 200 ps. The first maximum peak shows that the nearest distance corresponds to the oxygen-oxygen distance of hydrogen bonding (2.755 Å) of water. The second and third peaks appearing at 4.525 Å and 6.505 Å represent the distance of oxygen atoms in the hydrogen bonding of hydrate cages.

Table 4-2 shows the comparison between the major peaks in the RDFs of our work and previous studies for the methane hydrate system. The reported value represents the average of the major peaks in RDFs for different temperature and pressure conditions. The minimum and maximum errors are reported in Table 4-2. AAD% represents the average absolute deviation percentage. According to the magnitudes of AAD%, there is a very good agreement between the results of the current research investigation and previous studies available in the literature.

Table 4-2: RDFs of methane hydrate systems for this simulation and those reported in the literature.

RDF (Å)	Peak	Zhang et al.[23]	Ding et al.[43]	Zhang and Pan[19]	Erfan-Niya et al.[44]	Naeiji et al.[45]	This Work	Min. Error	Max. Error	AAD%*
Oxygen-Oxygen	First	2.75	2.78	2.75	2.775	2.75	2.755	0.211	0.666	0.435
	Second	4.40	4.53	4.49	4.425	4.45	4.525	0.876	2.428	1.502
	Third	6.67	6.35	6.37	6.375	6.60	6.505	1.839	2.259	2.090
Carbon-Carbone	First		4			4.25	3.965	2.976	5.76	4.035
	Second	7.5	6.6		6.525	6.65	6.665	0.861	5.47	1.444
	Third		11.3		11.925	10.75	11.02	3.79	5.16	4.401

* $ADD\%=100\times\frac{1}{n}\sum_{1}^{n}\left(\frac{RDF_{Litrature}-RDF_{This\ work}}{RDF_{This\ work}}\right)$; n represents the number of data points.

As observed in Figure 4-3, the peak of g_{oo} becomes lower but the peak valleys become higher with increasing temperature at a constant pressure. This behavior exhibits low stability of oxygen atoms in water molecules and hydrate cages due to the small ordering degree of oxygen atoms. Thus, the possibility of methane hydrate dissociation will increase at a constant pressure when an increase in the temperature is experienced. Figure 4-3(b) illustrates the RDF of carbon-carbon atoms in methane molecules at different temperatures for the methane hydrate system at 5 MPa and 200 ps. There is a considerable peak at around 6.6 Å that belongs to the distance of many methane molecules in the hydrate cages, implying that the nearest distance between the methane molecules in the hydrate structure is nearly 6.6 Å.

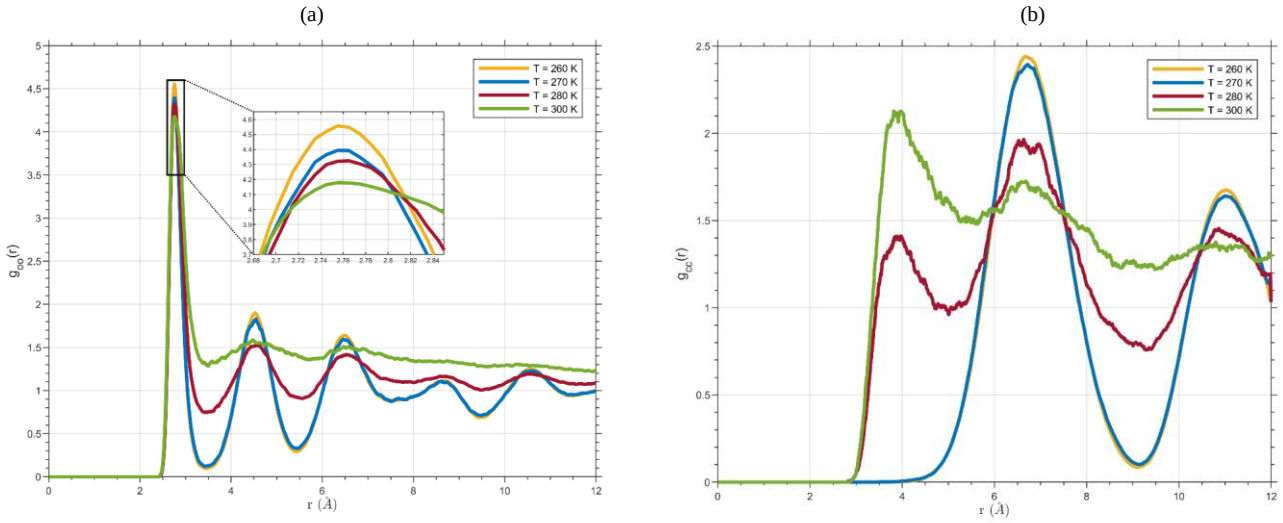

Figure 4-3: RDFs of (a) oxygen atoms in water molecules and (b) carbon atoms in methane molecules at P = 5 MPa, 200 ps, and different temperatures.

In addition, other peaks are found at around 10.9 Å,13.6 Å, and 16.5 Å in terms of methane molecules vibration in hydrate cages between each two methane molecules in the hydrate cages. The extent of g_{cc} lowers, but the distribution becomes wider with an increase in the temperature as a lower stability is attained for hydrate cavities at greater temperatures. After the decomposition process, a new peak is created at around 4 Å at temperatures of 280 K and 300 K, showing the minimum distance between methane molecules in the clusters. Figure 4-4 provides four snapshots of molecular dynamic simulations for the methane hydrate at various temperatures, a pressure of 5 MPa, and after time simulation 200 ps.

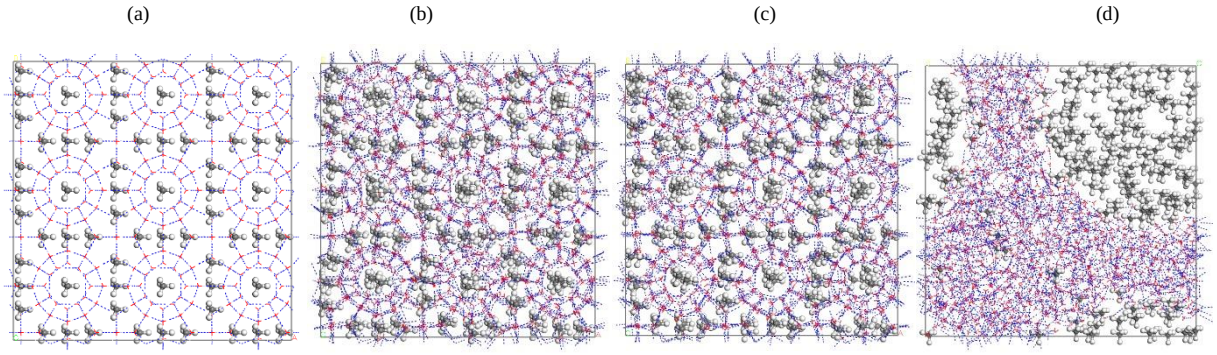

Figure 4-4:(a) Initial methane hydrate structure of simulation box; snapshots of molecular dynamic simulation after 200 ps at P = 5MPa (b) T = 260 K, (c) T = 270 K, and (d) T = 280 K.

The initial structure of the simulation box for methane hydrate with 100% cage occupancy is depicted in Figure 4a before conducting molecular simulations. Panels (b) and (c) of Figure 4-4 demonstrate the snapshots of molecular simulation of methane hydrate after 200 ps time at 5 MPa and temperatures of 260 K and 270 K, respectively. It is observed that the structure of cages is approximately consistent so that only methane molecules move to the center of the cages and hydrogen bonds of water molecules experience small changes. Thus, the structure of methane hydrates does not decompose at 5 MPa and 200 ps for both 260K and 270K. However, the cages of hydrate structure will disappear by increasing temperature to 280 K and

the methane hydrate structure will be decomposed by releasing the methane molecules and creating clusters, as shown in Figure 4-4d.

In this section, the RDF for oxygen-oxygen atoms of water molecules and for carbon-carbon atoms of methane molecules at a constant temperature upon pressure changes is calculated from NPT simulations. Panels (a) and (b) of Figure 4-5 describe the RDFs of oxygen-oxygen and carbon-carbon atoms at T = 280 K, but at different pressures. It is found that the height of peaks decreases and the valley of peaks becomes wider by decreasing pressure. The simulation runs reveal that the dissociation tendency of the methane hydrates becomes higher appreciably as the pressure is reduced; however, the pressure influence on the dissociation is not as much as the temperature effect. Thus, the temperature plays a more important role in the decomposition occurance.

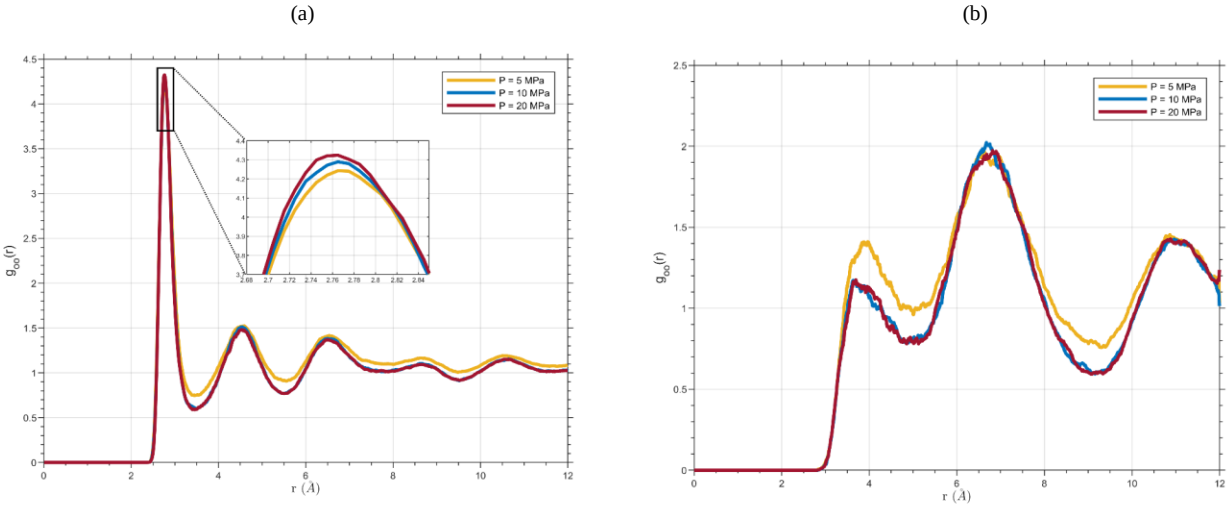

Figure 4-5:RDF plots of (a) oxygen atoms in water molecules and (b) carbon atoms in methane molecules at T = 280 K, 200 ps, and different pressures.

Cage Occupancy Impact. The NPT simulations are performed to investigate the decomposition process of the methane hydrate at various cage occupancies of 100%, 87.5%, and 75%. The details of the simulation runs are available in Table 4-1. The instability of the

methane hydrate increases by decreasing the cage occupancy from 100 % to 87.5% and 75%, as shown in Figure 4-6(a) and Figure 4-6(b), respectively where RDFs for the oxygen-oxygen atoms in water and methane molecules at 270 K and 5 MPa after 200 ps (as a simulation time) are presented for three different cage occupancies. The tendency of methane hydrate for decomposition is higher for partially occupied cages due to their instability, compared to the cages with 100% occupancy.

(a) (b)

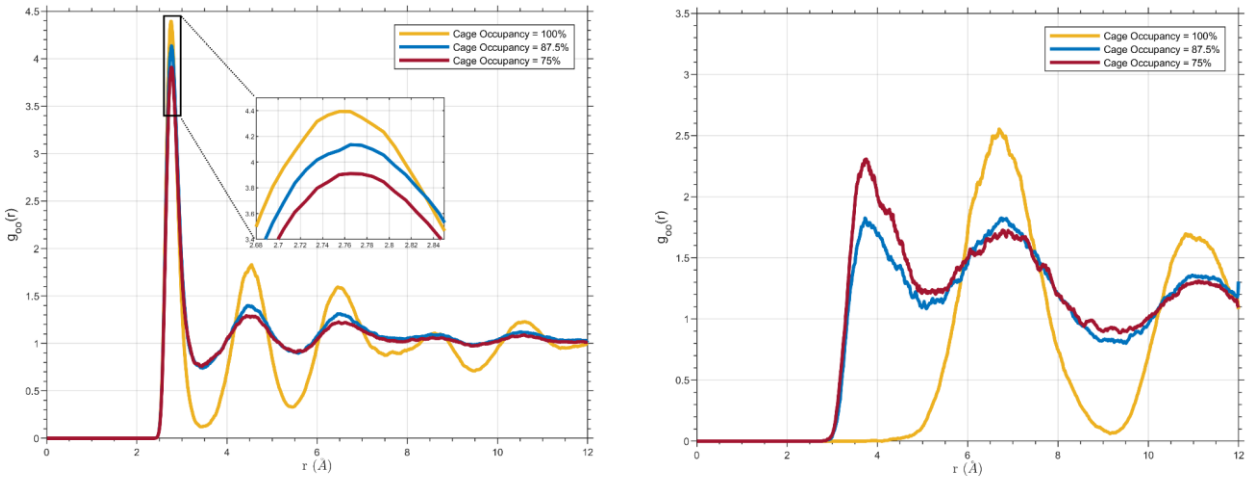

Figure 4-6:RDFs of (a) oxygen atoms in water molecules and (b) carbon atoms in methane molecules for various cage occupancies after 200 ps at P = 5 MPa and T = 270 K.

It was found that the RDF variation is higher when the cage occupancy is declined from 100% to 87.5%, compared to the case when the cage occupancy is reduced from 87.5% to 75%. Therefore, it confirmed that the hydrate cages with 100% cage occupancy are stable against the decomposition.

The final snapshot of simulation box for the methane hydrate with 100% cage occupancy is demonstrated in Figure 4-7(a) after 200 ps simulation at 270 K and 5 MPa. As mentioned earlier, no decomposition for this case occurs so that the structure of cages is almost firm/stable

and the methane molecules at the center of lattice are located. Figures 4-7(b) and 4-7(c) provide the last snapshots of molecular simulation of the methane hydrate after 200 ps time at 5 MPa and 270 K, where the cage occupancies are 87.5 % and 75 %, respectively. It is observed that the primary structure of the cages disappears completely and the methane hydrates are decomposed. Furthermore, some clusters of the methane molecules are observed at the end of the simulation run. It should be noted that the dissociation of methane hydrate structure happens at the time less than 200 ps at 5 MPa and 280 K for the case of 75 % as the lowest cage occupancy. Thus, it is logical to consider 200 ps as the simulation time while running NPT molecular simulation runs for the cage occupancies above 75%.

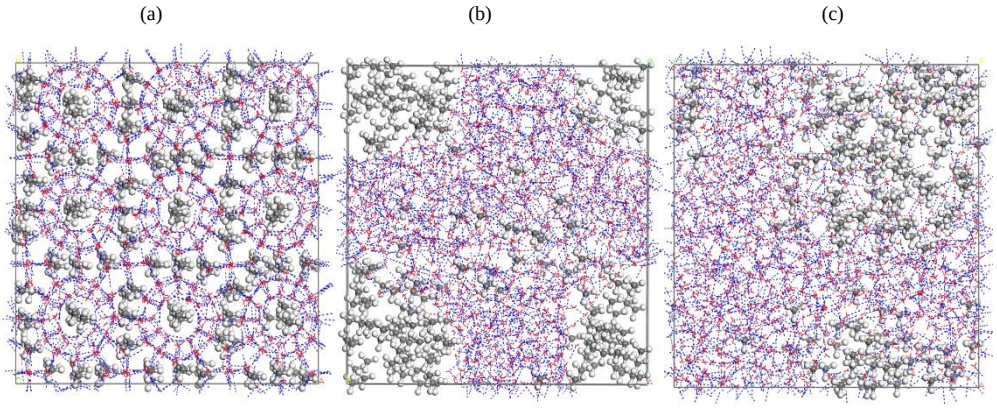

Figure 4-7: Final snapshots of molecular dynamic runs to simulate methane hydrate structure for various cage occupancies after 200 ps at P = 5MPa and T = 270 K for the cage occupancy of (a) 100%, (b) 87.5%, and (c)75%.

Inhibitor Impact. To demonstrate the effect of inhibitors in the decomposition process, we analyse the RDF of oxygen-oxygen of water molecules and the RDF of carbon-carbon atoms of two methanol (inhibitors) molecules in this section, according to Table 4-1. Based on NPT simulations, Figure 4-8(a) illustrates the g_{oo} for the water molecules at 270 K and 5 MPa for the two models in the absence and presence of methanol molecules, respectively. The positions/locations of peaks are almost the same, but the heights are different. The heights of

the peaks in the oxygen-oxygen RDF decrease and their widths become bigger upon inhibitor addition. It is concluded that the methanol injection into the methane hydrates changes the stability of the structure so that it would be more unstable. The RDF or g_{cc} (see Figure 4-8(b)) of methane molecules after 200 ps can be used to characterise the methane hydrate decomposition process. According to Figure 4-8(b), the new peak is created after adding two methanol molecules that replace two methane molecules.

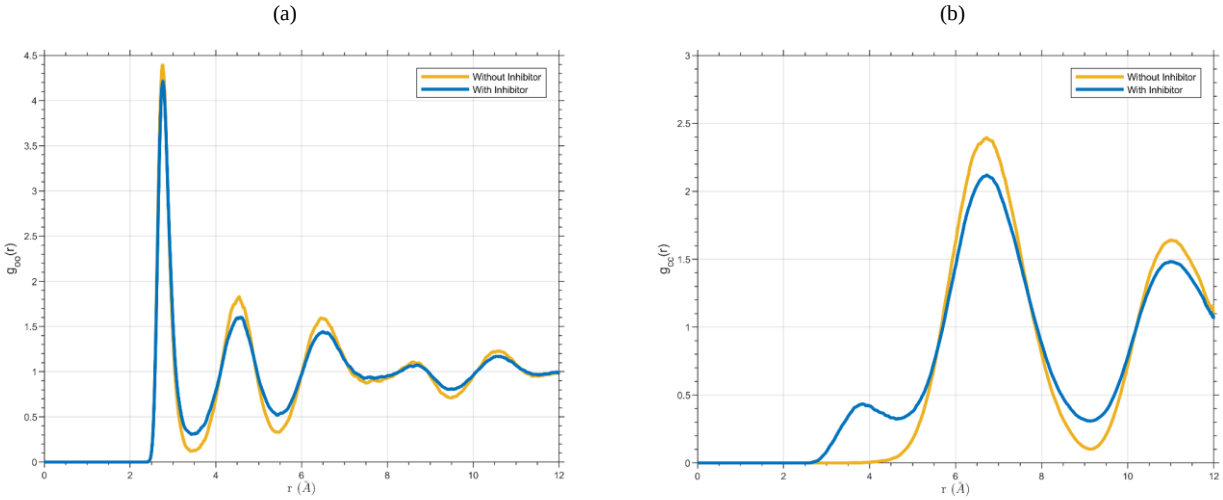

Figure 4-8: RDFs of (a) oxygen atoms in water molecules and (b) carbon atoms in methane molecules in the system with and without methanol molecules after 200 ps at P = 5 MPa and T = 270 K.

Figure 4-8 verifies that the methanol molecules play an important role to decrease the stability of methane hydrate structure, leading to facilitating the decomposition process. In next section, the potential energy difference of simple methane hydrate and inhibitor/hydrate molecules will be discussed.

4.3.2. Mean Square Displacement (MSD)

During simulations, the particles are moving in molecular simulation box. The mean square displacement (MSD) is used to analyse the particles position and movement. MSD is expressed by the following equation:

$$MSD = \left(\left| \bar{r}_i - \bar{r}_{i0} \right|^2 \right) = \frac{1}{N} \sum_{i=1}^{N} \left(\left| \bar{R}_i(t) - \bar{R}_i(t_0) \right|^2 \right) \tag{4-3}$$

In Equation (4-3), N represents the total number of particles; $\bar{R}_i(t)$ stands for the position of particle at t; and $\bar{R}_i(t_0)$ refers to the initial position of the particle. The mean square displacement increases linearly with time due to the position alteration of particles. The magnitude of MSD is determined for various temperatures based on 200 ps NPT simulation runs. Figures 4-9(a) and 4-9(b) illustrate the MSDs of water and methane molecules in the methane hydrate at temperatures of 260, 270, 280, and 300 K at a constant pressure (5MPa) after 200 ps.

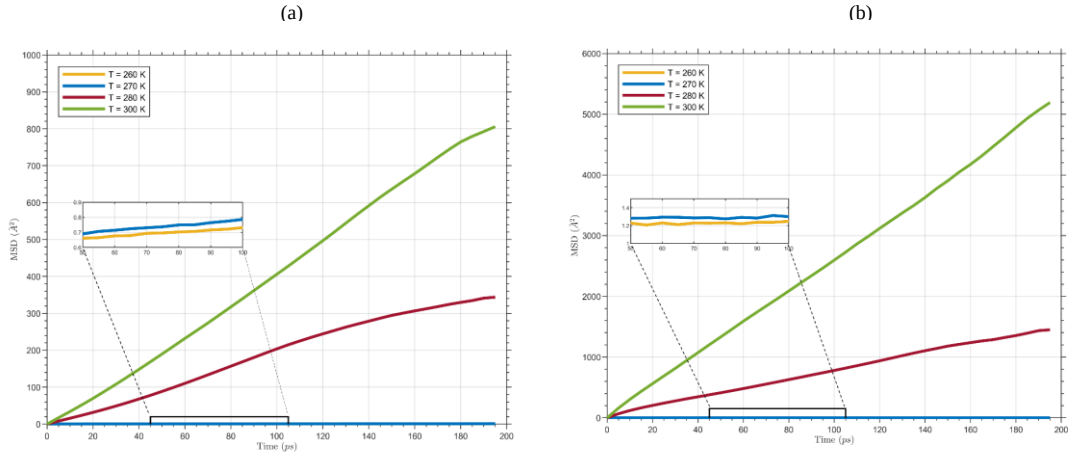

Figure 4-9: MSDs of (a) oxygen atoms in water molecules and (b) carbon atoms in methane molecules at P = 5 MPa, t=200 ps, and different temperatures.

At the temperatures of 260 and 270 K, the MSD changes of methane and water molecules are not as much as the MSD alteration at the temperatures of 280 and 300 K. Thus, the clathrate structure of methane hydrates is almost stable when the temperature is 260 and/or 270 K.

The minor change of MSDs for methane and water molecules at the temperatures of 260 and 270 K is attributed to vibration of methane and water molecules in the structure of the clathrate hydrate before decomposition, instead of moving out of the cages. The equilibrium temperature of the methane hydrate at a pressure of 5 MPa is lower than 280 K [46]. Thus, the acceptable results for hydrate dissociation temperature is achieved from our simulations due to the fact that the dissociation happens at 280 K and the structure remains stable at lower temperatures. It should be mentioned that under the dissociation condition at the temperatures above 280 K, the MSDs for methane and water molecules increase dramatically due to the breakage of hydrate cages. The MSD is a function of time so that the magnitude of MSD increases with time. Figure 4-10 provides the MSD of methane molecules in the methane hydrate structure versus simulation time at 280 K and 5 MPa.

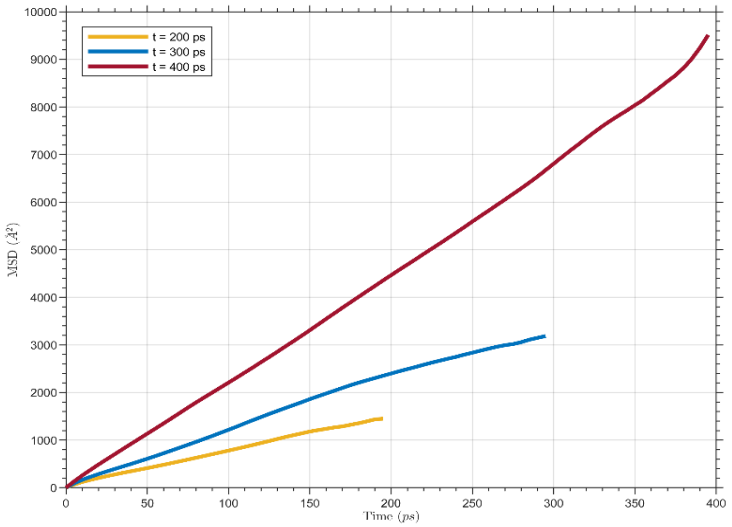

Figure 4-10: MSD of carbon atoms in methane molecules at various simulation times when T = 280 K and P = 5 MPa.

It can be concluded that the methane and water molecules in the hydrate structures rotate and vibrate in the crystal structure of methane hydrate; the methane clathrate hydrate collapses when the temperature or simulation time increases and eventually the methane and water molecules will abandon the clathrate structure.

4.3.3. Diffusion Coefficient

The diffusion coefficient is another important parameter to provide a different feature of simulation box in the MD simulations. The coefficient of diffusion is defined as the average of MSDs in certain nodes of simulation temperatures and pressures. The dissociation of gas hydrate can be investigated through calculating the diffusion coefficient of methane and water molecules, which can be written based on the Einstein relationship, as follows [47]:

$$6Dt = MSD \tag{4-4}$$

in which D introduces the diffusion coefficient; t refers to the simulation time; and MSD denotes the mean square displacement. Table 4-3 lists the diffusion coefficients of water and methane molecules in the simulation box for a variety of temperatures, pressures, and cage occupancies. According to the phase and nature of molecules, it is observed that the diffusion coefficient of the water molecules is much lower than that of the methane molecules in the methane hydrate system. On the basis of MSD concept, the water molecules vibrate around hydrate cages without movement in the stable hydrate structure. Hence, the diffusion coefficient of methane-water system is very low with an order of magnitude of 10^{-14} m^2/s, which is approximately equal to the solid diffusion coefficient. This can be seen in Table 4-3 for temperatures of 260K and 270 K at 5 MPa and 100% cage occupancy. The diffusion

coefficient of methane in the hydrate crystal increases after decomposition until it will equal the diffusion coefficient of gas /liquid systems with an order of magnitude of 10^{-9} m^2/s. In addition, Table 4-3 reports the diffusion coefficient for various cage occupancies. It is noticed that the structure of methane hydrate is more stable at low temperatures with a high cage occupancy; the diffusion coefficient increases with decreasing the cage occupancy from 100% to 87.5 % and 75%. The diffusion coefficient is a function of time. Thus, the decomposition process for different temperatures, pressures, and cage occupancies needs to be simulated at the same time. Like the diffusion coefficient of methane, the diffusion coefficient of water molecules can explain the dissociation process of methane hydrate structure for different nodes of the simulation well.

Table 4-3: Diffusion coefficient of methane and water molecules in methane hydrate systems at different conditions [200 ps simulation time and 5 MPa].

T (K)	Cage Occupancy	$D_{Methane} \times 10^{12}\ (m^2/s)$	$D_{Water} \times 10^{12}\ (m^2/s)$	T (K)	Cage Occupancy	$D_{Methane} \times 10^{12}\ (m^2/s)$	$D_{Water} \times 10^{12}\ (m^2/s)$
260	100%	1.07	0.72	260	100% + Inhibitors	1.038	0.488
270		1.21	0.85	270		173.17	71.4.01
280		1238.63	293.98	280		1424.79	295.26
300		4438.0.6	688.69	300		4601.72	694.77
260	75%	12.9	8.09	260	87.5%	271.06	117.23
270		930.041	235.71	270		658.11	257.12
280		1248.01	381.16	280		1504.32	362.62

4.3.4. Potential Energy

In the MD simulations, the potential energy consists of long-range Coulomb interactions and van der Waals interactions. Potential energy versus simulation time is shown in Figure 4-11 for two different case studies: simple methane hydrate with 100% cage occupancy and methane hydrate with two methanol (as an inhibitor) at a temperature of 280 K, a pressure of 5 MPa,

and 200ps for NPT simulation time. As illustrated in Figure 4-11, the potential energy of the simulation box exhibits different behaviours for the above systems. The hydrogen bonds between the water molecules of hydrate cages are not disturbed before decomposition and the potential energy varies around the equilibrium value because of the vibration and rotation of the water and methane molecules over the initial period of the simulation.

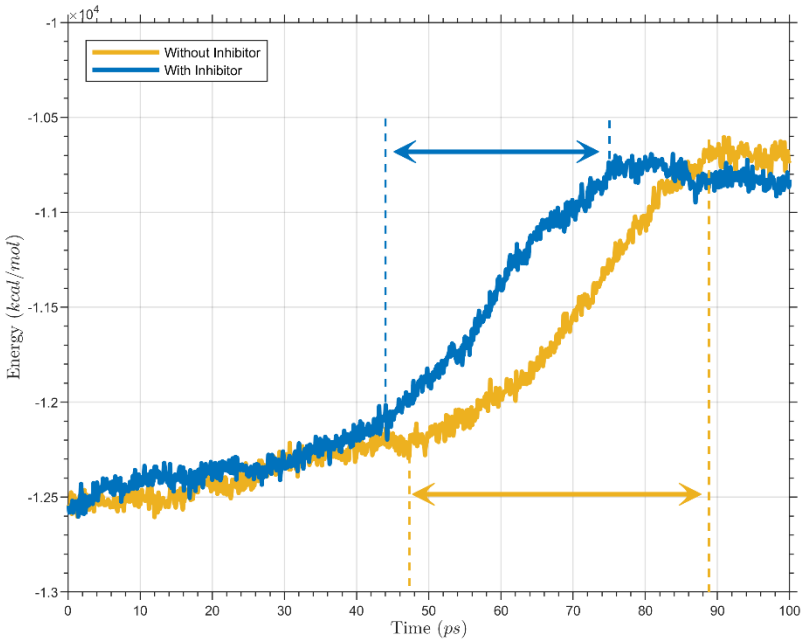

Figure 4-11: Potential energy for two different systems; methane hydrate with and without methanol molecules at T = 280 K and P = 5 MPa**.**

The potential energy of the first model is dramatically increased, implying that the hydrogen bonds of water molecules in the hydrate cages are decomposed between 47 and 89 ps. Therefore, it can be concluded that the dissociation time of the first model is around 47 ps. The structure of methane hydrate is decomposed completely after 42 ps, and the potential energy does not change any more so that it oscillates around one value. For the second case (methane hydrate structure with inhibitor molecules), the same behaviour is observed. The structure of hydrate has a stable condition during the initial period of the simulation before 45

ps. Within the time period between 45 and 78 ps, the total energy increases continuously, showing that the methane hydrate structure in the presence of two methanol molecules decomposes at a dissociation time about 33 ps. Subsequently, a new dynamic condition will be maintained as the potential energy fluctuates around one value and the decomposition process is ended. The difference between these two cases in the potential energy conveys the message that adding two methanol molecules as an inhibitor (less that 2 wt%) in small cages of methane hydrate can accelerate the dissociation process and decrease the decomposition time, as depicted in Figure 4-11 with horizontal blue and yellow arrows. The water molecules form hydrogen bond through hydroxyl group of alcohols. The addition of methanol in small cavities can facilitate the dissociation by making new hydrogen bonds between the water molecules in the cages and the hydroxyl group of methanol molecules. The oxygen atoms in the hydroxyl group of methanol can create new hydrogen bonds with molecules of waters. These new hydrogen bonds are able to disarrange and weaken the main (or primary) hydrogen bonds between the water molecules in the hydrate structure. Figure 4-12 demonstrates the new hydrogen bonds in the form of black circles. Methanol molecules effectively accelerate the hydrate decomposition phenomenon, leading to disrupting the great number of hydrogen bonds for water molecules in the cavities. It is worth noting that methanol plays two important roles in the gas hydrate decomposition: the hydroxyl group weakens the stability and structure of water cavities and the hydrocarbon placed at end part of the methanol molecule stimulates water molecules to form clusters.

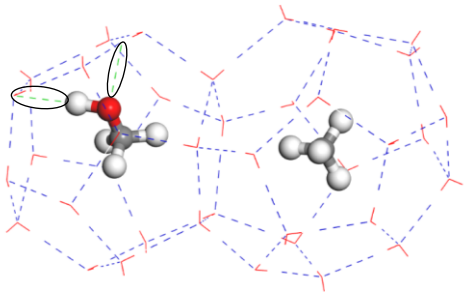

Figure 4-12: Structure of methane hydrate cages in the presence of methanol molecules with new hydrogen bonds between water and methanol molecules.

4.3.5. Methane Hydrate Density

The density alteration of gas hydrate in the simulation box can be used as a criterion to monitor the decomposition process. Figure 4-13 reveals the change of methane hydrate density for different cage occupancies based on the MD simulations at different temperatures. The density holds the highest value for 100% cage occupancy, which is equal to 890 kg/m^3.

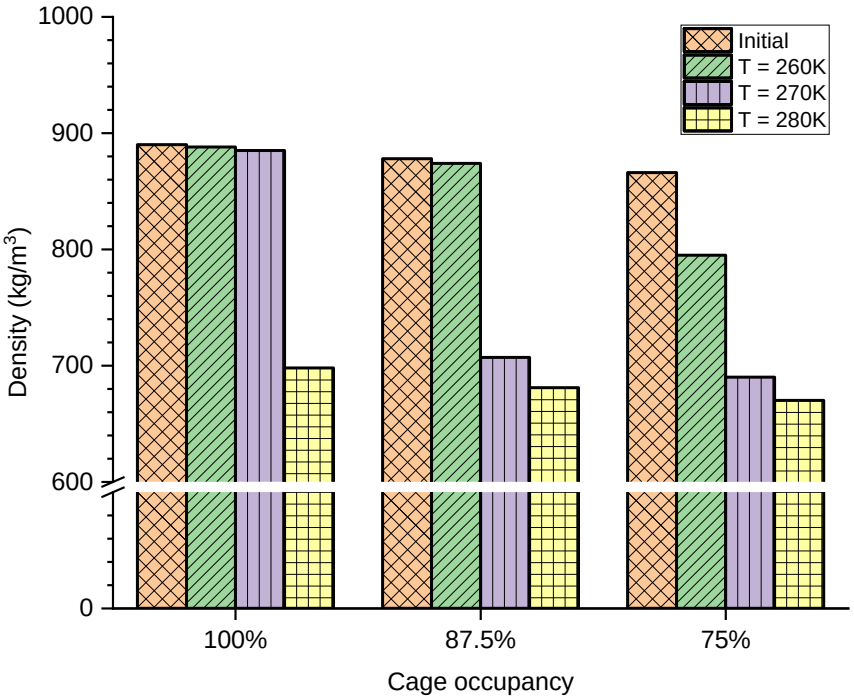

Figure 4-13: Density of methane gas hydrate for different cage occupancies before simulation and after 200 ps MD simulation at various temperatures.

The density remains at 890 kg/m^3 before reaching 280 K. It will then decrease dramatically so that it will become 700 kg/m^3. According to Figure 4-13, the decomposition for 100 % cage occupancy occurs at 280 K. Thus, the sharp drop in density value at the end of dynamic simulation demonstrates the decomposition of gas hydrate. The similar behavior/trend is found for the cage occupancies of 87.5% and 75 %; however, the decomposition is experienced at lower temperatures, compared to the case with 100 % cage occupancy.

4.3.6. Methane Hydrate Heat Capacity

The values of thermophysical properties of gas hydrate are required to estimate the amount (or rate) of gas hydrate production, to detect the sedimentary layers, and to determine the heat transfer rate during nucleation, formation, and decomposition stages. For instance, accurate determination of the heat capacity provides a reasonable estimation of natural gas production from gas hydrate reservoir with thermal stimulation strategy. There are studies in the literature that introduce various ways to calculate the heat capacity of hydrate for different guest molecules; however, they propose the methodologies which work for limited operating conditions. In addition, the experimental techniques are time-consuming and costly. MD simulation is a proper approach to calculate the thermophysical properties, particularly the heat capacity. In this research work, the amount of heat capacity of gas hydrate is obtained at different process and thermodynamic conditions. Figure 4-14 depicts the heat capacity for the methane hydrate at various pressures and temperatures. The experimental heat capacity reported in the previous works [48-52] have been obtained within wide range of hydrate condition. Various values for this parameter are attributed to the impurity of gas hydrate due to porosity, cage occupancy, and residual of ice and gas phases. Also, a weak relationship between the heat capacity and pressure and temperature is noticed. We calculate the heat

capacity of the initial simulation box before the decomposition. The values of heat capacity calculated in our research work at temperatures of 260, 270, and 280 K for 5, 10, and 15 MPa exhibit a good agreement with the available experimental data [48, 49, 52].

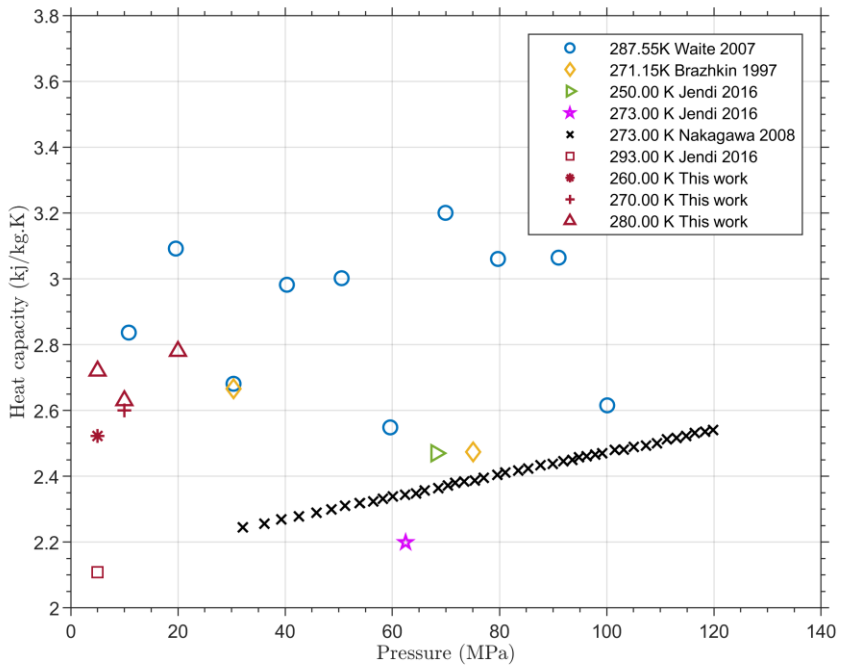

Figure 4-14: Heat capacity of methane hydrate at different pressures and temperatures.

It is recommended to study the decomposition of structure II and H of methane hydrates with the other gases (e.g., propane and butane) in the presence of different inhibitors in the future. It would be also interesting to investigate the impact of new molecules such as ionic liquids on the dissociation process.

Global energy demands are increasing over time. The gas hydrates as an energy source appear to be attractive in many countries containing this valuable energy source as utilization of methane produced from gas hydrates is considered a relatively climate friendly fuel, compared

to other hydrocarbons [12]. Hence, it seems vital to obtain deep and comprehensive understanding/knowledge regarding the gas hydrate behaviors and structures. To achieve this goal, the MD simulations assist researchers and engineers in gas and oil industries to accurately determine the physical and chemical properties. This important info can be utilized to modify the available thermodynamic equations of state. In addition, they can be incorporated in chemical and petroleum engineering software packages.

4.4. Conclusions

In this research work, the structural and dynamic properties of methane clathrate system during decomposition process are investigated through conducting molecular dynamic (MD) simulations by using the Materials Studio. In MD simulations, the CVFF force field and isobaric-isothermal (NPT) ensemble are used to study the methane hydrate stability or dissociation conditions. Various simulation runs at different temperature, pressure, and cage occupancy conditions are performed in this work. In addition, the methanol molecules are added to the hydrate cages to study the above aspects. To study the decomposition process, the structural properties including MSD and RDF are utilized. In the RDF curves of oxygen atoms in the water molecules and carbon atoms in the methane molecules, the height of peaks increases, and width of peaks in the methane hydrate system increases with lowering the pressure and increasing temperature, resulting in reduction of the hydrate stability. The similiar behaviours for MSD and diffusion coefficient are exprienced such that MSD and diffusion coefficient would be improved by increasing temperature and reducing pressure. The density of methane gas hydrate is calculated under different temperature conditions prior to the simulation runs and at the end of the simulation process; alteration of density in the simulation box can be used as another parameter to monitor decomposition of gas hydrate systems. The

trend of the heat capacity and density of methane hydrate obtained from the MD simulations shows a good match with the real data.

Analysing the hydrate properties, it can be concluded that the decomposition process of methane consists of two steps. Firstly, the water molecules vibrate around the structure of methane hydrate cages; the methane molecules inside the cages vibrate continuously and eventually the hydrogen bonds between the water molecules in hydrate cages will disturb. In the second step, the methane molecules start to escape from the damaged water cage.

The decomposition process is also investigated for different cage occupancies of methane hydrate structures at constant temperature and pressure. The methane hydrate dissociation at temperatures above the equilibrium condition can be seen when the cage occupancy decreases. The hydrate decomposition is not achieved at the equilibrium temperature at 100% cage occupancy; however, the decomposition of the methane hydrate lattice is observed when the cage occupancy reduces from 100% to 87.5% or 75% because of low stability and high diffusion coefficient of the methane molecules at low cage occupancies where the temperature and pressure are constant.

In the last phase of this study, the role of inhibitors in the methane hydrate decomposition process is studied. It is simulated in the work that the methanol molecules are injected into the small cages of Structure I methane hydrate. The development of new hydrogen bonds between the water and methanol can destroy a part of the forces between water molecules in the hydrate lattices, which can decrease the stability of the gas hydrate structure. Also, it causes that the decomposition happens earlier (e.g., lower dissociation time), compared to the case without methanol molecules.

Acknowledgements

We would like to thank Memorial University (Canada), Equinor, Innovate NL, and the Natural Sciences and Engineering Research Council of Canada (NSERC) for the financial support of the project.

Nomenclatures

Acronyms

ADD	Average absolute deviation percentage
$CVFF$	Consistent valence force field
MD	Molecular dynamic
MSD	Mean square displacement
NVT	Constant temperature, constant volume
NPT	Constant pressure, constant volume
RDF	Radial distribution function

Variables/Letters

b	Bond length
D	Diffusion coefficient and force constant in CVFF equation
F	Force constant in CVFF equation
H	Force constant in CVFF equation
n	Total number of data sets
n	Total number of particles α and β particles
P	Pressure
q	Charge of particles
r	Spherical distance and distance between particles in CVFF equation
R	Initial position of particles

S	Sign convention
t	Simulation time
T	Temperature
V	Volume of simulation box

Greek letters

ε	Well depth in vdW function
ϕ	Dihedral angle
θ	Bond angle
X	Out-of-plane parameter

Subscripts

0	Initial position of atoms
α	α particles
β	β particles
b	Bond length
C	Carbon atom
ε	Well depth in vdW function
i	i particles
j	j particles
O	Oxygen atom
θ	Bond angle
ϕ	Dihedral angle
X	Out-of-plane parameter

References

[1] Sloan Jr ED, Koh C. Clathrate hydrates of natural gases. CRC press; 2007.

[2] Englezos P, Lee JD. Gas hydrates: A cleaner source of energy and opportunity for innovative technologies. Korean J Chem Eng 2005;22(5):671-81.

[3] Fitzgerald A, Taylor M. Offshore gas-to-solids technology. Offshore Europe. Society of Petroleum Engineers; 2001.

[4] Kang S-P, Lee H. Recovery of CO2 from flue gas using gas hydrate: thermodynamic verification through phase equilibrium measurements. Environmental science & technology 2000;34(20):4397-400.

[5] Javanmardi J, Moshfeghian M. Energy consumption and economic evaluation of water desalination by hydrate phenomenon. QNRS Repository 2011;2011(1):622.

[6] Carroll JJ. Natural Gas Hydrates: A Guide for Engineers. 2009.

[7] Masuda Y, Fujinaga Y, Naganawa S, Fujita K, Sato K, Hayashi Y. Modelling and experimental studies on dissociation of methane gas hydrates in Berea sandstone cores; presented at 3rd International Conference on Gas Hydrates, July 18-22, Salt Lake City, Utah. Unpublished manuscript The University of Tokyo, Department of Geosystem Engineering, Tokyo, Japan 1999.

[8] Khairkhah D, Pooladi-Darvish M, Bishnoi P, Collett T, Dallimore S. Production potential of the Mallik field reservoir. BULLETIN-GEOLOGICAL SURVEY OF CANADA 1999:377-90.

[9] Clarke M, Bishnoi PR. Determination of the intrinsic rate of ethane gas hydrate decomposition. Chem Eng Sci 2000;55(21):4869-83.

[10] Ahmadi G, Ji C, Smith DH. Numerical solution for natural gas production from methane hydrate dissociation. Journal of Petroleum Science and Engineering 2004;41(4):269-85.

[11] Windmeier C, Oellrich LR. Theoretical study of gas hydrate decomposition kinetics - Model development. J Phys Chem A 2013;117(40):10151-61.

[12] Kondori J, Zendehboudi S, Hossain ME. A review on simulation of methane production from gas hydrate reservoirs: Molecular dynamics prospective. Journal of Petroleum Science and Engineering 2017;159:754-72.

[13] Sloan Jr ED. Fundamental principles and applications of natural gas hydrates. Nature 2003;426(6964):353-9.

[14] Dai Y, Zhong X, Jiang X, Wang S. Experiment of new additives effect on gas hydrate formation. Energy and Power Engineering 2014;6(06):133.

[15] Fan S, Zhang Y, Tian G, Liang D, Li D. Natural Gas Hydrate Dissociation by Presence of Ethylene Glycol. Energy & Fuels 2006;20(1):324-6.

[16] Luo H. Experiment of hydrate formation dynamics and model studying. China University Of Petroleum Beijing 2006.

[17] English NJ, MacElroy JMD. Theoretical studies of the kinetics of methane hydrate crystallization in external electromagnetic fields. J Chem Phys 2004;120(21):10247-56.

[18] Sarupria S, Debenedetti PG. Homogeneous nucleation of methane hydrate in microsecond molecular dynamics simulations. Journal of Physical Chemistry Letters 2012;3(20):2942-7.

[19] Zhang J, Pan Z. Effect of potential energy on the formation of methane hydrate. Journal of Petroleum Science and Engineering 2011;76(3):148-54.

[20] Okano Y, Yasuoka K. Free-energy calculation of structure-H hydrates. The Journal of chemical physics 2006;124(2):024510.

[21] Wei C, Hong-Yu Z. Molecular dynamics simulation of the structure I empty gas hydrate. Chinese physics letters 2002;19(5):609.

[22] Wan LH, Yan KF, Li XS, Fan SS. Molecular dynamics simulation of methane hydrate dissociation process in the presence of thermodynamic inhibitor. Wuli Huaxue Xuebao/ Acta Physico - Chimica Sinica 2009;25(3):486-94.

[23] Zhang J, Piana S, Freij-Ayoub R, Rivero M, Choi SK. Molecular dynamics study of methane in water: diffusion and structure. Molecular Simulation 2006;32(15):1279-86.

[24] Sakemoto R, Sakamoto H, Shiraiwa K, Ohmura R, Uchida T. Clathrate Hydrate Crystal Growth at the Seawater/Hydrophobic−Guest−Liquid Interface. Crystal Growth & Design 2010;10(3):1296-300.

[25] Waite WF, Santamarina JC, Cortes DD, Dugan B, Espinoza D, Germaine J, et al. Physical properties of hydrate-bearing sediments. Rev Geophys 2009;47(4).

[26] Kiefte H, Clouter M, Gagnon R. Determination of acoustic velocities of clathrate hydrates by Brillouin spectroscopy. The Journal of Physical Chemistry 1985;89(14):3103-8.

[27] Coluci VR, Pugno NM, Dantas SO, Galvao DS, Jorio A. Atomistic simulations of the mechanical properties of ‘super’carbon nanotubes. Nanotechnology 2007;18(33):335702.

[28] Rapaport DC. The art of molecular dynamics simulation. Cambridge: Cambridge University Press; 2004.

[29] Stoddard SD, Ford J. Numerical experiments on stochastic behavior of a Lennard-Jones gas system. Phys Rev A 1973;8.

[30] Verlet L. Computer" experiments" on classical fluids. I. Thermodynamical properties of Lennard-Jones molecules. Phys Rev 1967;159(1):98.

[31] Swope WC, Andersen HC, Berens PH, Wilson KR. A computer simulation method for the calculation of equilibrium constants for the formation of physical clusters of molecules: application to small water clusters. J Chem Phys 1982;76.

[32] Gear CW. Numerical initial value problems in ordinary differential equations. Prentice Hall PTR; 1971.

[33] Kalko SG, Gelpí JL, Fita I, Orozco M. Theoretical study of the mechanisms of substrate recognition by catalase. J Am Chem Soc 2001;123(39):9665-72.

[34] Ahalawat N, Murarka RK. Conformational changes and allosteric communications in human serum albumin due to ligand binding. J Biomol Struct Dyn 2015;33(10):2192-204.

[35] Biovia. Biovia Materials Studio. 18.1.0.2017 ed. San Diego, CA, USA; 2018.

[36] Takeuchi F, Hiratsuka M, Ohmura R, Alavi S, Sum AK, Yasuoka K. Water proton configurations in structures I, II, and H clathrate hydrate unit cells. The Journal of chemical physics 2013;138(12):124504.

[37] Dauber-Osguthorpe P, Roberts VA, Osguthorpe DJ, Wolff J, Genest M, Hagler AT. Structure and energetics of ligand binding to proteins: Escherichia coli dihydrofolate reductase-trimethoprim, a drug-receptor system. Proteins: Struct Funct Bioinformatics 1988;4.

[38] Liu Y, Zhao J, Xu J. Dissociation mechanism of carbon dioxide hydrate by molecular dynamic simulation and ab initio calculation. Computational and Theoretical Chemistry 2012;991:165-73.

[39] Burnham CJ, English NJ. Study of clathrate hydrates via equilibrium molecular-dynamics simulation employing polarisable and non-polarisable, rigid and flexible water models. The Journal of chemical physics 2016;144(16):164503.

[40] Hagler AT, Lifson S, Dauber P. Consistent force field studies of intermolecular forces in hydrogen-bonded crystals. 2. A benchmark for the objective comparison of alternative force fields. J Am Chem Soc 1979;101(18):5122-30.

[41] Hagler AT, Dauber P, Lifson S. Consistent force field studies of intermolecular forces in hydrogen-bonded crystals. 3. The C:O.cntdot..cntdot..cntdot.H-O hydrogen bond and the analysis of the energetics and packing of carboxylic acids. J Am Chem Soc 1979;101(18):5131-41.

[42] Berendsen HJ, Postma Jv, van Gunsteren WF, DiNola A, Haak J. Molecular dynamics with coupling to an external bath. The Journal of chemical physics 1984;81(8):3684-90.

[43] Ding LY, Geng CY, Zhao YH, Wen H. Molecular dynamics simulation on the dissociation process of methane hydrates. Molecular Simulation 2007;33(12):1005-16.

[44] Erfan-Niya H, Modarress H, Zaminpayma E. Molecular dynamics study on the structure I clathrate-hydrate of methane+ethane mixture. Energy Convers Manage 2011;52(1):523-31.

[45] Naeiji P, Varaminian F, Rahmati M. Comparison of the thermodynamic, structural and dynamical properties of methane/water and methane/water/hydrate systems using molecular dynamic simulations. Journal of Natural Gas Science and Engineering 2017;44:122-30.

[46] Kondori J, Zendehboudi S, James LA. Evaluation of Gas Hydrate Formation Temperature for Gas/Water/Salt/Alcohol Systems: Utilization of Extended UNIQUAC Model and PC-SAFT Equation of State. Industrial & Engineering Chemistry Research 2018.

[47] Allen MP, Tildesley DJ. Computer simulation of liquids. Oxford university press; 2017.

[48] Waite WF, Stern LA, Kirby S, Winters WJ, Mason D. Simultaneous determination of thermal conductivity, thermal diffusivity and specific heat in sI methane hydrate. Geophysical Journal International 2007;169(2):767-74.

[49] Nakagawa R, Hachikubo A, Shoji H. Dissociation and specific heats of gas hydrates under submarine and sublacustrine environments. 6th International Conference on Gas Hydrates, Chevron, Vancouver, BC, Canada. 2008.

[50] Ning F, Glavatskiy K, Ji Z, Kjelstrup S, Vlugt TH. Compressibility, thermal expansion coefficient and heat capacity of CH_4 and CO_2 hydrate mixtures using molecular dynamics simulations. PCCP 2015;17(4):2869-83.

[51] Jendi ZM, Rey AD, Servio P. Ab initio DFT study of structural and mechanical properties of methane and carbon dioxide hydrates. Molecular Simulation 2015;41(7):572-9.

[52] Handa Y. Compositions, enthalpies of dissociation, and heat capacities in the range 85 to 270 K for clathrate hydrates of methane, ethane, and propane, and enthalpy of dissociation of isobutane hydrate, as determined by a heat-flow calorimeter. The Journal of chemical thermodynamics 1986;18(10):915-21.

5. CHAPTER FIVE

Molecular Dynamic Simulations to Evaluate Dissociation of Hydrate Structure II in the Presence of Inhibitors: A Mechanistic Study (Published)

Preface

A version of this manuscript has been published in the Chemical Engineering Research and Design 149 (2019): 81-94. I am the primary author of this paper. All authors were involved in the objectives definition, development of methodology steps, and design of paper structure. I carried out a majority of the literature review, and the MD simulations with the aid of technical comments from co-authors, Sohrab Zendehboudi and Lesley James. I prepared the first draft of the manuscript and then revised the manuscript based on the co-authors' feedback and reviewers' comments received from the journal. The co-author, Sohrab Zendehboudi, had considerable contribution in revising the manuscript in terms of editorial and technical aspects. Lesley James also had a final look to edit the manuscript if some corrections were still needed.

Abstract

The present work aims to investigate stability and decomposition of hydrate structure II of methane, propane, and isobutane systems at various temperatures, pressures, and compositions in the absence and/or presence of inhibitor molecules. To assess the stability of gas hydrates, a comprehensive knowledge of the structural, thermodynamic, and dynamic properties of the hydrates is needed. The structure II of gas hydrates is embedded in a molecular dynamic (MD) approach and the simulations are carried out under constant temperature-constant volume (NVT) and constant temperature-constant pressure (NPT) conditions by employing the consistent valence force field (CVFF). In this work, first, the mean square displacement (MSD) and diffusion coefficient are evaluated to demonstrate the movement of host molecules. The radial displacement function is then utilized to display characteristic configurations of structure II under different process and thermodynamic conditions. In addition, other vital properties including lattice parameter and potential energy are determined. The effect of inhibitors on stability and/or decomposition of hydrate structure II is investigated. The achieved results are in good agreement with previous theoretical and experimental outputs, confirming reliability and appropriateness of the simulation method. The inhibition capability of different inhibitors based on the simulation results has the following order: methanol > ethanol > glycerol. The findings of this study can help for better understanding of hydrate dissociation in molecular scale as well as for proper selection and design of effective inhibitors for hydrates with different structures and characteristics.

Keywords: Gas hydrate structure II; Molecular dynamic simulation; Inhibitors; Decomposition; Stability

5.1. Introduction

Gas hydrates provide a valuable clean energy source to combat the energy crisis as each unit volume of gas hydrates can contain approximately 160 to 180 times the unit volume of natural gas under standard conditions [1]. The gas production and exploration from gas hydrate reservoirs are linked to the dissociation of gas hydrate structures. Depressurization, thermal stimulation, and chemical injection are three common techniques to decompose gas hydrates [2, 3]. The chemicals or additives alter the stability of the hydrate's structure and modify the temperature and pressure at which clathrate hydrates form or decompose [4-6]. Providing further information, adding additives in the form of promotors including silica and alumina particles can increase the rate of hydrate formation by improving the solubility of methane in water phase [7]. Liu et al. [8] showed that nanoparticles (e.g., zinc oxide nanoparticles) and sodium dodecyl sulfate are able to decrease the induction time and improve the storage capacity of methane hydrates. Thus, it is necessary to further investigate the effect of additives or chemicals on the stability of clathrate hydrates and decomposition phenomenon.

Clathrate hydrates are nonstoichiometric ice-like crystalline solids consisting of the gas molecules and polyhedral hydrogen-bonded cages of water molecules. The stability of the gas hydrate cages is maintained by the van der Waals interactions between gas molecules and caged water molecules. Water molecules in the form of hydrates are usually found in three different categories; namely, structure I, structure II, and structure H, depending on the temperature, pressure as well as gas molecule size [1]. Methane and ethane form the structure I of clathrate hydrates. However, the mixture of structure I and structure II might be created by methane and ethane components at particular thermodynamic conditions [9, 10]. N-butane

forms clathrate hydrates only when a help gas, such as methane or xenon, participates in the small cavities of structure II [1, 11].

Methane as a guest molecule can appear in different structures of hydrates if considerable variations in temperature and pressure occur [12, 13]. The natural gas usually includes methane, ethane, propane, and butane, which are guests in structure I and structure II of gas hydrates. Structure II of gas hydrate is formed by molecules with a high radius such as propane and butane due to the availability of bigger cages [1]. Although above 85% of natural gas is methane and it is stable in structure I, the structure II of methane hydrate can be formed by increasing temperature at constant pressure before formation of structure I. In general, the hydrate structure II is a thermodynamically stable structure for mixture of natural gases. The structure II can be formed by combinations of methane + propane and methane + isobutane, where the methane molecules are trapped in small cavities of structure II. Inhibitors such as methanol, ethanol, and glycerol are among the most efficient (and common) additives to prevent gas hydrate formation or accelerate gas hydrate decomposition. Thus, it appears to be important to systematically study the impact of inhibitors on gas hydrate structure II, which includes methane and other light components, in various scales particularly the molecular level.

The physical and dynamic properties of gas hydrates and natural gases have been studied through laboratory measurements [14-18]. As gas hydrates require high pressures and low temperatures for formation, the experimental runs should be conducted at specific thermodynamic conditions, which may cause various challenges in terms of economic, safety, and environmental aspects. Utilization of molecular simulation can solve these technical and practical issues through simulating the nucleation, formation, and decomposition of gas

hydrate systems at nanoscale. Recently, molecular dynamic (MD) simulations have been recognized as an efficient and powerful computer simulation method for investigation of the microscopic characteristics of gas hydrates. For example, nucleation [19, 20], growth [21], formation [22, 23], stability [24], decomposition [25], and characterization of gas hydrates (e.g., thermal conductivity and heat capacity) [26, 27] have been modelled using MD simulations. This effective strategy is able to determine the interactions between molecules and their motion through employing the empirical potential functions and Newton's Laws in small time steps. Recently, we have reviewed all potential functions that can be used for simulation of gas hydrates while implementing MD approach [3].

In the recent years, several studies have focused on gas hydrates by utilizing MD simulations in terms of stability, dissociation, and effect of additives on the structure and transport properties of gas hydrate systems. For instance, Ding et al. carried out a MD simulation study on the methane hydrate decomposition at a constant temperature and pressure. It was found that the dynamic transition occurs when the diffusion coefficient of the host molecules (water) is higher than that of the guest molecules (e.g., gases such as methane) [28]. Thus, it seems essential to systematically investigate the impact of various process/thermodynamic conditions on the stability and characteristics of clathrate hydrates and decomposition process.

Recently, we employed MD simulations to explore the influences of various parameters such as pressure, temperature, cage occupancy as well as the presence of inhibitor on methane hydrate stability and decomposition [29]. Smirnov and Stegailov used the MD simulations to describe the decomposition of methane hydrates at a pressure of 5000 MPa where different water potential functions were used [30]. It was concluded that the low cage occupancy can help to dissociate hydrates at lower temperatures. There are some research works in the

literature that analyze the hydrate dissociation in the presence of inhibitors. For example, Wan et al. conducted MD simulation runs to study the dissociation event of methane hydrate where the ethylene glycol is present in the system [25]. Wen et al. demonstrated that the decomposition and instability of hydrates will be prompted by using tetrahydrofuran molecules as a guest in the large cavities in structure II of hydrogen hydrates [31]. Choudhary et al. also showed that polyvinylpyrrolidone (PVP) at the interface of methane hydrate and liquid water can facilitate the decomposition of gas hydrates [32]. In another research study, Pal and Kundu concluded that methanol decreases the stability of methane hydrate cages [33]. According to a research investigation performed by Zi et al., the decomposition of methane hydrate can be improved by adding asphaltenes at high temperatures. Li et al. studied the structure and decomposition conditions of structure II of propane hydrate. They also investigated the influence of methanol on the dissociation process [34].

To the best of our knowledge, a majority of the previous works available in the open sources provide the basic knowledge of gas hydrates where the MD simulations are conducted. Much less attention has been paid to the dynamic and structural properties of structure II of gas hydrates. Although the role of inhibitors on the stability and dissociation of hydrate structures has been studied, there is no study in the literature that investigates the effect of various inhibitors on the hydrate structure II of natural gas mixtures as well as the inhibition effectiveness of the inhibitors at molecular scale. In addition, monitoring potential energy for the inhibitor/gas cases through the MD simulations adds further novelties to the current study, which can provide an effective strategy to obtain the decomposition time as well as decomposition duration. On the other hand, the measurement procedures of the physical and structural properties of gas hydrates are costly and not accurate enough due to the specific

thermodynamic conditions of gas hydrates. The above aspects/issues motivated us to employ the MD simulation approach for simulating the structure II of gas hydrate mixtures (in terms of stability) and determining vital physical properties of the gas hydrates.

The main goal of this study is to investigate the dynamic and structural properties of mixtures including methane, propane, and isobutane that appear in structure II of gas hydrates. The effect of three inhibitors including methanol, ethanol, and glycerol on the decomposition phenomenon is demonstrated through employing MD simulations. In addition, the influences of thermodynamic conditions such as temperature and pressure on the decomposition process are studied. We determine the radial distribution function (RDF), mean square displacement (MSD), potential energy, and diffusion coefficient of different molecules under a variety of process conditions (temperature, pressure, and composition). The density and lattice parameter of the simulation box are also calculated by employing the MD simulation approach.

After the introduction section, the theoretical aspects and methodology of the MD simulation strategy will be discussed in Section 2. The next section presents the research results and systematic discussion on the findings. The main conclusions of the research study are highlighted in the last section.

5.2. Computational Theory and Methodology

A variety of experimental and theoretical approaches are used to assess the hydrate stability and decomposition. Each research and/or engineering strategy might have advantages and drawbacks. Molecular dynamic (MD) simulations provide an effective way to investigate rare, expensive, and/or new components where the novel physical and chemical features and applications of targeted materials are identified. In fact, MD simulation is a strong and helpful method to obtain detailed information on the structural, dynamic, and thermodynamic

properties of complex systems at the microscopic scale. The initial position and summation of all energies are the first inputs, which are estimated for each atom's condition in the MD simulation approach. The energies for each atom are a summation of electrostatic, angle bending, van der Waals, and torsional rotation [3]. Over the years, in MD simulations, the Newton's law has been used to determine the position of each atom by using various algorithms such as Verlet, leap-frog, and Beeman algorithms to solve the equation of motion [35-37]. As an important feature, the atomic and intermolecular parameters are required parameters for MD simulations.

The MD simulations are performed by using Forcite module in the Materials Studio software [38] to investigate the stability of hydrate structure II of methane, propane, and isobutane mixtures. The current work plans to provide new insights into the effects of temperature, pressure, and inhibitors such as methanol, ethanol, and glycerol on the dissociation and stability of various hydrate systems of methane + propane, methane + isobutane hydrate, and methane + propane + isobutane. The position of oxygen atoms in the clathrate hydrate can be generally identified from X-ray single crystal diffraction measurements [39]. The hydrogen atoms of water molecules are arranged based on the restriction given by the Bernal-Fowler rule [40].

Providing further information on the computational methodology, a triclinic supercell with $\alpha = \beta = \gamma = 60^{\circ}$ of structure II hydrate is made of $3 \times 3 \times 3$ unit cells with initial dimensions of $3.56 \times 3.56 \times 3.56$ nm. Methane molecules are added to the center of small cavities in structure II of clathrate hydrate. Propane and isobutane are also placed at the center of large cavities for methane + propane, methane + isobutane, and methane + propane + isobutane hydrates to study different compositions. MD related information (composition and configuration) for methane,

propane, isobutane, and inhibitor molecules involved in different mixture systems is provided below:

Case 1- Composition (mole percent): Methane (66.7%) + Propane (33.3%); 54 Propane molecules in large cavities and 108 Methane molecules in small cavities.

Case 2- Composition (mole percent): Methane (66.7%) + Propane (32.0%) + Methanol (1.3%); 52 Propane molecules and 2 Methanol molecules in large cavities, and 108 Methane molecules in small cavities.

Case 3- Composition (mole percent): Methane (66.7%) + Propane (32.0%) + Ethanol (1.3%); 52 Propane molecules and 2 Ethanol molecules in large cavities, and 108 Methane molecules in small cavities.

Case 4- Composition (mole percent): Methane (66.7%) + Propane (32.0%) + Glycerol (1.3%); 52 Propane molecules and 2 Glycerol molecules in large cavities, and 108 Methane molecules in small cavities.

Case 5- Composition (mole percent): Methane (66.7%) + Isobutane (33.3%); 54 Isobutane molecules in large cavities and 108 Methane molecules in small cavities.

Case 6- Composition (mole percent): Methane (66.7%) + Isobutane (32.0%) + Methanol (1.3%); 52 Isobutane molecules and 2 Methanol molecules in large cavities, and 108 Methane molecules in small cavities.

Case 7- Composition (mole percent): Methane (66.7%) + Isobutane (32.0%) + Ethanol (1.3%); 52 Isobutane molecules and 2 Ethanol molecules in large cavities, and 108 Methane molecules in small cavities.

Case 8- Composition (mole percent): Methane (66.7%) + Isobutane (32.0%) + Glycerol (1.3%); 52 Isobutane molecules and 2 Glycerol molecules in large cavities, and 108 Methane molecules in small cavities.

Case 9- Composition (mole percent): Methane (66.6%) + Propane (16.7%) + Isobutane (16.7%); 27 Propane molecules and 27 Isobutane molecules in large cavities, and 108 Methane molecules in small cavities.

Case 10- Composition (mole percent): Methane (83.3%) + Propane (16.7%); 27 Propane molecules and 27 Methane molecules in large cavities, and 108 Methane molecules in small cavities.

Case 11- Composition (mole percent): Methane (83.3%) + Isobutane (16.7%); 27 Isobutane molecules and 27 Methane molecules in large cavities, and 108 Methane molecules in small cavities.

The lattice structure of water molecules for one small and one large cavity in structure II hydrate (for methane + propane system) is seen in Figure 5-1. All guest molecules are added to the center of cavities and allowed to move over the simulation run. The periodic boundary conditions are used in all directions of MD simulations. The consistent valence force field (CVFF) is utilized to describe the molecular interactions within the systems in the Forcite module. Further (and comprehensive) information about the CVFF model is found in our previous work [29]. Geometry optimization is performed on the initial simulation system to provide a stable initial configuration for simulation by using a smart algorithm, which includes the conjugate gradient, steepest descent, and Quasi-Newton methods [38]. The MD simulation is conducted by the initial 50 ps in NVT ensemble to reach an equilibrium condition. The NPT ensemble is carried out for 700 ps at different temperatures and the constant pressure of 20 MPa in the Materials Studio software [41]. The Ewald summation method is employed to

calculate the long-range columbic and van der Waals forces. In the NPT simulation, the Berendsen thermostat and barostat are applied to control the temperature and pressure with a decay of 0.2 ps and 0.1 ps, respectively. [42]. A cut-off distance of 12 Å is considered to obtain all van der Waals interactions in the simulation box. A brief procedure to perform MD simulations for investigation of gas hydrate structure II is described in Figure 5-1.

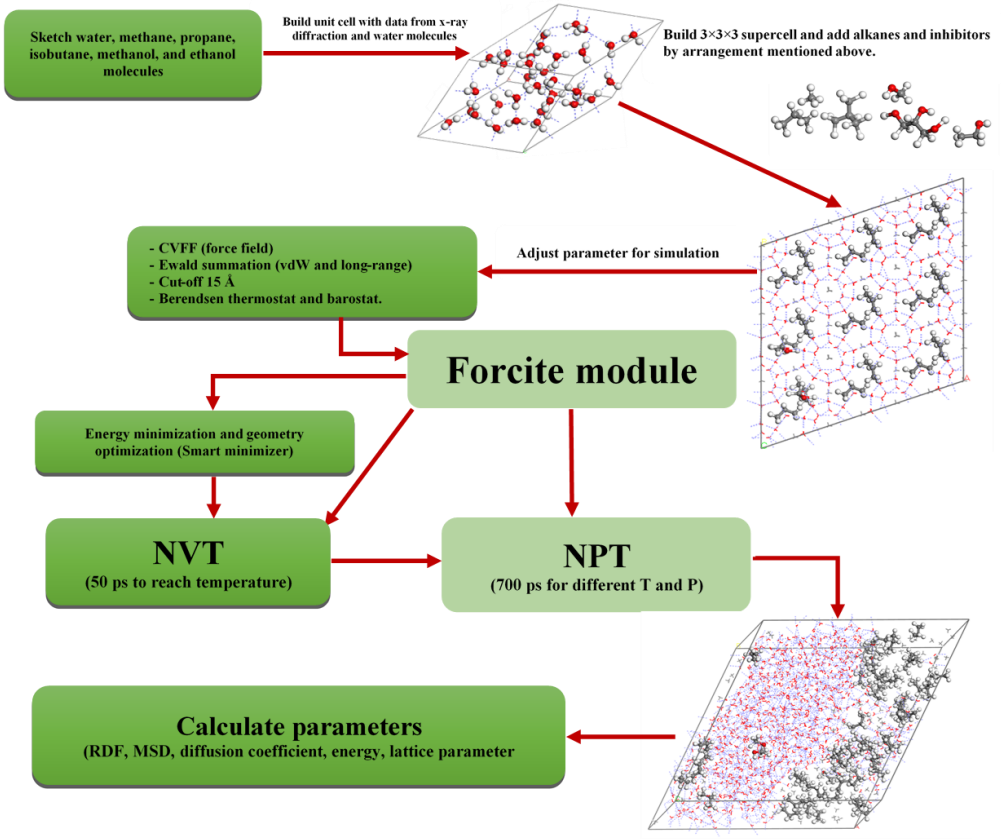

Figure 5-1: Main steps to implement molecular dynamic approach for simulation of dissociation occurrence in gas hydrae structure II.

There are cons and pros with the MD strategy. For instance, the MD simulations can be more useful for analyzing and characterizing of systems at very low and high temperature and pressure conditions. Another advantage of using MD simulation approach is that it allows to find/monitor complicated behaviors of molecules such as movement of enzyme molecules

through the channel of proteins [51, 52]. Additionally, it is one of the best methods to investigate the structural, mechanical, and thermodynamic parameters of rare and expensive materials such as proteins and polymers. Despite its benefits and broad applications, MD simulations technique has some drawbacks. The typical size of simulation box is in order of nm. Thus, a comprehensive structure should be defined that represents all features /properties of the simulation. The accuracy of the simulation is highly dependent on the type of the potential function. The MD modeling approach needs powerful computing systems with a strong central processing unit (CPU). In the MD simulations, the position of each particle is achieved by the classical mechanics (Newtonian equation of motion), whereas the motion of molecules can be more accurately described using Schrödinger's equation. Another problem with the MD simulations is that the method is not precise enough to simulate the interfacial and thermodynamic behaviors of very light components such as helium and hydrogen [51,52].

5.3. Results and Discussion

This section includes the MD results and technical discussion on the main findings of our research work. The structural and dynamic properties of methane + propane, methane + isobutane, and methane + propane + isobutane hydrate structure II are analyzed (cases 1, 5, and 9 -11). First, the radial distribution function (RDF), and mean square displacement (MSD) of the systems are obtained in the absence of inhibitors molecules. Then, the inhibitors molecules (methanol, ethanol, and glycerol) are injected into the hydrate structure and their influence on the dissociation process is studied. In addition, different mixtures of methane, propane, and isobutane are placed in large cavities (cases 9 to 11) to investigate the structural characteristics and stability of hydrate mixtures.

In the methane + propane and methane + isobutane systems (cases 1 and 5), the van der Waals interactions are responsible for the stability of clathrate hydrates, which occur between the methane, propane, and isobutane as the guest molecules and water molecules (as the host) in the cages. To evaluate variations of the structural and dynamic properties during the dissociation process, we display the snapshots for both systems/cases at different temperatures but at a constant pressure of 20 MPa for a 700 ps simulation time. The initial trajectories for methane + propane and methane + isobutane systems are illustrated in Figures 5-2(a) and 5-2(e), respectively. Panels (b), (c), and (d) of Figure 5-2 include snapshots of the simulation for the methane + propane case after 700 ps at 20 MPa and temperatures of 290 K, 300 K, and 310 K, respectively. In addition, Figures 5-2(f), 5-2(g), and 5-2(h) illustrate the snapshots of MD simulations for the methane + isobutane system after 700 ps at 20 MPa and temperatures of 310 K, 320 K, and 330 K, respectively. It is noticed that the clathrate hydrates of these different systems dissociate at different temperatures due to the differences in the gas type and mixture composition, where the pressure and dissociation time remain unchanged. In the following sections, the MSD, RDF, and diffusion coefficient are discussed for various systems where different temperatures and pressures are examined.

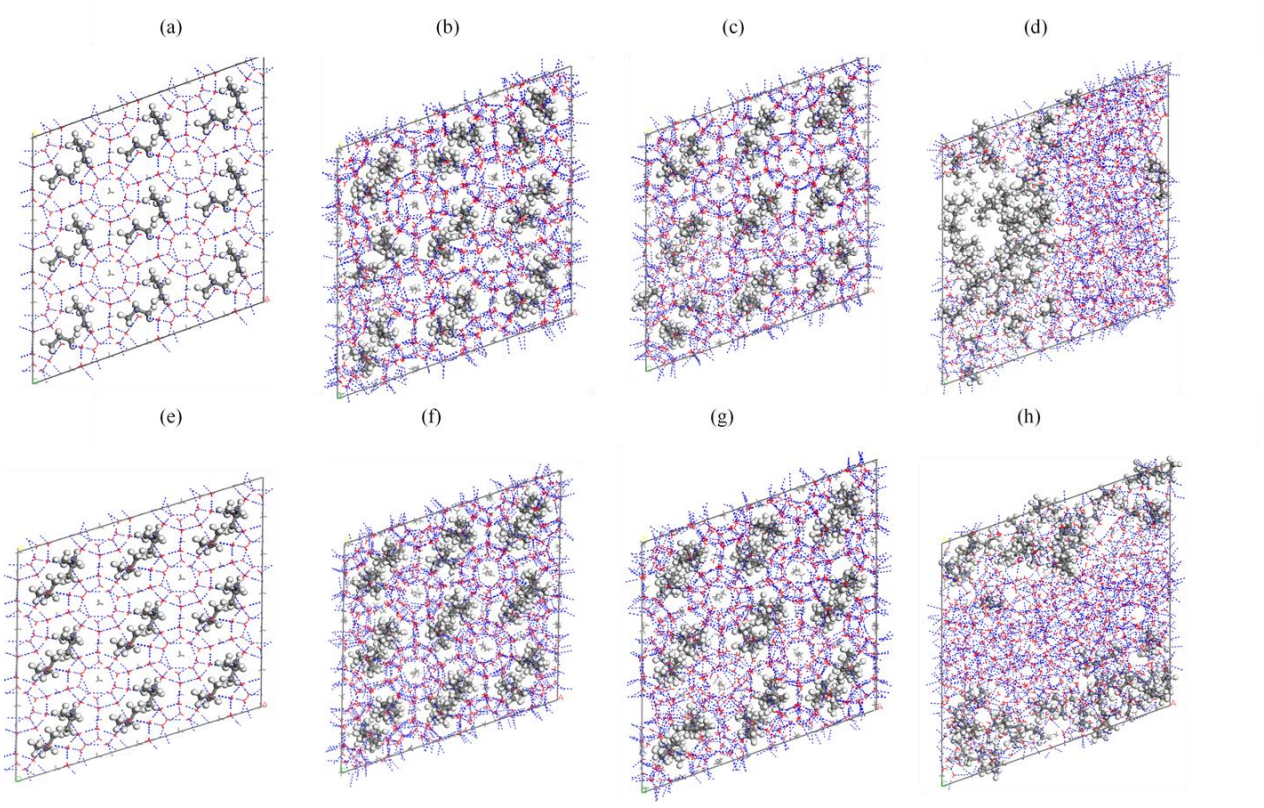

Figure 5-2: Initial condition (a) and final snapshots of molecular dynamic simulation after 700 ps at P = 20 MPa for T = 290 K (b), T = 300 K (c) and T = 310 K (d) for methane + propane case; Initial condition (e) and final snapshots of molecular dynamic simulation after 700 ps at P = 20 MPa for T = 310 K (f), T = 320 K (g) and T = 330 K (h) for methane + isobutane hydrate structure [methane molecules are in small cavities, propane and isobutane molecules are in large cavities, and red molecules are water].

RDF parameter. In this section, the structural and microscopic properties of methane clathrate hydrate in structure II are investigated to better comprehend the gas hydrate decomposition. The radial distribution function (RDF) is the occurrence possibility of differentiating a specific atom in the distance of r from another. The radial distribution function (RDF or $g_{\alpha\beta}$) to analyze the distance between two atoms, α and β, is obtained as follows:

$$g_{\alpha\beta}(r) = \frac{V}{N_\alpha N_\beta}\left(\sum_{i=1}^{N_\alpha}\frac{n_i\beta(r)}{4\pi r^2\Delta r}\right) \quad (5\text{-}1)$$

where N refers to the number of particles; $n_i\beta(r)$ represents the total number of atom β in the spherical distance of r from atom α; and V denotes the volume of the simulation box. The RDFs are obtained at different simulation conditions to study the stability of structure II of methane, propane, and isobutane mixtures. The RDFs of oxygen-oxygen atoms of water molecules ($g_{o-o}(r)$) and RDFs of carbon-carbon atoms of methane molecules ($g_{c-c}(r)$) are determined for different systems at various temperatures but with a constant pressure and simulation duration. To evaluate the influence of pressure on the MD simulation calculations, we also obtain the RDFs of oxygen atoms of water molecules for methane + isobutane system at 320 K but different pressures where the simulation time is 700 ps.

Figures 5-3a and 5-3b present the $g_{o-o}(r)$ and $g_{c-c}(r)$ attained from the molecular dynamic simulation of the methane + propane system at a variety of temperatures. The magnitudes of RDFs are zero at distances less than atomic diameter. For the distances above the atomic size, the RDFs hold different values because of various atom distances. According to $g_{o-o}(r)$ of oxygen-oxygen atoms in water molecules of the methane + propane structure II (see Figure 5-3(a)), there are three distinctive peaks: the first peak at the radius of 2.75 Å indicates the length between two hydrogen bonds for the nearest oxygen atoms in the hydrate cages [43]. The second peak of oxygen-oxygen pairs appears at r = 4.6 Å, which determines the tetrahedral hydrogen bonding structure of water molecules in the hydrate structure II [44]. The third peak at r = 6.53 Å shows mainly the distance of oxygen-oxygen pairs of the hexagonal rings, exhibiting a behaviour similar to the previous works [21, 43]. As clear from Figure 5-3(a), the peaks of $g_{o-o}(r)$ reach lower maximums by increasing temperature between 280 K to 300 K but the oxygen skeletons remain almost unchanged for the second and third peaks (tetrahedral and hexagonal rings) at different temperatures in the range of 280 K and 300 K. After that, the

RDF of the mixture is simulated for temperatures above 300 K. As it is clear, the second and third peaks almost disappear for the temperature cases of 310 K and 320 K. Hence, the structure of water cages in the clathrate hydrate is disintegrated. After the decomposition event, the height of peaks is again reduced with increasing temperature from 310 K to 320 K. As it is observed in Figures 5-3a and 5-3b, the decomposition temperature for the methane + propane hydrate structure II is greater than 300 K at P = 20 MPa. Panel (b) of Figure 5-3 demonstrates the $g_{c-c}(r)$ for the carbon-carbon atoms of methane molecules where different temperatures are examined but a constant pressure of 20 MPa for the 700 ps scenario is maintained. There is a distinct peak around r = 6.2 Å, which belongs to the minimum distance between the methane molecules in small cavities in structure II before the decomposition happens. Methane molecules are separated by water rings of the clathrate hydrate. A similar trend in terms of the RDFs of carbon atoms versus temperature can be observed as the instability is increased because of guest molecule vibrations in the center of cages. The height of peaks is declined with increasing temperature and the structure of hydrate is decomposed at the temperatures of 310 K and 320 K. In addition, the peaks disappear after decomposition and a new peak starts to grow around a distance of 4 Å at the temperatures of 310 K and 320 K. This new peak shows the minimum distance between two carbon atoms in the clusters of methane molecules. Based on the created clusters, the number of decomposed methane molecules increases with increasing the temperature, where the pressure and simulation duration are kept constant.

The RDFs for the pair of oxygen atoms in the water molecules and carbon-carbon in the methane molecules are presented in Figures 5-3c and 5-3d for structure II of methane + isobutane hydrate at different temperatures where the 700 ps NPT simulation is utilized. There are three major peaks in the oxygen RDF plots, which are similar to the oxygen trajectory for

structure II of the methane/propane gas hydrates. The trends/behaviours of oxygen skeleton and peaks in the structure II of the methane + propane system are similar to those of the methane + isobutane hydrate case in terms of the distance of oxygen molecules in the tetrahedral and hexagonal rings. In addition, the major peak in the $g_{c-c}(r)$ of the methane molecules for the methane + isobutane case appears at r = 6.2 Å, which is in agreement with the distance between the pair of carbon atoms in the methane molecules located in the samll cavities.

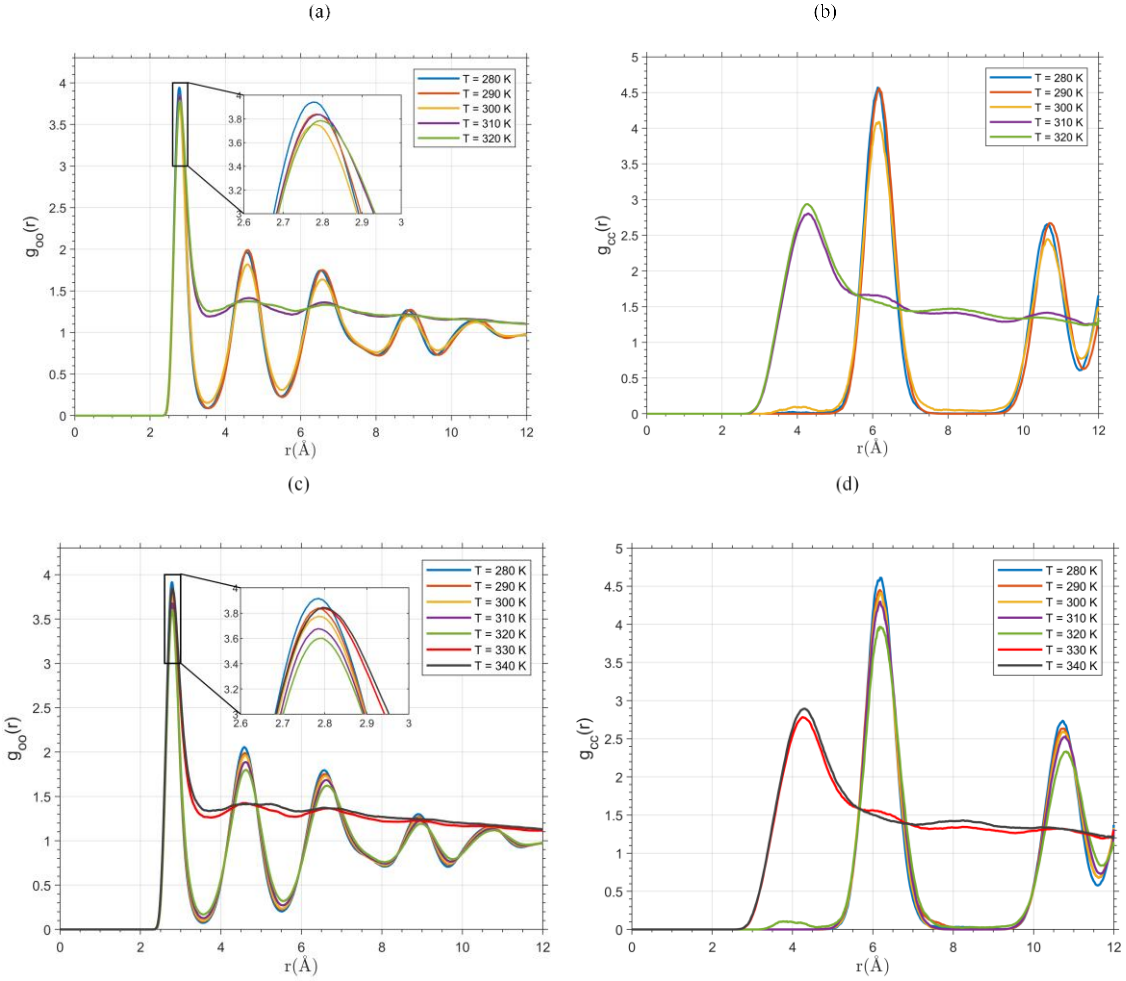

Figure 5-3: RDFs of oxygen atoms (a) in water molecules and carbon atoms (b) in the methane molecules for the methane + propane case; RDFs of oxygen atoms (c) in water molecules and carbon atoms (d) in the methane molecules for the methane + isobutane clathrate hydrate at P = 20 MPa and 700 ps, where the effect of temperature on RDF is studied.

As depicted in Figure 5-3(c), by increasing the temperature from 280 K to 320 K, the maximum value of each peak is lowered, and their height of valley is increased because of instability in the structure of the gas hydrate. At the temperatures above 320 K, the structure of methane + isobutane hydrate is decomposed and the second and third peaks (at r = 4.6 Å and r = 6.5 Å), which represent the tetrahedarl and hexahedaral rings in $g_{o-o}(r)$, are almost vanished since the tetrahedarl and hexahedaral rings in the structure of gas hydrates are destroyed. Figure 5-3(d) demonstrates the radial distribution functions (RDFs) for the pair of carbon atoms in the methane molecules. The behavouir of RDFs in the second system is similar to that in the methane + propane case. The main difference between these two cases is that the new peaks in the methane + isobutane grow at the temperatures higher than 320 K (e.g., 330 K and 340 K) when the decomposition temperature is attained. Providing further clarification, the RDF and MSD plots, and the magnitudes of density and diffusion coefficient show that the decomposition temperatures for propane + methane and methane + isobutane cases are different at the same pressure. Thus, the new (or third) peaks appear at different temperatures for these two cases. It should be noted that after the decomposition, a new peak is created at around 4 Å for the carbon-carbon pairs, showing the minimum distance between the methane molecules. The new peak confirms that the methane molecules escape from the hydrate cages (after the decomposition event) and create clusters in the simulation cell.

To illustrate the effect of pressure on the stability and decomposition of hydrates, the RDF for the pair of oxygen atoms in the water molecules is studied at different pressures for the methane + isobutane case where the temperature is 320 K and the simulation time is 700 ps. Figure 5-4 provides the $g_{o-o}(r)$ under various pressure conditions. According to Figure 5-4, the RDF reaches a higher peak when the pressure is increased and the stability of hydrate is improved. Thus, the gas hydrate structure becomes more stable with increasing pressure. It is concluded that the clathrate hydrate can decompose easily at high tempratures and low pressures.

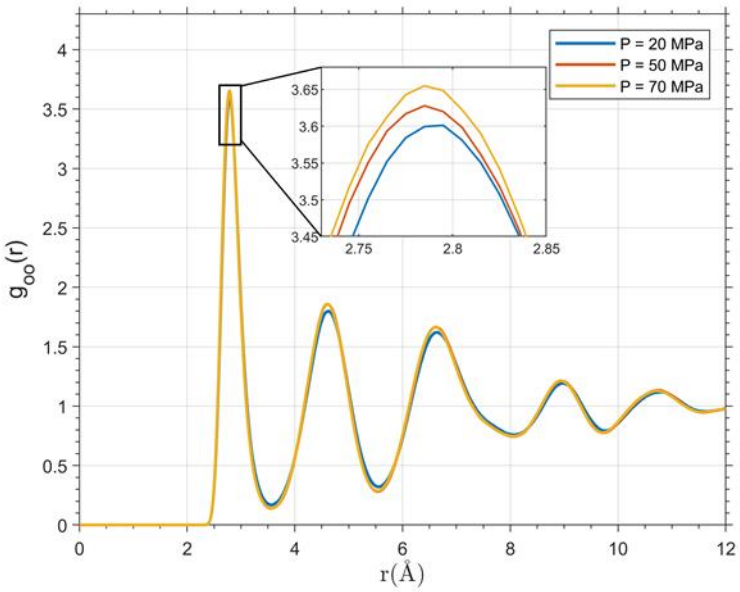

Figure 5-4: RDFs of oxygen atoms in water molecules for the methane + isobutane clathrate hydrate at T = 320 K, 700 ps, and different pressures.

MSD Parameter. This section describes the mean square displacement (MSD) behaviours of methane, propane, and isobutane as the guest molecules and water molecules (as the host) in the cages of gas hydrate structure II at different temperatures. The MSD is a parameter to show the real distance traveled by an identical particle, which is defined by the following equation:

$$\mathrm{MSD} = (|\bar{r}_i - \bar{r}_{i0}|^2) = \frac{1}{N}\sum_{i=1}^{N}(|\bar{R}_i(t) - \bar{R}_i(t_0)|^2) \quad (5\text{-}2)$$

In Equation (5-2), the summation is over all N identical molecules; $\bar{R}_i(t)$ and $\bar{R}_i(t_0)$ introduce the position of the particles at time t and reference time, respectively. The behaviour of molecules in the solid, liquid, and gas phases can be explored by analysing the MSD curves [45]. The magnitude of MSD increases linearly over the simulation time in the gas and liquid phases because of the random movement of molecules [46]. However, molecules cannot walk freely in the crystal phase (solid). Thus, the translational MSD in the crystals quickly approaches a constant value so that the slope of the MSD line will become close to zero in the solid (or hydrate) phase. Thus, the MSD can be a good indicator to recognize different phases. Figure 5-5 (a) depicts the MSD of the methane and propane molecules in the clathrate hydrate structure II at different temperatures (but at a constant pressure) with the simulation time of 700 ps. The MSD of the guest molecules at temperatures before decomposition (280 K and 290 K) is very small (and almost constant) due to the rotation of the molecules only in the center of cages. However, there is an appreciable difference between the values of MSD at 300 K and 320 K. It can be concluded that a small value of MSD over the simulation for some temperatures is related to the existence of clathrate hydrate. It is clear that the guest molecules can move freely in the simulation box with increasing temperature upon gas hydrate dissociation. This behaviour is observed in Figure 5-5(b), which shows the MSD of water molecules in the clathrate hydrate. As mentioned earlier, the small value of MSD is achieved at temperatures before the hydrate decomposition because of low vibrations of water molecules. However, the hydrogen bonds between water molecules in the cages are destroyed over the decomposition process and the MSD of water molecules becomes large.

Figures 5-5(c) and 5-5(d) depict the MSD versus time for water and guest molecules in the hydrate system of methane + isobutane at different temperatures. The magnitudes of MSD for water and guest molecules such as methane and isobutane are different (but slightly) between 280 K and 310 K conditions because of different vibrations and rotations for different molecules. However, the slope of the MSD lines is considerably increased as the temperature increases after the decomposition process (see Figures 5-5(c) and 5-5(d)).

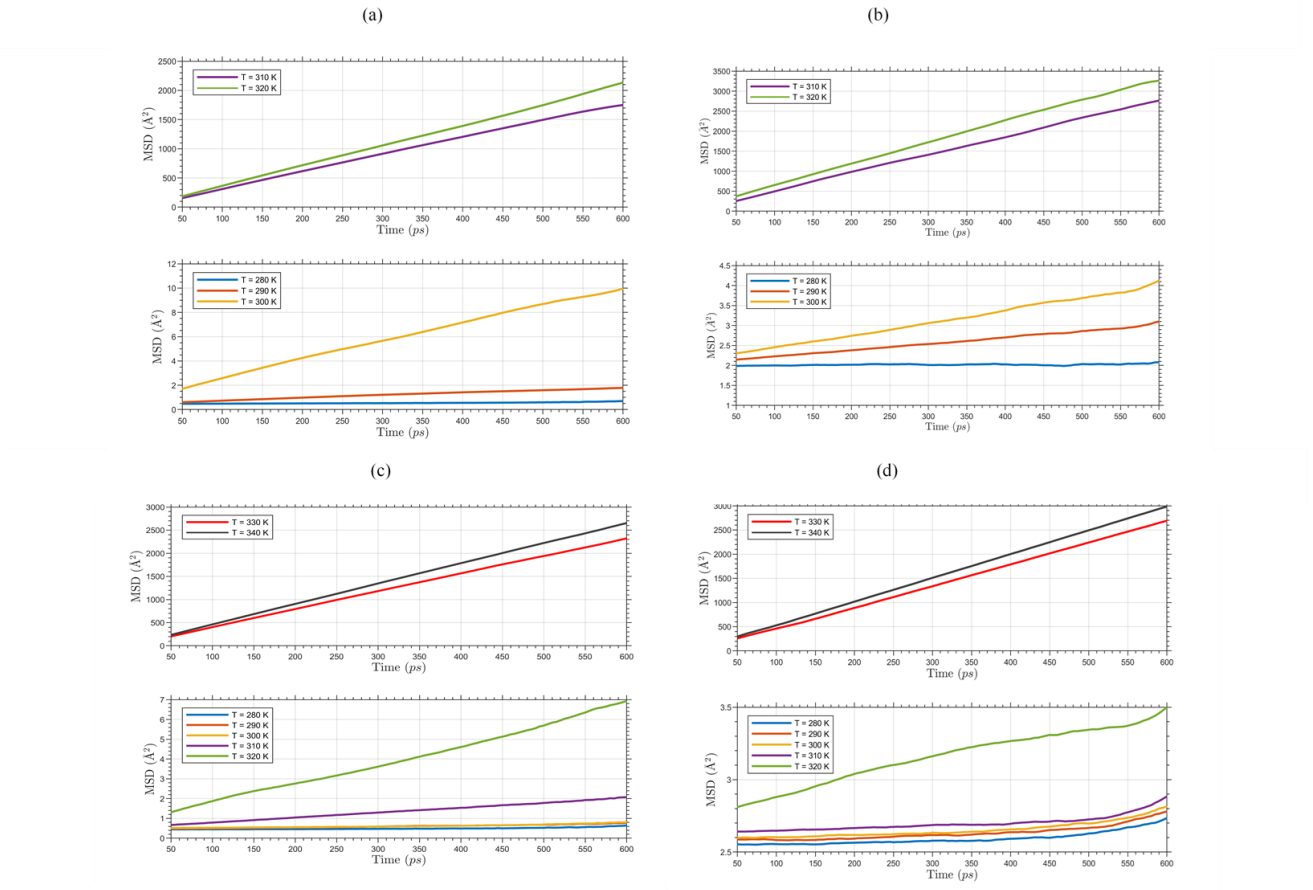

Figure 5-5: MSDs of water molecules (a) and guest molecules (b) in clathrate hydrate of the methane + propane system; MSD of water molecules (c) and guest molecules (d) in the methane + isobutane case at P = 20 MPa, 700 ps, and different temperatures.

Diffusion Coefficient. The diffusion coefficient of water molecules is calculated for the above-mentioned cases of hydrate structure II at various temperatures to provide further analysis of

dissociation behaviours. The diffusion coefficient can be calculated as a function of mean square displacement (MSD) of the specific particle, as shown below by the Einstein relationship [47]:

$$6\,D\,t = MSD \tag{5-3}$$

in which, D and t denote the diffusion coefficient and simulation time, respectively. Figure 6 presents the diffusion coefficient for the water and guest molecules (e.g., methane + propane and methane + isobutane) as a function of temperature. As it is seen in Figure 6, the diffusion coefficient of the molecules in the simulation box increases gradually with increasing temperature. As discussed earlier, the decomposition temperatures are above 300 K and 320 K for methane + propane and methane + isobutane, respectively. As the alkane molecules are captured and slightly rotated in the center of the hydrate cages, the diffusion coefficient of alkanes and water molecules holds a smaller value due to low vibrations of water molecules, compared to the condition after the decomposition event. However, the water molecules obtain a higher diffusion coefficient than alkanes for these two systems at a particular temperature condition, corresponding to the beginning of dissociation process, before the complete decomposition happens. This is because of high vibrations and movement of the water molecules at this condition, which may destroy the hydrogen bonds. At temperatures greater than decomposition temperature, the alkanes molecules move freely into the simulation box so that a higher diffusion coefficient is attained for the alkanes (compared to water) due to their molecular nature and greater movement.

In the first step of decomposition, destruction of hydrogen bonding leads to a considerable damage to the water molecules as the host in clathrate cages. After that, the encaged alkanes

molecules move freely and eventually, the alkanes bubbles are accumulated as clusters and the entire hydrate structure is completely decomposed.

(a) (b)

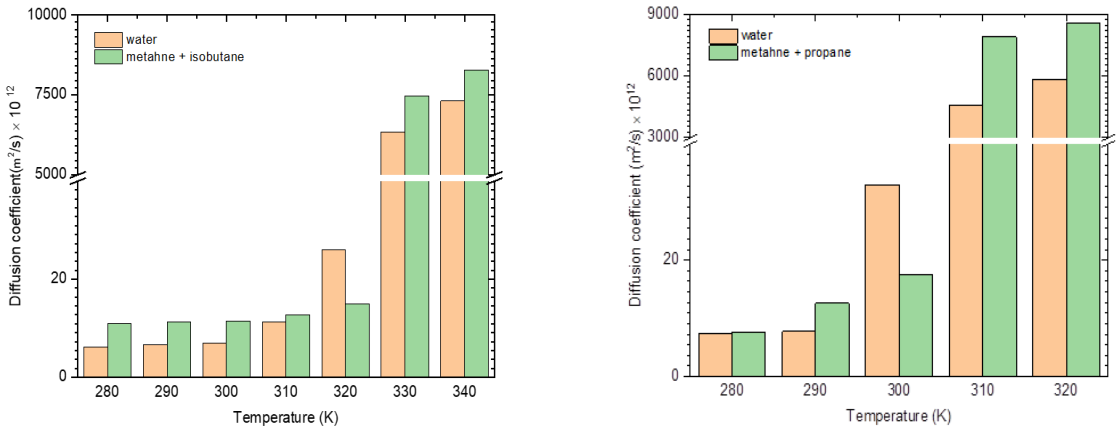

Figure 5-6: Diffusion coefficient of water and alkanes molecules for (a) methane + propane and (b) methane + isobutane hydrate at P = 20 MPa, 700 ps, and different temperatures.

Highlighting the importance of the research results, the molecular dynamic snapshots, RDFs plots, MSD curves, and the diffusion coefficient values provide adequate information on the structure and decomposition processes of the above hydrate systems.

Lattice Parameter. The network of the gas hydrate structure type II consists of small cages (5^{12}) and large cages ($5^{12}6^4$) where the small cages are connected in three dimensions and the remaining space between the cavities is filled with large cavities, which are joined through face-sharing of hexagons. Hence, the unit cell of structure II includes eight large cavities and 16 small cavities. In this work, MD simulations are conducted to calculate the lattice parameter under different thermodynamic conditions. Figure 5-7 depicts the lattice parameter for the methane + propane and methane + isobutane hydrate structure II versus temperature at the equilibrium condition. The lattice parameter for the smaller guest molecules is lower than that

for the guest molecules with a bigger radius as the larger guest molecules cause expansion of the cages as a result of the van der Waals repulsion.

The lattice parameter evaluated for the methane + propane and methane + isobutane hydrate systems is in a good agreement with the corresponding data available in the literature (see Figure 5-7). In addition, it is found that the lattice parameter for gas hydrates lowers with increasing pressure but increases with increasing temperature.

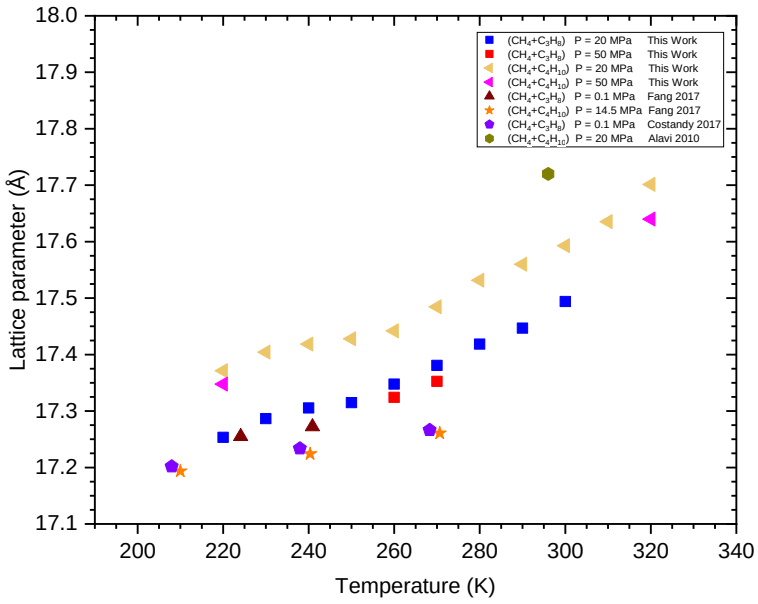

Figure 5-7: Lattice parameter for methane + propane and methane + isobutane hydrate cases as a function of temperature and pressure; The literature data are taken from [48-50].

Density. The variation of density with temperature for the gas hydrate structure II of two cases including methane + propane and methane + isobutane is obtained at a pressure of 20 MPa, as demonstrated in Figure 5-8. The density change is a proper parameter to monitor the dissociation process at various thermodynamic conditions. According to the results of MD

simulations, the density of the hydrate structure lowers with increasing temperature, particularly after the dissociation event (see Figure 5-8).

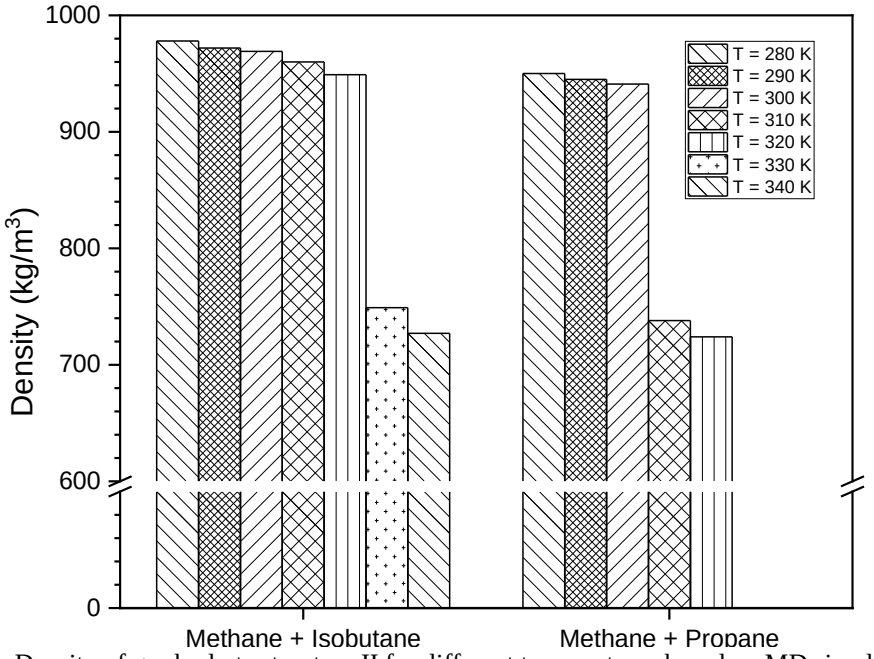

Figure 5-8: Density of gas hydrate structure II for different temperatures based on MD simulation approach.

The hydrate density is almost constant before the decomposition occurs so that it holds 970 kg/m^3 for the methane + propane hydrate case and 950 kg/m^3 for the methane + isobutane hydrate structure II. The values obtained for the density of gas hydrate structure II seem acceptable so the predicted densities for both cases are close to the values reported in the previous theoretical and experimental investigations. For instance, the reported density values are 975.14 kg/m^3 for propane + methane hydrate, 932 kg/m^3 for propane hydrate, 938 kg/m^3 for isobutane hydrate [51], and 940 and 934 kg/m^3 for gas the hydrate structure II [1, 5]. The density is significantly reduced after the decomposition occurrence so that it reaches about 740 kg/m^3. The similar trend in terms of density versus temperature is observed for both cases;

however, the magnitude of density for the methane/propane system is lower, compared to the case of methane/isobutane gas hydrate structure II (see Figure 5-8).

Effect of Composition. The influence of composition of methane/propane/ isobutane systems on the stability and decomposition of gas hydrate structure II is studied in this research work. Various configurations of the components are constructed in the hydrate phase by filling different gases in small and large cages. All five composition cases are listed in the methodology section. The MD simulations are run to simulate the behaviours of the mixtures before and after decomposition event. The RDF for hydrogen atoms in water molecules and RDF for carbon atoms in methane molecules within mixtures having different compositions are displayed in Figure 5-9. It was found before that the structures of methane + propane and methane + isobutane cases at 290 K and P = 20 MPa after 700 ps simulation remain stable. According to Figure 5-9, replacing propane and isobutane with methane molecules in large cavities can decrease the stability of gas hydrate structure, compared to the cases when higher numbers of isobutane and propane molecules are in the large cavities. Based on Figure 5-9, replacement of propane with isobutane molecules in large cavities (case 9) does not change the structure stability and the decomposition does not take place after 700 ps simulation. Thus, cases 1, 5, and 9 exhibit the same behaviours in terms of RDF and stability.

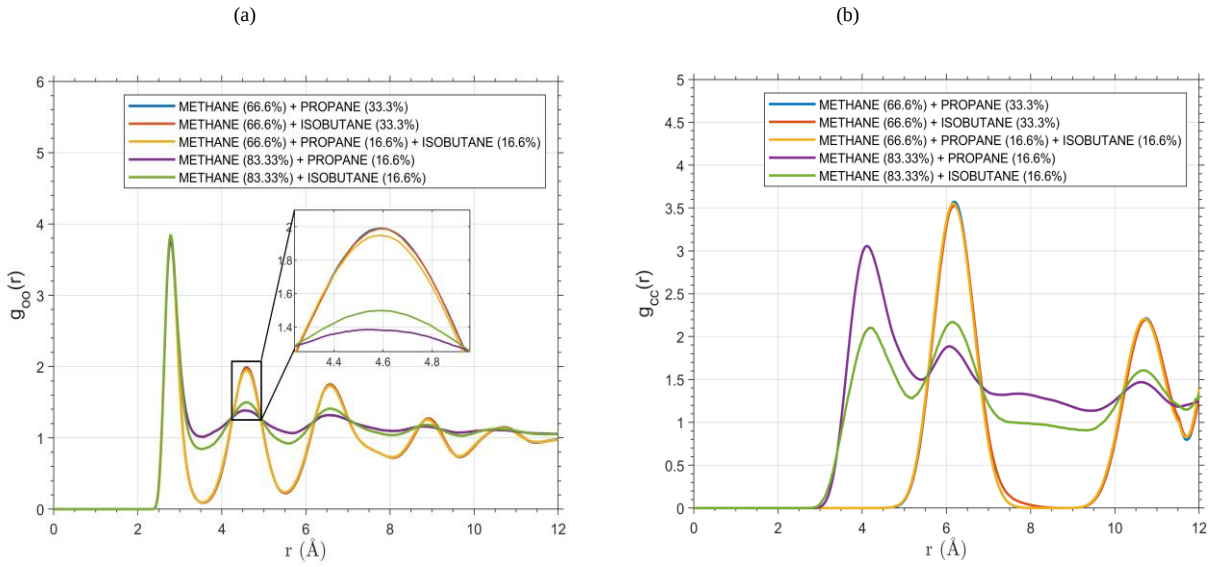

Figure 5-9: RDFs of (a) oxygen atoms in water molecules and (b) carbon atoms in methane molecules for different compositions of methane/propane/ isobutane clathrate hydrate structure II at P = 20 MPa, 700 ps, and T = 290 K.

Referring to Figure 5-10, the similar behaviour is observed for MSD plots of five different systems (cases 1, 5, and 9-11), where the same MD simulation condition is maintained. As it was discussed earlier, adding methane molecules lowers the stability of hydrate structure and the hydrate decomposition occurs earlier when the methane molecules occupy some large cavities. Figure 5-10 illustrates the MSD of water and methane molecules in the gas hydrate structure II where mixtures of methane/propane/ isobutane with different compositions are used. The value of MSD for the water molecules is increased for cases 10 and 11 when the propane and isobutane molecules are replaced with methane molecules in some large cavities. A high increase in the MSD shows the hydrate decomposition at the end of simulation time. It is concluded that the molecular dynamic trajectory simulates the decomposition behaviour of hydrate systems with different compositions of alkanes in three-phase systems. Thus, the presence of methane molecules in large cavities decreases the stability of gas hydrate structure

II for the mixtures of methane + propane, methane + isobutane, and methane + propane + isobutane.

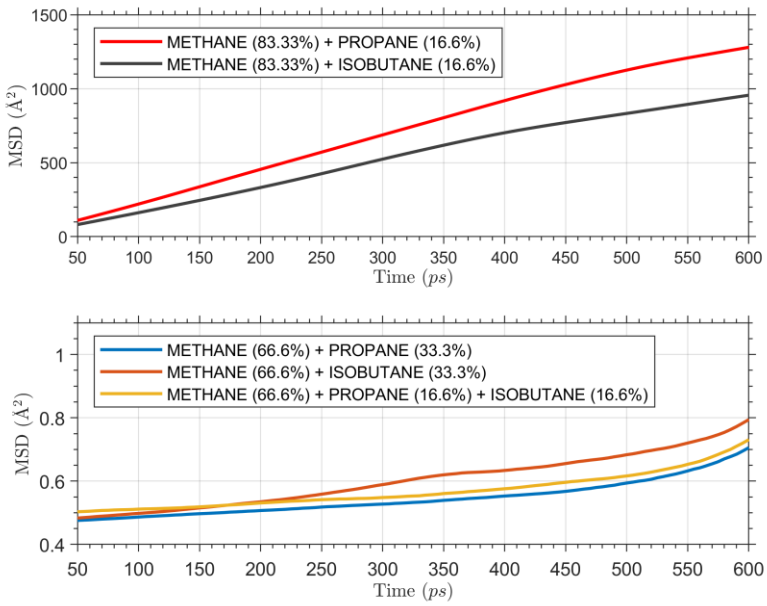

Figure 5-10: MSD of oxygen atom in water molecules at P = 20 MPa, 700 ps, and T =290 K for various mixtures.

Effect of Inhibitors. The effect of various inhibitor molecules on the hydrate decomposition is analysed in this section. By adding inhibitors to a gas hydrate system, the equilibrium condition of the gas hydrate is shifted. In this research, the gas molecules in two large cavities are replaced by the inhibitors and the MD simulations are carried out by 50 ps NVT to achieve the equilibrium condition, where the NPT ensemble is performed for 700 ps. We use three different inhibitors namely methanol, ethanol, and glycerol. The inhibition effectiveness of methanol, ethanol, and glycerol is assessed while considering methane + propane and methane + isobutane hydrate equilibria. The RDF and potential energy for the methane + propane and methane + isobutane systems in the presence and absence of inhibitors are studied to demonstrate the influence of inhibitors on the dissociation process. The new hydrogen bonds

are formed between the hydroxyl groups of inhibitors and water host molecules in the cages. The main reason for creation of the simultaneous hydrogen bonding between inhibitors (methanol, ethanol, and glycerol) and water molecules in the cages is because of the hydroxyl groups, which behave as both proton donors and proton acceptors.

Figure 5-11(a) depicts the RDF for carbon pairs of methane molecules, which occupy the small cavities. Methane molecules can clearly represent the behaviour of guest gas in the gas hydrate structure. The $g_{c-c}(r)$ is obtained at a temperature of 320 K, P = 20 MPa, and for 700 ps. The main peak appears at r = 6.2 Å, which is the distance between two methane molecules in small cages. It is clear that the structure of methane + isobutane will be stable after simulation; but when two inhibitor molecules such as methanol, ethanol, and glycerol are added to the large cavities, instead of isobutane molecules, the main peak will disappear after simulation due to decomposition of the gas hydrate structure. The decomposition can be detected when a new peak around r = 4.2 Å is observed and the methane molecules create a cluster. The same trend is noticed for the structure II of the methane + propane gas hydrate. It is found that adding even only two inhibitor molecules helps to decompose clathrate hydrate earlier, compared to the system without inhibitors, at the same condition of temperature and pressure.

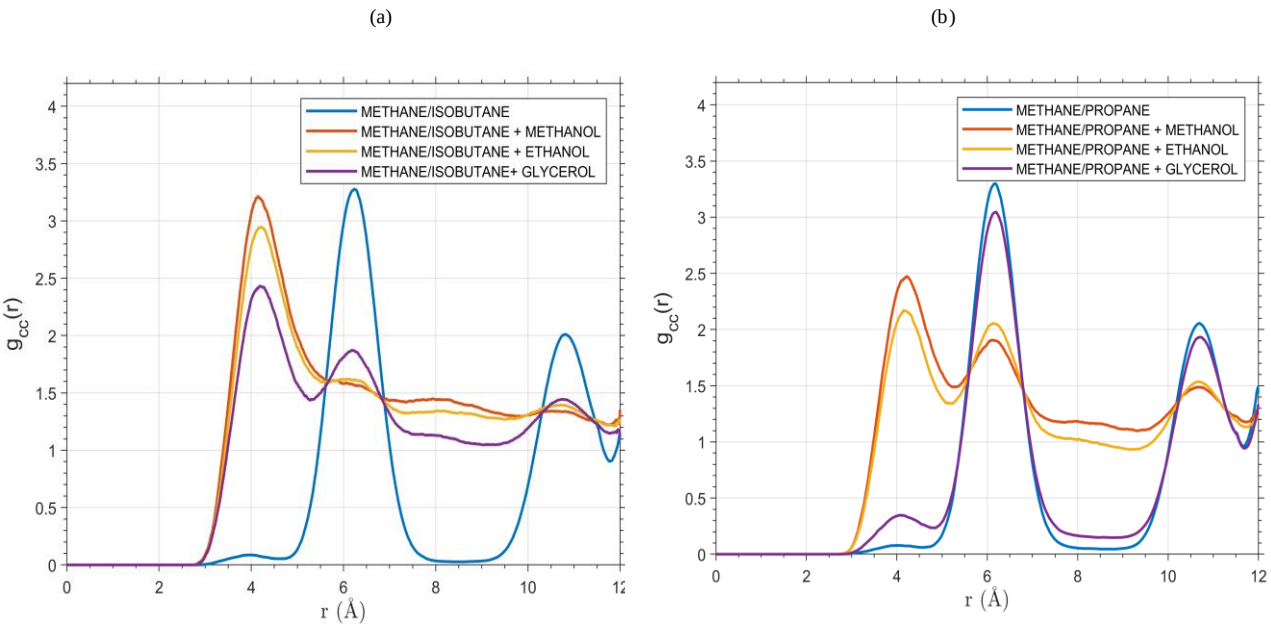

Figure 5-11: RDFs of carbon atoms in methane molecules for (a) methane + isobutane at T = 320 K and (b) methane + propane clathrate hydrate at T= 300 K, P = 20 MPa, and 700 ps in the absence and presence of inhibitors.

The potential energy in the molecular dynamic simulation is defined as the summation of van der Waals and Coulomb interactions. Figure 5-12 illustrates the potential energy alteration over the simulation run for two different systems in the presence and absence of inhibitor molecules. According to Figure 5-12, the potential energy changes around the equilibrium value before the decomposition phenomenon due to the rotation and vibration of the water and alkanes molecules. The potential energy of methane + propane system in the absence of inhibitor molecules reaches almost a constant value and the structure is stable during the simulation (see Figure 5-12(a)). The potential energy of the model with two methanol inhibitors is dramatically increased due to the structure decomposition between 120 and 185 ps. The decomposition duration for the methane + propane clathrate hydrate in the presence of methanol (as an inhibitor) is around 65 ps. However, the dissociation for the methane + propane case occurs at 195 and 595 ps in the presence of ethanol and glycerol, respectively. In addition, the

dissociation durations are about 75 and 86 ps for this system in the presence of ethanol and glycerol, respectively. After decomposition of the methane + propane hydrate structure in the presence of inhibitors, the potential energy remains almost constant so that no appreciable fluctuations are noticed. To figure out the order of inhibitors in terms of inhibition performance, the decomposition of the methane + isobutane system will be described by plotting the potential energy versus simulation time at a temperature of 330 K and P = 20 MPa. As mentioned before, the methane/ isobutane system at a pressure of 20 MPa will decompose at a temperature above 320 K. Hence, the structure dissociation occurs at a temperature higher than 320 K. The decomposition of hydrate for the methane/isobutane case without inhibitors happens after 140 ps. However, the decomposition occurs before 140 ps for the system of methane/ isobutane/inhibitor. The difference between the decomposition starting times is an acceptable parameter to rank the inhibition chemicals.

(a)

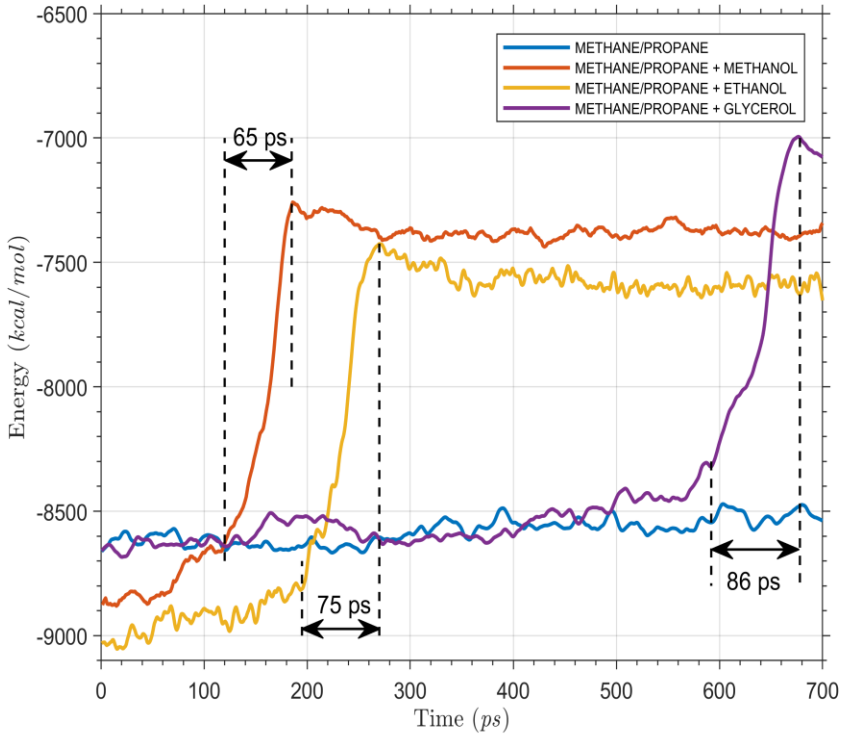

(b)

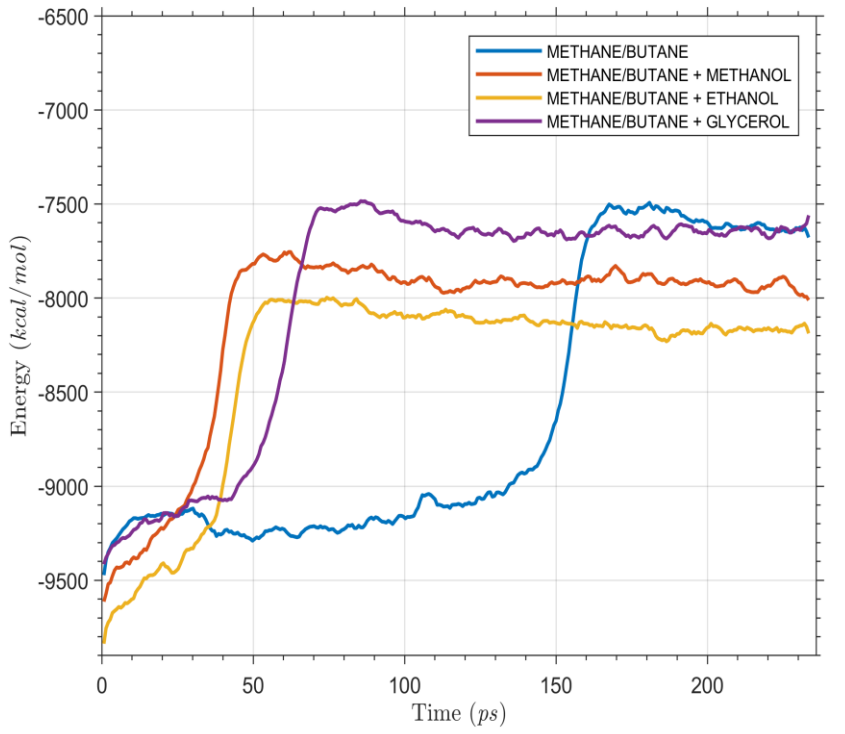

Figure 5-12: The potential energy versus time for (a) methane + propane at T = 300 K and (b) methane + isobutane clathrate hydrate at T= 330 K and P = 20 MPa.

The potential energy behaviour of the methane/propane system versus time is clearly shown in Figure 5-12(a) for before and after the decomposition. As can be seen in Figure 5-12(a), the system with methanol decomposes earlier than other cases. Considering the starting time of decomposition, the order for the inhibitors is as follows: methanol, ethanol, and glycerol. It is also concluded from panel b of Figure 5-12 that the effectiveness of inhibitors for decomposition of the methane + isobutane case is ranked in the following order: methanol > ethanol > glycerol. This ranking has been also confirmed in the previous studies [52, 53]. It seems more reasonable to consider the dissociation duration (instead of starting time of decomposition) as an important criterion to evaluate the inhibition performance. Based on Figure 5-12(a), the dissociation durations for the methanol, ethanol, and glycerol cases are 65, 75, and 86 ps, respectively, confirming the same conclusion/ranking as before. The difference between these four cases in terms of potential energy implies that adding two inhibitor molecules (less than 2 wt%) to the clathrate hydrate can lower the decomposition time, as displayed in Figure 5-12(a) with black two-way arrows. It is worth noting that the inhibitors can facilitate decomposition by creating new hydrogen bonds between the inhibitors and water molecules in the cages, which are able to weaken/destroy the hydrogen bonding balance between the water molecules in the hydrate cavities.

It is recommended to examine the effectiveness/behaviours of various molecules as inhibitors or promotors in hydrate systems at the atomic level. It seems interesting to study the stability and decomposition of various hydrate structures in the presence of clay, acids, and oils to obtain a better understanding of transport phenomena occurring in gas hydrate reservoirs.

The gas hydrate reservoirs are considered a valuable and available energy source in some countries around the world. To achieve a comprehensive/ deep knowledge about the structural,

dynamic, and thermodynamic parameters of gas hydrates, the molecular dynamic simulation strategy as a reliable and fairly inexpensive tool can assist researchers and engineers involved in various chemical and oil/gas industries in terms of some theoretical and practical prospects such as development of simulation/optimization software packages, prevention of pipe blockages, CO_2 capture, and inhibition of gas hydrate formation.

5.4. Conclusions

In this work, the decomposition and stability of gas hydrate type II for methane/propane, methane/isobutane, and methane/propane/isobutane are studied by employing the Forcite module in the Materials Studio molecular dynamic (MD) simulation. The influences of temperature, pressure, composition, and inhibitor on the decomposition phenomenon are analyzed. In addition, the dynamic and structural properties of the gas hydrate structure II are determined at various thermodynamic conditions. The density of simulation box, which is a key property to monitor the decomposition process, is calculated in the MD simulations. The best parameter to show the configuration of cages and distance between the guest molecules is the radial distribution function (RDF). In this study, the crystal structure of the hydrate structure II for methane/propane, methane/isobutane, and methane/propane/isobutane is well described by employing RDF. The main outcomes of this research work are summarized as follows:

- The stability of gas hydrate can be investigated in detail by utilizing the MD simulation approach. The RDF, MSD, and diffusion coefficient can be obtained from a set of NPT ensemble in MD simulation at different pressures and temperatures. According to the MD results, increasing temperature and decreasing pressure lead to instability of the gas hydrate structure.

- The dissociation of gas hydrates is observed at the molecular scale. First, the vibration of water molecules is continuously increasing so that the lattice parameter and diffusion coefficient increase over time. Eventually, the structure of cages in the gas hydrate disjoints. After this stage, the guest gases run away from the center of damaged cages and the diffusion coefficient of gas molecules experiences an increase after the decomposition.
- The lattice parameter for the methane/water and methane/isobutane systems is calculated at a variety of pressures and temperatures. A good agreement between the experimental data and simulation results is noticed.
- To study the effect of inhibitors on the decomposition process, two methane molecules are replaced by the inhibitors. As expected, the presence of inhibitors accelerates the decomposition process and results in the gas hydrate dissociation at lower temperatures.
- The hydroxyl groups in the inhibitors (used in this study) are the reason for the earlier decomposition, compared to the cases without inhibitors. The new hydrogen bonds are formed between the hydroxyl groups of inhibitors and water molecules, which disturb the arrangement and stability of cages.
- The relative importance of inhibitors in terms of gas hydrate decomposition duration is assessed. Based on this criterion, the inhibitors are ordered as follows: methanol > ethanol >glycerol.

Acknowledgments

We would like to thank Memorial University (NL, Canada), Equinor (formerly Statoil) Canada, Innovate NL, and the Natural Sciences and Engineering Research Council of Canada (NSERC) for their financial support.

Nomenclatures

Acronyms

$AAD\%$	Average absolute percent deviation
$CVFF$	Consistent valence force field
MD	Molecular dynamic
MSD	Mean square displacement
NVT	Constant temperature, constant volume
NPT	Constant pressure, constant volume
RDF	Radial distribution function

Variables/Letters

$g_{\alpha\beta}$	Radial distribution function of the atom β in the distance of r from the atom α.
D	Diffusion coefficient
N	Total number of particles α and β particles
n	Total number of data sets
P	Pressure
r	Spherical distance
R	Initial position of particles
t	Simulation time
T	Temperature

V Volume of simulation box

References

[1] Sloan, E.D. and C.A. Koh, *Clathrate Hydrates of Natural Gases*. 2008.

[2] Demirbas, A., *Methane hydrates as potential energy resource: Part 2–Methane production processes from gas hydrates.* Energy Conversion and Management, 2010. **51**(7): p. 1562-1571.

[3] Kondori, J., S. Zendehboudi, and M.E. Hossain, *A review on simulation of methane production from gas hydrate reservoirs: Molecular dynamics prospective.* Journal of Petroleum Science and Engineering, 2017. **159**: p. 754-772.

[4] Javanmardi, J., M. Moshfeghian, and R.N. Maddox, *An accurate model for prediction of gas hydrate formation conditions in mixtures of aqueous electrolyte solutions and alcohol.* Can. J. Chem. Eng., 2001. **79**(3): p. 367.

[5] Carroll, J.J., *Natural Gas Hydrates: A Guide for Engineers*. 2009.

[6] Kang, S.P., M.K. Chun, and H. Lee, *Phase equilibria of methane and carbon dioxide hydrates in the aqueous MgCl2 solutions.* Fluid Phase Equilib., 1998. **147**(1–2): p. 229.

[7] Abdi-Khanghah, M., M. Adelizadeh, Z. Naserzadeh, H. Barati, and Z. Zhang, *Methane hydrate formation in the presence of ZnO nanoparticle and SDS: Application to transportation and storage.* Journal of Natural Gas Science and Engineering, 2018. **54**: p. 120-130.

[8] Liu, Z., Z. Pan, Z. Zhang, P. Liu, L. Shang, and L. Bingfan, *Effect of Porous Media and SDS Complex System on Methane Hydrate Formation*. Vol. 32. 2018.

[9] Maekawa, T., *Equilibrium conditions for gas hydrates of methane and ethane mixtures in pure water and sodium chloride solution.* Geochemical Journal, 2001. **35**(1): p. 59-66.

[10] Kondori, J., S. Zendehboudi, and L. James, *Evaluation of Gas Hydrate Formation Temperature for Gas/Water/Salt/Alcohol Systems: Utilization of Extended UNIQUAC Model and PC-SAFT Equation of State.* Industrial & Engineering Chemistry Research, 2018.

[11] Strobel, T.A., K.C. Hester, E.D. Sloan, and C.A. Koh, *A Hydrogen Clathrate Hydrate with Cyclohexanone: Structure and Stability.* Journal of the American Chemical Society, 2007. **129**(31): p. 9544-9545.

[12] Sloan Jr, E. and F. Fleyfel, *A molecular mechanism for gas hydrate nucleation from ice.* AIChE Journal, 1991. **37**(9): p. 1281-1292.

[13] Davidson, D.W., Y.P. Handa, C.I. Ratcliffe, J.S. Tse, and B.M. Powell, *The ability of small molecules to form clathrate hydrates of structure II.* Nature, 1984. **311**: p. 142-143.

[14] Mehta, A.P. and E.D. Sloan Jr, *Structure H hydrate phase equilibria of methane+ liquid hydrocarbon mixtures.* Journal of Chemical and Engineering Data, 1993. **38**(4): p. 580-582.

[15] Loveday, J., R. Nelmes, M. Guthrie, S. Belmonte, D. Allan, D. Klug, J. Tse, and Y. Handa, *Stable methane hydrate above 2 GPa and the source of Titan's atmospheric methane.* Nature, 2001. **410**(6829): p. 661.

[16] Yang, L., C. Tulk, D. Klug, I. Moudrakovski, C. Ratcliffe, J. Ripmeester, B. Chakoumakos, L. Ehm, C. Martin, and J. Parise, *Synthesis and characterization of a*

new structure of gas hydrate. Proceedings of the National Academy of Sciences, 2009. **106**(15): p. 6060-6064.
[17] Qiu, X., S.P. Tan, M. Dejam, and H. Adidharma, *Novel isochoric measurement of the onset of vapor–liquid phase transition using differential scanning calorimetry.* Physical Chemistry Chemical Physics, 2018. **20**(41): p. 26241-26248.
[18] Qiu, X., S.P. Tan, M. Dejam, and H. Adidharma, *Simple and accurate isochoric differential scanning calorimetry measurements: phase transitions for pure fluids and mixtures in nanopores.* Physical Chemistry Chemical Physics, 2019. **21**(1): p. 224-231.
[19] Walsh, M.R., C.A. Koh, D.E. Sloan, A.K. Sum, and D.T. Wu, *Microsecond simulations of spontaneous methane hydrate nucleation and growth.* Science, 2009. **326**(5956): p. 1095-1098.
[20] Radhakrishnan, R. and B.L. Trout, *A new approach for studying nucleation phenomena using molecular simulations: Application to CO 2 hydrate clathrates.* The Journal of chemical physics, 2002. **117**(4): p. 1786-1796.
[21] Zhang, J. and Z. Pan, *Effect of potential energy on the formation of methane hydrate.* Journal of Petroleum Science and Engineering, 2011. **76**(3): p. 148-154.
[22] English, N.J., J.K. Johnson, and C.E. Taylor, *Molecular-dynamics simulations of methane hydrate dissociation.* Journal of Chemical Physics, 2005. **123**(24).
[23] Vatamanu, J. and P.G. Kusalik, *Molecular insights into the heterogeneous crystal growth of sI methane hydrate.* The Journal of Physical Chemistry B, 2006. **110**(32): p. 15896-15904.
[24] Okano, Y. and K. Yasuoka, *Free-energy calculation of structure-H hydrates.* The Journal of chemical physics, 2006. **124**(2): p. 024510.
[25] WAN, L.-H., K.-F. YA, X.-S. LI, and S.-S. FAN, *Molecular dynamics simulation of methane hydrate dissociation process in the presence of thermodynamic inhibitor.* Acta Physico-Chimica Sinica, 2009. **25**(3): p. 486-494.
[26] English, N.J. and J.M.D. Macelroy, *Structural and dynamical properties of methane clathrate hydrates.* Journal of Computational Chemistry, 2003. **24**(13): p. 1569-1581.
[27] Chialvo, A.A., M. Houssa, and P.T. Cummings, *Molecular dynamics study of the structure and thermophysical properties of model sI clathrate hydrates.* Journal of Physical Chemistry B, 2002. **106**(2): p. 442-451.
[28] Ding, L.Y., C.Y. Geng, Y.H. Zhao, and H. Wen, *Molecular dynamics simulation on the dissociation process of methane hydrates.* Molecular Simulation, 2007. **33**(12): p. 1005-1016.
[29] Kondori, J., S. Zendehboudi, and L. James, *New insights into methane hydrate dissociation: Utilization of molecular dynamics strategy.* Fuel, 2019. **249**: p. 264-276.
[30] Smirnov, G.S. and V.V. Stegailov, *Melting and superheating of sI methane hydrate: Molecular dynamics study.* Journal of Chemical Physics, 2012. **136**(4).
[31] Geng, C.-Y., Q.-Z. Han, H. Wen, Z.-Y. Dai, and C.-H. Song, *Molecular dynamics simulation on the decomposition of type SII hydrogen hydrate and the performance of tetrahydrofuran as a stabiliser.* Molecular Simulation, 2010. **36**(6): p. 474-483.
[32] Choudhary, N., S. Das, S. Roy, and R. Kumar, *Effect of polyvinylpyrrolidone at methane hydrate-liquid water interface. Application in flow assurance and natural gas hydrate exploitation.* Fuel, 2016. **186**: p. 613-622.
[33] Pal, S. and T. Kundu, *Pentagonal dodecahedron methane hydrate cage and methanol system—An ab initio study.* Journal of Chemical Sciences, 2013. **125**(2): p. 379-385.

[34] Li, K., R. Shi, Y. Huang, L. Tang, X. Cao, Y. Su, and J. Zhao, *Dissociation mechanism of propane hydrate with methanol additive: A molecular dynamics simulation.* Computational and Theoretical Chemistry, 2018. **1123**: p. 79-86.
[35] Verlet, L., *Computer" experiments" on classical fluids. I. Thermodynamical properties of Lennard-Jones molecules.* Physical review, 1967. **159**(1): p. 98.
[36] Swope, W.C., H.C. Andersen, P.H. Berens, and K.R. Wilson, *A computer simulation method for the calculation of equilibrium constants for the formation of physical clusters of molecules: application to small water clusters.* J Chem Phys, 1982. **76**.
[37] Gear, C.W., *Numerical initial value problems in ordinary differential equations*. 1971: Prentice Hall PTR.
[38] Biovia, *Biovia Materials Studio*. 2018: San Diego, CA, USA.
[39] Kirchner, M.T., R. Boese, W.E. Billups, and L.R. Norman, *Gas hydrate single-crystal structure analyses.* Journal of the American Chemical Society, 2004. **126**(30): p. 9407-9412.
[40] Bernal, J.D. and R.H. Fowler, *A theory of water and ionic solution, with particular reference to hydrogen and hydroxyl ions.* The Journal of Chemical Physics, 1933. **1**(8): p. 515-548.
[41] Berendsen, H.J., J.v. Postma, W.F. van Gunsteren, A. DiNola, and J. Haak, *Molecular dynamics with coupling to an external bath.* The Journal of chemical physics, 1984. **81**(8): p. 3684-3690.
[42] Zhang, J., S. Piana, R. Freij-Ayoub, M. Rivero, and S.K. Choi, *Molecular dynamics study of methane in water: diffusion and structure.* Molecular Simulation, 2006. **32**(15): p. 1279-1286.
[43] McLain, S.E., A.K. Soper, and A. Watts, *Water structure around dipeptides in aqueous solutions.* European Biophysics Journal, 2008. **37**(5): p. 647-655.
[44] Vatamanu, J. and P. Kusalik, *Molecular dynamics methodology to investigate steady-state heterogeneous crystal growth.* The Journal of chemical physics, 2007. **126**(12): p. 124703.
[45] Liang, S. and P.G. Kusalik, *Explorations of gas hydrate crystal growth by molecular simulations.* Chemical Physics Letters, 2010. **494**(4-6): p. 123-133.
[46] Allen, M.P. and D.J. Tildesley, *Computer simulation of liquids*. 2017: Oxford university press.
[47] Fang, B., F. Ning, P. Cao, L. Peng, J. Wu, Z. Zhang, T.J. Vlugt, and S. Kjelstrup, *Modeling Thermodynamic Properties of Propane or Tetrahydrofuran Mixed with Carbon Dioxide or Methane in Structure-II Clathrate Hydrates.* The Journal of Physical Chemistry C, 2017. **121**(43): p. 23911-23925.
[48] Costandy, J., V.K. Michalis, I.N. Tsimpanogiannis, A.K. Stubos, and I.G. Economou, *Lattice constants of pure methane and carbon dioxide hydrates at low temperatures. Implementing quantum corrections to classical molecular dynamics studies.* The Journal of chemical physics, 2016. **144**(12): p. 124512.
[49] Alavi, S., S. Takeya, R. Ohmura, T.K. Woo, and J.A. Ripmeester, *Hydrogen-bonding alcohol-water interactions in binary ethanol, 1-propanol, and 2-propanol+ methane structure II clathrate hydrates.* The Journal of chemical physics, 2010. **133**(7): p. 074505.

[50] Vlasic, T.M., P. Servio, and A.D. Rey, *Atomistic modeling of structure II gas hydrate mechanics: Compressibility and equations of state.* AIP Advances, 2016. **6**(8): p. 085317.
[51] Maekawa, T., *Equilibrium conditions of propane hydrates in aqueous solutions of alcohols, glycols, and glycerol.* Journal of Chemical & Engineering Data, 2008. **53**(12): p. 2838-2843.
[52] Maekawa, T., *Equilibrium conditions for carbon dioxide hydrates in the presence of aqueous solutions of alcohols, glycols, and glycerol.* Journal of Chemical & Engineering Data, 2010. **55**(3): p. 1280-1284.

Table of Contents (TOC) Graphic

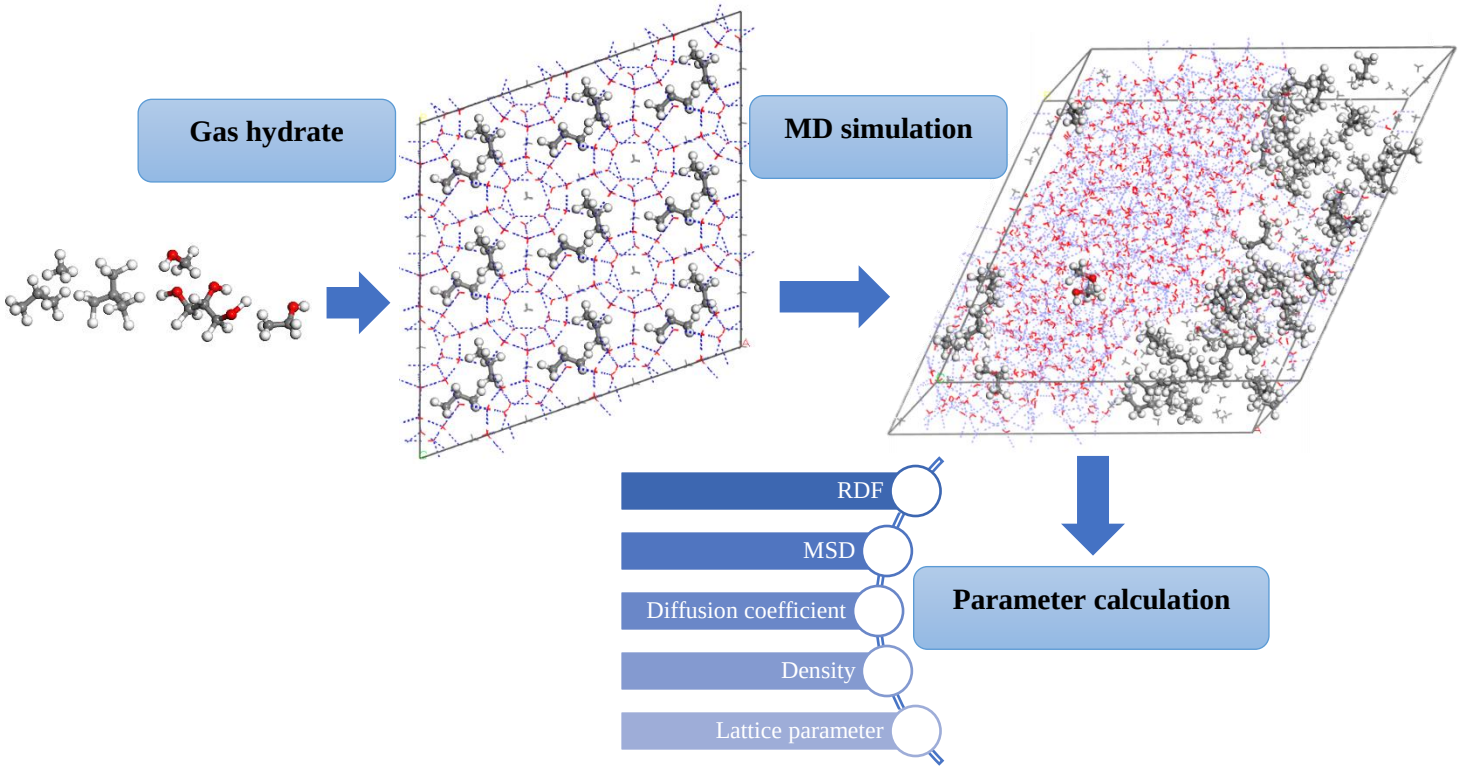

6.CHAPTER SIX

Molecular Scale Modeling Approach to Evaluate Stability and Dissociation of Methane and Carbon Dioxide Hydrates (in press)

Preface

A version of this manuscript has been published in the Journal of Molecular Liquids (2019). I am the primary author of this paper. Sohrab Zendehboudi, Lesley James, and I were involved in the literature review, definition of objectives, modeling approach, and design of the manuscript. I prepared the first draft of the manuscript and subsequently revised the manuscript based on the feedback/comments from the co-authors and the journal's reviewers. The co-author, Sohrab Zendehboudi, significantly helped in reviewing and revising the manuscript. The co-author, Lesley James, also provided several important comments/points to improve the quality of the manuscript.

Abstract

A comprehensive knowledge and precise estimation of the dynamic, structural, and thermodynamic characteristics of hydrates are needed to assess the stability of gas hydrates. Thermodynamic model and experimental studies can be utilized to compute the physical and dynamic properties of hydrate structures. The use of molecular dynamic (MD) simulation is a well-established approach in gas hydrate studies at the atomic level where the properties of interest are obtained from the numerical solution of Newtonian equations. The present work uses MD simulations by employing the constant temperature-constant pressure (NPT), constant temperature-constant volume (NVT) conditions, and the consistent valence force field (CVFF) to monitor the stability and decomposition of methane and carbon dioxide gas hydrates with different compositions. The effects of temperature and composition on the hydrate stability are investigated. In this study, we also compute the radial distribution function, mean square displacement, diffusion coefficient, lattice parameter, potential energy, dissociation enthalpy as well as the density of methane and carbon dioxide under various thermodynamic and process conditions. The formation of methane and carbon dioxide bubbles is studied to investigate bubble evolution in hydrate dissociation. The sizes of methane and carbon dioxide bubbles are not the same due to different solubility of methane and carbon dioxide in liquid water. In addition, the influences of pressure and temperature on the lattice parameter and density of clathrate hydrate are discussed. The obtained results are consistent with previous theoretical and experimental findings, implying that the methodology followed in this chapter is reliable. The most stable arrangement of methane and carbon dioxide molecules in the gas hydrate is found. The insights/findings of this study might be useful to further understand detailed transport phenomena (e.g., molecular interactions, gas production rate, carbon dioxide

replacement, and carbon dioxide capture) involved in the process of carbon dioxide injection into gas hydrate reservoirs.

Keywords: Molecular dynamic simulation; Carbon dioxide hydrate; Methane hydrate; Stability; Decomposition.

6.1. Introduction

Currently, gas hydrates have drawn growing interests because of their high importance and wide applications in the gas transportation [1], gas separation [2-8], future energy sources/storage [9-11], and water treatment operations [12]. Although gas hydrates might have considerable benefits to the energy and environment sectors, they generally lead to serious problems such as blockage and mechanical damage to equipment and pipeline systems in the oil and gas industries [13].

In terms of storage capacity, gas hydrate reservoirs provide massive and precious gas resources in permafrost and deep ocean regions because each cubic meter of methane or carbon dioxide hydrate offers about 120-180 cubic meters of natural gas in standard condition [14]. This high storage capacity of methane hydrates is an attractive technique to decrease CO_2 emissions to atmosphere and attract researchers' attention to study on carbon dioxide sequestration in methane hydrate reservoirs, which might be found in various marine sediments and geological formations [15].

Gas hydrates are ice-like components which are formed by water molecules at high pressure and low temperature conditions due to van der Waals interactions between caged water molecules and guest molecules as well as the hydrogen bonds in the frameworks of water

molecules. Depending on the pressure, temperature, and gas molecule size, three different types of gas hydrates are found (e.g., structures I, II, and H) [14]. These three types vary in the kind and number of cages in clathrate hydrates as well as the type and size of guest molecules. The unit cell parameter of cubic structure I is 12.05 Å, which includes two small (5^{12}, pentagonal dodecahedral) and six large ($5^{12}6^2$, tetrakaidekahedral) cages. The tetrakaidekahedral and pentagonal dodecahedral frameworks consist of 12 pentagonal plus two hexagonal faces and 12 pentagonal water rings, respectively. The variations of temperature and pressure in process equipment especially in pipelines may result in desirable conditions for formation of clathrate hydrates. Therefore, it is essential to propose effective, safe, and economical operating strategies in the oil and gas processes that may experience hydrate formation. In most recent studies, the depressurisation method has been recognised as the most promising approach for hydrate decomposition [15-19]. The additive and/or chemical injection also affects the hydrate dissociation or formation [18]. Hence, investigation of the molecular behaviours of additives in the hydrate formation inhibition and dissociation acceleration is valuable in terms of research contribution and practical implication. Several studies (in the open sources) carry out the important roles of additives in terms of dissociation [20], improving storage capacity [19], and formation rate [21] of gas hydrates.

One of the efficient methods for gas production from gas hydrate reservoirs is gas swapping [19]. This technique includes adding another guest molecules to the gas hydrate structure for hydrate formation so that new guest gas molecules occupy the place/space of methane, resulting in methane production. Graue et al. [20] developed a new approach using fluorine gas and microwave technology to exchange methane gas with carbon dioxide through CO_2 sequestration into natural gas hydrates. Park et al. [21]showed that the efficiency of gas

production by CO_2 is above 60%. This promising strategy offers advantages of both CO_2 sequestration and gas hydrate production operations. The Japan Oil, Gas, and Metals National Corporation, ConocoPhillips, and U.S. Department of Energy conducted a comprehensive study to investigate the potential of CO_2 replacement in methane hydrate reservoirs in the Alaska North Slope on May 5, 2012 [19]. Knowing important benefits of this process in terms of energy and environment prospects, further theoretical and experimental studies are required to confirm the economic and technical feasibility of this method for gas production from hydrates.

The controlling and monitoring of clathrate hydrate dissociation and/or formation through experimental works at low temperatures and high pressures are generally inaccurate, complicated, and problematic. Recently, MD simulations have been utilized as a valuable method to investigate the nucleation, formation [22], stability [23], growth [24], structure arrangement [25], and thermodynamic characteristics [26] of gas hydrates. For example, Baez and Clancy [27] carried out a MD simulation study to model hydrate decomposition at 270 K and 4 MPa. It was found that the hydrate dissociation is slower than the ice dissolution and the gas molecules form a gas cluster after dissociation. English et al. simulated formation of CO_2 hydrates using the MD approach. Their findings are in agreement with Baez's results [28, 29]. Ding et al. [30] performed MD simulation to study methane hydrate dissociation where they divided the decomposition process into two steps: firstly, the cell size is increased, and the cages are then decomposed and the guest molecules escape from decomposed clathrate hydrates. A series of MD simulation runs were conducted by Smirnov and Stegailov [31] to analyse the influences of temperature and cage occupancy on the stability and behaviours of methane hydrates at pressures below 500 MPa. The decomposition and/or stability of methane

hydrates were also investigated at different pressures and temperatures in the presence of alcohol as an inhibitor in our earlier work for structures I and II [32, 33].

Recently, considerable attention has been focused on the carbon dioxide injection into methane hydrate reserves to study the important aspects such as CO_2 storage in the ocean depth and separation process [34]. Geng et al. [35] worked on the MD simulation to study the CH_4 production by CO_2 replacement in the hydrate structure. This replacement in the molecular scale has also been investigated by Tung et al. [36]. They used a different potential function for water molecules to define interactions between the molecules. Moreover, the hydrate phase was identified using an angular order parameter (AOP) of water molecules. In another research work, the impacts of mass transfer, memory effect, and chemical potential of guest molecules on the stability of methane hydrate systems in the replacement process of CH_4 by CO_2 molecules were scrutinized by Bai et al. [37] using the MD simulation strategy.

The measurement of physical and structural properties of gas hydrates is relatively costly and erroneous because of the thermodynamic condition of gas hydrates (high pressure and low temperature). MD simulations have been employed as a powerful technique to overcome the drawbacks as mentioned earlier. To date, MD simulations have been conducted to measure the radial distribution function (RDF), mean square displacement (MSD), thermal expansion coefficient, diffusion coefficient [14], heat capacity, and thermal conductivity [38] for different structures of gas hydrates at various process and thermodynamic conditions.

In 1998, Gutt et al. were one of the pioneer researchers to calculate the structural and thermophysical properties of the structure I of gas hydrate as a function of temperature [38]. The lattice parameters of clathrate hydrates in structures I and II were obtained by Belosludov

et al. [39]. The structure I of methane and xenon and structure II of argon, krypton, and propane hydrate systems were analyzed to determine the structural parameters. Although their results differ from some recently published studies, they are consistent with the studies, which were conducted at low temperatures (below 100 K). Berite et al. [40] reported the lattice parameter for tetrahydrofuran and cyclobutanone in the structure II of the clathrate hydrates. Based on their findings, it was concluded that there is a relationship between the size of guest gases and stretching the hydrogen bonds in the cages. This provides a logical reason to obtain a high lattice parameter for large guest molecules.

Davidson et al. [41] carried out a study to determine the thermal expansion and lattice parameter of three structure I and 14 structure II hydrate systems using powder x-ray diffraction [23] at the temperature range of 100 to 170 K. They also calculated the unit cell parameters for 40 systems of type II at different temperatures. It was noticed that the cell size of structure II of hydrate increases by increasing the system temperature. In another research investigation, Ogienk et al. [42] measured the lattice parameter and thermal expansion for the mixture of methane and argon gases in the structure H of hydrates using the diffraction pattern at various temperatures within the range of 79-270 K. The temperature dependence of the unit cell parameter in the recent experimental works shows good agreement with Ogienk et al.'s results. Tse et al. [43] performed an isothermal-isobaric (NPT) MD simulation to calculate the RDF and lattice parameter of xenon hydrates. They concluded that the frequency of the translational modes causes the difference between the experimental and simulation values for lattice parameters. Chialvo et al. [44] accomplished a series of isothermal-isobaric (NPT) MD simulation runs to show the effect of different gas molecules on structural and thermal parameters of gas hydrates structure I for a mixture of methane and carbon dioxide. They also

used different water potential functions. The clathrate hydrate structure parameters were then determined, and they calculated the modified parameters which are currently used for hydrate phase equilibria calculations. In a recently published research work, Reshadi et al. [45] provided results of an MD simulation study for structure II of clathrate hydrates where different hydrocarbon gas molecules and krypton were employed. It offers valuable insights into why lattice parameters and density are different for various guest molecules at different temperatures and pressures. In addition, they found that the unit cell parameter increases with increasing temperature and declines with increasing pressure. The calculated lattice parameters are in agreement with those previously obtained by experiments. Also, Reshadi et al. [46] implemented an MD approach on the structure H of hydrate to obtain the thermodynamic and structural parameters of gas hydrates for different guest gases at various operating and thermodynamic conditions. They confirmed their previous results, showing that the lattice parameter of large guest hydrocarbons increases with increasing temperature and lowering pressure. It was also mentioned that the lattice parameter changes with the interaction energy, size of guest molecules, and dynamics of small cages. The diffusion coefficient of water molecules and structural parameter of methane hydrates were calculated by Zhang et al. [47] using MSD and RDF. Sakamaki et al. [48] investigated the mechanical and thermodynamic properties of methane hydrates within a wide range of pressure using the MD technique.Although the dynamic, structural, and thermodynamic characteristics of clathrate hydrates have been studied using experimental and thermodynamic approaches, only a limited number of research works have been found in the literature to determine the properties of various gas hydrate systems.

While the parameters mentioned above help to analyze all aspects related to stability and decomposition of methane and carbon dioxide hydrates, the gas bubble evolution can provide further information/data to characterize gas hydrate decomposition. Kim et al. [49] demonstrated that the gas bubble accumulation lowers the decomposition rate by influencing the heat transfer at the interface of hydrate decomposition. In a research study, Ripmeester et al. [50] examined the melting of methane hydrate; it was noticed that the gas hydrate decomposition rate declines due to gas bubble formation. More experimental and modeling research activities are needed to have proper (and deep) understanding of the structural and dynamic characteristics of the gas bubbles in methane and carbon dioxide hydrates. The molecular dynamic simulation appears to be a valuable tool for determination (and monitoring) of the properties of clathrate hydrates over different stages such as nucleation, formation, and dissociation.

Thermodynamically, the methane hydrate is the most common and available structure of natural gas hydrates. Carbone dioxide injection is an effective technique to produce methane from methane hydrate reservoirs, leading to acceleration of gas production rate. Hence, it seems essential to explore adding CO_2 to structure I of methane hydrates in terms of gas hydrate stability and carbon capture prospects. This study is planned to investigate the stability/ dissociation of CH_4 and CO_2 hydrates at different conditions such as compositions and temperatures. In addition, the vital physical and dynamic characteristics of the hydrate systems including lattice parameter and diffusion coefficient are determined. The formation and/or evolution of CH_4 and CO_2 bubbles after hydrate decomposition are then discussed.

This chapter is divided into three main sections. This chapter begins with the introduction section. The second section covers the theoretical aspects of our methodology and molecular

dynamic simulation. The third section deals with detailed discussion on the research results for different mixtures of CH_4 and CO_2 hydrates. The conclusions of this paper are finally presented.

6.2. Simulation Information and Procedure

Molecular dynamic (MD) simulation technique has emerged as a powerful tool in studying the behaviours of different systems and chemicals at the molecular level. MD simulations can contribute to a better understanding of structural, thermodynamic, and dynamic properties of simple and/or complex systems [51-53]. The MD simulation is based on Newton's laws, where atoms behave like hard-sphere solids. Firstly, the coordinates of atoms are obtained. The summation of all potential energies can provide the force of each atom. Then, the calculated forces are used to obtain new positions for atoms after a time step by employing a different algorithm to solve the Newton's equation [54-56]. The last step in MD simulations is to calculate different properties of the system.

A variety of theoretical, experimental, and molecular techniques are used to evaluate the hydrate decomposition and stability. Each approach has advantages and drawbacks. MD simulations can be more helpful for analysing and characterising systems at very high and low temperatures as well as a wide range of pressure. The second advantage of using the MD simulations is that only the intermolecular and atomic properties are needed to conduct the simulation runs.

Another benefit of MD simulation is the ability to detect the behaviour of molecules in the complex systems, such as movement of enzyme molecules through the channel of proteins [51, 52]. In addition, the MD simulation is the best technique to study the mechanical, structural,

and thermodynamic properties of expensive and rare molecules, namely polymers, enzymes, and proteins. In spite of the fact that the list of applications and advantages of the MD technique can be endless, MD simulations have some significant pitfalls. For example, the focal drawbacks of the MD simulations correspond to the simulation time and size of simulation box. Due to the fact that the size of simulation box is very small (in order of nm), an appropriate structure should be prepared to show all properties and aspects of the proposed system through the simulation runs. In addition, MD simulations need the utilization of strong computing systems/process units, leading to long-time computer runs.

The MD simulation will be used to describe the decomposition and stability of methane hydrates by including carbon dioxide at different pressures, temperatures, and compositions. The MD simulations are carried out by Materials Studio software through employing the Forcite modules and consistent valence force field (CVFF) in the Forcite module [57]. The x-ray diffraction data are used to construct a unit cell of hydrate structure I. All guest molecules are added at the centre of cages. The geometry of our system is optimized by employing Forcite geometry optimization, in which the position of particles is changed until the total energy of the simulation box is minimized. The force of all particles is computed based on selected forcefield and potential energy. A linear search is applied to the direction of energy drop in the steepest descent optimization methodology. In this technique, the highest magnitude of the energy is sought and then a new line search by the orthogonal direction with the initial point is found. Thus, the minimum energy in all directions can be achieved for all particles with an adequate tolerance. The steepest descent optimization is a commonly-used method for systems, which are not in equilibrium conditions. Although the steepest descent optimization has successfully identified the minimum case of total energy, it is very slow due to considerable

fluctuations to accede the required geometry. The combination of conjugate gradient and the method mentioned above is chosen to capture the geometry with a minimum energy to improve the convergence speed [57]. In this study, the energy and geometry of the simulation box are optimised using a smart algorithm, which is a combination of steepest descent, Quasi-Newton gradient, and conjugate methods [57].

The constant-temperature/constant-volume ensemble (NVT) is utilized to reach the thermodynamic temperature. The NVT ensemble or canonical ensemble is used to control thermodynamic temperature. The temperature of the system is adjusted based on the Berendsen Thermostats [58]. The change in temperature for each step in Berendsen method can be expressed by following equation [58]:

$$\lambda = \sqrt{1 + \frac{\Delta t}{\tau_T}\left(\frac{T_0}{T} - 1\right)} \tag{6-1}$$

where T_0 refers to the bath temperature (target temperature in K); T stands for the instantaneous temperature (K); and τ_T and Δt represent a characteristic relaxation time and time step (ps), respectively.

The initial 50 ps NVT simulation is run to achieve the desired temperature. The constant-temperature/constant-pressure ensemble (NPT) is employed to adjust the pressure and temperature. The pressure of the system is regulated by changing the volume of system.

The vectors of simulation box and position of particles are allowed to control the pressure of the system by adjusting the volume. This method is used only for periodic systems. In the Berendsen method the size of simulation box, not the shape, is allowed to change. The key advantage of the NPT method is that the both relaxation time (τ_T) and compressibility of the

system (λ) are utilized in the calculation of scaling factor (μ). For each step of the simulation, the x, y, and z coordinates of each particle are scaled by the following scaling factor:

$$\mu = \left[1 + \frac{\Delta t}{\tau_P}\lambda(P_0 - P)\right]^{\frac{1}{3}} \quad (6\text{-}2)$$

In Equation (6-2), P and P_0 resemble the target and instantaneous pressures, respectively. The units of compressibility and pressure in Equation (6-2) are Pa^{-1} and Pa, respectively. After NVT simulation, the NPT ensemble is performed for different pressures and temperatures in the Materials Studio software [57].

The consistent valence forcefield (CVFF) is used to assess the interactions between different particles in the Materials Studio package, which calculates the potential energy for different molecules such as amino acids, hydrocarbons, water, and many organic molecules [59]. The simple point charge (SPC) potential function is applied to determine the magnitudes of forces for water molecules in the CVFF forcefield. The charges for hydrogen and oxygen atoms in the water molecules are +0.41e and -0.82e, respectively. In addition, the charges on the carbon and hydrogen atoms of methane are -0.4e and +0.1e; and the charges on the oxygen and carbon atoms in carbon dioxide are +0.287e and +0.575e, respectively [60]. The energy in the CVFF forcefield is calculated by the following expression [57, 61, 62]:

$$
\begin{aligned}
E = \sum_{b} D_b \left[1 - e^{-\alpha(b-b_0)}\right] + \sum_{\theta} H_\theta \, (\theta - \theta_0)^2 + \sum_{\phi} H_\phi [1 - S\cos(n\phi)] \\
+ \sum_{\chi} H_\chi \chi^2 + \sum_{b} \sum_{b'} F_{bb'} \, (b - b_0)(b' - b_0') \\
+ \sum_{\theta} \sum_{\theta'} F_{\theta\theta'} (\theta - \theta_0)(\theta' - \theta_0') \\
+ \sum_{b} \sum_{\theta} F_{b\theta} \, (b - b_0)(\theta - \theta_0) \\
+ \sum_{\phi} F_{\phi\theta\theta'} \cos\phi (\theta - \theta_0)(\theta' - \theta_0') \\
+ \sum_{\chi} F_{\chi\chi'} \chi\chi' + \sum \varepsilon \left[\left(\frac{r^*}{r}\right)^{12} - 2\left(\frac{r^*}{r}\right)^{6}\right] + \frac{q_i q_j}{\varepsilon r_{ij}}
\end{aligned}
\tag{6-3}
$$

where χ, ϕ, b, and θ introduce the out-of-plane parameter, dihedral angle, bond length, and bond angle, respectively; F, H, and D represent the force constants; ε refers to the depth of well in van der Waals potential term; r_{ij} symbolizes the distance between atom *i* with charge q_i from particle *j* with charge q_j; and S and n denote the sign convention for the dihedral term and the nonnegative integer coefficient parameters, respectively. α in Equation (6-3) is expressed by the following equation:

$$
\alpha = \sqrt{\frac{K_0}{2D_0}} \tag{6-4}
$$

where K_0 is the force constant and D_0 stands for the equilibrium well depth.

The CVFF force field is used to compute the forces and interaction between particles in the methane /carbon dioxide hydrates. The van der Waals and long-range columbic forces are obtained using the Ewald summation; the cut-off distance to calculate the van der Waals forces is set to be 12 Å. The pressure and temperature of simulation are controlled by Berendsen barostat and instantaneous thermostat with a decay of 0.1 ps [58]. Figure 6-1 illustrates a brief algorithm for the MD simulations of methane + carbon dioxide hydrate decomposition for a variety of compositions using the Materials Studio.

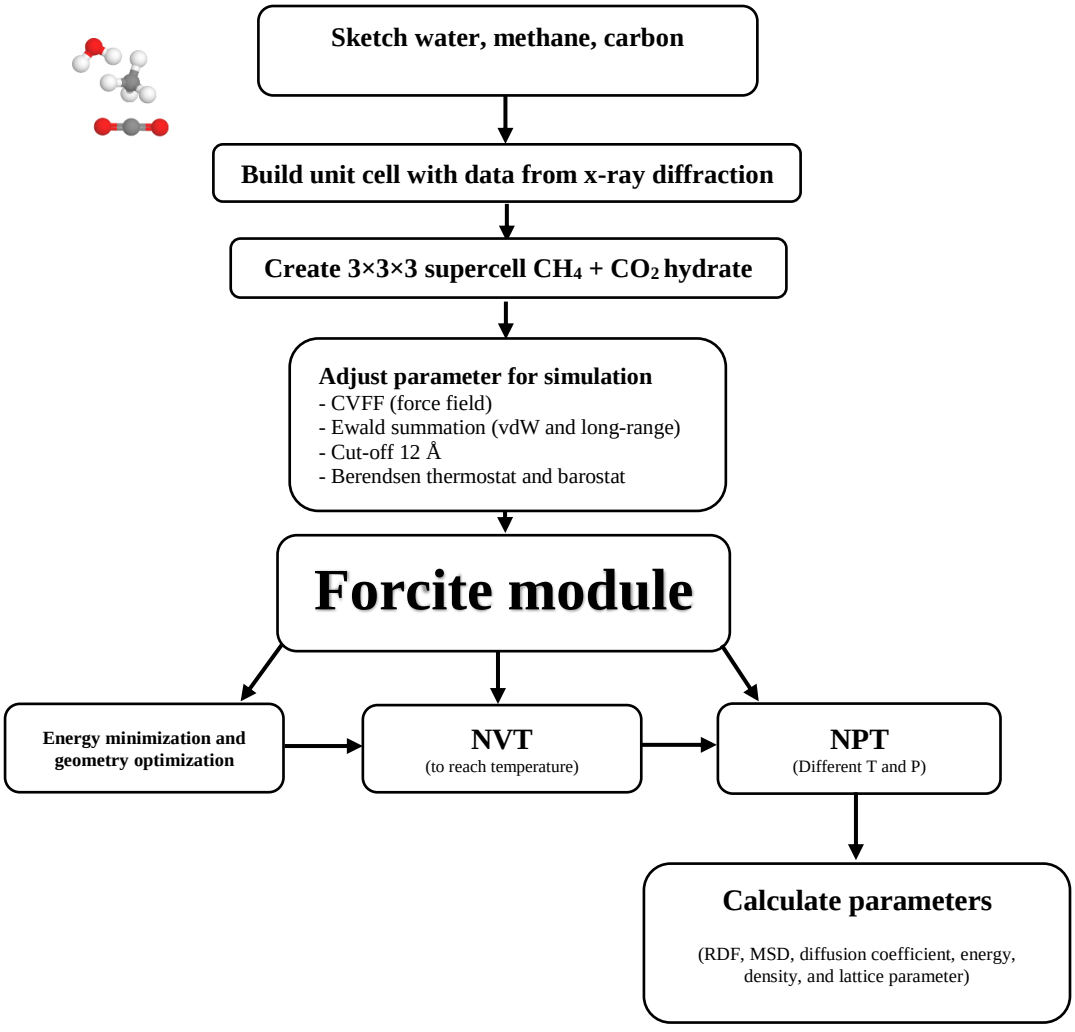

Figure 6-1: Main stages for molecular dynamic simulation of methane + carbon dioxide hydrate as well as methane hydrate.

6.3. Results and Discussion

In this section, the stability and decomposition process of methane and carbon dioxide hydrates at different compositions are studied. Also, the structural and physical properties are calculated. The radial distribution function, potential energy, diffusion coefficient, and mean square displacement are discussed to further understand the decomposition process and stability of hydrate structures at different process and thermodynamic conditions. This section covers the technical discussion and molecular dynamics findings on the decomposition of methane + carbon dioxide hydrates. The dynamic and structural characteristics of methane + carbon dioxide hydrates are investigated. In addition, the density and lattice parameter at different compositions and temperatures are calculated by employing MD simulation. In order to study the potential of methane replacement with carbon dioxide in the hydrate systems, the stability of the different compositions of methane and carbon dioxide hydrate cases are investigated. A cubic supercell of structure I hydrate is made by $3\times3\times3$ unit cells. Then, the guest molecules are placed at the center for different compositions to create various arrangements of molecules (see Table 6-1). MD simulations are performed for a 50 ps NVT and 400 ps NPT at a pressure of 5 MPa where different compositions and temperatures are applied. For instance, the MD simulations are carried out at 240, 250, 260, 270, 280, and 290 K to investigate the stability of the clathrate hydrates.

Radial distribution function (RDF). This parameter describes the ratio of density for a specific atom in the distance of *r* by overall density. Hence, it shows the variation of density around a given particle, as expressed below:

$$g_{\alpha\beta}(r) = \frac{V}{N_\alpha N_\beta}\left(\sum_{i=1}^{N_\alpha}\frac{n_i\beta(r)}{4\pi r^2\Delta r}\right) \quad (6\text{-}5)$$

where N_α and N_β stand for the total of α and β atoms; V denotes the volume of the simulation box; and $n_i\beta(r)$ resembles the number of particle β at the spherical distance of *r* from particle α. The methane and carbon dioxide molecules in different cavities of clathrate hydrate structure I are replaced with each other to simulate different compositions. The required information of all various mixtures is listed in Table 6-1.

Table 6-1: Summary of different systems in the simulation box.

No.	Molecules (molar fraction)	Small Cavity		Large Cavity	
		CH_4	CO_2	CH_4	CO_2
1	Methane (100%)	54	0	162	0
2	Methane (75%) + Carbon dioxide (25 %)	0	54	162	0
3	Methane (62.5%) + Carbon dioxide (37.5 %)	54	0	81	81
4	Methane (25%) + Carbon dioxide (75 %)	54	0	0	162
5	Carbon dioxide (100%)	0	54	0	162

The radial distribution function for carbon-carbon atoms in the guest molecules and oxygen-oxygen atoms in the water molecules are shown with $g_{c-c}(r)$ and $g_{o-o}(r)$, respectively. The RDFs are obtained for different temperatures but constant simulation time and pressure. The $g_{o-o}(r)$ of MD simulations at different composition and temperature conditions (at 5 MPa and after 400 ps simulation) are depicted in the left side of Figures 6-2(a) to 6-2(e). The first peak of the radial distribution function of oxygen pairs is around 2.75 Å. It shows the minimum distance between two oxygen atoms in two different waters molecules, which are linked with

the hydrogen bonds [47]. The magnitude of the second peak for $g_{o-o}(r)$ is 4.5 Å that originates from the hydrogen bonding in tetrahedral networks in the hydrate structures [63]. The distance of oxygen pairs in the hexagonal rings are represented by the third peak at r = 6.53 Å [24, 47]. The right side of Figures 6-2 (a) to 6-2 (e) provides the RDFs for carbon-carbon pairs of guest molecules (methane and carbon dioxide). The minimum distance between two guest molecules at the center of cages is shown by the first peak at 6.8 Å in the stable condition. A new peak appears after dissociation at r = 4.2 Å; consequently, the guest molecules move out from cages and start to create gas clusters. As can be seen after dissociation, the peak at 6.8 Å shifts to 4.2 Å, indicating the minimum distance between two carbon molecules in cluster of methane and carbon dioxide molecules. From the RDFs graphs, it is concluded that the structure of clathrate hydrates is progressively decomposed by increasing temperature. The dissociation temperatures are different for different compositions of methane and carbon dioxide. The dissociation temperature can be identified by finding a new peak in $g_{c-c}(r)$ or a sharp decrease in the height of the first peak for $g_{o-o}(r)$. For example, the decomposition temperature for methane (75%) + carbon dioxide (25 %) at P = 5 MPa is 270 K, where the methane and carbon dioxide molecules escape from the cages. The second and third peaks disappear in the $g_{o-o}(r)$ figures after decomposition due to disintegration of water cages in the hydrate structures. Hence, the hydrate stability and decomposition behavoiur can be pursued by the second and third peaks in $g_{o-o}(r)$. In addition,

creation of a new peak at r = 4.2 Å in $g_{c-c}(r)$ shows the hydrate decomposition where the guest molecules leave the cages.

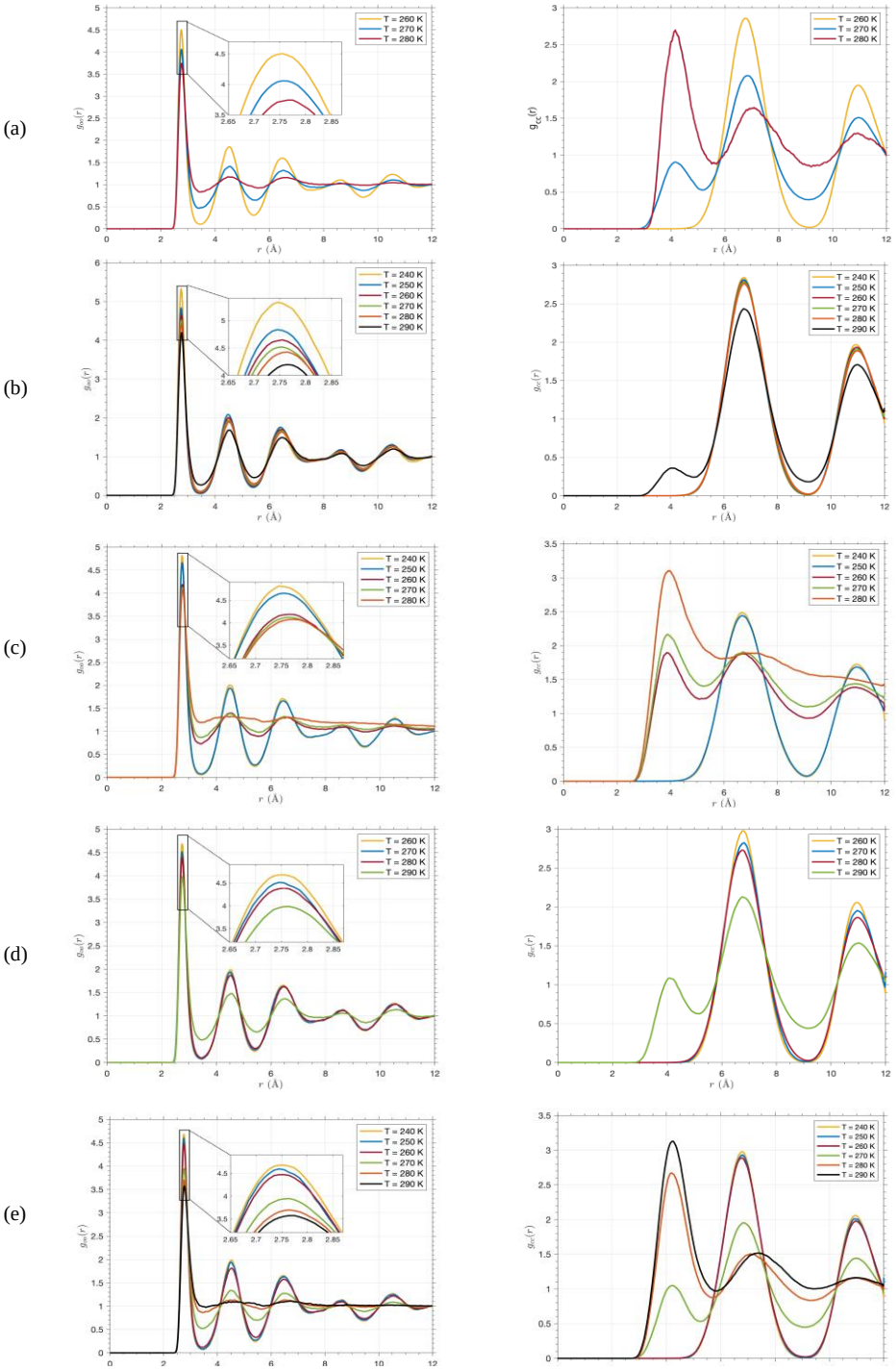

Figure 6-2: RDFs of oxygen atoms in water molecules (left side) and carbon atoms in methane molecules (right side) for (a) methane, (b) methane (75%) + carbon dioxide (25%), (c) methane (62.5%) + carbon dioxide (37.5 %), (d) methane (25%) + carbon dioxide (75%), and (e) carbon dioxide hydrate, at P=5 MPa, 400 ps, and different temperatures.

The MD simulations are performed at different temperatures for 5 systems at a pressure of 5 MPa for 400 ps. The objective of obtaining different RDFs is to explore the stability of various compositions of guest gas in different cages at various temperatures. For instance, the third system (methane (62.5%) + carbon dioxide (37.5 %)) is stable at a temperature less than 270 K, implying that the water cages are almost rigid during simulation, and the hydrate is decomposed after 270 K where the water cages are destroyed and guest molecules escape. Highlighting the main results of this phase of study, the RDFs at different temperatures demonstrate that the system with a composition of methane (25%) + carbon dioxide (75 %) is almost stable between 260 and 290 K where the carbon dioxide molecules are in large cages and the methane molecules are present in small cavities. In another hydrate system, the large cavities are shared between the carbon dioxide and methane molecules (methane (62.5%) + carbon dioxide (37.5 %)). As it is clear from Figure 6-2(d), the clathrate hydrate decomposes at 290 K and the height of the new peak in $g_{c-c}(r)$ is larger than that in Figure 6-2 (e). The carbon dioxide molecules are placed in small cages and methane molecules are located in large cages in the second system. However, this replacement decreases the stability of clathrate hydrate in comparison with the fourth case when the carbon dioxide molecules are in large cavities. In addition, the stability of systems with pure methane and pure carbon dioxide (the first and last systems) is minimal, compared with the the hydrate systems that contain a mixture of CH_4 and CO_2 gases. According to the results, it is found that the mixture of methane + carbon dioxide hydrate is more stable than carbon dioxide hydrate and methane hydrate cases. The hydrate structures with 87.5 % and 75 % cage occupancy of carbon dioxide are almost stable at temperatures below 290 K where the pressure is constant (e.g., 5 MPa).

To demonstrate the impact of pressure on hydrate dissociation, the RDF of oxygen-oxygen atoms in the water molecules and that of carbon-carbon atoms in carbon dioxide molecules is obtained from NPT simulations at a constant temperature, but variable pressures. Panels (a) and (b) of Figure 6-3 illustrate the RDFs of oxygen-oxygen and carbon-carbon atoms at T = 270 K, where different pressures of 5,10, and 50 MPa are examained. It is clear that the the valley of peaks becomes narrow and the height of peaks increases with increasing pressure. The same behavouir can be found in the RDFs of CO_2 molecules; the tendency of CO_2 hydrate dissociation is higher at lower pressures due to formation of clusters of CO_2 molecules after decomposition, compared to the cages with higher pressures.

The molecular dynamic simulations reveal that the probability of CO_2 hydrate decomposition becomes lower noticeably as the pressure is increased. In addition, the efffect of pressure on hydrate decomposition phenomenon is not pronounced as much as the temperature influence.

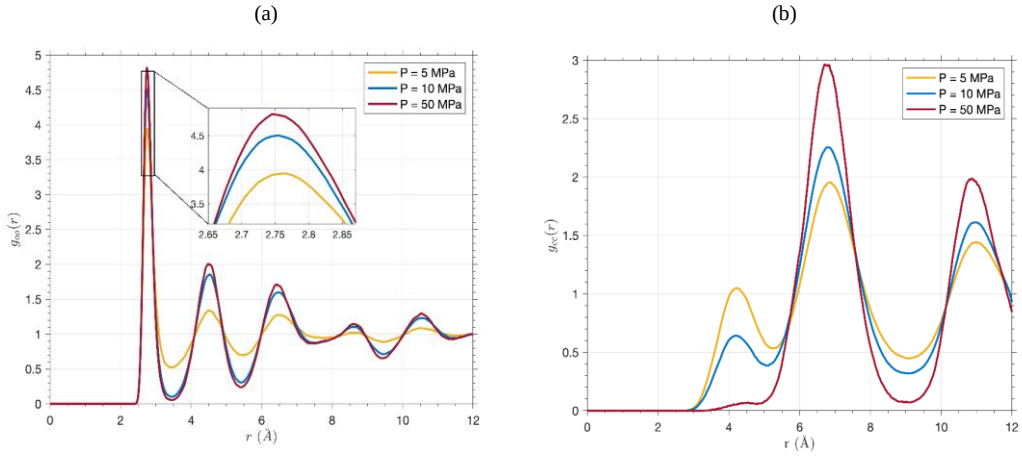

Figure 6- 3: RDF plots of (a) oxygen atoms in water molecules and (b) carbon atoms in carbon dioxide at T = 270 K, 400 ps, and different pressures.

Mean square displacement and diffusion coefficient. The mean square displacement (MSD) and diffusion coefficient for guest molecules and water in the hydrate structures are studied in

this section for various composition and temperature conditions. The movement and vibration of each molecule can be represented by MSD, as defined by the following equation:

$$MSD = \left(\left| \bar{r}_i - \bar{r}_{i0} \right|^2 \right) = \frac{1}{N} \sum_{i=1}^{N} \left(\left| \bar{R}_i(t) - \bar{R}_i(t_0) \right|^2 \right) \quad (6\text{-}6)$$

where $\bar{R}_i(t)$ resembles the position of atoms at t; and $\bar{R}_i(t_0)$ introduces the initial position of the particle; N stands for the total number of particles. The movement and behaviour of molecules in the various phases can be investigated using MSD curves [64]. Figures 6-4(a)-6-4(e) provide the MSDs for guest molecules (methane and/or carbon dioxide) and water molecules in the framework of hydrate at different temperatures and compositions of methane and carbon dioxide after 400 ps MD simulation. The decomposition temperatures for a variety of systems were obtained in the previous section. Based on Figures 6-4(a) to 6-4(e), there is a slight change in MSDs of guest gases and water molecules at the temperatures below the decomposition temperature. This behaviour/trend is due to rotation and vibration of molecules before decomposition when the structure of hydrate is almost stable. Hence, the slope of MSD curves is almost zero in the crystals of hydrates. However, the value of MSDs increases sharply after decomposition owing to the breakage of hydrate cages. In addition, the value of MSD for guest molecules at the same temperature shows that the fourth system (methane (25%) + carbon dioxide (75%)) is more stable than other cases in which the carbon dioxide and methane molecules fill the large and small cavities, respectively. It can be inferred that using MSD graphs we are able to recognize different phases, stability, and decomposition in clathrate hydrates.

(a)

(b)

(c)

(d)

(e)

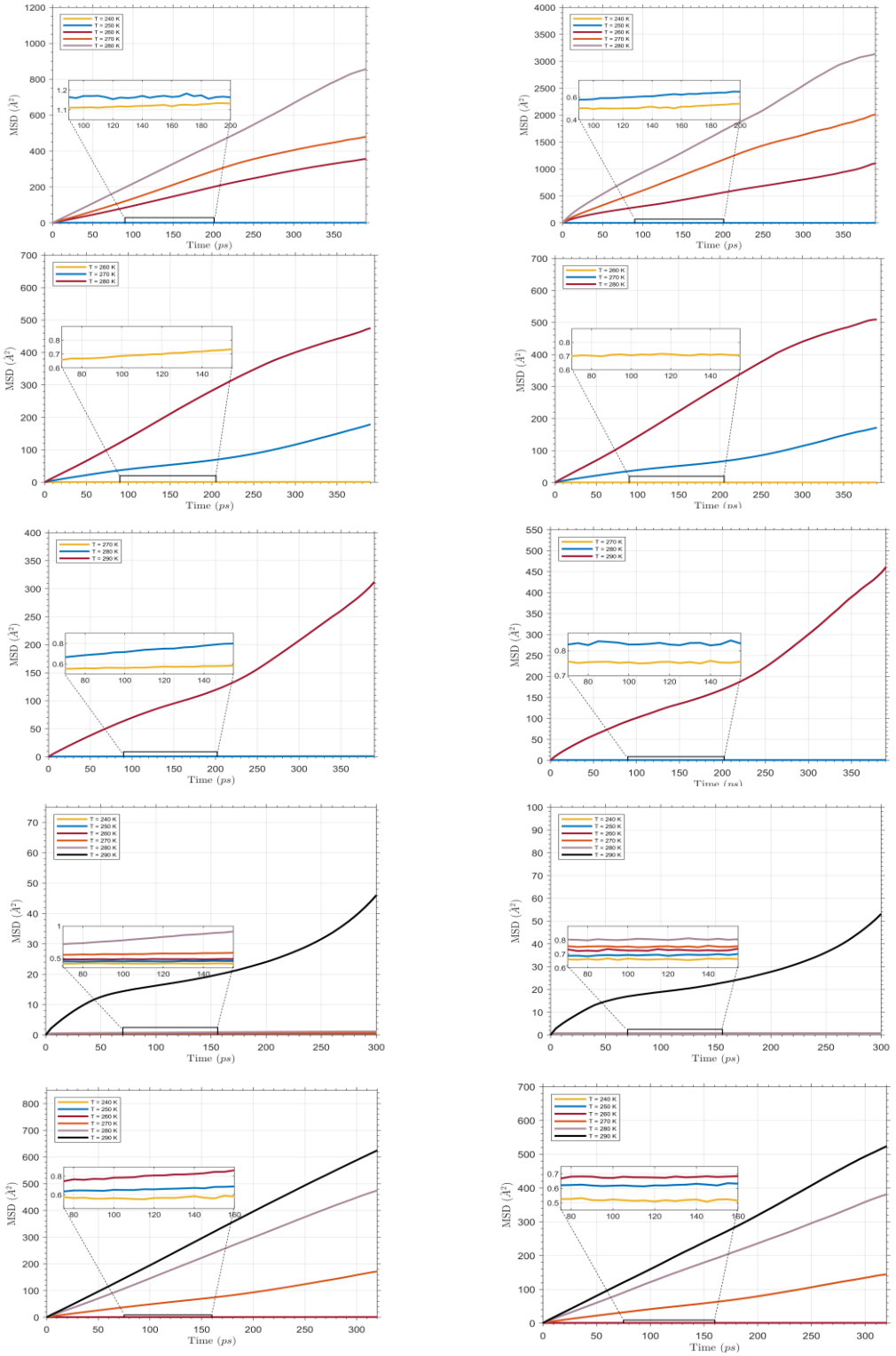

Figure 6-4: MSDs of oxygen atoms in water molecules (left side) and carbon atoms in guest molecules (right side) for (a) methane, (b) methane (75%) + carbon dioxide (25%), (c) methane (62.5%) + carbon dioxide (37.5 %), (d) methane (25%) + carbon dioxide (75%), and (e) carbon dioxide hydrate, at P=5 MPa, 400 ps, and different temperatures.

The diffusion coefficient is another important parameter to monitor the stability and decomposition of the hydrate phase, which is obtained by using the MD simulation technique. The trend of diffusion coefficient for different molecules provides valuable information on the hydrate structure behaviors at different temperatures. The diffusivity for all the aforementioned systems is calculated directly by using MSD of the targeted molecule, as expressed by the following equation [55]:

$$6Dt = MSD \tag{6-7}$$

In Equation (6-7), D and t stand for the coefficient of diffusion and simulation time, respectively. Figure 6-4 illustrates the coefficient of diffusion for water molecules at different compositions of methane and carbon dioxide hydrate systems as a function of temperature at a pressure of 5 MPa after 400 ps simulation. As it is clear from Figure 6-5, the diffusion coefficient of water molecules increases gradually with temperature due to vibration of water molecules in the hydrate cages.

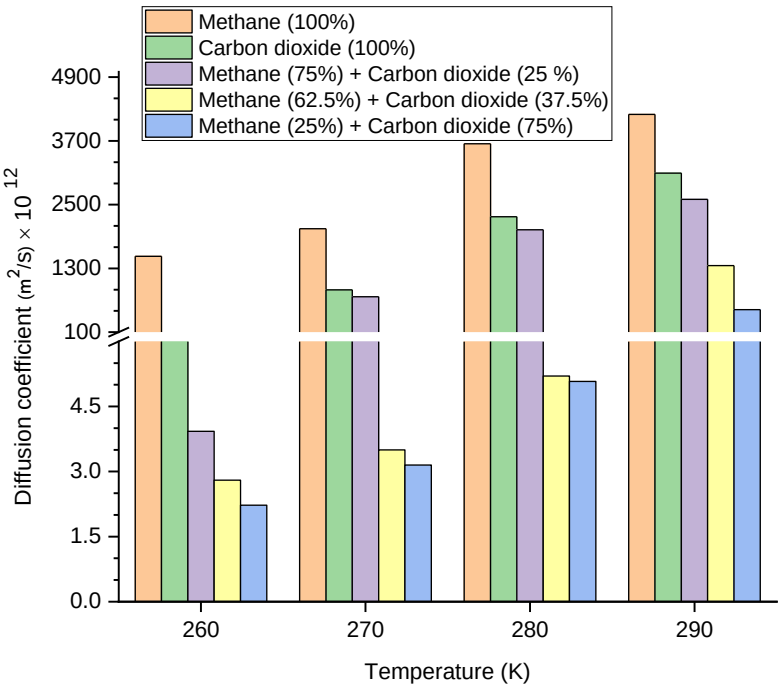

Figure 6- 5: Diffusion coefficient of water molecules in various hydrate systems versus temperature at P = 20 MPa, 400 ps.

The higher diffusion coefficient after the decomposition temperature is due to movement and rotation of water molecules instead of vibration. It is worth noting that the stability of different systems can be determined based on the magnitudes of diffusion coefficient. The trend/behaviour of diffusion coefficient for different systems with respect to temperature change confirms our earlier findings regarding RDFs and MSDs. The variation of coefficient diffusion for guest molecules (methane and/or carbon dioxide) with temperature is demonstrated in Figure 6-6 for various hydrate systems. According to Figure 6-6, there is a considerable difference between the magnitudes of the diffusion coefficient of guest molecules before and after decomposition.

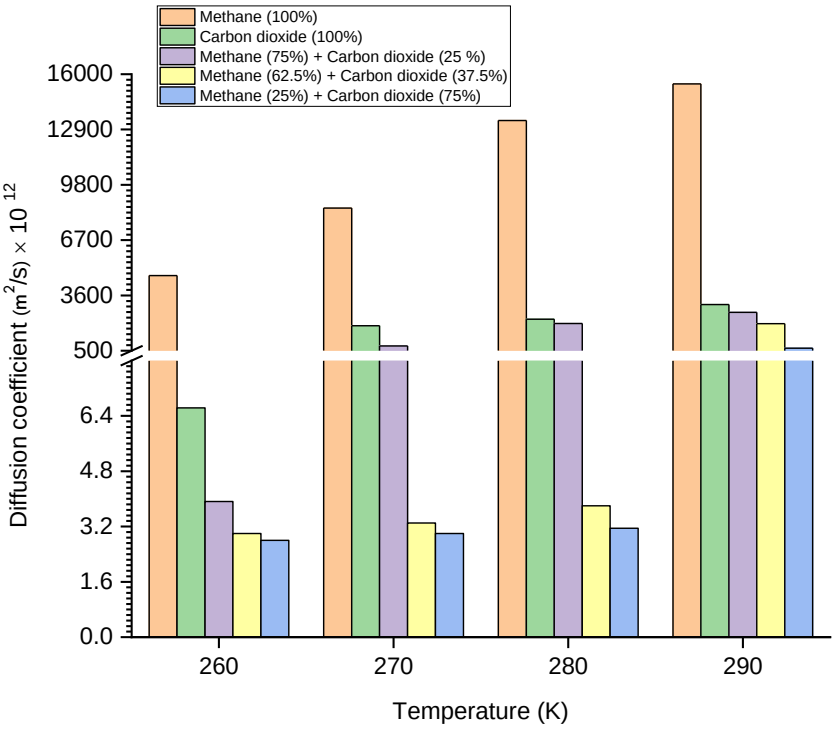

Figure 6-6: Diffusion coefficient of guest molecules for various systems at P = 20 MPa, 400 ps, and different temperatures.

The primary reason of this difference is that the captured guest molecules rotate in the center of frameworks and the values of MSDs and diffusion coefficients remain at a lower level; however, the guest molecules move out freely from the cages after decomposition. Hence, higher values for MSDs and diffusion coefficient are expected because of their movement and molecular nature.

Lattice parameter. In order to investigate the most vital aspects in the clathrate hydrates, the lattice parameter of gas hydrates are assessed under different conditions of temperature, pressure, and composition. The unit cell of cubic structure I includes six large ($5^{12}6^2$) and two small (5^{12}) cages. The tetrakaidekahedral (large) and pentagonal dodecahedral (small) cages

are made of 12 pentagonal plus two hexagonal rings (large) and 12 pentagonal (small) water faces.

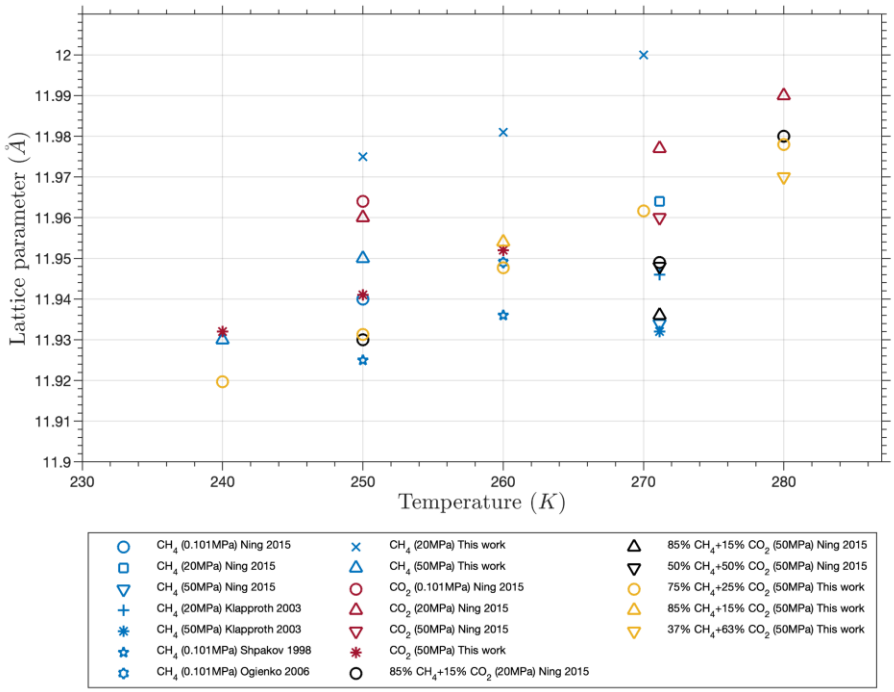

Figure 6-7: Unit cell parameter for methane + carbon dioxide hydrate as a function of temperature and pressure [32, 56-58].

The unit cell parameter for the smaller guests is lower than that for the bigger guest molecules, due to the fact that the van der Waals repulsion results in a greater cage expansion. The unit cell parameter for the methane and carbon dioxide molecules under different thermodynamic conditions and compositions is obtained by using MD simulation. Figure 6-7 demonstrates the unit cell for the methane + carbon dioxide structure I at various temperatures under the equilibrium condition. Effects of temperature and pressure on the value of lattice parameters are reviewed through studying the previous works. Based on Figure 6-7, the calculated lattice parameters are consistent with those reported in the previous experimental and simulation

studies. Also, it can be concluded that the lattice parameter is increased by increasing temperature and size of guest molecules; however, it is lowered as the pressure increases.

Density. The alteration of density with temperature for the gas hydrate structure I of methane + carbon dioxide is discussed for three different pressures, as depicted in Figure 6-8. The density calculated for the carbon dioxide hydrate is above 1150 kg/m3; the densities of carbon dioxide hydrate predicted at different temperatures are in good agreement with the values given in recent experimental and theoretical research investigations [44, 68-72]. When the methane molecules are added to hydrate cages, the density of hydrate decreases slightly due to the lower molecular weight of methane, in comparison with carbon dioxide.

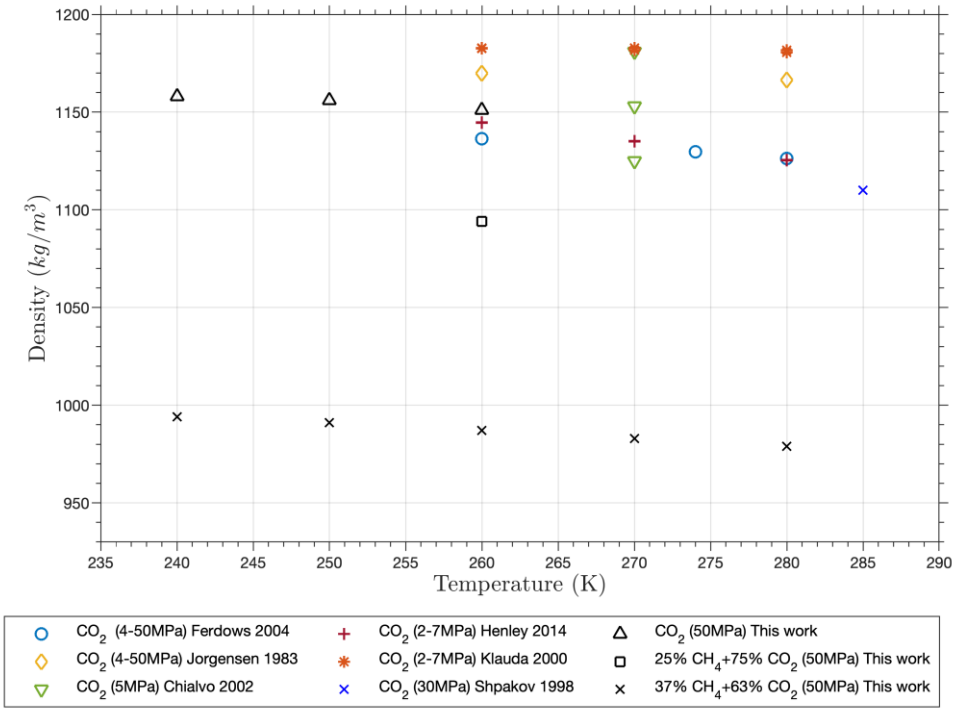

Figure 6-8: Density of methane + carbon dioxide hydrate at different temperatures and compositions [34, 58-62].

Figure 6-9 presents the density of methane hydrate structure calculated by using MD simulation technique, in terms of temperature and pressure. According to Figures 6-8 and 6-9, the hydrate density is lowered with increasing temperature and pressure, which is logical. Thus, it can be concluded that the MD simulation is an appropriate method to calculate density of the clathrate hydrate cases.

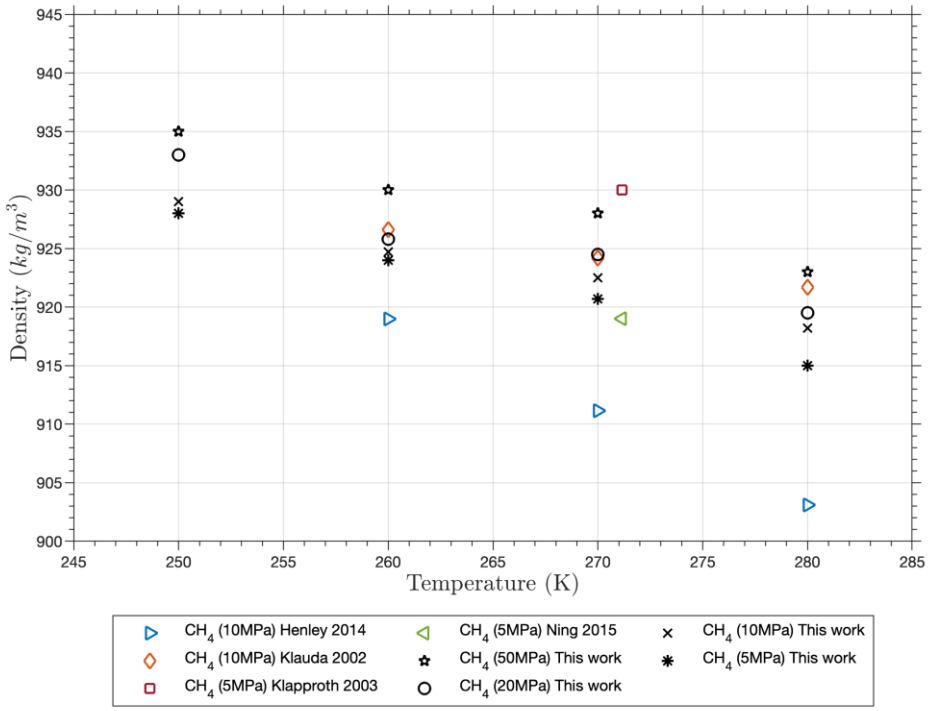

Figure 6-9: Density of methane hydrate under different temperature and pressure conditions [56, 57, 61, 62].

The effect of different pressure and temperature on the density of methane and carbon dioxide hydrate are shown in Figures 6-8 and 6-9. It can be found that hydrate density is declining with increasing temperature and pressure. The findings indicate that the MD simulation is an appropriate method to calculate density for the clathrate hydrate.

Angular order parameter (AOP). The stability of clathrate hydrate can be monitored by the angular order parameter (AOP) of water molecules in the hydrate cages [36]. AOP is defined by the following expression:

$$AOP = \sum [cos\theta|cos\theta| + cos^2(109.47°)]^2 \quad (6\text{-}8)$$

in which, $\boldsymbol{\theta}$ is the angle created by any oxygen atom in a central water molecule with any two oxygen atoms of the neighboring water molecules within a radius of 3.5 Å. Figure 6-10 demonstrates an example for some calculated angles for the neighboring water molecules with a central water molecule (the black dash lines represents the distance between oxygen atoms).

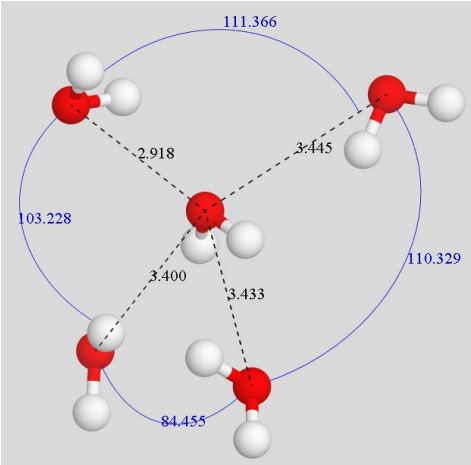

Figure 6- 10: Different angles for a water molecule with four water molecule neighbors within radius of 3.5 Å.

The magnitude of AOP for hydrate and liquid phases are 0 to 0.1 and about 0.8, respectively. Figure 6-11 provides the AOP distribution of water molecules during decomposition of methane

According to Figure 6-11, the value of AOP before decomposition fluctuate is between 0 and 0.1. However, a remarkable increase in the extent of AOP is noticed after the decomposition event (t = 200 ps). A higher value of AOP (compared with stable structure) shows the disordered and turbulent conditions of water molecules. In addition, the layer between the liquid water and solid hydrate is separated by a layer. This interface layer reaches the AOP with a value within the range of 0.3 to 0.7, confirming that the hydrate dissociates layer by layer. Hence, the AOP can be employed to monitor/investigate the decomposition and stability of hydrate structures.

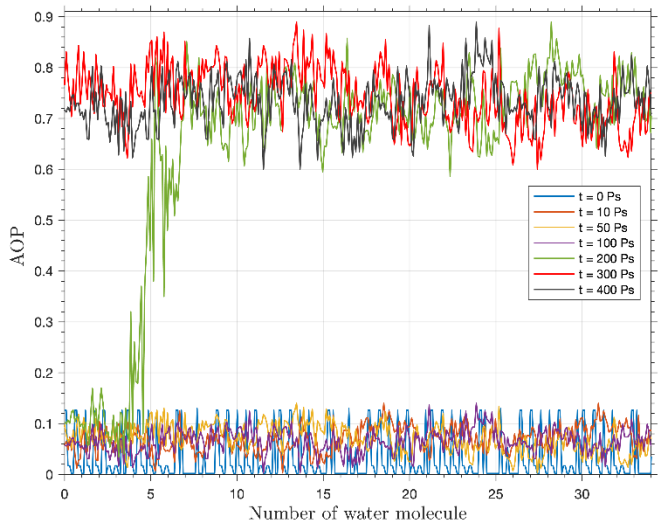

Figure 6- 11: AOP of different water molecules during decomposition of methane hydrate.

MD analysis of CH_4 and CO_2 bubbles. In this section, we aim to show the evolution of gas bubbles composed of methane and/or carbon dioxide in the hydrate systems after decomposition. The objective of this section is to further understand the behavior and effect of bubbles on the hydrate stability while producing gas from hydrates. The behavior and size of bubbles for the hydrate systems considered in this study are different due to different stability of hydrate cages and solubility of gasses in the water phase. MD simulation runs are conducted

at 300 K, 5 MPa, and 1ns. As mentioned earlier, all hydrate systems dissociate at temperatures above 290 K. Hence, higher temperatures are chosen to model decomposition within a reasonable simulation time. The simulation runs at temperatures lower than 300 K are not fast to maintain methane and carbon dioxide supersaturation condition in the water phase.

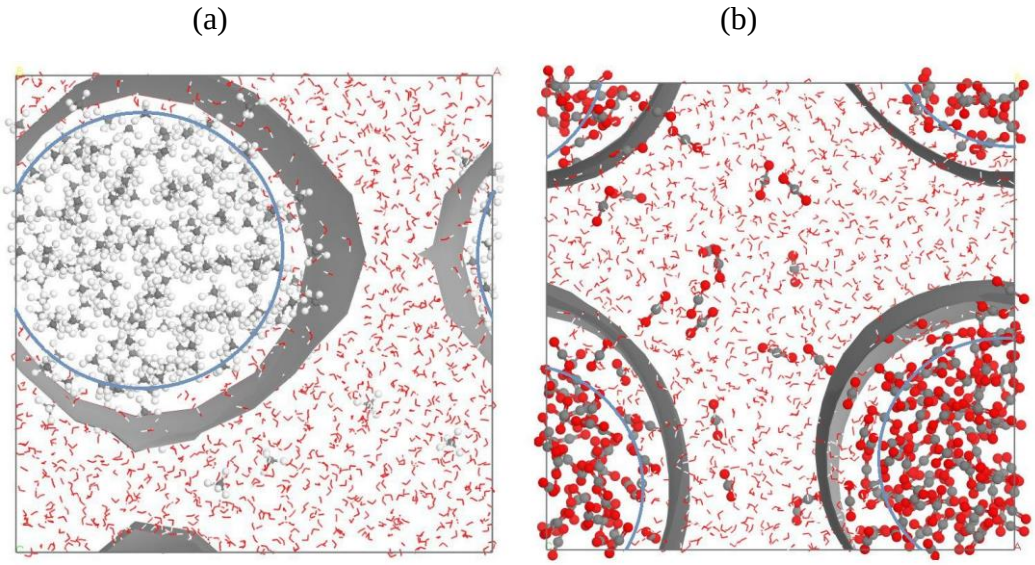

Figure 6-12: Bubble formation after gas hydrate dissociation for (a) methane hydrate (b) carbon dioxide hydrate at T = 300 K and P = 5 MPa after 1 ns simulation.

The final snapshot of the hydrate dissociation at 1000 ps for methane and carbon dioxide hydrate cases is depicted in Figure 6-12 where the temperature is 300 K and the pressure is 5 MPa. After decomposition, the gas molecules escape from hydrate cages and appear in the water phase in the form of bubbles. The bubbles grow in all directions. When the diameter of bubbles is equal to the cell size in any direction, the spherical bubbles change to cylindrical bubbles because of a periodic boundary condition in our simulation.

The equal number of methane and carbon dioxide molecules are considered for both simulation runs. The size of the methane bubbles is noticeably larger than that of carbon dioxide bubbles. It seems that the size difference is due to the lower solubility of methane in liquid water,

compared to that of carbon dioxide in the water. It is clear that only six water molecules remain in the water phase in the simulation. On the other hand, the number of carbon dioxide molecules is higher than that of methane molecules in the water phase due to the high solubility of carbon dioxide in water. The difference between the size of bubbles implies that the formation of CH_4 bubbles has a more important impact on the hydrate decomposition, in comparison with the bubbles in the CO_2 hydrate case. Interestingly, there is also a difference in the concentration of carbon dioxide and methane molecules at the interface between the bubbles and liquid phase. This might be related to the lower surface tension of CO_2 molecules at the interface. The same composition of CO_2, CH_4, and water as well as the decomposition conditions are applied to investigate the hydrate dissociation. It should be mentioned that the size and shape of the bubbles may be affected by the size of the simulation box. A large spherical bubble can be created at a large simulation box so that the bubble diameter is equal to the length of the simulation box. Although this study successfully demonstrates the difference between the size and behavior of CO_2 and CH_4 bubbles after hydrate decomposition, it has limitations in terms of dimensions of the simulation box due to computational cost (or time) restriction.

The formation of methane bubble is chosen to capture the bubble growth after hydrate dissociation. Figure 6-13 provides different snapshots of MD simulation for methane decomposition at the temperature of 300 K (above equilibrium condition) at different times.

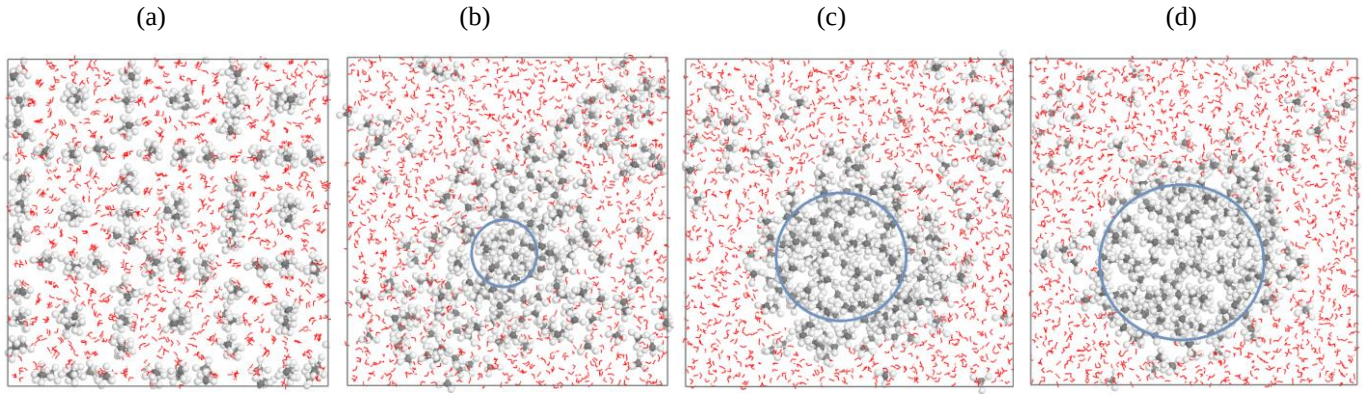

Figure 6-13: Snapshots of the decomposition of the methane hydrate at T = 300 K after (a) 50 ps, (b) 200 ps, (c) 400 ps, and (d) 600 ps.

The blue circles show the size of bubbles in the water molecules after hydrate decomposition. As the simulation time increases, the structure of methane hydrates starts to break and forms a bubble due to high concentration of gas molecules in water molecules (above the gas solubility in the water). The shape of bubble will be quasi-sphere at the primary stage of dissociation due to the limited size of simulation box. After that, it changes to a cylinder to reach a lower interfacial tension. It is clear that the bubble size increases immediately after decomposition and it will be almost stable at the end of simulation. The interesting point about the methane molecules in Figure 6-13 is that the number of methane molecules between water molecules decreases over the simulation run due to low solubility of methane molecules in the water.

Figure 6-14 illustrates the relative concentration distribution of methane molecules against the z coordinate of the simulation box at T = 280 K, P = 5 MPa while examining different simulation times. Different methane concentration curves for gas hydrate decomposition

provide the microscopic characteristics of the molecules involved in the hydrates. As can be seen from Figure 6-14, the relative concentration of methane molecules before decomposition fluctuates around 1.

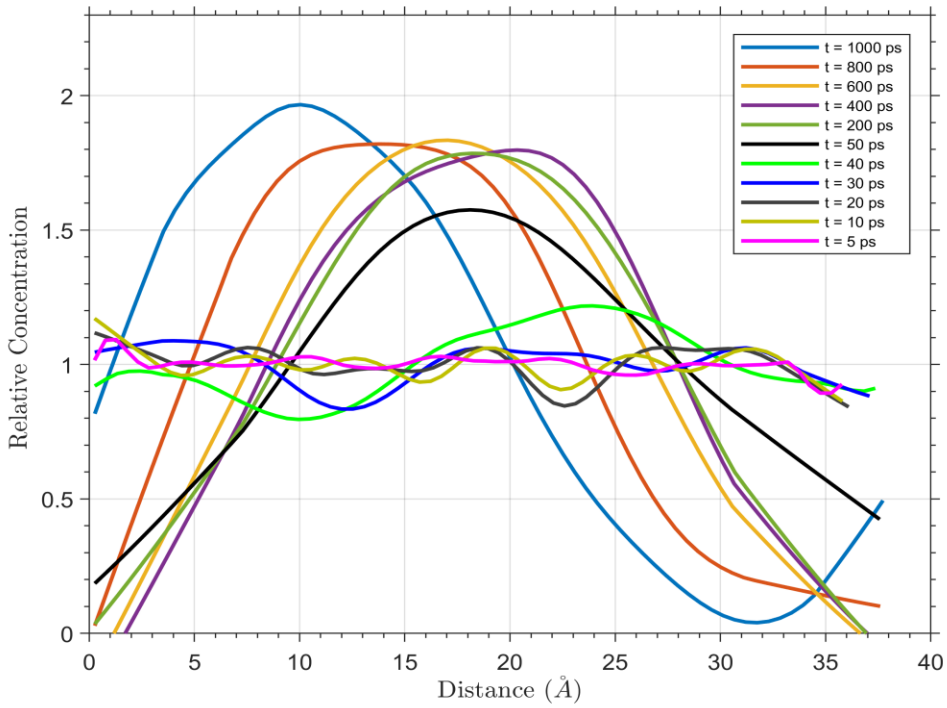

Figure 6-14: The relative concentration of methane molecules for different simulation time at T = 280 K and P = 5 MPa

However, after decomposition (for the simulation time above 20ps), the relative concertation reaches a maximum value which shows the bubble formation in the simulation box. The size of bubble increases over the simulation period. The bubble size is then changed along the Z direction after 50 ps.

Potential energy. The potential energy includes the van der Waals interactions and long-range Coulomb interactions. Figure 6-15 depicts the potential energy versus simulation time for all the systems (studied in this work) at a temperature of 280 K, a pressure of 5 MPa, and 400ps for NPT simulation time before and after hydrate decomposition. As shown in Figure 6-15, the

potential energy varies around the equilibrium value before the dissociation phenomenon due to the vibration and rotation of the guest and water and molecules in the center of cages. The potential energy of the methane hydrate is sharply increased at the beginning of MD simulation, due to decomposition of hydrogen bonds between the water molecules in the cages. Therefore, it can be concluded that the methane hydrate is not stable at a temperature of 280 K. The clathrate hydrate is dissociated after a short period of time (about 30 ps), and it oscillates around a constant extent. Based on Figure 6-15, carbon dioxide hydrate is decomposed after methane hydrate. After that, the system with a composition of methane (75%) + carbon dioxide (25%) is dissociated. The potential energies of methane (25%) + carbon dioxide (75 %) and methane (62.5%) + carbon dioxide (37.5 %) systems are almost constant and the structure is stable throughout the simulation run at a temperature of 280 K. The difference between all hydrate cases in terms of potential energy implies that we are able to monitor the decomposition and stability of gas hydrates using potential energy curves for different systems. The MSD, RDF, and potential energy graphs are at a good agreement in terms of predicting the decomposition time.

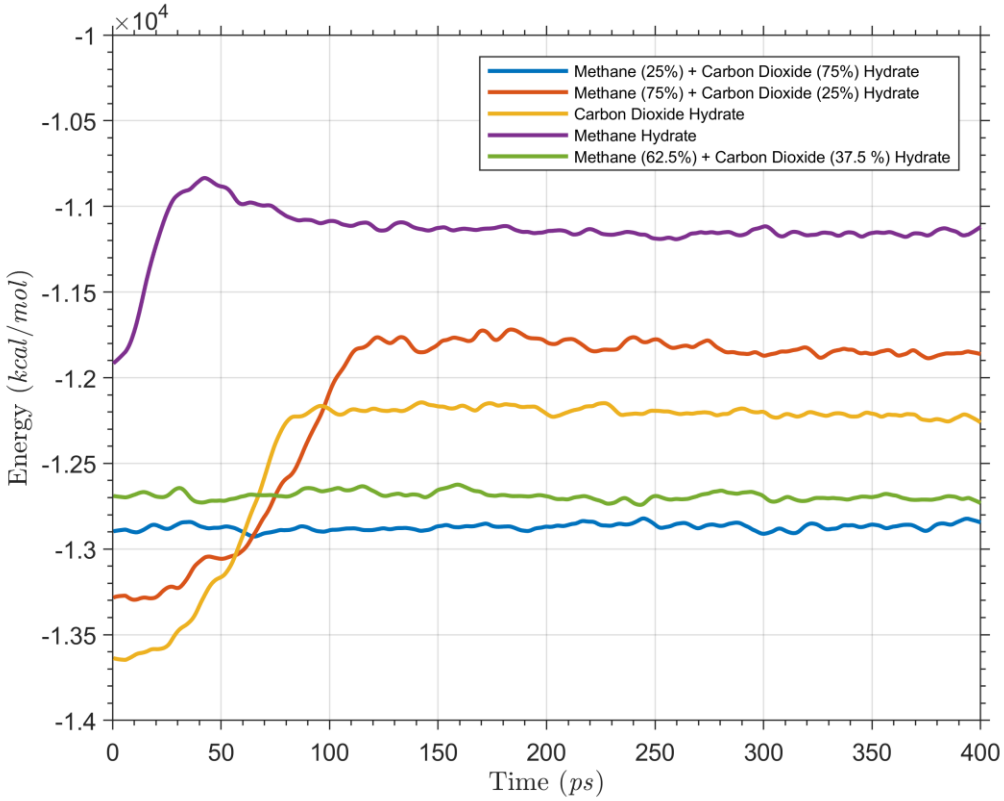

Figure 6- 15: The potential energy versus time for different systems at T = 280 K and P = 5 MPa.

Enthalpy of dissociation. Generally, decomposition of the gas hydrate structure can be represented by this reaction, $G.nH_2O(s) \rightarrow G(g) + nH_2O(l)$, where G refers to the guest gas molecules in the system, and n denotes the hydration number. In addition, *s*, *g*, and *l* represent the molecule phases as solid, liquid, and gas, respectively. The enthalpy of gas hydrate dissociation is the amount of heat required to dissociate hydrate structure to produce one mole of gas molecules. As mentioned earlier, the guest molecules have van der Waals interactions with water molecules and the hydrogen bonds create the hydrate cages. Thus, the amount of dissociation enthalpy changes with the interactions between guest and host molecules and the number of hydrogen bonds per guest gas molecules.

In this research study, the structure I of clathrate hydrate for methane and carbon dioxide is investigated. Hence, the type of cages and number of hydrogen bonds are constant. It implies that only different interactions between the guest and host molecules influence the enthalpy of dissociation of gas hydrates. Carbon dioxide is bigger than methane. Thus, it has a greater enthalpy of dissociation [73, 74]. In this work, dissociation enthalpy of gas hydrates is calculated by using MD simulation at different compositions of methane and carbon dioxide. The magnitudes of molar enthalpy of dissociation for various mixtures are listed in Table 6-2. As it is clear from Table 6-2, the molar dissociation enthalpy values of pure components as well as CH_4 /CO_2 mixture hydrates are in good agreement with the results found in the previous works [73, 74].

Table 6-2: Molar enthalpy of dissociation for systems of CH_4 / CO_2 hydrates.

No.	Molecules (mole fraction)	Enthalpy of dissociation (kJ/mol. gas)							
		This work	Kwon et al. [75]	Handa [76]	Gupta et al. [77]	Rydzy et al. [73]	Anderson [78, 79]	Yoon et al. [80]	Nagayev et al.[81]
1	**CH_4 (100%)**	53.27	-	54.19	54.44	51.6	52.9	53.81	54,674
2	**CH_4 (85%) + CO_2 (15%)**	-	-	-	-	-	53.4	-	-
3	**CH_4 (75%) + CO_2 (25%)**	55.41	-	-	-	-	-	-	-
4	**CH_4 (70%) + CO_2 (30 %)**	-	-	-	-	-	53	-	-
5	**CH_4 (60%) + CO_2 (40%)**	--	57.23	-	-	-	-	-	-
6	**CH_4 (62.5%) + CO_2 (37.5%)**	56.9	-	-	-	-	-	-	-
7	**CH_4 (29%) + CO_2 (71%)**	-	62.82	-	-	-	-	-	-
8	**CH_4 (25%) + CO_2 (75%)**	61.32	-	-	-	-	-	-	-
9	**CO_2 (100%)**	64.01	-	-	-	-	57.7 - 63.6	57.66	57.98

Based on Table 6-2, the interesting finding is that the calculated molar enthalpies of hydrate dissociation of CH_4/CO_2 hydrates are almost between those of pure methane and carbon dioxide hydrates. Hence, the dissociation enthalpy increases with including a higher number of larger molecules in the hydrate structures [73, 74].

Molecular dynamic approach is helpful to obtain further detailed knowledge such that the attained data/information can assist engineers and researchers in oil and gas industries. The accurate thermodynamic and physical characteristics of gas hydrates, which are calculated by MD simulation, can be used to improve the performance/effectiveness of available simulation and modeling tools in the hydrate area.

6.4. Summary and Conclusions

The main goal of the current study is to investigate the stability and dissociation of gas hydrate structure I for methane + carbon dioxide cases by using MD simulation in the Forcite module of Materials studio software. The impacts of temperature and composition on structure and stability of the hydrates are analyzed. A variety of properties for gas hydrates such as radial distribution function (RDF), mean square displacement (MSD), lattice parameter, density, potential energy, and diffusion coefficient of molecules involved in the hydrate structure are obtained at different conditions through employing the MD simulation strategy. A summary of the main findings is provided below:

- The MD simulation methodology is able to evaluate the stability of gas hydrates in the molecular scale. This effective technique can assist to calculate the RDF, MSD, AOP, dissociation enthalpy, and diffusion coefficient at various temperatures and simulation

time. Based on our result, the stability of hydrates lowers as the temperature and time increase.

- Different compositions of methane and carbon dioxide hydrate systems are studied to find the most stable case at different thermodynamic conditions. According to the MD results, the structure with a composition of methane (25%) + carbon dioxide (75%) is stable under 300 K at 5 MPa; it means the best configuration to attain a stable structure is when the carbon dioxide and methane molecules are in large and small cavities, respectively.
- The physical properties such as density and lattice parameter for different compositions of methane + carbon dioxide hydrate cases are computed. The findings are in good agreement with the experimental and theoretical data/outputs in the literature. This confirms the reliability and accuracy of the model implemented in this research work.
- The MD technique is utilized to investigate the bubble formation and evolution of carbon dioxide and methane molecules after dissociation. The size of bubbles (for methane and carbon dioxide) is different; however, the shape of both methane and carbon dioxide molecules are almost cylindrical.

Acknowledgements

The financial assistance of the Natural Sciences and Engineering Research Council of Canada (NSERC), Memorial University (Canada), Innovate NL, and Equinor Canada is highly appreciated.

Nomenclatures

Acronyms

ADD	Average absolute deviation percentage
AOP	Angular order parameter
CVFF	Consistent valence force field
MD	Molecular dynamic
MSD	Mean square displacement
NVT	Constant temperature, constant volume
NPT	Constant pressure, constant volume
RDF	Radial distribution function

Variables/Letters

b	Bond length
D	Diffusion coefficient and force constant in CVFF equation
F	Force constant in CVFF equation
H	Force constant in CVFF equation
n	Total number of data sets
n	Total number of particles α and β particles
P	Pressure
q	Charge of particles
r	Spherical distance and distance between particles in CVFF equation
R	Initial position of particles
S	Sign convention
t	Simulation time

T	Temperature
V	Volume of simulation box

Greek letters

ε	Well depth in vdW function
ϕ	Dihedral angle
θ	Bond angle
X	Out-of-plane parameter

Subscripts

0	Initial position of atoms
α	α particles
β	β particles
b	Bond length
C	Carbon atom
ε	Well depth in vdW function
i	i particles
j	j particles
O	Oxygen atom
θ	Bond angle
ϕ	Dihedral angle
X	Out-of-plane parameter

References

[1] Fitzgerald, A. and M. Taylor. *Offshore gas-to-solids technology*. in *Offshore Europe*. 2001. Society of Petroleum Engineers.

[2] Kang, S.-P. and H. Lee, *Recovery of CO2 from flue gas using gas hydrate: thermodynamic verification through phase equilibrium measurements.* Environmental science & technology, 2000. **34**(20): p. 4397-4400.
[3] Kou, Z., M. Dejam, D. R., and K.V. R., *Dispersion due to combined pressure-driven and electro-osmotic flows in a channel surrounded by a permeable porous medium*

Electrokinetic dispersion in capillary electrophoresis. Physics of Fluids, 2019. **31**(5): p. 056603.
[4] M., D., *Derivation of dispersion coefficient in an electro-osmotic flow of a viscoelastic fluid through a porous-walled microchannel.* Chem. Eng. Sci., 2019. **204**: p. 298.
[5] M., D., *Hydrodynamic dispersion due to a variety of flow velocity profiles in a porous-walled microfluidic channel.* Int. J. Heat Mass Transfer, 2019. **136**: p. 87.
[6] M., D., H. H., and C.Z. X., *Shear dispersion in a rough-walled fracture.* Soc. Pet. Eng. J., 2018. **23**: p. 1669.
[7] M., D., H. H., and C.Z. X., *Shear dispersion in combined pressure-driven and electro-osmotic flows in a channel with porous walls.* Chem. Eng. Sci., 2015. **137**: p. 205.
[8] M., D., H. H., and C.Z. X., *Shear dispersion in combined pressure-driven and electro-osmotic flows in a capillary tube with a porous wall.* AICHE J., 2015. **61**: p. 3981.
[9] Englezos, P. and J.D. Lee, *Gas hydrates: A cleaner source of energy and opportunity for innovative technologies.* Korean Journal of Chemical Engineering, 2005. **22**(5): p. 671-681.
[10] Dejam, M. and H. Hassanzadeh, *Diffusive leakage of brine from aquifers during CO2 geological storage.* Advances in Water Resources, 2018. **111**: p. 36-57.
[11] Dejam, M. and H. Hassanzadeh, *The role of natural fractures of finite double-porosity aquifers on diffusive leakage of brine during geological storage of CO2*. Vol. 78. 2018. 177-197.
[12] Javanmardi, J. and M. Moshfeghian, *Energy consumption and economic evaluation of water desalination by hydrate phenomenon.* QNRS Repository, 2011. **2011**(1): p. 622.
[13] Carroll, J.J., *Natural Gas Hydrates: A Guide for Engineers*. 2009.
[14] Sloan, D.E. and C.A. Koh, *Clathrate Hydrates of Natural Gases*. 2008.
[15] Demirbas, A., *Methane hydrates as potential energy resource: Part 2–Methane production processes from gas hydrates.* Energy Conversion and Management, 2010. **51**(7): p. 1562-1571.
[16] Kurihara, M., A. Sato, H. Ouchi, H. Narita, Y. Masuda, T. Saeki, and T. Fujii. *Prediction of gas productivity from eastern Nankai Trough methane hydrate reservoirs*. in *Offshore Technology Conference*. 2008. Offshore Technology Conference.
[17] Moridis, G. *Numerical studies of gas production from methane hydrates*. in *SPE Gas Technology Symposium*. 2002. Society of Petroleum Engineers.
[18] Liu, Y., M. Strumendo, and H. Arastoopour, *Simulation of methane production from hydrates by depressurization and thermal stimulation.* Industrial & Engineering Chemistry Research, 2008. **48**(5): p. 2451-2464.

[19] Kondori, J., S. Zendehboudi, and M.E. Hossain, *A review on simulation of methane production from gas hydrate reservoirs: Molecular dynamics prospective.* Journal of Petroleum Science and Engineering, 2017. **159**: p. 754-772.
[20] Graue, A., B. Kvamme, B. Baldwin, J. Stevens, J.J. Howard, E. Aspenes, G. Ersland, J. Husebo, and D. Zornes, *MRI visualization of spontaneous methane production from hydrates in sandstone core plugs when exposed to CO2.* SPE Journal, 2008. **13**(02): p. 146-152.
[21] Park, Y., M. Cha, J.-H. Cha, K. Shin, H. Lee, K.-P. Park, D.-G. Huh, H.-Y. Lee, S.-J. Kim, and J. Lee. *Swapping carbon dioxide for complex gas hydrate structures*. in *ICGH 6th International Conference on Gas Hydrates*. 2008. Citeseer.
[22] Sarupria, S. and P.G. Debenedetti, *Homogeneous nucleation of methane hydrate in microsecond molecular dynamics simulations.* Journal of Physical Chemistry Letters, 2012. **3**(20): p. 2942-2947.
[23] Okano, Y. and K. Yasuoka, *Free-energy calculation of structure-H hydrates.* The Journal of chemical physics, 2006. **124**(2): p. 024510.
[24] Zhang, J. and Z. Pan, *Effect of potential energy on the formation of methane hydrate.* Journal of Petroleum Science and Engineering, 2011. **76**(3): p. 148-154.
[25] English, N.J. and J.M.D. MacElroy, *Theoretical studies of the kinetics of methane hydrate crystallization in external electromagnetic fields.* Journal of Chemical Physics, 2004. **120**(21): p. 10247-10256.
[26] Wei, C. and Z. Hong-Yu, *Molecular dynamics simulation of the structure I empty gas hydrate.* Chinese physics letters, 2002. **19**(5): p. 609.
[27] Baez, L.A. and P. Clancy, *Computer simulation of the crystal growth and dissolution of natural gas hydrates.* Annals of the New York Academy of Sciences, 1994. **715**: p. 177-186.
[28] English, N.J., J.K. Johnson, and C.E. Taylor, *Molecular-dynamics simulations of methane hydrate dissociation.* Journal of Chemical Physics, 2005. **123**(24).
[29] English, N.J. and E.T. Clarke, *Molecular dynamics study of CO2 hydrate dissociation: Fluctuation-dissipation and non-equilibrium analysis.* Journal of Chemical Physics, 2013. **139**(9).
[30] Ding, L.Y., C.Y. Geng, Y.H. Zhao, and H. Wen, *Molecular dynamics simulation on the dissociation process of methane hydrates.* Molecular Simulation, 2007. **33**(12): p. 1005-1016.
[31] Smirnov, G.S. and V.V. Stegailov, *Melting and superheating of sI methane hydrate: Molecular dynamics study.* Journal of Chemical Physics, 2012. **136**(4).
[32] Kondori, J., S. Zendehboudi, and L. James, *New insights into methane hydrate dissociation: Utilization of molecular dynamics strategy.* Fuel, 2019. **249**: p. 264-276.
[33] Kondori, J., S. Zendehboudi, and L. James, *Molecular Dynamic Simulations to Evaluate Dissociation of Hydrate Structure II in the Presence of Inhibitors: A Mechanistic Study.* Chemical Engineering Research and Design, 2019.
[34] Chatti, I., A. Delahaye, L. Fournaison, and J.P. Petitet, *Benefits and drawbacks of clathrate hydrates: A review of their areas of interest.* Energy Conversion and Management, 2005. **46**(9-10): p. 1333-1343.
[35] Geng, C.-Y., H. Wen, and H. Zhou, *Molecular simulation of the potential of methane reoccupation during the replacement of methane hydrate by CO2.* The Journal of Physical Chemistry A, 2009. **113**(18): p. 5463-5469.

[36] Tung, Y.-T., L.-J. Chen, Y.-P. Chen, and S.-T. Lin, *In situ methane recovery and carbon dioxide sequestration in methane hydrates: A molecular dynamics simulation study.* The Journal of Physical Chemistry B, 2011. **115**(51): p. 15295-15302.
[37] Bai, D., X. Zhang, G. Chen, and W. Wang, *Replacement mechanism of methane hydrate with carbon dioxide from microsecond molecular dynamics simulations.* Energy and Environmental Science, 2012. **5**(5): p. 7033-7041.
[38] Gutt, C., B. Asmussen, W. Press, M.R. Johnson, Y.P. Handa, and J.S. Tse, *The structure of deuterated methane-hydrate.* Journal of Chemical Physics, 2000. **113**(11): p. 4713-4721.
[39] Belosludov, V.R., T.M. Inerbaev, O.S. Subbotin, R.V. Belosludov, J.-i. Kudoh, and Y. Kawazoe, *Thermal expansion and lattice distortion of clathrate hydrates of cubic structures I and II.* Journal of Supramolecular Chemistry, 2002. **2**(4-5): p. 453-458.
[40] Bertie, J.E. and S.M. Jacobs, *Infrared spectra from 300 to 10 cm-1 of structure II clathrate hydrates at 4.3°K.* The Journal of Chemical Physics, 1978. **69**(9): p. 4105-4113.
[41] Davidson, D.W., Y.P. Handa, C.I. Ratcliffe, J.A. Ripmeester, J.S. Tse, J.R. Dahn, F. Lee, and L.D. Calvert, *Crystallographic Studies of Clathrate Hydrates. Part I.* Molecular Crystals and Liquid Crystals, 1986. **141**(1-2): p. 141-149.
[42] Ogienko, A.G., A.V. Kurnosov, A.Y. Manakov, E.G. Larionov, A.I. Ancharov, M.A. Sheromov, and A.N. Nesterov, *Gas Hydrates of Argon and Methane Synthesized at High Pressures: Composition, Thermal Expansion, and Self-Preservation.* The Journal of Physical Chemistry B, 2006. **110**(6): p. 2840-2846.
[43] Tse, J., M. L. Klein, and I. R. McDonald, *Dynamical Properties of the Structure I Clathrate Hydrate of Xenon*. Vol. 78. 1983. 2096-2097.
[44] Chialvo, A.A., M. Houssa, and P.T. Cummings, *Molecular dynamics study of the structure and thermophysical properties of model sI clathrate hydrates.* Journal of Physical Chemistry B, 2002. **106**(2): p. 442-451.
[45] Reshadi, P., H. Modarress, B. Dabir, and S. Amjad-Iranagh, *A study on dissociation of sII krypton hydrate and the effect of hydrocarbon guest molecules as stabilizer by molecular dynamics simulation.* Phase Transitions, 2017. **90**(11): p. 1128-1142.
[46] Reshadi, P., H. Modarress, B. Dabir, and S. Amjad-Iranagh, *Molecular dynamics simulation for studying the stability of structure H clathrate-hydrates of argon and large guest molecules.* Journal of Dispersion Science and Technology, 2018. **39**(11): p. 1572-1581.
[47] Zhang, J., S. Piana, R. Freij-Ayoub, M. Rivero, and S.K. Choi, *Molecular dynamics study of methane in water: diffusion and structure.* Molecular Simulation, 2006. **32**(15): p. 1279-1286.
[48] Sakemoto, R., H. Sakamoto, K. Shiraiwa, R. Ohmura, and T. Uchida, *Clathrate Hydrate Crystal Growth at the Seawater/Hydrophobic−Guest−Liquid Interface.* Crystal Growth & Design, 2010. **10**(3): p. 1296-1300.
[49] Kim, H.C., P.R. Bishnoi, R.A. Heidemann, and S.S.H. Rizvi, *Kinetics of Methane Hydrate Decomposition.* Chem. Eng. Sci., 1987. **42**(7): p. 1645.
[50] Ripmeester, J.A., S. Hosseini, P. Englezos, and S. Alavi. *Fundamentals of methane hydrate decomposition*. in *Canadian Unconventional Resources and International Petroleum Conference*. 2010. Society of Petroleum Engineers.

[51] Coluci, V.R., N.M. Pugno, S.O. Dantas, D.S. Galvao, and A. Jorio, *Atomistic simulations of the mechanical properties of 'super'carbon nanotubes.* Nanotechnology, 2007. **18**(33): p. 335702.
[52] Rapaport, D.C., *The art of molecular dynamics simulation*. 2004, Cambridge: Cambridge University Press.
[53] Stoddard, S.D. and J. Ford, *Numerical experiments on stochastic behavior of a Lennard-Jones gas system.* Phys Rev A, 1973. **8**.
[54] Verlet, L., *Computer" experiments" on classical fluids. I. Thermodynamical properties of Lennard-Jones molecules.* Physical review, 1967. **159**(1): p. 98.
[55] Swope, W.C., H.C. Andersen, P.H. Berens, and K.R. Wilson, *A computer simulation method for the calculation of equilibrium constants for the formation of physical clusters of molecules: application to small water clusters.* J Chem Phys, 1982. **76**.
[56] Gear, C.W., *Numerical initial value problems in ordinary differential equations*. 1971: Prentice Hall PTR.
[57] Biovia, *Biovia Materials Studio*. 2018: San Diego, CA, USA.
[58] Berendsen, H.J., J.v. Postma, W.F. van Gunsteren, A. DiNola, and J. Haak, *Molecular dynamics with coupling to an external bath.* The Journal of chemical physics, 1984. **81**(8): p. 3684-3690.
[59] Dauber-Osguthorpe, P., V.A. Roberts, D.J. Osguthorpe, J. Wolff, M. Genest, and A.T. Hagler, *Structure and energetics of ligand binding to proteins: Escherichia coli dihydrofolate reductase-trimethoprim, a drug-receptor system.* Proteins: Struct Funct Bioinformatics, 1988. **4**.
[60] Liu, Y., J. Zhao, and J. Xu, *Dissociation mechanism of carbon dioxide hydrate by molecular dynamic simulation and ab initio calculation.* Computational and Theoretical Chemistry, 2012. **991**: p. 165-173.
[61] Hagler, A.T., S. Lifson, and P. Dauber, *Consistent force field studies of intermolecular forces in hydrogen-bonded crystals. 2. A benchmark for the objective comparison of alternative force fields.* Journal of the American Chemical Society, 1979. **101**(18): p. 5122-5130.
[62] Hagler, A.T., P. Dauber, and S. Lifson, *Consistent force field studies of intermolecular forces in hydrogen-bonded crystals. 3. The C:O.cntdot..cntdot..cntdot.H-O hydrogen bond and the analysis of the energetics and packing of carboxylic acids.* Journal of the American Chemical Society, 1979. **101**(18): p. 5131-5141.
[63] McLain, S.E., A.K. Soper, and A. Watts, *Water structure around dipeptides in aqueous solutions.* European Biophysics Journal, 2008. **37**(5): p. 647-655.
[64] Vatamanu, J. and P. Kusalik, *Molecular dynamics methodology to investigate steady-state heterogeneous crystal growth.* The Journal of chemical physics, 2007. **126**(12): p. 124703.
[65] Allen, M.P. and D.J. Tildesley, *Computer simulation of liquids*. 2017: Oxford university press.
[66] Ning, F., K. Glavatskiy, Z. Ji, S. Kjelstrup, and T.H. Vlugt, *Compressibility, thermal expansion coefficient and heat capacity of CH 4 and CO 2 hydrate mixtures using molecular dynamics simulations.* Physical Chemistry Chemical Physics, 2015. **17**(4): p. 2869-2883.

[67] Klapproth, A., E. Goreshnik, D. Staykova, H. Klein, and W.F. Kuhs, *Structural studies of gas hydrates.* Canadian Journal of Physics, 2003. **81**(1-2): p. 503-518.
[68] Shpakov, V., J. Tse, C. Tulk, B. Kvamme, and V.R. Belosludov, *Elastic Module Calculation and Instability in Structure I Methane Clathrate Hydrate*. Vol. 282. 1998. 107-114.
[69] Ferdows, M. and M. Ota, *Density of CO2 Hydrate by Monte Carlo Simulation.* Proceedings of the Institution of Mechanical Engineers, Part C: Journal of Mechanical Engineering Science, 2006. **220**(5): p. 691-696.
[70] Jorgensen, W.L., J. Chandrasekhar, J.D. Madura, R.W. Impey, and M.L. Klein, *Comparison of simple potential functions for simulating liquid water.* The Journal of Chemical Physics, 1983. **79**(2): p. 926-935.
[71] Henley, H., E. Thomas, and A. Lucia, *Density and phase equilibrium for ice and structure I hydrates using the Gibbs–Helmholtz constrained equation of state.* Chemical Engineering Research and Design, 2014. **92**(12): p. 2977-2991.
[72] Klauda, J.B. and S.I. Sandler, *A fugacity model for gas hydrate phase equilibria.* Industrial & engineering chemistry research, 2000. **39**(9): p. 3377-3386.
[73] Rydzy, M.B., J.M. Schicks, R. Naumann, and J. Erzinger, *Dissociation enthalpies of synthesized multicomponent gas hydrates with respect to the guest composition and cage occupancy.* The Journal of Physical Chemistry B, 2007. **111**(32): p. 9539-9545.
[74] Hachikubo, A., R. Nakagawa, D. Kubota, H. Sakagami, N. Takahashi, and H. Shoji. *Dissociation heat of mixed-gas hydrate composed of methane and ethane*. in *Proceedings of the 6th International Conference on Gas Hydrates (ICGH-2008)*. 2008.
[75] Kwon, T.-H., T.J. Kneafsey, and E.V. Rees, *Thermal dissociation behavior and dissociation enthalpies of methane–carbon dioxide mixed hydrates.* The Journal of Physical Chemistry B, 2011. **115**(25): p. 8169-8175.
[76] Handa, Y., *Compositions, enthalpies of dissociation, and heat capacities in the range 85 to 270 K for clathrate hydrates of methane, ethane, and propane, and enthalpy of dissociation of isobutane hydrate, as determined by a heat-flow calorimeter.* The Journal of chemical thermodynamics, 1986. **18**(10): p. 915-921.
[77] Gupta, A., J. Lachance, E. Sloan Jr, and C.A. Koh, *Measurements of methane hydrate heat of dissociation using high pressure differential scanning calorimetry.* Chemical Engineering Science, 2008. **63**(24): p. 5848-5853.
[78] Anderson, G.K., *Enthalpy of dissociation and hydration number of carbon dioxide hydrate from the Clapeyron equation.* The Journal of Chemical Thermodynamics, 2003. **35**(7): p. 1171-1183.
[79] Anderson, G.K., *Enthalpy of dissociation and hydration number of methane hydrate from the Clapeyron equation.* The Journal of Chemical Thermodynamics, 2004. **36**(12): p. 1119-1127.
[80] Yoon, J.-H., Y. Yamamoto, T. Komai, H. Haneda, and T. Kawamura, *Rigorous approach to the prediction of the heat of dissociation of gas hydrates.* Industrial & engineering chemistry research, 2003. **42**(5): p. 1111-1114.
[81] Nagayev, V., A. Gritsenko, and V. Murin. *A new method for enhanced production of gas hydrates with CO2*. in *All-union Conference on Calorimetry and Chemical Thermodynamics. Ivonovo, Proc*. 1979.

7. CHAPTER SEVEN

Summary and Recommendations for Future Work

This study focuses on the gas hydrate decomposition process. A thermodynamic model is used to calculate the gas hydrate decomposition conditions for different systems under various temperatures, pressures, and compositions. In addition, the molecular dynamic simulation is used by employing Materials Studio package to investigate the molecular properties and behaviour of gas hydrate structures I and II. This thesis includes five sections: literature review (Chapter Two), thermodynamic model (Chapter Three), molecular dynamic simulation for methane hydrate (Chapter Four), molecular dynamic simulation for methane + propane and methane + isobutane hydrate structure II (Chapter Five), and molecular dynamic simulation for methane + carbon dioxide hydrate structure I (Chapter Six).

7.1. Literature Review (Chapter 2)

A large amount of methane is stored in gas hydrate reserves around the world, nearly 10^{17} cubic meters. Due to this high potential energy source and the massive extent of gas hydrates, the hydrates have attracted a great attention from governments and scientists. This phase of study provides an overview of the research works conducted on the decomposition of methane hydrates in reservoirs. The main findings/conclusions of the first phase are as follows:

- There are a few studies about the hydrate formation and decomposition of methane hydrate at the microscopic level. Considering various uses of gas hydrates, further experimental and theoretical investigations should be conducted in this field so that more accurate and cost-effective techniques are developed.
- An appropriate gas reservoir simulation should be able to identify the key characteristics of gas reservoirs, to predict the future of reservoir production, and to develop effective hydrocarbon withdrawal plans. Therefore, a

systematic/comprehensive simulation and modeling strategy for investigation of gas hydrate production mechanisms seems inevitable.

- One of the main challenges in the area of gas hydrates is how to accurately model the behaviors of brine/gas/hydrates where the permeability, porosity, and temperature of underground formations hold high values. In addition, further experimental and theoretical studies at micro to macro scales are required to assess the free gas layer and intermediate zones in gas hydrate reserves. Despite of various engineering and research works reported in the literature on the gas hydrate formation and dissociation, comprehensive and precise models (e.g., for prediction of thermo-physical properties, reaction kinetics, and production rate) for natural gas hydrate reservoir cases should be developed through using real data and theoretical information.
- With the aid of MD simulation, it is feasible to determine the geometric parameters of gas hydrate molecules, to explore the interfacial phenomena of various water/gas/hydrate/porous medium systems, and to obtain electromagnetic fields for the hydrate cages and potential functions for methane, water, and carbon dioxide over the hydrate formation and gas production processes in gas hydrate reservoirs. In addition, it is important to explore new features of hydrate cages and their impact on decomposition rate, and combination of two or three practical methods for hydrate decomposition using MD in order to choose an effective production approach.
- The interface between the liquid water and methane hydrate during methane hydrate decomposition can be systematically explored by a new powerful approach, called molecular dynamics simulations. New potential functions are substantial to investigate

the detailed molecular nature and to figure out the mechanisms of hydrate decomposition.

7.2. Thermodynamic Model (Chapter 3)

The main objective of this phase of the thesis is to conduct a new thermodynamic modeling through using PC-SAFT equation of state for calculation of formation conditions of single and mixed clathrate hydrates. In this study, the binary and ternary gas systems of methane, ethane, propane, isobutane, carbon dioxide, nitrogen, and hydrogen sulfide are considered. The association contribution and UNIQUAC model are incorporated in the modeling strategy. The association contributions between water, methanol, and ethanol are taken into account to obtain the thermodynamic conditions for the methane hydrate systems. A very good agreement is noticed between the modeling results and the experimental data so that the value of average error percentage for PC-SAFT equation of state is lower, compared to the previous EOS/thermodynamic models. The binary interaction parameters for different binary components are investigated by using experimental hydrate data, leading to better outcome compared with results obtained through fitting the vapor liquid equilibrium (VLE) data. In addition to attaining a higher accuracy, the current study provides the best values for the physical parameters of PC-SAFT equation of state in gas hydrate systems.

7.3. Molecular Dynamic Approach (Chapter 3, 5, and 6)

This phase of the study investigates the stability and decomposition process of gas hydrates at different conditions (chapters 4 to 6). The structural and dynamic properties of methane clathrate systems during decomposition process are evaluated through conducting molecular dynamic (MD) simulations by using the Materials Studio. In the MD simulations, the CVFF

force field and isobaric-isothermal (NPT) ensemble are used to study the methane hydrate stability or dissociation conditions. Various simulation runs at different temperature, pressure, and cage occupancy conditions are performed. The main outcomes of this modeling approach are as follows:

- The stability of gas hydrate can be systematically investigated by utilizing the MD simulation approach. The RDF, MSD, and diffusion coefficient can be obtained from a set of NPT ensemble in MD simulation at different pressures and temperatures. According to the MD results, increasing temperature and decreasing pressure lead to instability of the gas hydrate structures.
- The dissociation of gas hydrates is observed at the molecular scale. First, the vibration of water molecules continuously increases so that the lattice parameter and diffusion coefficient increase over time. Eventually, the structure of cages in the gas hydrate disjoints. After this stage, the guest gases run away from the center of damaged cages and the diffusion coefficient of gas molecules experiences an increase after the decomposition.
- The lattice parameter for the methane/water, methane/isobutane, methane/carbon dioxide, methane/ propane systems is calculated at a variety of pressures and temperatures. A good agreement between the experimental data and simulation results is noticed.
- To study the effect of inhibitors on the decomposition process, two methane molecules are replaced by the inhibitors. As expected, the presence of inhibitors accelerates the decomposition process and results in the gas hydrate dissociation at lower temperatures.

- The hydroxyl groups in the inhibitors (used in this study) are the reason for the earlier decomposition, compared to the cases without inhibitors. The new hydrogen bonds are formed between the hydroxyl groups of inhibitors and water molecules, which disturb the arrangement and stability of cages.
- Different compositions of methane and carbon dioxide are analyzed to find the most stable case(s) at various temperatures. According to the MD results, the structure with methane (25%) + carbon dioxide (75%) composition is stable at 300 K and 5 MPa; it means the best configuration to have a stable structure is when carbon dioxide and methane molecules are placed in large and small cavities, respectively.
- The density and heat capacity for different compositions of methane, methane/ carbon dioxide, methane/ propane, and methane/ isobutane are obtained, which are in good agreement with those determined by common experimental and theoretical techniques.
- MD technique is employed to assess the dynamic and thermodynamic behaviors of carbon dioxide and methane bubbles after dissociation. The size of bubbles for different molecules is different. However, the methane and carbon dioxide molecules are almost cylindrical.
- In the decomposition process, two methane molecules are replaced by the inhibitors. As expected, the presence of inhibitors accelerates the decomposition process and results in the gas hydrate dissociation at lower.

7.4. Recommendations for Future Work

Employing the thermodynamic approach and molecular dynamic simulation strategy, the following recommendations for future work are summarized:

- In further work, the thermodynamic approach can be used for various systems /structures of gas hydrates. The influence of additives such as alcohols, promotors, and ionic liquids on gas hydrate decomposition can be studied through using various extended EOSs where association and non-association terms are considered.
- It is recommended to assess the impact of different additives on the hydrate stability using the MD approach where various force fields are examined.
- We recommend that all structures of hydrate systems are modeled using MD technique. Interactions between hydrate structures and density distribution of hydrate structures at a variety of process and thermodynamic conditions seem interesting to be studied.
- Further experimental and modeling studies are needed to validate the MD results concerning the physical and structure properties.
- The stability of gas hydrates in hydrate reservoirs can be studied by incorporating the effect of pore size and structure.
- The type and composition of rocks (and clays) and fatty acids can affect the hydrate stability and decomposition. Thus, these important aspects can be considered in the future work.
- The change in thermodynamic properties (entropy, enthalpy, and Gibbs free energy) before and after hydrate decomposition is recommended to be determined with a higher accuracy and reliability through integration of MD and thermodynamic approaches.
- With the aid of stochastic and/or non-stochastic optimization methods, it is possible to find the optimal concentration of additives (inhibitors and promotors) to control hydrate formation at different conditions. The hybrid MD/EOS strategy can lead to considerable contribution in this research area.

- In future work, MD simulations can be employed to design new effective inhibitors/chemicals, where inhibition performance, cost aspect, and environmental prospect are taken into account.
- Hydrate, gas, and/or water phase properties such as oil composition, density, heat capacity, and diffusion coefficient can be calculated for simple and/or complex systems of hydrates by employing MD simulation. Further modelling/simulation works need to be conducted to determine physical and thermos-physical characteristics of hydrate systems with high reliability and precise.